Cover Page



Universiteit Leiden



The handle http://hdl.handle.net/1887/37413 holds various files of this Leiden University dissertation

Author: Piers, S.R.D.
Title: Understanding ventricular tachycardia : towards individualized substrate-based therapy
Issue Date: 2016-01-28

S.R.D. PIERS

Understanding Ventricular Tachycardia:

Towards Individualized

Understanding Ventricular Tachycardia:

Towards Individualized Substrate-based Therapy

S.R.D. Piers

Understanding Ventricular Tachycardia:
Towards Individualized Substrate-based Therapy
S.R.D. Piers

Thesis Leiden University, Faculty of Medicine, with summary in Dutch
Proefschrift Universiteit Leiden, faculteit Geneeskunde, met een samenvatting in het Nederlands

Copyright © S.R.D. Piers 2015
All right reserved. No parts of this thesis may be reproduced, stored in a retrieval system of any nature or transmitted in any form or by any means, electronic, mechanical, photocopying, recording or otherwise, without prior permission of the author, or when appropriate, the publishers of the papers.

ISBN: 978-94-6169-791-2

Lay-out and printed by: Optima Grafische Communicatie, Rotterdam, the Netherlands.

The printing of this thesis was financially supported by St. Jude Medical, Biotronik, Bayer HealthCare, Sanofi Aventis, Chipsoft, Medis Medical Imaging and Toshiba Medical Systems.

Understanding Ventricular Tachycardia: Towards Individualized Substrate-based Therapy

Proefschrift

ter verkrijging van
de graad van Doctor aan de Universiteit Leiden,
op gezag van Rector Magnificus prof. mr. C.J.J.M. Stolker,
volgens besluit van het College voor Promoties
te verdedigen op donderdag 28 januari 2016
klokke 16:15 uur

door

Sebastiaan Roderick Daniël Piers
geboren te Utrecht
in 1986

Promotores:
Prof. dr. K. Zeppenfeld
Prof. dr. M.J. Schalij

Promotiecommissie:
Prof. dr. J.M.T. de Bakker (Universiteit van Amsterdam)
Prof. dr. N.A. Blom
Dr. A. Meijer (Catharina Ziekenhuis, Eindhoven)
Prof. dr. L. Mont (Hospital Clinic, Barcelona)
Dr. D.A. Pijnappels
Dr. Q. Tao

Het verschijnen van dit proefschrift werd mede mogelijk gemaakt door de steun van de Nederlandse Hartstichting en de Stichting Wetenschap en Onderzoek Interne Geneeskunde Onze Lieve Vrouwe Gasthuis.

CONTENTS

Chapter 1 **General introduction and outline of thesis** **9**

Part I Imaging-guided VT ablation

Chapter 2 **Imaging-guided ventricular tachycardia ablation** **27**
Piers SRD, Zeppenfeld K
Arrhythmia & Electrophysiology Review 2013;2(2):128-34

Chapter 3 **Epicardial substrate mapping for ventricular tachycardia ablation in patients with non-ischemic cardiomyopathy: a new algorithm to differentiate between scar and viable myocardium developed by simultaneous integration of computed tomography and contrast-enhanced magnetic resonance imaging** **49**
Piers SRD, van Huls van Taxis CF, Tao Q, van der Geest RJ, Askar SF, Siebelink HM, Schalij MJ, Zeppenfeld K
European Heart Journal 2013;34(8):586-96

Chapter 4 **Contrast-enhanced MRI-derived scar patterns and associated ventricular tachycardias in nonischemic cardiomyopathy: implications for the ablation strategy** **71**
Piers SRD, Tao Q, van Huls van Taxis CF, Schalij MJ, van der Geest RJ, Zeppenfeld K
Circulation: Arrhythmia & Electrophysiology 2013;6(5):875-83

Chapter 5 **CMR-based identification of critical isthmus sites of ischemic and nonischemic ventricular tachycardia** **91**
Piers SRD, Tao Q, de Riva Silva M, Siebelink HM, Schalij MJ, van der Geest RJ, Zeppenfeld K
JACC: Cardiovascular Imaging 2014;7(8):774-84

Part II From Substrate and VT Features to Therapy and Outcome

Chapter 6 **Endocardial or epicardial ventricular tachycardia in nonischemic cardiomyopathy: The role of 12-lead ECG criteria in clinical practice** **115**

Piers SRD, de Riva Silva M, Kapel GF, Trines SA, Schalij MJ, Zeppenfeld K
Heart Rhythm 2014;11(6):1031-9

Chapter 7 **Influence of steroid therapy on the incidence of pericarditis and atrial fibrillation after percutaneous epicardial mapping and ablation for ventricular tachycardia** **135**

Piers SRD, Dyrda K, van Huls van Taxis CF, Schalij MJ, Zeppenfeld K
Circulation: Arrhythmia & Electrophysiology 2014;7(4):671-6

Chapter 8 **Outcomes of ventricular tachycardia ablation in patients with nonischemic cardiomyopathy: the impact of noninducibility** **149**

Piers SRD, Leong DP, van Taxis CF, Tayyebi M, Trines SA, Pijnappels DA, Delgado V, Schalij MJ, Zeppenfeld K
Circulation: Arrhythmia & Electrophysiology 2013;6(3):513-21

Chapter 9 **Early reperfusion therapy affects inducibility, cycle length and occurrence of ventricular tachycardia late after myocardial infarction** **171**

Piers SRD, Wijnmaalen AP, Borleffs CJ, van Huls van Taxis CF, Thijssen J, van Rees JB, Cannegieter SC, Bax JJ, Schalij MJ, Zeppenfeld K
Circulation: Arrhythmia & Electrophysiology 2011;4(2):195-201

Chapter 10 **Myocardial scar predicts monomorphic VT but not polymorphic VT or VF in non-ischemic dilated cardiomyopathy** **189**

Piers SRD, Everaerts K, van der Geest RJ, Hazebroek MR, Siebelink HM, Pison LAFG, Schalij MJ, Bekkers SCAM, Heymans S, Zeppenfeld K
Heart Rhythm 2015;12(10):2106-14

Chapter 11 **Critical QRS prolongation after premature stimulation is associated with polymorphic ventricular tachycardia in nonischemic cardiomyopathy: results from the Leiden Nonischemic Cardiomyopathy Study** **213**

Piers SRD, Askar SFA, Venlet J, Kapel GFL, de Riva Silva M, Jongbloed JJDH, van Tintelen JP, Schalij MJ, Pijnappels DA, Zeppenfeld K
Accepted for publication in Heart Rhythm

Chapter 12 **Summary, conclusions and future perspectives: Towards more effective, individualized substrate-based therapies for ventricular arrhythmias.** **237**

Nederlandse samenvatting **249**

Dankwoord **255**

List of publications **257**

Curriculum vitae **263**

Chapter 1

General Introduction and Outline of Thesis

GENERAL INTRODUCTION AND OUTLINE OF THESIS

Background

Although important scientific advances have shed some light onto the substrate and mechanisms of ventricular arrhythmias in patients with structural heart disease, many aspects remain incompletely understood. Meanwhile, a pragmatic approach has been adopted, employing implantable cardioverter defibrillators (ICDs) to reduce sudden cardiac death in patients who survived cardiac arrest due to sustained ventricular tachycardia (VT) or ventricular fibrillation (VF),[1-3] and in selected patients who are considered to be at high risk for sudden cardiac death.[4-6] ICDs can usually effectively terminate ventricular arrhythmias and have thus saved numerous lives, but it is important to realize that they do not prevent the occurrence of arrhythmias. ICD shocks are associated with significant morbidity and even with increased mortality,[7] although there may not be a *causal* relation with the latter.[8,9] Therapies to control recurring ventricular arrhythmias and ICD shocks, such as anti-arrhythmic drugs and endocardial or epicardial catheter ablation, have thus become even more important and indispensable in the era of ICDs.

In the past, catheter ablation was only applied in patients with hemodynamically stable VT.[10] The development of substrate and pace mapping has allowed catheter ablation of hemodynamically unstable VTs,[11] which are inducible in the majority of patients with prior myocardial infarction[12] or nonischemic cardiomyopathy (NICM).[13] Catheter ablation is typically performed in patients with recurrent VT despite anti-arrhythmic drugs, but is also recommended in patients who do not prefer or tolerate anti-arrhythmic drugs[14] and may even be applied after a first episode of VT in patients after myocardial infarction, as a direct adjunct to ICD implantation for secondary prevention to prevent future appropriate ICD shocks.[15,16] Despite these recommendations and potential applications, the vast majority of clinicians restrict VT ablation to patients who experience multiple ICD shocks or electrical storm,[17] suggesting that '*there is a need to catch up with current recommendations*'.[18] One potential reason for the poor implementation rate of VT ablation may be the disappointing long-term outcomes, with 6 month recurrence rates of 47% in one large multicenter study in patients with VT after myocardial infarction,[12] and 12-month recurrence rates of 43% and 59% in patients after infarction and with NICM, respectively, in a large tertiary care facility.[19] Notably, although VT ablation may not completely prevent VT recurrence in around 50% of patients, the 6-month VT burden is reduced by ≥75% in approximately 67% of patients.[12] It is unclear whether, and to what extent, the high VT recurrence rates are attributable to not identified or not reachable substrates, imperfect ablation, lesion recovery, arrhythmogenic substrates that evolve over time, progressive heart failure, or other factors.

The key to more effective primary and secondary preventive therapies for ventricular arrhythmias may be improved understanding of different types of ventricular arrhyth-

mias, and of its underlying substrate and mechanisms. Improved understanding may lead both to more accurate risk stratification and to development of more effective, individualized and substrate-based therapies.

Myocardial Fibrosis and Monomorphic Ventricular Tachycardia

In patients with prior myocardial infarction and other causes of replacement fibrosis (e.g., laminopathy[20], myocarditis[21,22]), surviving bundles of myocytes may be located within regions of fibrosis, resulting in slow conduction.[23,24] Classically, slow conduction in fibrotic regions has been attributed to increased path length (so-called *zig-zag* course of activation[23]), but there is also emerging evidence for functional components, which may be unmasked by premature stimulation.[25] The presence of inexcitable barriers, slow conduction and unidirectional conduction block may allow for stable re-entrant activation through a central slow-conducting critical isthmus, which manifests as VT. For hemodynamically stable VTs, activation and entrainment mapping can be performed to identify the slow-conducting critical isthmus during ongoing arrhythmia, so that the arrhythmia can be slowed and terminated by ablation.[26-28] In case of hemodynamically unstable VT, substrate mapping and ablation are typically performed to localize and eliminate the slow-conducting isthmuses during stable rhythm, thereby preventing VT recurrence.[11,29-31]

Nonischemic scars are different from post-infarct scars as they exhibit less late potentials[32] and are frequently located intramurally or subepicardially,[32] limiting the efficacy of endocardial VT ablation. Epicardial mapping and ablation may therefore be required to abolish VT.[33,34] Substrate mapping may however be hampered at the epicardium by interposed epicardial adipose tissue, which is typically not only present in the atrioventricular and interventricular grooves, but also at the acute margin and in other areas.[35,36] In patients undergoing catheter ablation for ventricular arrhythmias, on average 25% of the epicardial surface is covered by >4 mm of fat.[36] The integration of CT-derived fat thickness during VT ablation procedures has demonstrated that fat reduces bipolar electrogram amplitudes,[35,36] thereby preventing accurate delineation of scar regions. The combined integration of both CT and LGE-MRI may compensate for this limitation, allowing distinguishing between scar, viable myocardium and epicardial fat.

Although the '*grass may appear greener*' on the opposite (i.e., epicardial) side of the wall during endocardial mapping (Tung et al.[37]), not all patients with NICM have VTs originating from the epicardium[34] and as a consequence, pericardial puncture and its associated risks (including RV perforation, severe pericardial bleeding, coronary stenosis and occlusion, and liver injury[38]) are not required in all patients with NICM. Also, even if the arrhythmogenic substrate is located subepicardially, it may not be amenable to epicardial ablation because of overlying coronary arteries and/or epicardial fat.[36] Patients with isolated septal substrates are unlikely to benefit from epicardial ablation.[39]

Pre-procedural imaging studies, scar patterns, and associated VT morphologies may be very helpful to identify patients who are not expected to benefit from epicardial VT ablation.

During VT ablation procedures, the slow-conducting critical isthmuses that cause VT are typically located in or adjacent to regions with low bipolar voltage based on electro-anatomical mapping studies,[11,29-34,40,41] and in or adjacent to regions with late gadolinium enhancement (LGE) on MRI based on image integration studies,[42-46] which are both considered to be indicative of focal myocardial fibrosis, based on histological correlation studies.[47-49] There is however limited data on more specific features of the area harboring critical isthmuses of VT. Some evidence suggests that fibrosis density may play a role,[50] and that higher scar transmurality is related to slow conduction.[43,50,51] Improved insights into LGE characteristics at critical isthmuses may improve our understanding of VT and the integration of LGE-MRI-derived data may be of significant added value during catheter ablation procedures if MRI-derived features can lead to critical isthmus sites, in particular in the setting of hemodynamically unstable VT,[12] inducibility of multiple VTs,[12] intramural re-entry circuits[52,53] and epicardial fat overlying the area of interest.[35,36] Finally, LGE-MRI characteristics at critical isthmus sites may facilitate improved risk stratification for VT in broader populations and in particular in patients with non-myocardial infarction scars in the future. The potential benefits of image integration during VT ablation are discussed in more detail in Chapter 2.

From Substrate and VT Features to Therapy and Outcome

The 12-lead ECG of epicardial VTs has been reported to exhibit specific features that may be useful for identification of VTs with an epicardial origin,[54-59] and for guidance of the procedural strategy (i.e., endocardial, epicardial, or both). Based on these ECG features, specific criteria have been developed, which all indicate either the initial direction of the activation wave front from epicardium to endocardium (e.g., initial Q-waves in the inferior leads in VTs with a superior axis), or a delayed and slurred onset of the QRS-complex in the precordial leads consistent with late activation of the endocardially located conduction system (e.g. pseudodelta wave, intrinsicoid deflection time in lead V2).[54-59] The ECG criteria have however previously only been analyzed during pacing and in induced VTs, using electronic calipers at a sweep speed of 200 mm/second on electrophysiology recording systems. To guide the procedural strategy and to select patients that need an epicardial approach, the criteria should be derived from regular 25 mm/second ECGs of clinically documented VTs. The accuracy of the criteria in this setting is unclear.

If epicardial mapping and ablation are performed, post-procedural pericarditic chest pain,[38,60] atrial fibrillation[61] and adhesions[62] may occur. Animal experiments demonstrated that intrapericardial installation of triamcinolone can reduce the development of adhesions.[62] In humans, the effects of intrapericardial triamcinolone or systemic steroids

on pericarditic chest pain and on ECG changes after epicardial mapping has never been investigated.

After VT ablation, programmed electrical stimulation is typically performed to assess for inducibility of clinical and non-clinical VTs. The value of programmed electrical stimulation (PES) after ablation as a procedural endpoint is however unclear in patients with NICM; it has mainly been analyzed in patients after myocardial infarction.[63,64] Patients after infarction do however have a different substrate, higher acute success rates and lower VT recurrence rates.[32,63] Moreover, even in patients after infarction data are inconsistent, possibly due to differences in induction protocols, incomplete application of protocols but also changes in VT ablation populations over time.[12,25,63-65] The predictive value of PES as a procedural endpoint in NICM has only been analyzed in two small studies.[32,66] Also, VT ablation is now more frequently performed in patients without an ICD and off amiodarone, and fast hemodynamically unstable VTs are typically inducible, with uncertain clinical significance. Novel substrate-based endpoints have been proposed as an alternative to post-ablation PES,[25,67] but are arbitrarily defined and to date, their independent predictive value for long-term outcomes has not been reported.

Post-infarct scar features such as transmurality are known to be influenced by reperfusion therapy,[68] which may have important implications for VT. In patients undergoing VT ablation, it has recently been demonstrated that reperfused patients had non-transmural, patchy scars that were associated with faster VTs, whereas non-reperfused patients typically had more transmural, confluent scars that were associated with slower VTs.[69] The effect of reperfusion therapy on VT characteristics has not yet been analyzed in a broader population of patients at risk for VT after myocardial infarction.

Ventricular Arrhythmias: Are All the Same?

Importantly, patients with prior infarction and NICM are not only at risk for monomorphic VT, but also for potentially fatal polymorphic VT and VF.[70,71] Myocardial scar on LGE-MRI has been identified as an important novel predictor of sudden cardiac death, appropriate ICD therapy and combined arrhythmic endpoints in patients after infarction and in NICM.[72-78] In the setting of NICM, the absence of LGE on MRI has been associated with (very) low arrhythmic event rates,[73,75,77] which has led to questions regarding the benefit of ICD implantation in these patients. However, none of these studies has analyzed the predictive value of LGE for monomorphic VT and polymorphic VT/VF separately. Based on LGE-MRI studies in patients with and without inducible VT,[79] and on LGE-MRI integration during VT ablation procedures,[42] monomorphic VT is expected to be related to regions of LGE on MRI. It is unclear whether LGE on MRI also contributes to the initiation and/or maintenance of polymorphic VT/VF.

Polymorphic VT and VF have been attributed to different causes, such as conduction and repolarization abnormalities and electrolyte imbalances.[80-83] For example, progres-

sive activation delay after premature stimulation was associated with a history of VF in the setting of various nonischemic heart diseases.[83] More specifically, the increase in RV intracardiac electrogram duration was larger in patients with prior VF than in those without VF, and the premature stimulus coupling intervals at which the electrogram durations started to increase were longer. There are limited data on the underlying substrate and mechanisms of this electrophysiological phenomenon. An *in vitro* study has found tissue discontinuities as a cause for abnormal conduction velocity restitution,[84] studies in Langendorff-perfused mouse hearts have demonstrated that reduced sodium channel expression and severely reduced Cx43 expression can affect conduction velocity restitution,[85] and finally, two studies in 5-6 explanted hearts from patients with end-stage heart failure have demonstrated conduction abnormalities to occur in regions with long fibrotic strands.[82,86] The underlying substrate and mechanisms of activation delay after premature stimulation have however never been studied in humans with NICM before end-stage heart failure developed.

AIM AND OUTLINE OF THESIS

The present thesis aims to contribute to an improved understanding of different types of ventricular arrhythmias, in both ischemic and nonischemic heart disease. An improved understanding is mandatory for the development of novel, more effective, individualized and substrate-based therapies in the future.

In **part I**, it is demonstrated how image integration strategies can provide insights into the substrate for monomorphic VT in patients with ischemic and nonischemic heart disease. **Chapter 2** provides a detailed overview of the current literature on this topic. Computed tomography-derived epicardial fat thickness and MRI-derived scars are integrated with epicardial substrate maps in **chapter 3** in order to obtain insights into the effects of scar, viable myocardium and epicardial fat on bipolar and unipolar voltages and on electrogram characteristics during epicardial substrate mapping. **Chapter 4** analyzes typical MRI-derived scar patterns in patients with nonischemic cardiomyopathy, the associated 12-lead ECG morphologies of VTs, and their potential use to assess the need for epicardial VT ablation. Specific MRI-derived scar characteristics at electroanatomical mapping-based critical isthmus sites of monomorphic VTs are analyzed in **chapter 5**. These scar characteristics may be used to restrict VT substrate mapping and ablation to limited MRI-identified areas that are likely to contain the critical isthmus for VT.

In **part II**, additional strategies are used to improve our understanding of sustained monomorphic VT and of polymorphic VT and VF. Previously proposed 12-lead ECG criteria to identify an epicardial origin of VTs in nonischemic cardiomyopathy are analyzed in **chapter 6**. The study focuses on the effect of amiodarone and VT cycle length on the

reliability of ECG criteria, and more importantly, on its value in clinical practice. If epicardial substrate mapping and VT ablation are performed, patients may experience post-procedural pericarditic chest pain and pericarditic ECG changes. **Chapter 7** analyzes the effects of systemic and intrapericardial steroids on these adverse procedural effects. The outcomes of VT ablation and the predictive value of post-ablation programmed electrical stimulation are analyzed in **chapter 8**, with a special emphasis on the predictive value of persistent inducibility of non-clinical VTs for VT recurrence during follow-up. In **chapter 9**, it is demonstrated how early reperfusion therapy may have an important impact on monomorphic VTs late after myocardial infarction. The last two chapters will focus on distinct substrates for different types of arrhythmias in nonischemic cardiomyopathy. In **chapter 10**, the predictive value of the presence and extent of MRI-based myocardial scar for monomorphic VT and for polymorphic VT and VF is analyzed. Several mechanisms have been proposed as potential causes for polymorphic VT and VF. In **chapter 11**, it is demonstrated how activation delay after premature stimulation can be quantified simply by measuring the QRS duration during a standard electrophysiological study, and how it relates to inducible polymorphic VT and to underlying fibrosis in endomyocardial biopsy specimens. Finally, a summary, conclusions and future perspectives are provided in **chapter 12**.

REFERENCE LIST

1. A comparison of antiarrhythmic-drug therapy with implantable defibrillators in patients resuscitated from near-fatal ventricular arrhythmias. The Antiarrhythmics versus Implantable Defibrillators (AVID) Investigators. N Engl J Med 1997; 337(22):1576-83.
2. Connolly SJ, Gent M, Roberts RS, Dorian P, Roy D, Sheldon RS, Mitchell LB, Green MS, Klein GJ, O'Brien B. Canadian implantable defibrillator study (CIDS) : a randomized trial of the implantable cardioverter defibrillator against amiodarone. Circulation 2000;101(11):1297-302.
3. Kuck KH, Cappato R, Siebels J, Ruppel R. Randomized comparison of antiarrhythmic drug therapy with implantable defibrillators in patients resuscitated from cardiac arrest : the Cardiac Arrest Study Hamburg (CASH). Circulation 2000;102(7):748-54.
4. Bardy GH, Lee KL, Mark DB et al. Amiodarone or an implantable cardioverter-defibrillator for congestive heart failure. N Engl J Med 2005;352(3):225-37.
5. Kadish A, Dyer A, Daubert JP et al. Prophylactic defibrillator implantation in patients with nonischemic dilated cardiomyopathy. N Engl J Med 2004;350(21):2151-8.
6. Moss AJ, Zareba W, Hall WJ, Klein H, Wilber DJ, Cannom DS, Daubert JP, Higgins SL, Brown MW, Andrews ML. Prophylactic implantation of a defibrillator in patients with myocardial infarction and reduced ejection fraction. N Engl J Med 2002; 346(12):877-83.
7. Poole JE, Johnson GW, Hellkamp AS et al. Prognostic importance of defibrillator shocks in patients with heart failure. N Engl J Med 2008;359(10):1009-17.
8. Powell BD, Saxon LA, Boehmer JP, Day JD, Gilliam FR, III, Heidenreich PA, Jones PW, Rousseau MJ, Hayes DL. Survival after shock therapy in implantable cardioverter-defibrillator and cardiac resynchronization therapy-defibrillator recipients according to rhythm shocked. The ALTITUDE survival by rhythm study. J Am Coll Cardiol 2013; 62(18):1674-9.
9. Dorian P. Counterpoint: implantable cardioverter-defibrillator shocks for ventricular tachyarrhythmias do not increase mortality. Heart Rhythm 2012;9(6): 988-91.
10. Morady F, Harvey M, Kalbfleisch SJ, el-Atassi R, Calkins H, Langberg JJ. Radiofrequency catheter ablation of ventricular tachycardia in patients with coronary artery disease. Circulation 1993;87(2):363-72.
11. Marchlinski FE, Callans DJ, Gottlieb CD, Zado E. Linear ablation lesions for control of unmappable ventricular tachycardia in patients with ischemic and nonischemic cardiomyopathy. Circulation 2000;101(11): 1288-96.
12. Stevenson WG, Wilber DJ, Natale A et al. Irrigated radiofrequency catheter ablation guided by electroanatomic mapping for recurrent ventricular tachycardia after myocardial infarction: the multicenter thermocool ventricular tachycardia ablation trial. Circulation 2008;118(25):2773-82.
13. Tokuda M, Tedrow UB, Kojodjojo P, Inada K, Koplan BA, Michaud GF, John RM, Epstein LM, Stevenson WG. Catheter ablation of ventricular tachycardia in nonischemic heart disease. Circ Arrhythm Electrophysiol 2012;5(5):992-1000.
14. Aliot EM, Stevenson WG, Almendral-Garrote JM et al. EHRA/HRS Expert Consensus on Catheter Ablation of Ventricular Arrhythmias: developed in a partnership with the European Heart Rhythm Association (EHRA), a Registered Branch of the European Society of Cardiology (ESC),

and the Heart Rhythm Society (HRS); in collaboration with the American College of Cardiology (ACC) and the American Heart Association (AHA). Heart Rhythm 2009;6(6): 886-933.

15. Kuck KH, Schaumann A, Eckardt L, Willems S, Ventura R, Delacretaz E, Pitschner HF, Kautzner J, Schumacher B, Hansen PS. Catheter ablation of stable ventricular tachycardia before defibrillator implantation in patients with coronary heart disease (VTACH): a multicentre randomised controlled trial. Lancet 2010;375(9708): 31-40.
16. Reddy VY, Reynolds MR, Neuzil P, Richardson AW, Taborsky M, Jongnarangsin K, Kralovec S, Sediva L, Ruskin JN, Josephson ME. Prophylactic catheter ablation for the prevention of defibrillator therapy. N Engl J Med 2007;357(26):2657-65.
17. Dagres N, Cantu F, Geelen P, Lewalter T, Proclemer A, Blomstrom-Lundqvist C. Current practice of ventricular tachycardia ablation in patients with implantable cardioverter-defibrillators. Europace 2012; 14(1):135-7.
18. Zeppenfeld K. Ventricular tachycardia ablation in implantable cardioverter-defibrillator recipients: a need to catch up with current recommendations. Europace 2012;14(6):778-80.
19. Dinov B, Fiedler L, Schonbauer R, Bollmann A, Rolf S, Piorkowski C, Hindricks G, Arya A. Outcomes in Catheter Ablation of Ventricular Tachycardia in Dilated Nonischemic Cardiomyopathy Compared With Ischemic Cardiomyopathy: Results From the Prospective Heart Centre of Leipzig VT (HELP-VT) Study. Circulation 2014;129(7):728-36.
20. Holmstrom M, Kivisto S, Helio T et al. Late gadolinium enhanced cardiovascular magnetic resonance of lamin A/C gene mutation related dilated cardiomyopathy. J Cardiovasc Magn Reson 2011;13(30.
21. Mahrholdt H, Goedecke C, Wagner A, Meinhardt G, Athanasiadis A, Vogelsberg H, Fritz P, Klingel K, Kandolf R, Sechtem U. Cardiovascular magnetic resonance assessment of human myocarditis: a comparison to histology and molecular pathology. Circulation 2004;109(10):1250-8.
22. Mahrholdt H, Wagner A, Deluigi CC et al. Presentation, patterns of myocardial damage, and clinical course of viral myocarditis. Circulation 2006;114(15):1581-90.
23. de Bakker JM, van Capelle FJ, Janse MJ, Tasseron S, Vermeulen JT, de JN, Lahpor JR. Slow conduction in the infarcted human heart. 'Zigzag' course of activation. Circulation 1993;88(3):915-26.
24. de Bakker JM, van Capelle FJ, Janse MJ, Tasseron S, Vermeulen JT, de JN, Lahpor JR. Fractionated electrograms in dilated cardiomyopathy: origin and relation to abnormal conduction. J Am Coll Cardiol 1996;27(5):1071-8.
25. Jais P, Maury P, Khairy P et al. Elimination of local abnormal ventricular activities: a new end point for substrate modification in patients with scar-related ventricular tachycardia. Circulation 2012;125(18): 2184-96.
26. Calkins H, Epstein A, Packer D et al. Catheter ablation of ventricular tachycardia in patients with structural heart disease using cooled radiofrequency energy: results of a prospective multicenter study. Cooled RF Multi Center Investigators Group. J Am Coll Cardiol 2000;35(7):1905-14.
27. Stevenson WG, Nademanee K, Weiss JN, Wiener I, Baron K, Yeatman LA, Sherman CT. Programmed electrical stimulation at potential ventricular reentry circuit sites. Comparison of observations in humans with predictions from computer simulations. Circulation 1989;80(4):793-806.
28. Stevenson WG, Khan H, Sager P, Saxon LA, Middlekauff HR, Natterson PD, Wiener I.

Identification of reentry circuit sites during catheter mapping and radiofrequency ablation of ventricular tachycardia late after myocardial infarction. Circulation 1993;88(4 Pt 1):1647-70.

29. Brunckhorst CB, Stevenson WG, Jackman WM, Kuck KH, Soejima K, Nakagawa H, Cappato R, Ben-Haim SA. Ventricular mapping during atrial and ventricular pacing. Relationship of multipotential electrograms to ventricular tachycardia reentry circuits after myocardial infarction. Eur Heart J 2002;23(14):1131-8.
30. Brunckhorst CB, Delacretaz E, Soejima K, Maisel WH, Friedman PL, Stevenson WG. Identification of the ventricular tachycardia isthmus after infarction by pace mapping. Circulation 2004;110(6):652-9.
31. Soejima K, Suzuki M, Maisel WH, Brunckhorst CB, Delacretaz E, Blier L, Tung S, Khan H, Stevenson WG. Catheter ablation in patients with multiple and unstable ventricular tachycardias after myocardial infarction: short ablation lines guided by reentry circuit isthmuses and sinus rhythm mapping. Circulation 2001;104(6):664-9.
32. Nakahara S, Tung R, Ramirez RJ, Michowitz Y, Vaseghi M, Buch E, Gima J, Wiener I, Mahajan A, Boyle NG, Shivkumar K. Characterization of the arrhythmogenic substrate in ischemic and nonischemic cardiomyopathy implications for catheter ablation of hemodynamically unstable ventricular tachycardia. J Am Coll Cardiol 2010;55(21):2355-65.
33. Cano O, Hutchinson M, Lin D et al. Electroanatomic substrate and ablation outcome for suspected epicardial ventricular tachycardia in left ventricular nonischemic cardiomyopathy. J Am Coll Cardiol 2009; 54(9):799-808.
34. Soejima K, Stevenson WG, Sapp JL, Selwyn AP, Couper G, Epstein LM. Endocardial and epicardial radiofrequency ablation of ventricular tachycardia associated with dilated cardiomyopathy: the importance of low-voltage scars. J Am Coll Cardiol 2004; 43(10):1834-42.
35. Desjardins B, Morady F, Bogun F. Effect of epicardial fat on electroanatomical mapping and epicardial catheter ablation. J Am Coll Cardiol 2010;56(16):1320-7.
36. van Huls van Taxis CF, Wijnmaalen AP, Piers SR, van der Geest RJ, Schalij MJ, Zeppenfeld K. Real-Time Integration of MDCT-Derived Coronary Anatomy and Epicardial Fat: Impact on Epicardial Electroanatomic Mapping and Ablation for Ventricular Arrhythmias. JACC Cardiovasc Imaging 2013;6(1):42-52.
37. Tung R, Shivkumar K. The value of image integration for epicardial catheter ablation of ventricular tachycardia. JACC Cardiovasc Imaging 2013;6(1):53-5.
38. Sacher F, Roberts-Thomson K, Maury P et al. Epicardial ventricular tachycardia ablation a multicenter safety study. J Am Coll Cardiol 2010;55(21):2366-72.
39. Haqqani HM, Tschabrunn CM, Tzou WS et al. Isolated septal substrate for ventricular tachycardia in nonischemic dilated cardiomyopathy: incidence, characterization, and implications. Heart Rhythm 2011;8(8): 1169-76.
40. Arenal A, Glez-Torrecilla E, Ortiz M, Villacastin J, Fdez-Portales J, Sousa E, del CS, Perez d, I, Jimenez J, Almendral J. Ablation of electrograms with an isolated, delayed component as treatment of unmappable monomorphic ventricular tachycardias in patients with structural heart disease. J Am Coll Cardiol 2003;41(1):81-92.
41. Bogun F, Good E, Reich S et al. Isolated potentials during sinus rhythm and pace-mapping within scars as guides for ablation of post-infarction ventricular tachycardia. J Am Coll Cardiol 2006;47(10):2013-9.
42. Bogun FM, Desjardins B, Good E, Gupta

S, Crawford T, Oral H, Ebinger M, Pelosi F, Chugh A, Jongnarangsin K, Morady F. Delayed-enhanced magnetic resonance imaging in nonischemic cardiomyopathy: utility for identifying the ventricular arrhythmia substrate. J Am Coll Cardiol 2009;53(13):1138-45.

43. Dickfeld T, Tian J, Ahmad G, Jimenez A, Turgeman A, Kuk R, Peters M, Saliaris A, Saba M, Shorofsky S, Jeudy J. MRI-Guided ventricular tachycardia ablation: integration of late gadolinium-enhanced 3D scar in patients with implantable cardioverter-defibrillators. Circ Arrhythm Electrophysiol 2011;4(2):172-84.
44. Fernandez-Armenta J, Berruezo A, Andreu D et al. Three-dimensional Architecture of Scar and Conducting Channels Based on High Resolution ce-CMR: Insights for Ventricular Tachycardia Ablation. Circ Arrhythm Electrophysiol 2013;6(3):528-37.
45. Perez-David E, Arenal A, Rubio-Guivernau JL et al. Noninvasive identification of ventricular tachycardia-related conducting channels using contrast-enhanced magnetic resonance imaging in patients with chronic myocardial infarction: comparison of signal intensity scar mapping and endocardial voltage mapping. J Am Coll Cardiol 2011;57(2):184-94.
46. Wijnmaalen AP, van der Geest RJ, van Huls van Taxis CF, Siebelink HM, Kroft LJ, Bax JJ, Reiber JH, Schalij MJ, Zeppenfeld K. Head-to-head comparison of contrast-enhanced magnetic resonance imaging and electroanatomical voltage mapping to assess post-infarct scar characteristics in patients with ventricular tachycardias: real-time image integration and reversed registration. Eur Heart J 2011;32(1):104-14.
47. Ashikaga H, Sasano T, Dong J et al. Magnetic resonance-based anatomical analysis of scar-related ventricular tachycardia: implications for catheter ablation. Circ Res 2007;101(9):939-47.
48. Callans DJ, Ren JF, Michele J, Marchlinski FE, Dillon SM. Electroanatomic left ventricular mapping in the porcine model of healed anterior myocardial infarction. Correlation with intracardiac echocardiography and pathological analysis. Circulation 1999; 100(16):1744-50.
49. Kim RJ, Fieno DS, Parrish TB, Harris K, Chen EL, Simonetti O, Bundy J, Finn JP, Klocke FJ, Judd RM. Relationship of MRI delayed contrast enhancement to irreversible injury, infarct age, and contractile function. Circulation 1999;100(19):1992-2002.
50. Desjardins B, Crawford T, Good E, Oral H, Chugh A, Pelosi F, Morady F, Bogun F. Infarct architecture and characteristics on delayed enhanced magnetic resonance imaging and electroanatomic mapping in patients with postinfarction ventricular arrhythmia. Heart Rhythm 2009;6(5):644-51.
51. Sasaki T, Miller CF, Hansford R et al. Myocardial structural associations with local electrograms: a study of postinfarct ventricular tachycardia pathophysiology and magnetic resonance-based noninvasive mapping. Circ Arrhythm Electrophysiol 2012;5(6):1081-90.
52. Betensky BP, Kapa S, Desjardins B, Garcia FC, Callans DJ, Dixit S, Frankel DS, Hutchinson MD, Supple GE, Zado ES, Marchlinski FE. Characterization of trans-septal activation during septal pacing: criteria for identification of intramural ventricular tachycardia substrate in nonischemic cardiomyopathy. Circ Arrhythm Electrophysiol 2013;6(6): 1123-30.
53. Desjardins B, Yokokawa M, Good E et al. Characteristics of intramural scar in patients with nonischemic cardiomyopathy and relation to intramural ventricular arrhythmias. Circ Arrhythm Electrophysiol 2013; 6(5):891-7.

54. Bazan V, Bala R, Garcia FC, Sussman JS, Gerstenfeld EP, Dixit S, Callans DJ, Zado E, Marchlinski FE. Twelve-lead ECG features to identify ventricular tachycardia arising from the epicardial right ventricle. Heart Rhythm 2006;3(10):1132-9.

55. Bazan V, Gerstenfeld EP, Garcia FC, Bala R, Rivas N, Dixit S, Zado E, Callans DJ, Marchlinski FE. Site-specific twelve-lead ECG features to identify an epicardial origin for left ventricular tachycardia in the absence of myocardial infarction. Heart Rhythm 2007;4(11):1403-10.

56. Berruezo A, Mont L, Nava S, Chueca E, Bartholomay E, Brugada J. Electrocardiographic recognition of the epicardial origin of ventricular tachycardias. Circulation 2004;109(15):1842-7.

57. Daniels DV, Lu YY, Morton JB, Santucci PA, Akar JG, Green A, Wilber DJ. Idiopathic epicardial left ventricular tachycardia originating remote from the sinus of Valsalva: electrophysiological characteristics, catheter ablation, and identification from the 12-lead electrocardiogram. Circulation 2006;113(13):1659-66.

58. Martinek M, Stevenson WG, Inada K, Tokuda M, Tedrow UB. QRS characteristics fail to reliably identify ventricular tachycardias that require epicardial ablation in ischemic heart disease. J Cardiovasc Electrophysiol 2012;23(2):188-93.

59. Valles E, Bazan V, Marchlinski FE. ECG criteria to identify epicardial ventricular tachycardia in nonischemic cardiomyopathy. Circ Arrhythm Electrophysiol 2010;3(1): 63-71.

60. Della BP, Brugada J, Zeppenfeld K, Merino J, Neuzil P, Maury P, Maccabelli G, Vergara P, Baratto F, Berruezo A, Wijnmaalen AP. Epicardial ablation for ventricular tachycardia: a European multicenter study. Circ Arrhythm Electrophysiol 2011;4(5):653-9.

61. Mahapatra S, LaPar DJ, Bhamidipati CM, McDaniel G, Kamath S, Bunch TJ, Ailawadi G. Incidence, risk factors, and consequences of new-onset atrial fibrillation following epicardial ablation for ventricular tachycardia. Europace 2011;13(4):548-54.

62. d'Avila A, Neuzil P, Thiagalingam A, Gutierrez P, Aleong R, Ruskin JN, Reddy VY. Experimental efficacy of pericardial instillation of anti-inflammatory agents during percutaneous epicardial catheter ablation to prevent postprocedure pericarditis. J Cardiovasc Electrophysiol 2007;18(11): 1178-83.

63. Carbucicchio C, Santamaria M, Trevisi N, Maccabelli G, Giraldi F, Fassini G, Riva S, Moltrasio M, Cireddu M, Veglia F, Della BP. Catheter ablation for the treatment of electrical storm in patients with implantable cardioverter-defibrillators: short- and long-term outcomes in a prospective single-center study. Circulation 2008; 117(4):462-9.

64. Della Bella P, De Ponti R., Uriarte JA, Tondo C, Klersy C, Carbucicchio C, Storti C, Riva S, Longobardi M. Catheter ablation and antiarrhythmic drugs for haemodynamically tolerated post-infarction ventricular tachycardia; long-term outcome in relation to acute electrophysiological findings. Eur Heart J 2002;23(5):414-24.

65. Della Bella P, Riva S, Fassini G, Giraldi F, Berti M, Klersy C, Trevisi N. Incidence and significance of pleomorphism in patients with postmyocardial infarction ventricular tachycardia. Acute and long-term outcome of radiofrequency catheter ablation. Eur Heart J 2004;25(13):1127-38.

66. Arya A, Bode K, Piorkowski C, Bollmann A, Sommer P, Gaspar T, Wetzel U, Husser D, Kottkamp H, Hindricks G. Catheter ablation of electrical storm due to monomorphic ventricular tachycardia in patients with nonischemic cardiomyopathy: acute results

and its effect on long-term survival. Pacing Clin Electrophysiol 2010;33(12):1504-9.

67. Vergara P, Trevisi N, Ricco A, Petracca F, Baratto F, Cireddu M, Bisceglia C, Maccabelli G, Della BP. Late Potentials Abolition as an Additional Technique for Reduction of Arrhythmia Recurrence in Scar Related Ventricular Tachycardia Ablation. J Cardiovasc Electrophysiol 2012.
68. Reimer KA, Lowe JE, Rasmussen MM, Jennings RB. The wavefront phenomenon of ischemic cell death. 1. Myocardial infarct size vs duration of coronary occlusion in dogs. Circulation 1977;56(5):786-94.
69. Wijnmaalen AP, Schalij MJ, von der Thusen JH, Klautz RJ, Zeppenfeld K. Early reperfusion during acute myocardial infarction affects ventricular tachycardia characteristics and the chronic electroanatomic and histological substrate. Circulation 2010; 121(17):1887-95.
70. Zaim S, Zaim B, Rottman J, Mendoza I, Nasir N, Jr., Pacifico A. Characterization of spontaneous recurrent ventricular arrhythmias detected by electrogram-storing defibrillators in sudden cardiac death survivors with no inducible ventricular arrhythmias at baseline electrophysiologic testing. Am Heart J 1996;132(2 Pt 1):274-9.
71. Daubert JP, Zareba W, Hall WJ, Schuger C, Corsello A, Leon AR, Andrews ML, McNitt S, Huang DT, Moss AJ. Predictive value of ventricular arrhythmia inducibility for subsequent ventricular tachycardia or ventricular fibrillation in Multicenter Automatic Defibrillator Implantation Trial (MADIT) II patients. J Am Coll Cardiol 2006; 47(1):98-107.
72. Gao P, Yee R, Gula L et al. Prediction of arrhythmic events in ischemic and dilated cardiomyopathy patients referred for implantable cardiac defibrillator: evaluation of multiple scar quantification measures for late gadolinium enhancement magnetic resonance imaging. Circ Cardiovasc Imaging 2012;5(4):448-56.
73. Assomull RG, Prasad SK, Lyne J, Smith G, Burman ED, Khan M, Sheppard MN, Poole-Wilson PA, Pennell DJ. Cardiovascular magnetic resonance, fibrosis, and prognosis in dilated cardiomyopathy. J Am Coll Cardiol 2006;48(10):1977-85.
74. de Haan S, Meijers TA, Knaapen P, Beek AM, van Rossum AC, Allaart CP. Scar size and characteristics assessed by CMR predict ventricular arrhythmias in ischaemic cardiomyopathy: comparison of previously validated models. Heart 2011;97(23): 1951-6.
75. Gulati A, Jabbour A, Ismail TF et al. Association of fibrosis with mortality and sudden cardiac death in patients with nonischemic dilated cardiomyopathy. JAMA 2013;309(9): 896-908.
76. Iles L, Pfluger H, Lefkovits L, Butler MJ, Kistler PM, Kaye DM, Taylor AJ. Myocardial fibrosis predicts appropriate device therapy in patients with implantable cardioverter-defibrillators for primary prevention of sudden cardiac death. J Am Coll Cardiol 2011;57(7):821-8.
77. Lehrke S, Lossnitzer D, Schob M et al. Use of cardiovascular magnetic resonance for risk stratification in chronic heart failure: prognostic value of late gadolinium enhancement in patients with non-ischaemic dilated cardiomyopathy. Heart 2011;97(9): 727-32.
78. Schmidt A, Azevedo CF, Cheng A et al. Infarct tissue heterogeneity by magnetic resonance imaging identifies enhanced cardiac arrhythmia susceptibility in patients with left ventricular dysfunction. Circulation 2007;115(15):2006-14.
79. Nazarian S, Bluemke DA, Lardo AC et al. Magnetic resonance assessment of the substrate for inducible ventricular

tachycardia in nonischemic cardiomyopathy. Circulation 2005;112(18):2821-5.

80. Higham PD, Adams PC, Murray A, Campbell RW. Plasma potassium, serum magnesium and ventricular fibrillation: a prospective study. Q J Med 1993;86(9):609-17.
81. Akar FG, Rosenbaum DS. Transmural electrophysiological heterogeneities underlying arrhythmogenesis in heart failure. Circ Res 2003;93(7):638-45.
82. Kawara T, Derksen R, de Groot JR, Coronel R, Tasseron S, Linnenbank AC, Hauer RN, Kirkels H, Janse MJ, de Bakker JM. Activation delay after premature stimulation in chronically diseased human myocardium relates to the architecture of interstitial fibrosis. Circulation 2001;104(25):3069-75.
83. Saumarez RC, Chojnowska L, Derksen R, Pytkowski M, Sterlinski M, Huang CL, Sadoul N, Hauer RN, Ruzyllo W, Grace AA. Sudden death in noncoronary heart disease is associated with delayed paced ventricular activation. Circulation 2003; 107(20):2595-600.
84. Derksen R, van Rijen HV, Wilders R, Tasseron S, Hauer RN, Rutten WL, de Bakker JM. Tissue discontinuities affect conduction velocity restitution: a mechanism by which structural barriers may promote wave break. Circulation 2003;108(7):882-8.
85. Stein M, van Veen TA, Hauer RN, de Bakker JM, van Rijen HV. A 50% reduction of excitability but not of intercellular coupling affects conduction velocity restitution and activation delay in the mouse heart. PLoS One 2011;6(6):e20310.
86. Glukhov AV, Fedorov VV, Kalish PW, Ravikumar VK, Lou Q, Janks D, Schuessler RB, Moazami N, Efimov IR. Conduction remodeling in human end-stage nonischemic left ventricular cardiomyopathy. Circulation 2012;125(15):1835-47.

Part I

Imaging-guided VT ablation

Chapter 2

Imaging-guided Ventricular Tachycardia Ablation

Sebastiaan R.D. Piers, MD, Katja Zeppenfeld, MD, PhD

Arrhythmia & Electrophysiology Review 2013;2(2):128-34

ABSTRACT

Over the past decades important advances have been made in the field of ventricular tachycardia (VT) ablation and as a result, VT ablation is now more widely being performed. The identification of ablation target sites still relies on electroanatomical substrate mapping, which is time-consuming, hampered by the intramural location of some scars and limited by epicardial fat. The potential of various imaging modalities to overcome these limitations have stimulated clinical electrophysiologists to perform studies on image integration during VT ablation. Imaging guidance has been used to identify, delineate and characterize the substrate for VT, to provide detailed anatomical information, to avoid ablation on coronary arteries, to delineate epicardial fat tissue and to assess ablation lesions. In this review reported applications and the potential advantages and limitations of different imaging modalities are discussed.

INTRODUCTION

Over the last 20 years ventricular tachycardia (VT) ablation has evolved from a treatment modality for selected patients with recurrent hemodynamically tolerated VT (which can be mapped during ongoing arrhythmia), to a therapeutic option for patients with tolerated and untolerated VT using substrate-based ablation strategies.[1] The substrate for VT after myocardial infarction (MI) consists of areas of myocardial fibrosis interspersed with viable myocytes creating slow conduction through the scar.[2] The latter is an important precondition for re-entry, the most common underlying mechanism of scar-related VT. Inhomogeneous scars also occur in other diseases such as nonischemic cardiomyopathy (NICM), sarcoidosis and repaired congenital heart disease.[3-5] Substrate-based VT ablation procedures currently depend on extensive electroanatomical mapping (EAM) to delineate bipolar[1,6] and unipolar[7,8] low voltage areas and to identify abnormal electrograms such as fragmented electrograms and late potentials.[4,9-11] The limitations of EAM (time-consuming, inaccurate delineation of intramural scars, attenuation of electrograms by epicardial fat) on the one hand, and the availability of different imaging modalities (providing detailed anatomical information[12-15], characterizing myocardial scars[12,16-22], delineating epicardial fat[15,23]) as well as the progress in imaging acquisition and processing on the other hand, have stimulated clinical electrophysiologists to study image integration during VT ablation procedures. Various imaging modalities such as multidetector computed tomography (MDCT), contrast-enhanced magnetic resonance imaging (CE-MRI), intracardiac echocardiography (ICE) and nuclear imaging modalities have been applied, however, most available data are derived from MDCT and CE-MRI studies conducted in the post-MI patients; MDCT because of the higher spatial resolution if compared to CE-MRI and nuclear imaging modalities, and CE-MRI as current gold standard to visualize fibrosis. Image integration has been used to identify and delineate the substrate for VT during the procedure[12,16-22], to avoid ablation in the vicinity of coronary arteries[15,23], to delineate epicardial fat tissue[15,21] and to assess ablation lesions.[24,25] In this review reported applications and the potential advantages and limitations of the different imaging modalities are discussed.

Image registration

An important prerequisite for the use of image integration to guide mapping and ablation is the accurate registration of EAM and imaging data. Of note, image registration has mainly been performed during stable sinus or paced rhythm, and may be less reliable during VT activation mapping due to potential differences in cardiac morphology. An overview of studies on integration of imaging data with ventricular EAM and the reported registration accuracy is provided in Table 1. It is important to realize that a small registration error (the distance from an imaging surface to the EAM surface) does

Table 1. Registration methods and accuracy.

Imaging modality	Author	Publication year	Registration error (mm)	Registration method	Landmarks (if applicable)	Registration mode
MRI	Codreanu et al.	2008	N/R	LM	Aorta, LV apex, MA	offline
	Desjardins et al.	2009	4.3	LM + SURF	Aorta, LV apex, MA	offline
	Bogun et al.	2009	4.8	LM + SURF	Aorta, LV apex, MA	online
	Ilg et al.	2010	3.5	LM + SURF	Not reported	online
	Andreu et al.	2011	3.4	LM + SURF	Aorta, LV apex, MA, RV	online
	Wijnmaalen et al.	2011	3.8	LM + SURF	Left main	online
	Dickfeld et al.	2011	3.9	VA	N/A	online
	Perez-David et al.	2011	N/R	LM	LV apex and MA	offline
	Tao et al.	2012	4.3	SURF	N/A	offline
	Gupta et al.	2012	3.8	LM + SURF	Aorta, LV apex, MA	online
	Piers et al.	2012	3.2	LM + VA	Left main	online
	Spears et al.	2012	3.6	LM + SURF	Aorta, LV apex, MA or His	offline
	Sasaki et al.	2012	2.8	LM + SURF	Aorta, LV apex, MA, RV septal insertions	offline
	Cochet et al.*	2013	N/R	LM + SURF	Aorta, CS, left atrium, MA	online
MDCT	Desjardins et al.	2010	3.0	LM + SURF	Epicardial apex, most lateral tricuspid and MA	offline
	Tian et al.	2010	3.3	VA + SURF	N/A	online
	v Huls v Taxis et al.	2013	2.8	LM + SURF	Left main	online
	Piers et al.	2012	2.0	LM + SURF	Left main	online
	Komatsu et al.	2013	N/R	LM + SURF	CS, aortic root, LV apex and MA	online
PET/CT	Fahmy et al.	2008	5.1	LM + SURF	Coronary ostia, cusps, apex	online**
	Dickfeld et al.	2008	3.7	VA	N/A	online
	Tian et al.	2009	4.3	VA + SURF	N/A	online
SPECT	Tian et al.	2012	4.4	LM + SURF	MA	offline

* Combined MDCT and MRI. ** 16/19 patients. CS indicates coronary sinus; LM, landmark; LV, left ventricular; MA, MA; N/A, not applicable; N/R, not reported; RV, right ventricle; SURF, surface registration; VA, visual alignment

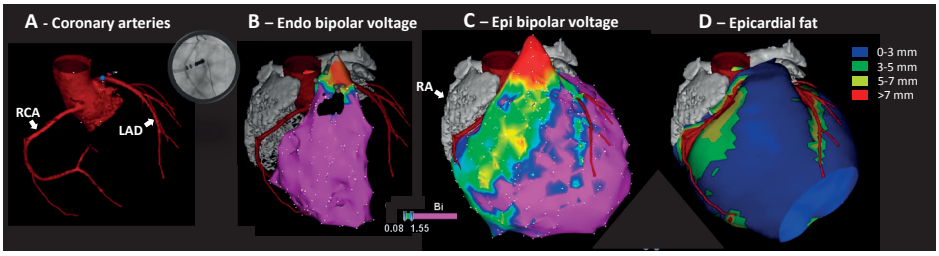


Figure 1. Integration of MRI-derived scar and MDCT-derived coronary artery anatomy and epicardial fat with electroanatomical maps in a patient with a scar in the epicardial RVOT.

The coronary artery anatomy is derived from the MDCT scan using special software (Medis medical imaging systems BV, Leiden, the Netherlands), allowing visualization of small branches (panel A). During the procedure the position of the left main coronary artery (confirmed by contrast injection, circle in panel A), was tagged on the map to integrate the MDCT-derived coronary artery anatomy and MRI-derived scar (displayed in black) with the endocardial EAM (panel B). Subsequent epicardial EAM revealed low voltage areas around the atrioventricular groove, interventricular groove and acute margin which are consistent with MDCT-derived epicardial fat (panels C and D), but also a low voltage area at the epicardial right ventricular outflow tract corresponding with the location of the MRI-derived scar. Fragmented electrograms were observed in this area, supporting the presence of scar. LAD indicates left anterior descending coronary artery; RA, right atrium; RCA, right coronary artery.

not necessarily imply good registration accuracy. Automated surface registration tools which are provided by commercially available 3D mapping systems[13,15,22,25-30] typically minimize this distance by translation movements and circumferential and axial rotation. These registration algorithms may result in significant rotation errors in particular if only the symmetrically shaped LV is mapped and low resolution imaging modalities are used.[31] Indeed, the registration accuracy of MRI images with left ventricular (LV) EAM has been evaluated using different registration models and it could be demonstrated that the best correlation between bipolar voltage and scar transmurality could be achieved by avoiding any circumferential or axial rotation during the registration process.[32] Mapping of well-defined anatomical structures such as the ostium of the left main artery or additional chambers can improve the registration accuracy. In a phantom model incorporation of EAM of the aorta in the registration process resulted in substantial improvement, as assessed visually and by the EAM-to-MRI surface distance of both LV and aorta.[31] Several clinical studies have used the aorta and the ostia of the coronary arteries, which correct position can be confirmed by contrast injection if an open irrigated-tip catheter is used (Figure 1, panel A),[15,21,22] or a coronary sinus catheter[12,13] to improve registration accuracy or to monitor the registration stability throughout the procedure.

Lessons learned from Integration of pre-acquired MRI images

The feasibility of MRI integration during EAM of the LV was first demonstrated by Reddy et al. in phantom and animal models in 2004.[31] To evaluate the registration accuracy iron

oxide injections were performed in 5 pigs before MRI acquisition. Their position was marked on the integrated MRI image and subsequently targeted for radiofrequency (RF) catheter ablation. At gross pathology the ablation lesions were localized close (mean distance 1.8±0.5 mm) to the iron oxide targets, suggesting that MRI integration may allow imaging-guided ablation of MRI-derived target sites.

In humans off-line comparison of EAM data and CE-MRI-derived scar data could demonstrate a good overall correlation between the MRI-reconstructed post-MI scar surface and low bipolar voltage areas. However, CE-MRI allowed even improved identification of scar areas not sufficiently delineated by EAM, thereby paving the way for true MRI guidance during the VT ablation procedure.[18,33] The first study on real-time integration of MRI-derived scar distribution during VT ablation could demonstrate that the integrated scar information facilitated substrate mapping and could be used as a guide to VT isthmus sites in 15 post-MI patients.[22] These findings were confirmed in a second series of 13 patients with frequent PVCs and 10 patients with VT after MI.[28] Of importance, although scars due to MI are predominantly localized subendocardially, in particular non-transmural parts of the scar remain undetected by bipolar voltage mapping (example in Figure 2).[22] These parts of the scar may however contain critical parts of the VT re-entry circuits, and can be visualized during real-time integration of the CE-MRI-derived scar information supporting the important complementary information provided by MRI.[22]

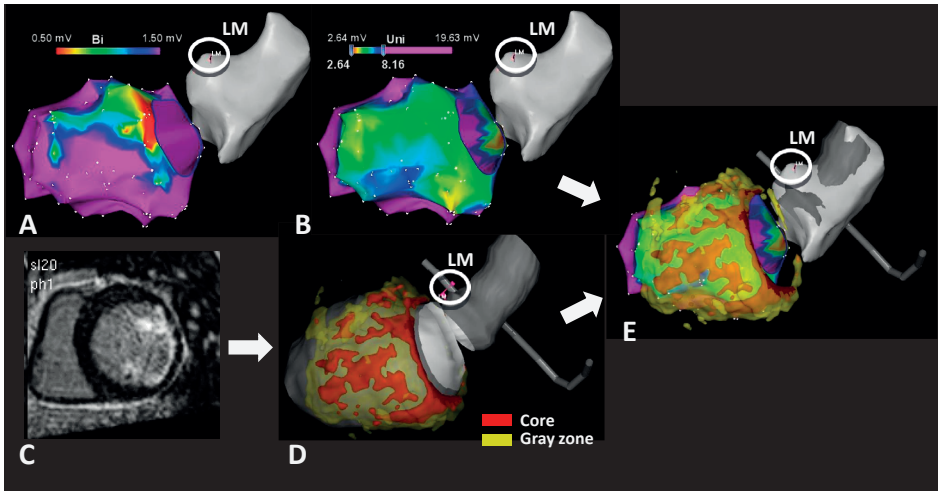


Figure 2. MRI-derived 3D scar reconstruction integrated with EAM

The endocardial bipolar voltage map (panel A) shows only a limited low voltage area, smaller than the MRI-based non-transmural scar (panels C and D). The unipolar voltage map (panel B) reveals a larger low voltage area which is more consistent with the true size of the scar area. The MRI-derived scar is integrated with the electroanatomical maps based on the left main (LM) landmark (panel E).

The limitation of electroanatomical voltage mapping to fully delineate the 3D geometry of scar has also been reported in patients with NICM, in whom scars are typically localized intramurally or subepicardially.[17,21,34] Intraprocedural registration of MRI-derived scars in patients with NICM has demonstrated that critical components of ventricular arrhythmias are confined to scar tissue,[17] and it has been reported that MRI integration in patients presenting with VT can reveal scars not identified by EAM, which may have important diagnostic and therapeutic consequences.[25] In a small series of NICM patients the distribution of contrast enhancement, which was classified as endocardial, intramural or epicardial, corresponded with the location (endocardium or epicardium) containing critical components of the VT circuit. This finding suggests an important role for MRI in choosing the appropriate procedural strategy which can be either endocardial, epicardial or both.[17] Notably, half of the patients had predominantly endocardial scar in this study,[17] which is reported to be less common in patients with NICM.[35] Further studies are required before MRI-derived scar distribution can be used to guide preprocedural planning.

Not only the presence of enhanced regions, but also MRI-derived scar characteristics have been correlated with VT-related sites and local electrophysiological findings in patients with prior MI and NICM. Isolated potentials and critical sites of re-entrant VT (based on pace and entrainment mapping) were associated with high infarct scar transmurality.[30] In another study, also conducted in post-MI patients, 71% of VT isthmus sites were localized within the infarct core (defined as signal intensity [SI] >3 standard deviations above remote myocardium), while the remaining isthmus sites were localized in transmural border zone with SI slightly lower than this cutoff.[33] Electrogram characteristics consistent with slow conduction such as prolonged duration, late potentials and fractionated electrograms were also related to higher scar transmurality in patients with NICM.[21] The association between MRI-derived scar characteristics and EAM-based electrophysiological parameters has recently been used to create non-invasive 3D substrate maps in post-MI patients. These MRI-derived substrate maps showed a remarkably high resemblance to the endocardial electroanatomical substrate maps.[30]

Similar to the method that adapts bipolar voltage thresholds of EAM to display channels of relatively higher voltages within low voltage regions,[36] some investigators have attempted to identify relatively low SI channels within higher SI post-MI scars on MRI.[16,20,37] Using variable SI and voltage thresholds a good correlation regarding the location (segments) and orientation (perpendicular or parallel to the mitral annulus) of relatively low SI channels and relatively high voltage channels has been reported.[20] In a recent paper a favorable association between lower SI channels within high SI regions based on "pixel SI scanning" (i.e. modifying the thresholds to 60±5% and 40±5%[37]) and channels of slow conduction identified by high density endocardial activation mapping during sinus rhythm has been reported (example in Figure 3). Of importance, 17 of these

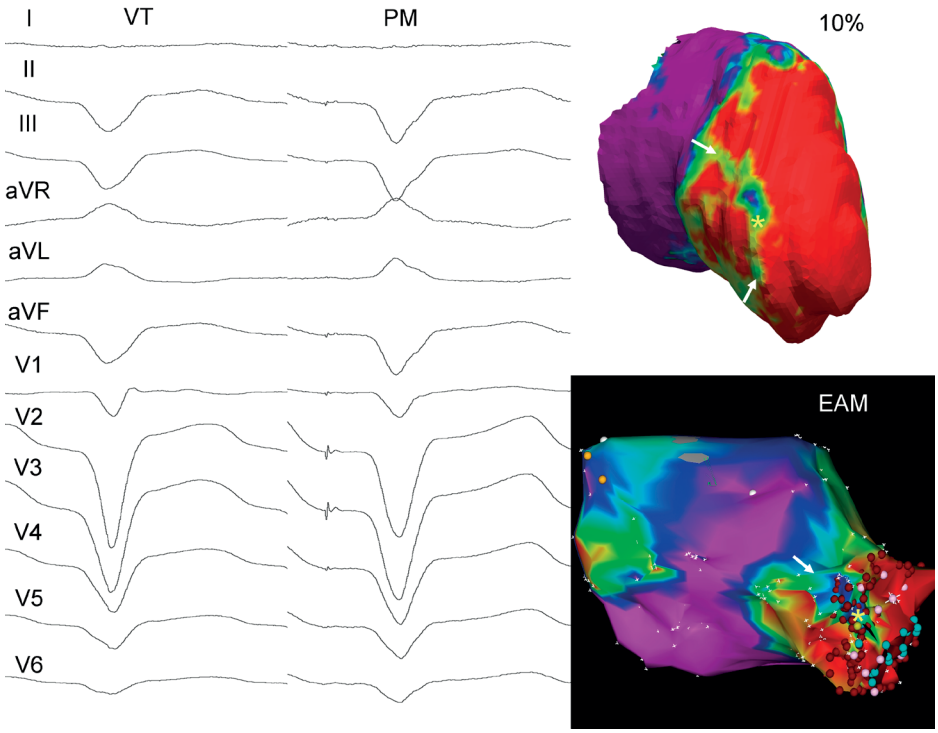


Figure 3. MRI-based border zone channel identification
Subendocardial (10%) pixel signal intensity map and endocardial bipolar voltage map, with an extensive area of scar in the anterior wall. A border zone channel is shown in the 10% shell, consistent with the conduction channel identified on the voltage map (white arrows). The 12-lead electrocardiogram on the left shows the induced monomorphic ventricular tachycardia. Electrocardiogram on the right shows pace map from the middle of the conduction channel (yellow asterisk in both maps). Pacing from the channel reproduces the induced VT morphology with a long stimulus-to-QRS delay, as expected by the location of the stimulus delivery on the channel. Additionally, there is a late potential channel in the EAM (blue dots) not visible on the cardiac magnetic resonance. EAM indicates electroanatomic map; PM, pace mapping; VT, ventricular tachycardia. Derived from Fernández-Armenta J et al. Circ Arrhythm Electrophysiol 2013;6:528-537.

45 identified SI channels were related to VT based on pace mapping and entrainment mapping, and on localization within the same AHA segment with the same orientation (parallel or perpendicular to the mitral annulus or intermediate).[37] The validation of 3D lower SI channels within high density scars is limited by the lack of a gold standard, which would be histological 3D scar reconstruction. Application of different scar identification methods and cut-off values impede the comparison of reported data. Considering the known limited field of view of bipolar mapping,[38] simply correlating the 3D CE-MRI-derived SI channels with 2D bipolar voltage channels or with progressively delayed low voltage electrogram channels cannot overcome these limitations.[7] In addition, advanced imaging techniques providing relatively high spatial resolution CE-MRI

(1.4 x 1.4 x 1.4 mm in a recent paper[37]) are still unlikely to delineate channels at a microscopic level[2], which produce very low amplitude late potentials during sinus rhythm[4] and diastolic potentials during VT.[39] Despite all current limitations the integration of high resolution CE-MRI-derived 3D scar characteristics with EAM is exciting. Additional studies are however required to determine the intraobserver and interobserver variability of the channel identification process, both on MRI images and on EAM (including different applied scar detection methods and cut-off values for SI). Ideally, the identified channels should be compared to histology, and the clinical relevance of the channels needs to be determined by assessing the impact of ablation of CE-MRI-derived channels on procedural outcome.

Compared to other imaging modalities, the advantages of MRI integration include a higher resolution for detection and localization of non-transmural scar areas, and the possibility of tissue characterization (T1-weighted sequences after gadolinium administration to assess for extracellular matrix, T2-weighted sequences to assess for myocardial edema). However, currently MRI integration requires extensive and time-consuming (± 1 hour) image pre-processing by specialists experienced in CE-MRI, which restrict its wide applicability. The most important limitation of MRI is its use in device recipients, as the majority of patients undergoing VT ablation have an implantable cardioverter defibrillator (ICD). Although ICDs may not necessarily preclude MRI if appropriate safety measures are taken, detailed evaluation of important parts of the LV (in particular the anterior segments) is hampered by artifacts due to the pulse generator.[19,30] However, also based on the results of 2 recently published randomized controlled trials conducted in post-MI patients,[40,41] early VT ablation may be considered in an increasing number of patients before ICD implantation, suggesting that CE-MRI integration may play an increasing role in the future.

CE-MRI as a gold standard

Although considered a gold standard, the technique of CE-MRI to delineate 3D scar geometry still has limitations. First, contrast enhancement is not specific for fibrosis; T2-weighted sequences should therefore also be performed to assess for myocardial oedema.[42] Second, the delineation of scars and in particular border zones is hampered by the partial volume effect (i.e. the averaging that occurs between high and low SI regions) which may cause overestimation of the scar size.[43] Third, current scar identification methods vary between studies (e.g. full-width half-maximum method, standard deviation of remote region based methods) and although scar characteristics predict ventricular tachyarrhythmias in patients after MI independent of the scar identification method used, the size of the border zone varies by a factor five depending on the method.[44] Finally, the present scar identification methods are based on the SI of scar and/or remote myocardium in a look-locker sequence, which depend on the amount

of diffuse fibrosis in remote myocardium, and on the maximum density of fibrosis in the scar area, the heart rate, contrast dose, glomerular filtration rate, hematocrit, and other variables;[45] scars are therefore not directly comparable between patients. Novel techniques are required to allow more accurate and objective characterization of scars. A general disadvantage of integrating pre-acquired imaging data during VT ablation is the potential change that may occur between scan and procedure (e.g. volume, orientation of the heart) – a logical next step would therefore be on-site MRI.

On-site MRI guidance

On-site MRI may provide an all-in-one solution during VT ablation, allowing catheter tracking without fluoroscopy, anatomical guidance, substrate delineation (including intramural and subepicardial scars), MRI-based identification of ablation target sites, and evaluation of ablation lesions. In 2008 the feasibility of real-time MRI-based catheter tracking to perform an electrophysiology study was first demonstrated in 10 mongrel dogs and 2 humans.[46] In another study in pigs, a real-time MRI-tracked mapping catheter could be visualized on pre-acquired magnetic resonance angiography (MRA) and CE-MRI images. Real-time MRI based tracking could be used to construct an EAM of the LV, which matched well with the pathological specimen.[47] Although in both studies RF filters were applied to remove MRI-induced artifacts, significant artifacts remained interfering with both the surface electrocardiogram (ECG) and the intracardiac electrograms, which is an important current limitation. Although the use of CE-MRI has been reported to allow evaluation of ablation lesions hours to months after RF energy application,[24,29] no study has analyzed the value of MRI to characterize and assess acute lesion formation during VT ablation yet. The required continuous gadolinium contrast infusion is only one of the problems that need to be solved. However, despite these hurdles, direct evaluation of lesion formation would be desirable to assess completeness of linear lesion but also to monitor substrate-based ablation targeting intramural scar, or scar covered by epicardial fat.

Integration of pre-acquired MDCT images

The high resolution of current MDCT images allows the detailed anatomic reconstruction of the heart, including the cardiac chambers, aortic sinus cusps, coronary vessels, epicardial fat thickness and the atrial appendages.[15] The feasibility of MDCT-guided catheter manipulation was first reported in a porcine model in 2003,[48] and the accuracy of MDCT-guided RF applications was demonstrated in 9 mongrel dogs with a 2.1±1.1 mm position accuracy of RF lesions with respect to the targeted MDCT markers.[26] In humans, integration of the anatomic reconstruction of the coronary artery anatomy has been used to avoid RF energy applications at, or in close proximity to coronary arteries, thereby potentially preventing complications of epicardial ablation (example

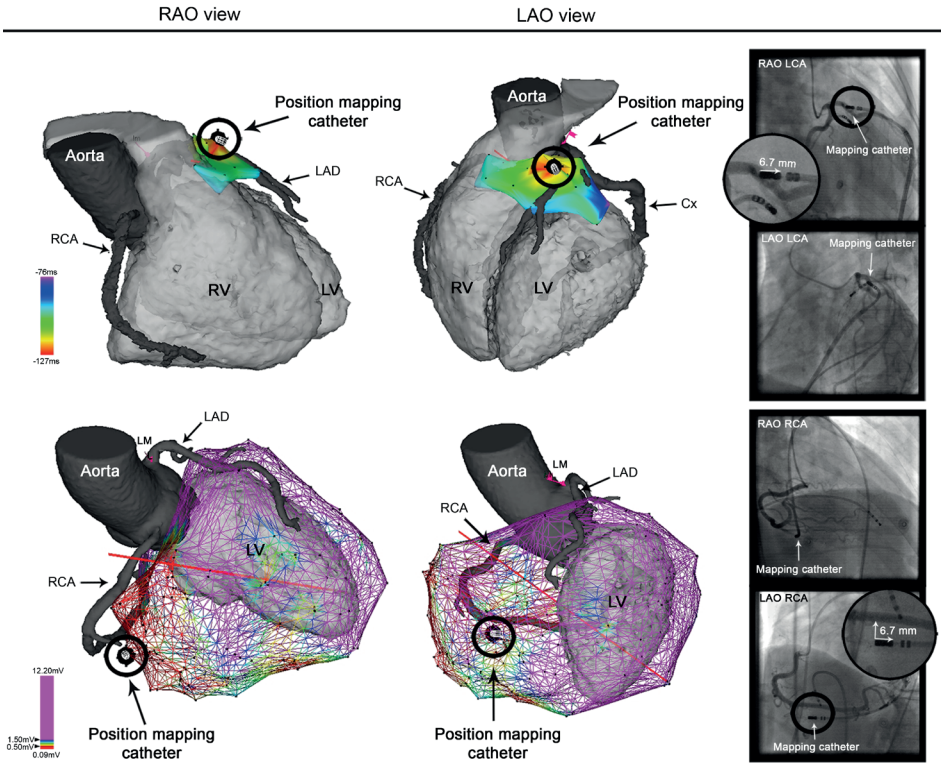


Figure 4. Integration of MDCT-derived images to assess the proximity of coronary arteries at ablation target sites

The distance between the catheter tip and coronary arteries on integrated MDCT images and coronary angiography is shown in a right anterior oblique (RAO) view (left) and left anterior oblique (LAO) view (right) in 2 patients. In one, limited activation mapping identified a target site located on the left coronary artery (LCA) on both MDCT and angiography (upper panels). In another, the target site (based on pace mapping) was located < 7 mm from the right coronary artery (RCA) confirmed by angiography (lower panels). LM indicates left main; LV, left ventricle; PA, pulmonary artery; RV, right ventricle. Reproduced from reference 15 with permission.

in Figure 4). The registration accuracy was confirmed by coronary angiograms in various angulations in a case report[23] and in a study in 28 patients.[15] The high accuracy which can be evaluated by a single coronary injection is important as coronary angiography in some (in particular caudal) angulations can be precluded by the location pad of the EAM system, hampering accurate estimation of the distance to coronary arteries by angiography. The integration of MDCT images can also facilitate catheter ablation in patients with complex anatomy due to congenital heart disease.[49]

Apart from the coronary arteries an important limitation for epicardial mapping and ablation is the presence of epicardial fat.[15,50,51] Epicardial fat can be delineated by MDCT with high spatial resolution and has been shown to cover significant parts of the

ventricles, with on average 25% of surface being covered with > 4mm fat in patients undergoing epicardial PVC or VT ablation.[15] In particular the acute margin, anterior right ventricular (RV) free wall, interventricular groove and atrioventricular groove may be covered by significant fat layers (example in Figure 1).[15,52] Importantly, not only scar but also epicardial fat attenuates bipolar electrogram amplitudes, thereby limiting the accuracy of epicardial substrate mapping.[15,21,51] In addition, epicardial RF energy applications may be ineffective in the presence of >7 mm fat.[15,51] The integration of MDCT-derived fat thickness can therefore be very helpful to classify low voltage areas (due to fat or true scar in the absence of fat, Figure 1) and to predict and explain ineffective RF energy applications during epicardial VT ablation.

In patients with epicardial idiopathic ventricular arrhythmias the approximate site of origin can often be estimated based on electroanatomical activation mapping of the endocardial RV, LV, aortic cusps and coronary sinus, if appropriate. The integration of MDCT images with EAM data may predict epicardial ablation failure in selected patients, which can be due to the close proximity of coronary arteries and/or a thick epicardial fat layer at the predicted epicardial site of origin (example in Figure 5), thereby potentially preventing unnecessary pericardial puncture and its associated risks.[15]

Detailed contrast-enhanced MDCT scans can provide important anatomic (wall thickness, example in Figure 6), dynamic (wall thickening) and perfusion (hypoenhancement) information, which may guide to MI areas during VT ablation.[14] However, in a small series of 13 post-MI patients, 87% of abnormal electrograms, but only 46% of termination sites

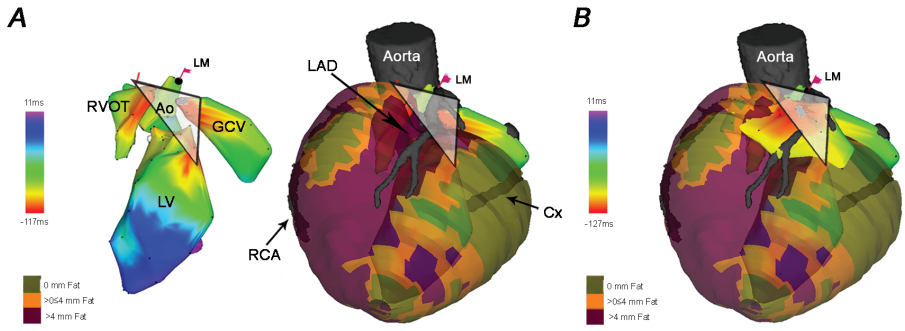


Figure 5. Prediction of an epicardial target site and the proximity of coronary arteries and epicardial fat

Endocardial electroanatomical activation maps of the LV, right ventricle outflow tract (RVOT), aorta (Ao), and great cardiac vein (GCV) (panel A). Similar activation time of the LV, RVOT, and GCV was observed. The white triangle demonstrates the predicted epicardial target area in the vicinity of the LAD, covered by >4 mm of fat. The final fusion image was registered with the endocardial maps, using the left main coronary artery (LM) landmark. Limited epicardial activation mapping confirmed the earliest activation within the predicted area not suitable for ablation (panel B). Reproduced from reference 15 with permission.

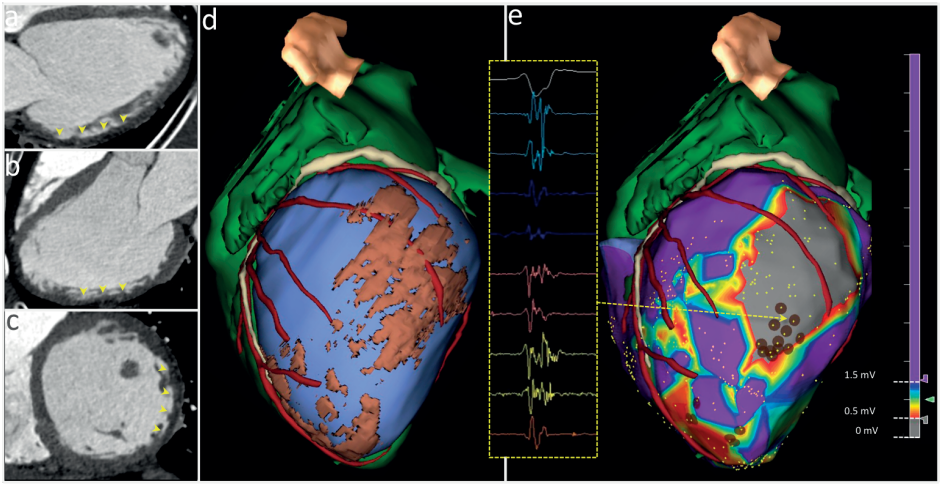


Figure 6. MDCT-derived wall thinning areas and the electroanatomical substrate in a patient with nonischemic dilated cardiomyopathy.

Correlation between voltage and wall thinning at MDCT in a patient with nonischemic dilated cardiomyopathy. Myocardial wall thinning is seen in the lateral wall of the left ventricle on 4 chambers (panel A), 3 chambers (panel B), and short axis (panel C) reconstructions of the contrast-enhanced MDCT volume. No delayed enhancement was seen at MRI. Areas of wall thickness <5mm are mapped on the epicardial surface and integrated in the NavX system (panel D). The epicardial voltage map is registered to the imaging model, demonstrating a match between wall thinning and low voltage (panel E). Brown dots indicate sites of local abnormal ventricular activities targeted by ablation. A high-frequency fragmented signal occurring during the far field ventricular electrogram is seen (yellow frame), indicating the presence of persisting local electrical activity within scar. Please note that these high-frequency signals are fractionated but not late as they are recorded within the QRS. Reproduced from reference 12 with permission.

were localized within 5mm of MDCT-derived wall thinning areas, perhaps suggesting a limited value of MDCT-derived wall thinning for identification of the VT substrate.[13] Data on the use of MDCT for detection of the arrhythmogenic substrate in patients with NICM are remarkably sparse, with only 3 patients being included in one study.[12]

Compared to other imaging modalities the main advantage of MDCT integration during VT ablation is its superior spatial resolution. Furthermore, MDCT can be performed without precautions in patients with implantable devices, and with only minor lead artifacts. Pre-processing of MDCT images is relatively easy when segmentation is performed on the CARTO system (± 15-30 minutes), but may be time-consuming if advanced coronary artery and epicardial fat images are required (± 2 hours). As a main limitation, contrast-enhanced MDCT is associated with significant radiation exposure (currently ±2 to 12 mSv depending on acquisitions[14,53]).

Intracardiac echocardiography

Intracardiac echocardiography (ICE) provides real-time anatomical information and allows monitoring of catheter-tissue contact, lesion formation and potential complications without radiation exposure.[54-58] The anatomical information provided by ICE has been shown to be useful to guide catheter ablation of the papillary muscles,[54,55] or to avoid RF delivery near the coronary artery ostia and on the aortic leaflets, as has been demonstrated in one series of 5 patients.[58] An experimental study in 7 pigs after left anterior descending infarction demonstrated a close correlation between ICE-derived infarct size and low voltage (≤ 2 mV) areas.[59] Akinetic and thinned areas on ICE corresponded with the electroanatomic scar during VT ablation in one study in 18 humans (15/18 post-MI).[54] In a series of 18 patients with NICM and abnormal echogenicity on ICE imaging it could be demonstrated that the areas of increased echogenicity in the lateral wall corresponded with the endocardial and/or epicardial electroanatomical substrate.[56] In these studies ICE images were visually interpreted, and data on interobserver and intraobserver variability are not available. Whether ICE-derived reconstruction of scar areas in post-MI patients and patients with NICM provides complementary substrate information to EAM data requires further investigation. Important limitations of ICE include the two-dimensional nature of ICE images, the considerable costs and the time required to acquire and interpret ICE images.

Nuclear image guidance

Nuclear imaging has the advantage of not being limited by the presence of implantable devices. Three studies have analyzed the value of hybrid positron emission tomography (PET)/CT imaging, combining low-resolution metabolic activity information from PET scans with high-resolution anatomic information from MDCT scans.[27,60,61] Although areas with low metabolic activity corresponded well with low voltage areas, the net benefit of PET integration during VT ablation may be limited due to the inferior resolution of PET (currently 4-7 mm[62]), significant radiation exposure, high costs, and the time required to create mapping system-compatible images from the PET data.[63] Notably, the value of PET for identification of intramural and subepicardial scars, which are common in NICM, remains unclear as only 2 of the 41 patients in these studies had NICM.[27,60,61] PET scanning is limited by the high costs of cyclotrons, which are required to produce radionuclides. Single-photon emission computed tomography (SPECT) images are more widely available but have an even lower resolution (±12 mm[64]). SPECT-derived scar images were integrated with EAM in a small series of 10 patients, demonstrating that all successful ablation sites were located within 1 cm of the SPECT-derived scar area.[64] Similar to PET, the added value of SPECT integration to EAM during VT ablation may be limited due to its poor resolution.

Bimodality or multimodality image integration

Different imaging modalities can provide complementary information, which may be important during complex ablation procedures as has been illustrated in several case reports.[49,65] In a study conducted in 10 patients with NICM, MDCT-derived fat images and MRI-derived scar images were integrated with the epicardial EAM during VT ablation and provided important insights in the complex interplay between scar, viable myocardium and epicardial fat. It could be demonstrated that in the presence of > 2.8 mm fat neither bipolar nor unipolar voltage mapping can distinguish scar from fat. Specific electrogram morphologies were not affected by fat, but identified only 25% of all scar sites.[21] In a second series, MDCT and MRI-derived images were fused and integrated during VT ablation procedures in 9 patients with various underlying diseases to provide detailed anatomical information (e.g., coronary artery anatomy during epicardial VT ablation) and to guide to the arrhythmogenic substrate (using MRI-derived scar areas and MDCT-derived wall thinning areas).[12] These data illustrate the potential clinical applications of advanced bimodality image integration.[12,21]

Future perspectives

Currently integration of MDCT, MRI and nuclear images requires pre-processing of imaging data, which is time-consuming (typically 1-2 hours based on one study[12] and our own experience[15,21,22]) and requires experienced observers and special software. Development of advanced software to allow more efficient or even automated analysis of imaging data would therefore be of interest, and would also make advanced image integration techniques available to electrophysiologists who do not have supporting imaging specialists.

Integration of MRI-derived images has been shown to accurately delineate ventricular scar without time-consuming EAM. Real-time image integration would be even more valuable if more specific scar features that are related to VT could be identified and displayed. In the future, MRI-based identification of critical re-entry circuit sites may then allow MRI-guided delivery of RF energy applications and thereby true imaging-guided VT ablation, which has already been demonstrated feasible and accurate in an animal model.[31]

Although image integration has provided important insights into the substrate for VT, to date it has not been demonstrated that the integration of MDCT, MRI or nuclear imaging data is cost-effective, improves preprocedural planning, total radiation exposure (including both imaging-related radiation and intraprocedural fluoroscopy), EAM time and, most importantly, the outcome of VT ablation. Prospective randomized studies comparing imaging-guided VT ablation to standard VT ablation in the setting of different diseases are required to determine whether the promising technology translates into improved acute and long-term outcome.

REFERENCE LIST

1. Marchlinski FE, Callans DJ, Gottlieb CD, Zado E. Linear ablation lesions for control of unmappable ventricular tachycardia in patients with ischemic and nonischemic cardiomyopathy. Circulation 2000;101(11): 1288-96.
2. de Bakker JM, van Capelle FJ, Janse MJ, Tasseron S, Vermeulen JT, de JN, Lahpor JR. Slow conduction in the infarcted human heart. 'Zigzag' course of activation. Circulation 1993;88(3):915-26.
3. Koplan BA, Soejima K, Baughman K, Epstein LM, Stevenson WG. Refractory ventricular tachycardia secondary to cardiac sarcoid: electrophysiologic characteristics, mapping, and ablation. Heart Rhythm 2006; 3(8):924-9.
4. Nakahara S, Tung R, Ramirez RJ, Michowitz Y, Vaseghi M, Buch E, Gima J, Wiener I, Mahajan A, Boyle NG, Shivkumar K. Characterization of the arrhythmogenic substrate in ischemic and nonischemic cardiomyopathy implications for catheter ablation of hemodynamically unstable ventricular tachycardia. J Am Coll Cardiol 2010;55(21):2355-65.
5. Zeppenfeld K, Schalij MJ, Bartelings MM, Tedrow UB, Koplan BA, Soejima K, Stevenson WG. Catheter ablation of ventricular tachycardia after repair of congenital heart disease: electroanatomic identification of the critical right ventricular isthmus. Circulation 2007;116(20):2241-52.
6. Hsia HH, Callans DJ, Marchlinski FE. Characterization of endocardial electrophysiological substrate in patients with nonischemic cardiomyopathy and monomorphic ventricular tachycardia. Circulation 2003;108(6):704-10.
7. Hutchinson MD, Gerstenfeld EP, Desjardins B et al. Endocardial unipolar voltage mapping to detect epicardial ventricular tachycardia substrate in patients with nonischemic left ventricular cardiomyopathy. Circ Arrhythm Electrophysiol 2011;4(1): 49-55.
8. Polin GM, Haqqani H, Tzou W, Hutchinson MD, Garcia FC, Callans DJ, Zado ES, Marchlinski FE. Endocardial unipolar voltage mapping to identify epicardial substrate in arrhythmogenic right ventricular cardiomyopathy/dysplasia. Heart Rhythm 2011;8(1): 76-83.
9. Arenal A, Glez-Torrecilla E, Ortiz M, Villacastin J, Fdez-Portales J, Sousa E, del CS, Perez d, I, Jimenez J, Almendral J. Ablation of electrograms with an isolated, delayed component as treatment of unmappable monomorphic ventricular tachycardias in patients with structural heart disease. J Am Coll Cardiol 2003;41(1):81-92.
10. Bogun F, Good E, Reich S et al. Isolated potentials during sinus rhythm and pace-mapping within scars as guides for ablation of post-infarction ventricular tachycardia. J Am Coll Cardiol 2006;47(10):2013-9.
11. Brunckhorst CB, Stevenson WG, Jackman WM, Kuck KH, Soejima K, Nakagawa H, Cappato R, Ben-Haim SA. Ventricular mapping during atrial and ventricular pacing. Relationship of multipotential electrograms to ventricular tachycardia reentry circuits after myocardial infarction. Eur Heart J 2002;23(14):1131-8.
12. Cochet H, Komatsu Y, Sacher F et al. Integration of merged delayed-enhanced magnetic resonance imaging and multidetector computed tomography for the guidance of ventricular tachycardia ablation: a pilot study. J Cardiovasc Electrophysiol 2013;24(4):419-26.
13. Komatsu Y, Cochet H, Jadidi A et al. Regional myocardial wall thinning at multidetector computed tomography

correlates to arrhythmogenic substrate in postinfarction ventricular tachycardia: assessment of structural and electrical substrate. Circ Arrhythm Electrophysiol 2013;6(2):342-50.

14. Tian J, Jeudy J, Smith MF et al. Three-dimensional contrast-enhanced multidetector CT for anatomic, dynamic, and perfusion characterization of abnormal myocardium to guide ventricular tachycardia ablations. Circ Arrhythm Electrophysiol 2010;3(5): 496-504.
15. van Huls van Taxis CF, Wijnmaalen AP, Piers SR, van der Geest RJ, Schalij MJ, Zeppenfeld K. Real-Time Integration of MDCT-Derived Coronary Anatomy and Epicardial Fat: Impact on Epicardial Electroanatomic Mapping and Ablation for Ventricular Arrhythmias. JACC Cardiovasc Imaging 2013;6(1):42-52.
16. Andreu D, Berruezo A, Ortiz-Perez JT, Silva E, Mont L, Borras R, de Caralt TM, Perea RJ, Fernandez-Armenta J, Zeljko H, Brugada J. Integration of 3D electroanatomic maps and magnetic resonance scar characterization into the navigation system to guide ventricular tachycardia ablation. Circ Arrhythm Electrophysiol 2011;4(5):674-83.
17. Bogun FM, Desjardins B, Good E, Gupta S, Crawford T, Oral H, Ebinger M, Pelosi F, Chugh A, Jongnarangsin K, Morady F. Delayed-enhanced magnetic resonance imaging in nonischemic cardiomyopathy: utility for identifying the ventricular arrhythmia substrate. J Am Coll Cardiol 2009;53(13):1138-45.
18. Codreanu A, Odille F, Aliot E, Marie PY, Magnin-Poull I, Andronache M, Mandry D, Djaballah W, Regent D, Felblinger J, de CC. Electroanatomic characterization of post-infarct scars comparison with 3-dimensional myocardial scar reconstruction based on magnetic resonance imaging. J Am Coll Cardiol 2008;52(10):839-42.
19. Dickfeld T, Tian J, Ahmad G, Jimenez A, Turgeman A, Kuk R, Peters M, Saliaris A, Saba M, Shorofsky S, Jeudy J. MRI-Guided ventricular tachycardia ablation: integration of late gadolinium-enhanced 3D scar in patients with implantable cardioverter-defibrillators. Circ Arrhythm Electrophysiol 2011;4(2):172-84.
20. Perez-David E, Arenal A, Rubio-Guivernau JL et al. Noninvasive identification of ventricular tachycardia-related conducting channels using contrast-enhanced magnetic resonance imaging in patients with chronic myocardial infarction: comparison of signal intensity scar mapping and endocardial voltage mapping. J Am Coll Cardiol 2011;57(2):184-94.
21. Piers SR, van Huls van Taxis CF, Tao Q, van der Geest RJ, Askar SF, Siebelink HM, Schalij MJ, Zeppenfeld K. Epicardial substrate mapping for ventricular tachycardia ablation in patients with non-ischaemic cardiomyopathy: a new algorithm to differentiate between scar and viable myocardium developed by simultaneous integration of computed tomography and contrast-enhanced magnetic resonance imaging. Eur Heart J 2012;34(8):586-96.
22. Wijnmaalen AP, van der Geest RJ, van Huls van Taxis CF, Siebelink HM, Kroft LJ, Bax JJ, Reiber JH, Schalij MJ, Zeppenfeld K. Head-to-head comparison of contrast-enhanced magnetic resonance imaging and electroanatomical voltage mapping to assess post-infarct scar characteristics in patients with ventricular tachycardias: real-time image integration and reversed registration. Eur Heart J 2011;32(1):104-14.
23. Zeppenfeld K, Tops LF, Bax JJ, Schalij MJ. Images in cardiovascular medicine. Epicardial radiofrequency catheter ablation of ventricular tachycardia in the vicinity of coronary arteries is facilitated by fusion of 3-dimensional electroanatomical mapping

with multislice computed tomography. Circulation 2006;114(3):e51-e52.

24. Dickfeld T, Kato R, Zviman M, Lai S, Meininger G, Lardo AC, Roguin A, Blumke D, Berger R, Calkins H, Halperin H. Characterization of radiofrequency ablation lesions with gadolinium-enhanced cardiovascular magnetic resonance imaging. J Am Coll Cardiol 2006;47(2):370-8.
25. Tian J, Ahmad G, Mesubi O, Jeudy J, Dickfeld T. Three-dimensional delayed-enhanced cardiac MRI reconstructions to guide ventricular tachycardia ablations and assess ablation lesions. Circ Arrhythm Electrophysiol 2012;5(2):e31-e35.
26. Dong J, Calkins H, Solomon SB, Lai S, Dalal D, Lardo AC, Brem E, Preiss A, Berger RD, Halperin H, Dickfeld T. Integrated electroanatomic mapping with three-dimensional computed tomographic images for real-time guided ablations. Circulation 2006; 113(2):186-94.
27. Fahmy TS, Wazni OM, Jaber WA et al. Integration of positron emission tomography/computed tomography with electroanatomical mapping: a novel approach for ablation of scar-related ventricular tachycardia. Heart Rhythm 2008; 5(11):1538-45.
28. Gupta S, Desjardins B, Baman T, Ilg K, Good E, Crawford T, Oral H, Pelosi F, Chugh A, Morady F, Bogun F. Delayed-enhanced MR scar imaging and intraprocedural registration into an electroanatomical mapping system in post-infarction patients. JACC Cardiovasc Imaging 2012;5(2):207-10.
29. Ilg K, Baman TS, Gupta SK et al. Assessment of radiofrequency ablation lesions by CMR imaging after ablation of idiopathic ventricular arrhythmias. JACC Cardiovasc Imaging 2010;3(3):278-85.
30. Sasaki T, Miller CF, Hansford R et al. Myocardial structural associations with local electrograms: a study of postinfarct ventricular tachycardia pathophysiology and magnetic resonance-based noninvasive mapping. Circ Arrhythm Electrophysiol 2012;5(6):1081-90.
31. Reddy VY, Malchano ZJ, Holmvang G, Schmidt EJ, d'Avila A, Houghtaling C, Chan RC, Ruskin JN. Integration of cardiac magnetic resonance imaging with three-dimensional electroanatomic mapping to guide left ventricular catheter manipulation: feasibility in a porcine model of healed myocardial infarction. J Am Coll Cardiol 2004;44(11):2202-13.
32. Tao Q, Milles J, VAN Huls VAN, Lamb HJ, Reiber JH, Zeppenfeld K, van der Geest RJ. Toward magnetic resonance-guided electroanatomical voltage mapping for catheter ablation of scar-related ventricular tachycardia: a comparison of registration methods. J Cardiovasc Electrophysiol 2012; 23(1):74-80.
33. Desjardins B, Crawford T, Good E, Oral H, Chugh A, Pelosi F, Morady F, Bogun F. Infarct architecture and characteristics on delayed enhanced magnetic resonance imaging and electroanatomic mapping in patients with postinfarction ventricular arrhythmia. Heart Rhythm 2009;6(5):644-51.
34. Spears DA, Suszko AM, Dalvi R, Crean AM, Ivanov J, Nanthakumar K, Downar E, Chauhan VS. Relationship of bipolar and unipolar electrogram voltage to scar transmurality and composition derived by magnetic resonance imaging in patients with nonischemic cardiomyopathy undergoing VT ablation. Heart Rhythm 2012;9(11):1837-46.
35. McCrohon JA, Moon JC, Prasad SK, McKenna WJ, Lorenz CH, Coats AJ, Pennell DJ. Differentiation of heart failure related to dilated cardiomyopathy and coronary artery disease using gadolinium-enhanced cardiovascular magnetic resonance. Circulation 2003;108(1):54-9.

36. Arenal A, del CS, Gonzalez-Torrecilla E, Atienza F, Ortiz M, Jimenez J, Puchol A, Garcia J, Almendral J. Tachycardia-related channel in the scar tissue in patients with sustained monomorphic ventricular tachycardias: influence of the voltage scar definition. Circulation 2004;110(17): 2568-74.

37. Fernandez-Armenta J, Berruezo A, Andreu D et al. Three-dimensional Architecture of Scar and Conducting Channels Based on High Resolution ce-CMR: Insights for Ventricular Tachycardia Ablation. Circ Arrhythm Electrophysiol 2013;6(3):528-37.

38. Piers SR, Tao Q, van Huls van Taxis CF, Schalij MJ, van der Geest RJ, Zeppenfeld K. Contrast-Enhanced MRI-Derived Scar Patterns and Associated Ventricular Tachycardias in Nonischemic Cardiomyopathy: Implications for the Ablation Strategy. Circ Arrhythm Electrophysiol 2013;6(5):875-83.

39. Stevenson WG, Khan H, Sager P, Saxon LA, Middlekauff HR, Natterson PD, Wiener I. Identification of reentry circuit sites during catheter mapping and radiofrequency ablation of ventricular tachycardia late after myocardial infarction. Circulation 1993;88(4 Pt 1):1647-70.

40. Kuck KH, Schaumann A, Eckardt L, Willems S, Ventura R, Delacretaz E, Pitschner HF, Kautzner J, Schumacher B, Hansen PS. Catheter ablation of stable ventricular tachycardia before defibrillator implantation in patients with coronary heart disease (VTACH): a multicentre randomised controlled trial. Lancet 2010;375(9708): 31-40.

41. Reddy VY, Reynolds MR, Neuzil P, Richardson AW, Taborsky M, Jongnarangsin K, Kralovec S, Sediva L, Ruskin JN, Josephson ME. Prophylactic catheter ablation for the prevention of defibrillator therapy. N Engl J Med 2007;357(26):2657-65.

42. Friedrich MG, Sechtem U, Schulz-Menger J et al. Cardiovascular magnetic resonance in myocarditis: A JACC White Paper. J Am Coll Cardiol 2009;53(17):1475-87.

43. Kim RJ, Fieno DS, Parrish TB, Harris K, Chen EL, Simonetti O, Bundy J, Finn JP, Klocke FJ, Judd RM. Relationship of MRI delayed contrast enhancement to irreversible injury, infarct age, and contractile function. Circulation 1999;100(19):1992-2002.

44. de Haan S, Meijers TA, Knaapen P, Beek AM, van Rossum AC, Allaart CP. Scar size and characteristics assessed by CMR predict ventricular arrhythmias in ischaemic cardiomyopathy: comparison of previously validated models. Heart 2011;97(23): 1951-6.

45. Gai N, Turkbey EB, Nazarian S, van der Geest RJ, Liu CY, Lima JA, Bluemke DA. T1 mapping of the gadolinium-enhanced myocardium: adjustment for factors affecting interpatient comparison. Magn Reson Med 2011;65(5):1407-15.

46. Nazarian S, Kolandaivelu A, Zviman MM et al. Feasibility of real-time magnetic resonance imaging for catheter guidance in electrophysiology studies. Circulation 2008; 118(3):223-9.

47. Dukkipati SR, Mallozzi R, Schmidt EJ et al. Electroanatomic mapping of the left ventricle in a porcine model of chronic myocardial infarction with magnetic resonance-based catheter tracking. Circulation 2008;118(8):853-62.

48. Solomon SB, Dickfeld T, Calkins H. Real-time cardiac catheter navigation on three-dimensional CT images. J Interv Card Electrophysiol 2003;8(1):27-36.

49. Piers SR, Dyrda K, Tao Q, Zeppenfeld K. Bipolar ablation of ventricular tachycardia in a patient after atrial switch operation for dextro-transposition of the great arteries. Circ Arrhythm Electrophysiol 2012;5(2): e38-e40.

50. d'Avila A, Houghtaling C, Gutierrez P,

Vragovic O, Ruskin JN, Josephson ME, Reddy VY. Catheter ablation of ventricular epicardial tissue: a comparison of standard and cooled-tip radiofrequency energy. Circulation 2004;109(19):2363-9.

51. Desjardins B, Morady F, Bogun F. Effect of epicardial fat on electroanatomical mapping and epicardial catheter ablation. J Am Coll Cardiol 2010;56(16):1320-7.
52. Abbara S, Desai JC, Cury RC, Butler J, Nieman K, Reddy V. Mapping epicardial fat with multi-detector computed tomography to facilitate percutaneous transepicardial arrhythmia ablation. Eur J Radiol 2006; 57(3):417-22.
53. van der Bijl N, Joemai RM, Geleijns J, Bax JJ, Schuijf JD, de RA, Kroft LJ. Assessment of Agatston coronary artery calcium score using contrast-enhanced CT coronary angiography. AJR Am J Roentgenol 2010; 195(6):1299-305.
54. Bunch TJ, Weiss JP, Crandall BG, Day JD, DiMarco JP, Ferguson JD, Mason PK, McDaniel G, Osborn JS, Wiggins D, Mahapatra S. Image integration using intracardiac ultrasound and 3D reconstruction for scar mapping and ablation of ventricular tachycardia. J Cardiovasc Electrophysiol 2010;21(6):678-84.
55. Seiler J, Lee JC, Roberts-Thomson KC, Stevenson WG. Intracardiac echocardiography guided catheter ablation of incessant ventricular tachycardia from the posterior papillary muscle causing tachycardia--mediated cardiomyopathy. Heart Rhythm 2009;6(3):389-92.
56. Bala R, Ren JF, Hutchinson MD et al. Assessing epicardial substrate using intracardiac echocardiography during VT ablation. Circ Arrhythm Electrophysiol 2011;4(5):667-73.
57. Jongbloed MR, Bax JJ, van der Burg AE, van der Wall EE, Schalij MJ. Radiofrequency catheter ablation of ventricular tachycardia guided by intracardiac echocardiography. Eur J Echocardiogr 2004;5(1):34-40.
58. Lamberti F, Calo' L, Pandozi C, Castro A, Loricchio ML, Boggi A, Toscano S, Ricci R, Drago F, Santini M. Radiofrequency catheter ablation of idiopathic left ventricular outflow tract tachycardia: utility of intracardiac echocardiography. J Cardiovasc Electrophysiol 2001;12(5):529-35.
59. Callans DJ, Ren JF, Michele J, Marchlinski FE, Dillon SM. Electroanatomic left ventricular mapping in the porcine model of healed anterior myocardial infarction. Correlation with intracardiac echocardiography and pathological analysis. Circulation 1999; 100(16):1744-50.
60. Dickfeld T, Lei P, Dilsizian V, Jeudy J, Dong J, Voudouris A, Peters R, Saba M, Shekhar R, Shorofsky S. Integration of three-dimensional scar maps for ventricular tachycardia ablation with positron emission tomography-computed tomography. JACC Cardiovasc Imaging 2008;1(1):73-82.
61. Tian J, Smith MF, Chinnadurai P et al. Clinical Application of PET/CT Fusion Imaging for Three-Dimensional Myocardial Scar and Left Ventricular Anatomy during Ventricular Tachycardia Ablation. J Cardiovasc Electrophysiol 2008.
62. Pichler BJ, Wehrl HF, Judenhofer MS. Latest advances in molecular imaging instrumentation. J Nucl Med 2008;49 Suppl 2(5S-23S.
63. Bengel FM, Higuchi T, Javadi MS, Lautamaki R. Cardiac positron emission tomography. J Am Coll Cardiol 2009;54(1):1-15.
64. Tian J, Smith MF, Ahmad G, Dilsizian V, Jimenez A, Dickfeld T. Integration of 3-dimensional scar models from SPECT to guide ventricular tachycardia ablation. J Nucl Med 2012;53(6):894-901.
65. Tian J, Smith MF, Jeudy J, Dickfeld T. Multimodality fusion imaging using delayed-enhanced cardiac magnetic resonance imaging, computed tomogra-

phy, positron emission tomography, and real-time intracardiac echocardiography to guide ventricular tachycardia ablation in implantable cardioverter-defibrillator patients. Heart Rhythm 2009;6(6):825-8.

Chapter 3

Epicardial substrate mapping for ventricular tachycardia ablation in patients with nonischemic cardiomyopathy

A new algorithm to differentiate between scar and viable myocardium developed by simultaneous integration of CT and contrast-enhanced MRI

Sebastiaan R.D. Piers, MD, Carine F.B. van Huls van Taxis, MD, Qian Tao, PhD, Rob J. van der Geest, PhD, Said F. Askar, Hans-Marc J. Siebelink, MD, PhD, Martin J. Schalij, MD, PhD, Katja Zeppenfeld, MD, PhD

European Heart Journal 2013;34(8):586-96

ABSTRACT

Aims

During epicardial electroanatomical mapping (EAM) it is difficult to differentiate between fibrosis and fat, as both exhibit attenuated bipolar voltage (BV). The purpose of this study was to assess whether unipolar voltage (UV), BV and electrogram characteristics (EC) can distinguish fibrosis from viable myocardium and fat during epicardial EAM for ventricular tachycardia (VT) ablation in nonischemic cardiomyopathy (NICM).

Methods and Results

Ten NICM patients (7 males, 56±13 years) with VT underwent epicardial EAM with real-time integration of CT-derived epicardial fat and contrast-enhanced MRI-derived scar. BV (filtered 30-400Hz), UV (filtered 1-240Hz) and EC (duration and morphology) were correlated with the presence of fat and scar. At sites devoid of fat, the optimal cutoff values to differentiate between scar and myocardium were 1.81mV for BV and 7.95mV for UV. BV, UV and electrogram duration >50ms distinguished scar from myocardium in areas covered with <2.8mm fat (all $p<0.001$), but not ≥2.8mm fat. In contrast, electrogram morphology-characteristics could also detect scar covered with ≥2.8mm fat ($p=0.001$). A newly developed 3-step algorithm combining electrogram morphology, duration and UV could correctly identify scar with a sensitivity of 75%. UV but not BV could detect intramural scar in the absence of fat.

Conclusions

Both BV≤1.81mV and UV≤7.95mV are useful for detection of scar during epicardial EAM, in the absence of ≥2.8mm fat. However, EC can be used to detect scar covered with fat. A newly developed algorithm combining UV and EC can differentiate between scar and viable myocardium. UV but not BV could detect intramural scar.

INTRODUCTION

The substrate for ventricular tachycardia (VT) in patients with left ventricular (LV) nonischemic cardiomyopathy (NICM) is frequently located intramurally or epicardially and may require an epicardial ablation approach.[1,2] Since the majority of induced VTs are hemodynamically unstable,[3] substrate mapping is indispensable for successful ablation. Epicardial substrate mapping is however challenging. Firstly, it may be difficult to differentiate between scar and epicardial fat, since both exhibit attenuated bipolar electrogram amplitudes.[4,5] Secondly, even in the absence of epicardial fat, scar may be difficult to detect if located intramural.

Electrogram characteristics have been proposed to distinguish scar from epicardial fat[4] since long electrogram duration, fragmented electrograms and late potentials indicate slow conduction typical for inhomogeneous scar.[6] However, subtle bipolar electrogram abnormalities such as low-amplitude late potentials may be reduced to noise level by the interposition of epicardial fat. Unipolar voltage has been demonstrated to have a larger field of view,[7] which may allow detection of scar covered by fat and intramural scar.

Computed tomography (CT) and contrast-enhanced magnetic resonance imaging (CE-MRI) are considered gold standards for delineation of fat and fibrosis. Prior studies have demonstrated the feasibility and accuracy of integration of CT-derived epicardial fat[5] and CE-MRI-derived fibrosis[8,9] with electroanatomical maps (EAM). By integrating both CT- and CE-MRI-derived data during substrate mapping, gold standards for the presence of fat and fibrosis become available.

The purpose of this study was to (1) establish bipolar and unipolar voltage cutoff values for scar detection during epicardial EAM, (2) assess whether voltages and electrogram characteristics can distinguish scar from viable myocardium in the presence of fat, (3) develop an algorithm that differentiates between scar and viable myocardium and (4) to determine whether the epicardial area of interest containing ablation target sites can be delineated using voltage or electrogram characteristics.

METHODS

Patients

The study population consisted of 10 out of 11 consecutive patients with NICM referred for combined endocardial and epicardial VT ablation, with integration of both CT-derived epicardial fat and CE-MRI-derived scar information. One patient was excluded because of imaging artifacts causing non-interpretable CE-MRI image data. Coronary artery disease was excluded by coronary angiography in all patients. Seven patients

underwent combined endocardial and epicardial VT ablation after endocardial ablation failure which was presumed to be due to an epicardial VT exit site based on the lack of early endocardial activation during VT and/or an endocardial substrate for VT. In the remaining 3 patients, an epicardial VT exit site was suspected based on the 12-lead ECG morphology of the clinical VT.[10]

Six patients with idiopathic ventricular arrhythmias (VA) who underwent endocardial and epicardial EAM with CT integration served as controls for voltages and electrogram characteristics. Structural heart disease was excluded by echocardiography and CT in 6 patients (100%), by coronary angiography in 5 patients (83%) and by MRI in 4 patients (67%). All 6 patients underwent combined endocardial and epicardial ablation after endocardial ablation failure and an endocardial activation pattern consistent with an epicardial site of origin.

All patients were treated according to the clinical protocol and provided informed consent.

CT acquisition and processing

Before the procedure, electrocardiogram-gated cardiac CT imaging was performed with intravenous iodinated contrast agent either on a 64-detector row helical scanner or a 320-detector row volumetric scanner (Toshiba Medical Systems, Otawara, Japan). Using in-house developed software (Mass, V2009-EXP LKEB, Leiden, The Netherlands) the endocardial, epicardial and pericardial contours were manually traced on short-axis reformatted CT slices (0.5x0.5mm resolution, 2mm thickness, 2mm inter-slice gap) to create 3D meshes (Figure 1). Fat thickness was computed by calculating the distance between epicardial and pericardial contours and the vertices of the epicardial 3D mesh were color-coded for fat thickness. Subsequently, the original CT data and the meshes were imported into the mapping system (CARTO XP™, Biosense Webster Inc, Diamond Bar, CA, USA). Using CARTOMerge (IPE) software, which enables integration of multiple datasets, the ventricles, aorta and coronary arteries were segmented and merged with the 3D meshes.

CE-MRI acquisition and processing

Contrast-enhanced MRI was performed on a 1.5 T Gyroscan ACS-NT/Intera MR system (Philips Medical Systems, Best, The Netherlands). A standardized protocol was followed, including a black-blood turbo spin-echo sequence for the proximal aorta.[9] Contrast-enhanced images were acquired 15min after bolus injection of gadolinium. The heart was imaged in one breath-hold with 20–24 imaging levels (dependent on heart size) in short-axis views.

The images were post-processed as described previously.[9] The centerline of the proximal coronary arteries was manually defined in the black-blood spin-echo image data

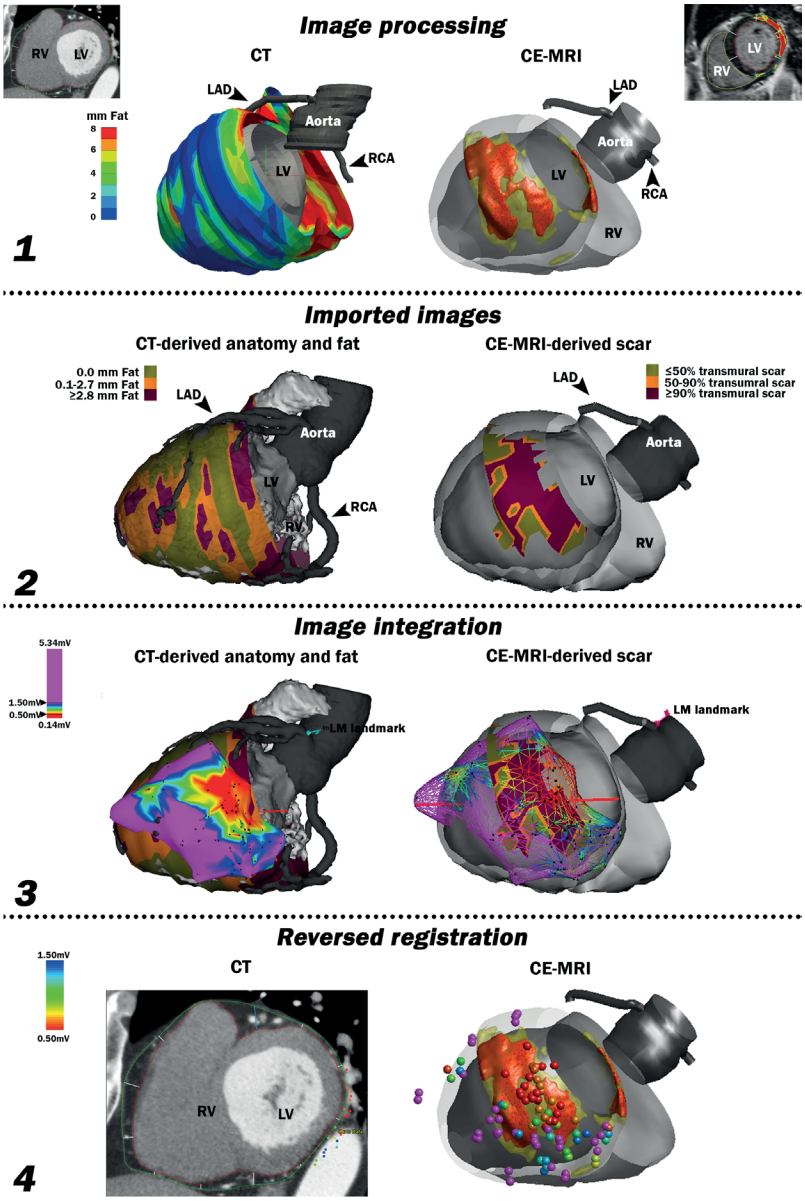


Figure 1. Processing and integration of CT and contrast-enhanced MRI

Step 1. Epicardial fat meshes and 3D scar reconstructions were created from the short-axis CT and CE-MRI slices. Step 2. Before the procedure, the CT was segmented and all meshes were imported into the mapping system. Step 3. During the procedure, CT- and CE-MRI-derived images were integrated with the electroanatomical map (displayed as a mesh to better visualize the scar distribution [right]) Step 4. After the procedure, points were projected on the corresponding short-axis CT slices and the 3D scar reconstruction to determine fat thickness and the presence of underlying scar.

CE-MRI denotes contrast-enhanced MRI; LAD, left anterior descending; LM, left main; LV, left ventricle; RCA, right coronary artery; RV, right ventricle.

and the aortic, endocardial and epicardial contours were semi-automatically detected on the short axis views. The contours were converted into 3D meshes (Mass research software, Figure 1). Myocardial tissue with ≥35% of maximal signal intensity was considered scar. The vertices of the LV endocardial and epicardial meshes were color-coded with scar transmurality for the inner and outer half of the wall, respectively. All meshes were imported into the CARTO system using CARTOMerge (IPE) software.

Electrophysiological evaluation

Anti-arrhythmic drugs were discontinued for ≥5 half-lives with the exception of amiodarone (n=1). Programmed electrical stimulation was performed under conscious sedation (3 drive cycle lengths [600, 500 and 400ms], 1-3 ventricular extrastimuli [≥200ms] from 2 right ventricular (RV) sites and burst pacing (CL≥200ms), repeated with isoproterenol (2-10μg/min) when necessary). A positive endpoint for stimulation was the induction of sustained monomorphic VT lasting >30s or requiring termination because of hemodynamic compromise.

Electroanatomical mapping, real-time image integration and ablation

Pericardial access was obtained through a subxyphoid puncture followed by intravenous heparin administration. Electroanatomical mapping was performed using a 3.5mm irrigated-tip catheter with a 2mm ring electrode and a 1mm interelectrode spacing (NaviStar ThermoCool, Biosense Webster Inc, Diamond Bar, CA, USA) and the CARTO^{XP} system. Electrograms were filtered at 30-400Hz (bipolar) and 1-240Hz (unipolar). Limited EAM of the aortic root was performed and the left main coronary artery position, confirmed by undiluted contrast injection through the mapping catheter, was tagged on the map. Secondly, an endocardial map of the LV was created using a retrograde approach via the aorta. An RV map was created if indicated. CT-derived images were visually aligned with the EAM using the left main landmark to overcome rotation errors. The LV surfaces were automatically aligned using CARTOMerge software and the mean surface registration error was calculated.

CE-MRI-derived images were visually aligned with the EAM using the left main landmark. Then, the LV surfaces were aligned with the translation tool until the lowest mean surface registration error was reached.

After image registration, epicardial EAM of the target area was performed. Endocardial and epicardial ablation target sites were identified based on activation mapping and entrainment mapping for stable VT, and substrate mapping (electrogram characteristics and pace-mapping) for unstable VT. Radiofrequency energy was applied at 30-45W (maximum temperature 45°C, flow 20-30ml/min, 60s) for endocardial sites and up to 50W (flow 20ml/min) for epicardial sites.

Electrogram analysis

All bipolar electrograms were displayed at the same gain (reference caliper 0.20mV, Figure 2) and categorized as normal (≤4 sharp spikes) or abnormal (>4 sharp spikes).[11] The latter were subdivided into the following morphologies: double potentials (amplitude ratio ≤1.5), continuously fragmented electrograms (amplitude/duration [mV/msec] ratio ≤0.05), late potentials (inscribing after QRS and separated by an isoelectric segment >20ms) or other abnormal morphologies (>4 spikes but none of the previous; Figure 2). In addition, electrogram duration was measured from the first to the last sharp spike[11] and categorized into 4 predefined categories: ≤50ms, 51-60ms, 61-70ms or >70ms.

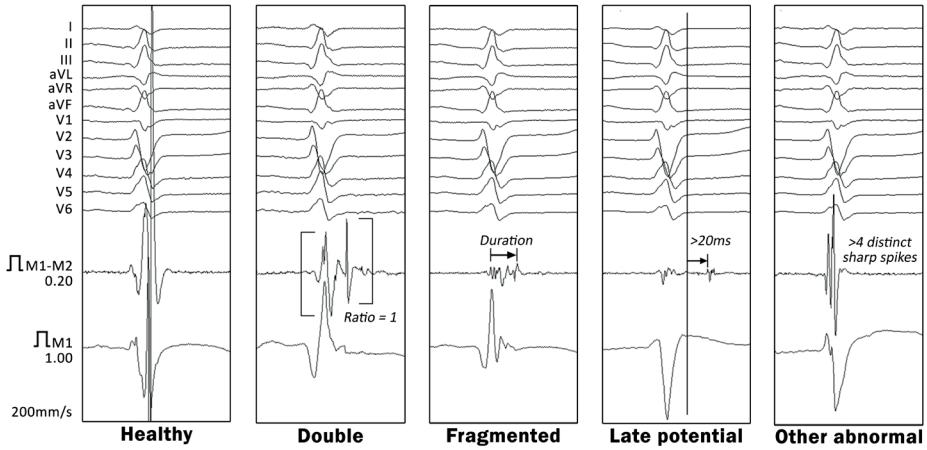


Figure 2. Electrogram morphology categories.

Post-procedural reverse registration of electroanatomical maps with both CT and CE-MRI

After the procedure, all points were superimposed on the corresponding short-axis CT slice using the reversed registration matrix and point coordinates (Mass research software). The epicardial fat thickness was calculated for each point and categorized as 0.0mm, 0.1-2.7mm or ≥2.8mm. Sites with 0.0mm fat were analyzed separately to assess the impact of scar on electroanatomical mapping parameters in the absence of fat. The 2.8mm cutoff has been demonstrated to separate low (<1.5mV) from normal bipolar voltage.[5]

All points were also superimposed on a 3D reconstruction of the CE-MRI, which was created using the short-axis slices (MATLAB software, version 2009b). Centered around each mapping point that was projected on the LV epicardial surface, a 5mm-diameter transmural cylinder was created and divided into three layers of equal thickness. Points with late enhancement (LE) in the endocardial 1/3 or 2/3 were categorized as endocardial scar, those with LE only in the intramural layer as intramural scar, those with LE in the epicardial 1/3 or 2/3 as epicardial scar and points with LE in all 3 layers as transmural

scar. All LV epicardial ablation target sites with a ≥11/12 pacemap were evaluated for voltages, electrogram characteristics and the presence of LE.

Endomyocardial biopsy

After ablation, when indicated by current guidelines[12] endomyocardial biopsy was performed (6 patients, interventricular septum [n=4] and/or apicolateral LV [n=3]). Tissue was fixed in 4% formaldehyde. After embedding the tissue in paraffin, cross-sections were cut at 4μm and stained for collagen content by Picro-sirius Red staining. Nuclei were counterstained with Mayer's hematoxylin. High resolution images were taken by microscopy and collagen content was quantified as a percentage of the total biopsy surface using dedicated software (ImageJ, National Institutes of Health, USA). The amount and pattern of fibrosis (compact and/or interstitial) were compared with CE-MRI and EAM findings.

Statistical analysis

Categorical variables are displayed as number (percentage) and continuous variables as mean±SD or median (interquartile range). Data were analyzed using the χ^2 test, Fisher's exact test, Mann-Whitney *U* test or Kruskal-Wallis test when appropriate. Receiver-operating characteristic curve analysis was performed to determine the optimal cutoff values of bipolar and unipolar voltage for detection of scar, which were defined as the values maximizing the sum of sensitivity and specificity. The area under the curve (AUC) was calculated to evaluate the accuracy of the mapping parameters. To create an algorithm for differentiation between scar and viable myocardium, independent predictors of scar were identified using multivariable logistic regression analysis and backward stepwise selection (inclusion $p<0.10$, exclusion $p>0.20$). The algorithm outcome was positive for scar if any of the incorporated parameters was abnormal. McNemar's test was used to compare the sensitivity and specificity for the different steps of the algorithm. All analyses were performed with SPSS v18.0 (SPSS Inc., Chicago, Illinois). All p-values were two-sided and a p-value of <0.05 was considered significant.

RESULTS

Patients

Ten patients with NICM (7 males, 56±13 years) and 6 patients with idiopathic VA (5 males, 55±19 years) were studied. Baseline characteristics are summarized in Table 1. Mapping of the LV (NICM mean 110±66 points [median 102, min 33 – max 254], idiopathic mean 50±27 points [median 50, min 21 – max 90]) and epicardium (NICM mean 137±78 points [median 138, min 55 – max 247], idiopathic mean 80±51 points [median 81, min 28 –

Table 1. Baseline characteristics.

	Patients with NICM (n=10)	Patients without SHD (n=6)
Male gender (%)	7 (70%)	5 (83%)
Age, years	56±13	55±19
Body mass index, kg/m^2	25±4	28±5
LV ejection fraction, %	39±13	56±7
LV end-diastolic volume, mL	243±99	112±33
Hypertension (%)	3 (30%)	3 (30%)
Diabetes Mellitus (%)	1 (10%)	3 (50%)
Creatinin clearance < 60 mL/min	2 (20%)	2 (33%)
Atrial flutter / fibrillation (%)	1 (10%)	0
PVC (%)	0	5 (83%)
VT (%)	10 (100%)	2 (33%)

LV = left ventricular, NICM = nonischemic cardiomyopathy, PVC = premature ventricular contraction, SHD = structural heart disease, VT = ventricular tachycardia

max 164]) was performed focusing on the area of interest based on the 12-lead ECG of spontaneous and induced VA.

Image integration was successfully performed in all patients (CT surface registration error 2.0±0.3mm in NICM patients and 3.5±1.8mm in patients with idiopathic VA; CE-MRI surface registration error 3.2±0.4mm) (figure 3).

Fat and epicardial voltages

Of 1374 epicardial mapping points acquired in patients with NICM, 476 (35%) points were projected on the RV and excluded. Epicardial fat thickness was 0.0mm at 423 (47%) epicardial LV sites, 0.1-2.7mm at 296 (33%) sites and ≥2.8mm at 179 (20%) sites. LE on MRI was present at 558 (62%) points and no LE at 340 (38%). In patients with idiopathic VA, 268 points were analyzed. Epicardial fat thickness was 0.0mm fat at 37 (14%) epicardial LV sites, 0.1-2.7mm at 48 (18%) sites and ≥2.8mm at 183 (68%) sites. Both bipolar and unipolar electrogram amplitudes at sites without LE were attenuated by fat in NICM ($p<0.001$, Figure 4A-B) and controls ($p<0.001$, data not shown).

Bipolar and unipolar voltages: scar vs. viable myocardium

Bipolar and unipolar voltages in areas without scar on CE-MRI or fat on CT were similar in NICM patients and controls (Figure 4A-B). In patients with NICM, cutoff values of 1.81mV for bipolar voltage (AUC 0.73, sensitivity 59% and specificity 78%) and 7.95mV for unipolar voltage (AUC 0.79, sensitivity 80% and specificity 72%) could best differentiate between the absence and presence of scar in areas devoid of fat. In areas covered by ≥2.8mm fat neither bipolar nor unipolar voltage could differentiate between the

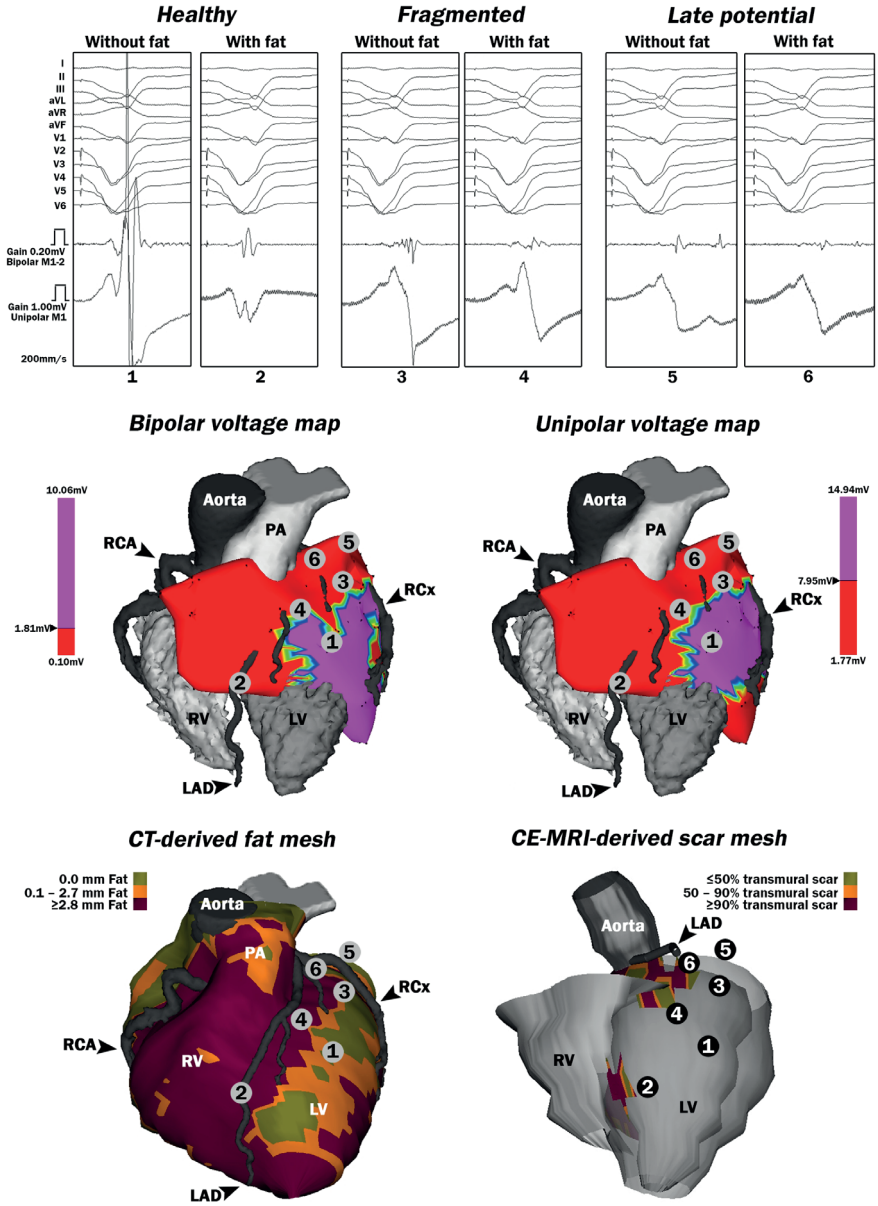


Figure 3. Example of simultaneous CT and contrast-enhanced MRI integration during epicardial electroanatomical mapping.

Substrate mapping demonstrates low voltage areas consistent with epicardial fat, scar or both. Late potentials were detected at the basal LV low voltage area, while an apparently healthy but attenuated electrogram was found at the interventricular groove. Integrated CT-derived fat meshes demonstrate that the interventricular groove and the RV are covered by thick fat layers, possibly explaining the attenuated electrogram amplitudes. The late potentials were caused by a basal scar, which was identified by the integrated CE-MRI-derived scar mesh. RVOT=RV outflow tract. Other abbreviations as in Figure 1.

Table 2. Diagnostic performance of electroanatomical mapping parameters to detect scar for areas with <2.8mm fat and ≥2.8mm fat.

Fat thickness (mm)	AUC*		PPV		NPV		Sensitivity		Specificity	
	<2.8	≥2.8	<2.8	≥2.8	<2.8	≥2.8	<2.8	≥2.8	<2.8	≥2.8
Mapping parameters										
Bipolar voltage ≤1.8mV	0.73	0.57	78%	58%	53%	48%	65%	69%	68%	35%
Unipolar voltage ≤7.95mV	0.78	0.58	80%	60%	64%	52%	79%	71%	66%	39%
Electrogram duration >50ms	0.70	0.58	89%	69%	50%	50%	50%	36%	89%	80%
Electrogram morphology - any abnormal	-	-	80%	69%	58%	55%	72%	56%	68%	68%
Algorithm										
STEP 1: Electrogram morphology - only double, fragmented, late potential	-	-	91%	92%	42%	50%	25%	24%	96%	98%
STEP 1+2: As above, *OR* duration >50ms †	-	-	88%	70%	54%	51%	58%	42%	86%	77%
STEP 1+2+3: As above, *OR* unipolar voltage ≤7.95mV †	-	-	78%	70%	66%	51%	83%	42%	60%	77%

* Parameters are analyzed as a continuous variable.
† Overall sensitivity and specificity compared to previous step by McNemar's test, p<0.001.
AUC denotes area under the curve; NPV, negative predictive value; PPV, positive predictive value.

absence or presence of scar. A summary of the value of EAM parameters for identification of scar is provided in Table 2.

Electrogram characteristics: scar vs. viable myocardium

In NICM patients electrograms were prolonged (>50ms) at 263 (47%) sites with scar, as compared to only 45 (13%) sites without evidence of scar on CE-MRI (p<0.001). Electrograms at scar sites with <2.8mm fat were more often prolonged (>50ms) than electrograms at scar sites with ≥2.8mm fat (50% vs. 36%, p=0.02, Figure 5A-B).

The electrogram morphology at sites with scar was categorized as normal in 173 (31%), double-equal in 61 (11%), fragmented in 57 (10%), late potential in 22 (4%) and other abnormal morphologies in 245 (44%) points. The double-equal, fragmented and late potential morphologies were unaffected by fat thickness (p=0.90), while the other abnormal electrogram morphologies were affected by fat thickness (p<0.001, Figure 5A-B, Table 2).

Algorithm for differentiation between scar and viable myocardium

The variables that were independently associated with scar by multivariable logistic regression analysis were electrogram morphology, electrogram duration and unipolar voltage, but not bipolar voltage. The 3 independently associated variables were used to create a 3-step algorithm, which is displayed in Figure 6.

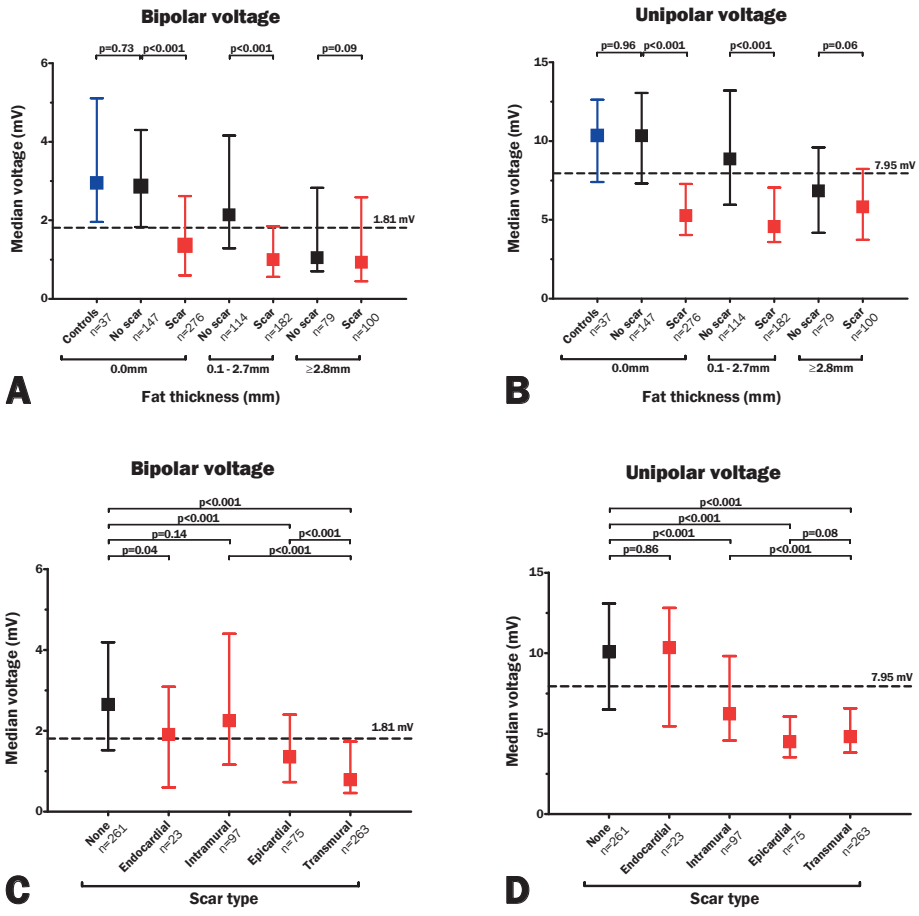


Figure 4. Scar, fat and bipolar & unipolar voltages.
Median and interquartile range of bipolar and unipolar voltage at scar and non-scar sites for different fat thicknesses (Panel A-B) and scar types (Panel C-D).

The complete algorithm had an overall sensitivity of 75%. The sensitivity was 83% in areas covered with <2.8mm fat, which decreased to 42% in the presence of ≥2.8mm fat (Table 2). However, in contrast to bipolar and unipolar voltage, the algorithm maintained a high specificity in areas covered with ≥2.8mm fat.

Using the complete algorithm 84% of transmural, 73% of epicardial and 64% of intramural scar sites could be identified, as compared to only 36% of endocardial scar sites.

Bipolar & unipolar voltage, electrogram characteristics and scar type

To determine the accuracy of bipolar and unipolar voltage for detection of different types of scar, sites covered by ≥2.8mm fat were excluded. Both bipolar and unipolar

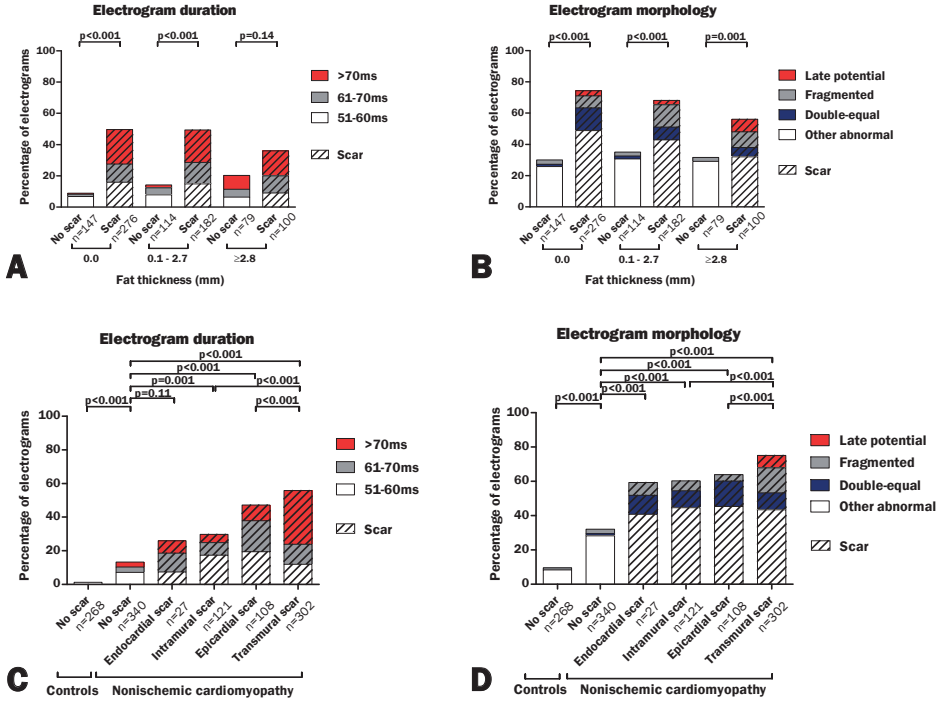


Figure 5. Scar, fat and electrogram characteristics.
Electrogram duration and electrogram morphology at scar and non-scar sites for different fat thicknesses in nonischemic cardiomyopathy (Panel A-B) and for different scar types in nonischemic cardiomyopathy and controls (Panel C-D).

voltage were reduced in the presence of epicardial and transmural scar (all p<0.001, Figure 4C-D), but only unipolar voltage was affected by intramural scar (p<0.001). Sites with transmural scar more often had prolonged (>50ms) and morphologically abnormal electrograms than sites with epicardial, intramural or endocardial scar (all p<0.001, Figure 5C-D). Epicardial scar in turn resulted in more prolonged (>50ms) electrograms than intramural (p=0.007) or endocardial scar (p=0.046). Late potentials were only observed at sites with transmural scar.

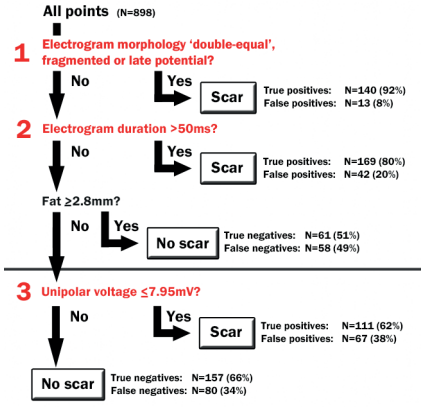


Figure 6. Algorithm for differentiation between scar and viable myocardium.

Ablation target sites

A total of 40 VTs was induced (cycle length 310±77ms). A ≥11/12 pacemap could be produced for 17 VTs (43%). At 9 of these 17 sites (53%), diastolic potentials were identified during VT and at 4 (24%) VT slowed and terminated during ablation. Eight (47%) target sites were located at the LV epicardium, 3 (18%) in the LV, 3 (18%) in the aortic root, 2 (12%) at the epicardial RV outflow tract and 1 (6%) at the RV side of the interventricular septum. At all LV epicardial target sites bipolar voltage was ≤1.81mV, unipolar voltage ≤7.95mV, electrogram duration >50ms and electrogram morphology abnormal (5 late potential, 1 fragmented, 2 other abnormal). Late enhancement was present at all LV epicardial target sites (6 transmural, 1 subepicardial, 1 intramural). Six of 8 VTs (75%) were not inducible after ablation. One VT could not be abolished presumably due to a deep intramural circuit (intramural LE on MRI) and another due to interposition of a coronary artery and >10mm epicardial fat.

Histology

Endomyocardial biopsy from the interventricular septum was performed in 4 patients (3 specimens each) distant from areas with LE on MRI. In 3 patients, voltages and electrograms were normal at the biopsy site, although both interstitial and limited compact fibrosis was identified in 2 of 3 patients (both 8% of surface, supplemental Figure). In the fourth patient, bipolar voltage was 1.40mV, unipolar voltage 4.46mV, electrogram duration 65ms and electrogram morphology 'other abnormal'. Histology revealed more severe compact and interstitial fibrosis (46% of surface).

Endomyocardial biopsy from the apicolateral LV was performed in 3 patients (3 specimens each). Voltages and electrograms were normal at the biopsy site, while both interstitial and limited compact fibrosis were found in all 3 patients (2, 13 and 16% of surface). None of the biopsy sites corresponded to an area of LE.

DISCUSSION

The present study is the first to compare voltage maps, electrogram characteristics, fat and scar by integration of both CT and CE-MRI with epicardial EAM. In addition, the distribution and amount of fibrosis as identified by histology, were also compared with EAM and CE-MRI. The main findings can be summarized as follows: (1) bipolar voltage ≤1.81mV and unipolar voltage ≤7.95mV are the optimal cutoff values for identification of scar during epicardial EAM of areas devoid of fat, (2) electrogram characteristics, but not bipolar or unipolar voltages, can detect scar covered by fat, (3) the proposed algorithm can be applied to differentiate between scar and viable myocardium and (4) unipolar voltage can be used to identify intramural scar.

Bipolar and unipolar voltage, scar and fat

In the current study, epicardial bipolar and unipolar cutoff values for detection of scar were determined based on CT and CE-MRI. In a prior study by Cano et al.[2], normal epicardial bipolar voltage values were assessed by excluding a 1.5cm wide area along the course of the coronary arteries and the atrioventricular groove. Thick fat layers often found in other areas[13] may explain the reported lower bipolar voltage cutoff value of 1.0mV. In another study, CT-derived fat was integrated with EAM, but a gold standard for the presence of scar was lacking.[5] The currently presented cutoff values of 1.81mV for bipolar voltage and 7.95mV for unipolar voltage are likely to be more accurate since detailed information on fat and scar was available.

It has been postulated that having a larger 'field of view', unipolar voltage could detect scar covered by fat, thereby compensating for the limitation of bipolar voltage mapping. However, in the NICM population unipolar voltage could not differentiate between presence or absence of scar at sites with ≥2.8mm fat, suggesting a limited field of view.

Electrogram characteristics, scar and fat

Prolonged bipolar electrograms with an abnormal morphology are likely to indicate slow conduction in inhomogeneous scar, perhaps related to VT. Since bipolar electrogram amplitudes are attenuated by epicardial fat, low amplitude components such as late potentials may be reduced to noise level. In this study, both CT-derived fat and CE-MRI-derived scar information were integrated, which for the first time allowed evaluation of the value of different EAM parameters. Electrograms were prolonged at only 47% of sites with LE, suggesting that CE-MRI and EAM may provide complementary information, with CE-MRI more accurately delineating (intramural) fibrosis and EAM providing functional information. Importantly, double-equal, fragmented and late potentials were not affected by fat and almost exclusively detected in scar areas, whereas other (more subtle) abnormal electrogram morphologies were affected by fat and also frequently found in non-scar areas. Subtle electrogram abnormalities may be caused by small amounts of fibrosis not detected by CE-MRI, as was found in the biopsy specimens. Late potentials may indicate the presence of slow conduction caused by large amounts of scar, which is supported by the presence of transmural scar at all sites with late potentials.

Algorithm

If CE-MRI is not available, the proposed easy-to-apply 3-step algorithm may be used to improve the accuracy of scar delineation during epicardial EAM. In areas with ≥2.8mm fat (as delineated by CT, which can be acquired irrespective of prior device implantation) only the first and second step should be used to maintain specificity, whereas the third step may be used for sites with <2.8mm fat (on average 80% of mapping sites). When CT scans are not available, step 1 and 2 of the algorithm can be used, although with

lower sensitivity. When only the electrogram morphology (any abnormal) is applied, the sensitivity is acceptable and the specificity is unaffected by fat thickness.

Voltage mapping and scar type

In the current study, for the first time it is demonstrated that epicardial unipolar voltage can be used to identify intramural scar. However, due to the limited field of view unipolar voltages cannot be used to detect subendocardial scar. Previously, Hutchinson et al. demonstrated that 61% of endocardial low unipolar voltage areas (≤8.27mV) overlapped with epicardial low bipolar voltage areas.[7] This may however also be explained by epicardial scar extending towards the endocardium. Further studies are needed to assess the exact 'field of view'.

Ablation target sites

Since extensive epicardial EAM is time-consuming, it may be preferable to map the area of interest only. Importantly, all target sites were projected on areas with transmural LE on MRI, suggesting that CE-MRI may be used to delineate the area of interest. The combination of all EAM parameters may be used when CE-MRI is not available.

Histology

Histology is the true gold standard to detect, quantify and characterize fibrosis, but its results, unlike CE-MRI, are not readily available during the procedure. Biopsy specimens revealed both interstitial and compact fibrosis in the majority of cases, although LE on MRI was only found remote from these areas. These findings may explain why electrogram characteristics were frequently abnormal even in the absence of LE on MRI. Interstitial fibrosis and small amounts of compact fibrosis not detected by CE-MRI may cause electrogram abnormalities, as activation fronts curve around lines of block created by such strands of fibrosis.[14] This is an important finding when considering CE-MRI as a gold standard for detection of fibrosis in NICM. Whether areas of fibrosis not detectable on CE-MRI are related to VT needs further evaluation.

Limitations

This study only analyzed mapping points that were projected on the LV epicardium and therefore, our findings do not apply to the RV epicardium. In addition, our findings only apply to the commonly used 3.5mm-tip catheters with a 2mm ring electrode and a 1mm interelectrode spacing. Although low voltage may have been caused by poor contact, this was unlikely as pericardial effusions were absent and the irrigant was removed frequently. One patient with an electroanatomical small basolateral scar not clearly visible on CE-MRI due to imaging artifacts, was excluded illustrating that CE-MRI and EAM may still be used in a complementary manner.

It should be noted that obtaining pre-procedural CT scans requires pre-procedural planning and is associated with radiation exposure. However, CT-derived coronary anatomy may also reduce the number of contrast injections before epicardial ablation and thus, reduce the radiation exposure during the procedure.

The relatively small number of mapping points, particularly in patients with idiopathic VA, may have limited the accuracy of the maps. The number of controls was small due to the fact that epicardial ablation is not required in the majority of patients with idiopathic VA. The number of NICM patients studied was also small because implanted devices frequently impeded CE-MRI acquisition. For patients in whom CE-MRI is not available during the procedure, we provide tools to distinguish scar from viable myocardium and fat.[9]

Clinical implications

Substrate mapping is of key importance during epicardial VT ablation since activation mapping cannot be performed in the majority of VTs. However, during epicardial EAM it may be difficult to distinguish scar from fat, as both are associated with attenuated bipolar electrogram amplitudes. Moreover, even in the absence of epicardial fat, scars may be difficult to detect if located intramurally. The current study provides insight into the value of different epicardial EAM parameters for detection of scar in patients with NICM. Our findings have important implications when EAM is performed at areas covered by ≥2.8mm fat, such as the basal LV[13] which is often affected in patients with NICM[3,15]. In addition, epicardial unipolar voltage mapping may be particularly useful for detection of intramural scars, which are common in patients with NICM[1] and cannot reliably be detected based on bipolar voltage and electrogram characteristics alone.

Magnetic resonance imaging is limited by the presence of devices and even if safe, it is significantly hampered by artifacts.[8] Computed tomography is however available in all patients and may be important not only to prove, but also to exclude the presence of epicardial fat. The combination of CT, unipolar voltage mapping and electrogram characteristics is likely to improve the accuracy of epicardial substrate mapping, which is important for successful catheter ablation of VT.

CONCLUSION

Bipolar voltage ≤1.81mV and unipolar voltage ≤7.95mV are the optimal cutoff values to differentiate between scar and viable myocardium during epicardial EAM, but both are attenuated by epicardial fat. Specific electrogram morphologies are not affected by fat, but can identify only one quarter of all scar sites. The proposed easy-to-use algorithm allows more accurate differentiation between scar and viable myocardium during epicardial EAM. Unipolar voltage, but not bipolar voltage can be used to identify intramural scar.

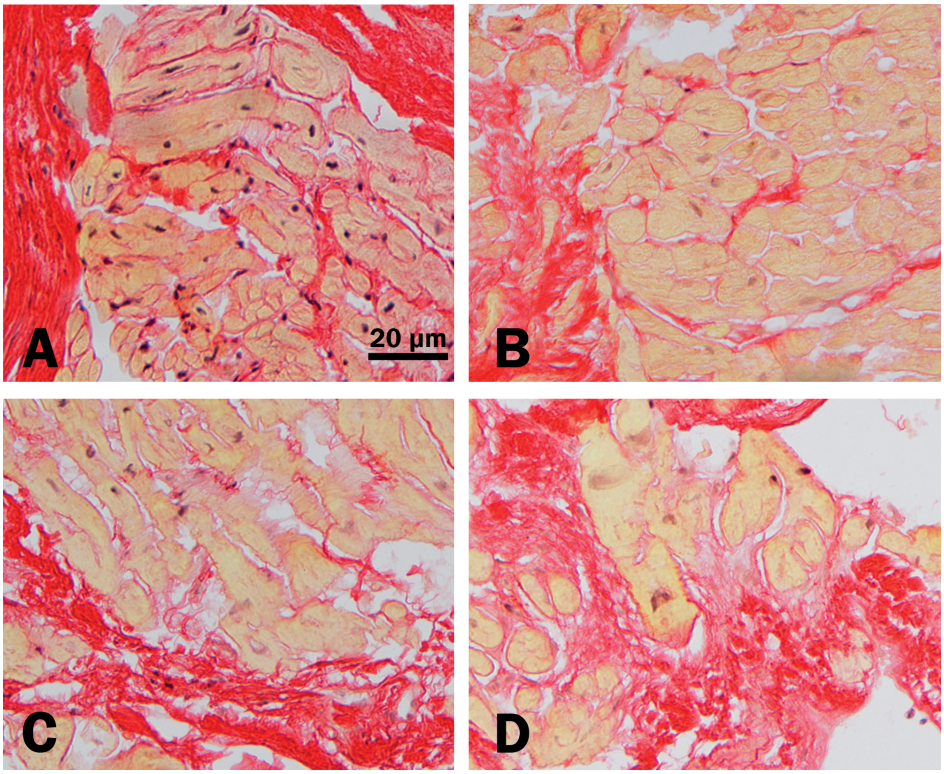
REFERENCE LIST

1. Bogun FM, Desjardins B, Good E, Gupta S, Crawford T, Oral H, Ebinger M, Pelosi F, Chugh A, Jongnarangsin K, Morady F. Delayed-enhanced magnetic resonance imaging in nonischemic cardiomyopathy: utility for identifying the ventricular arrhythmia substrate. J Am Coll Cardiol 2009;53(13):1138-45.
2. Cano O, Hutchinson M, Lin D et al. Electroanatomic substrate and ablation outcome for suspected epicardial ventricular tachycardia in left ventricular nonischemic cardiomyopathy. J Am Coll Cardiol 2009; 54(9):799-808.
3. Nakahara S, Tung R, Ramirez RJ, Michowitz Y, Vaseghi M, Buch E, Gima J, Wiener I, Mahajan A, Boyle NG, Shivkumar K. Characterization of the arrhythmogenic substrate in ischemic and nonischemic cardiomyopathy implications for catheter ablation of hemodynamically unstable ventricular tachycardia. J Am Coll Cardiol 2010;55(21):2355-65.
4. Tung R, Nakahara S, Ramirez R, Lai C, Fishbein MC, Shivkumar K. Distinguishing epicardial fat from scar: analysis of electrograms using high-density electroanatomic mapping in a novel porcine infarct model. Heart Rhythm 2010;7(3):389-95.
5. Desjardins B, Morady F, Bogun F. Effect of epicardial fat on electroanatomical mapping and epicardial catheter ablation. J Am Coll Cardiol 2010;56(16):1320-7.
6. de Bakker JM, van Capelle FJ, Janse MJ, Tasseron S, Vermeulen JT, de JN, Lahpor JR. Slow conduction in the infarcted human heart. 'Zigzag' course of activation. Circulation 1993;88(3):915-26.
7. Hutchinson MD, Gerstenfeld EP, Desjardins B et al. Endocardial unipolar voltage mapping to detect epicardial ventricular tachycardia substrate in patients with nonischemic left ventricular cardiomyopathy. Circ Arrhythm Electrophysiol 2011;4(1):49-55.
8. Dickfeld T, Tian J, Ahmad G, Jimenez A, Turgeman A, Kuk R, Peters M, Saliaris A, Saba M, Shorofsky S, Jeudy J. MRI-Guided ventricular tachycardia ablation: integration of late gadolinium-enhanced 3D scar in patients with implantable cardioverter-defibrillators. Circ Arrhythm Electrophysiol 2011;4(2):172-84.
9. Wijnmaalen AP, van der Geest RJ, van Huls van Taxis CF, Siebelink HM, Kroft LJ, Bax JJ, Reiber JH, Schalij MJ, Zeppenfeld K. Head-to-head comparison of contrast-enhanced magnetic resonance imaging and electroanatomical voltage mapping to assess post-infarct scar characteristics in patients with ventricular tachycardias: real-time image integration and reversed registration. Eur Heart J 2011;32(1):104-14.
10. Valles E, Bazan V, Marchlinski FE. ECG criteria to identify epicardial ventricular tachycardia in nonischemic cardiomyopathy. Circ Arrhythm Electrophysiol 2010;3(1):63-71.
11. Zeppenfeld K, Kies P, Wijffels MC, Bootsma M, van Erven L, Schalij MJ. Identification of successful catheter ablation sites in patients with ventricular tachycardia based on electrogram characteristics during sinus rhythm. Heart Rhythm 2005;2(9):940-50.
12. Cooper LT, Baughman KL, Feldman AM, Frustaci A, Jessup M, Kuhl U, Levine GN, Narula J, Starling RC, Towbin J, Virmani R. The role of endomyocardial biopsy in the management of cardiovascular disease: a scientific statement from the American Heart Association, the American College of Cardiology, and the European Society of Cardiology. Endorsed by the Heart Failure Society of America and the Heart Failure Association of the European Society of Cardiology. J Am Coll Cardiol 2007;50(19): 1914-31.

13. Abbara S, Desai JC, Cury RC, Butler J, Nieman K, Reddy V. Mapping epicardial fat with multi-detector computed tomography to facilitate percutaneous transepicardial arrhythmia ablation. Eur J Radiol 2006;57(3): 417-22.

14. de Bakker JM, van Capelle FJ, Janse MJ, Tasseron S, Vermeulen JT, de JN, Lahpor JR. Fractionated electrograms in dilated cardiomyopathy: origin and relation to abnormal conduction. J Am Coll Cardiol 1996;27(5):1071-8.

15. Hsia HH, Callans DJ, Marchlinski FE. Characterization of endocardial electrophysiological substrate in patients with nonischemic cardiomyopathy and monomorphic ventricular tachycardia. Circulation 2003; 108(6):704-10.



Supplemental Figure 1. Histologic examination of scar architecture in biopsy specimens.
Endomyocardial biopsy specimens from the right ventricular septum (upper panels) and from the apicolateral left ventricle (lower panels) distant from areas with late enhancement on MRI. All reveal both compact and interstitial fibrosis.

Chapter 4

Contrast-enhanced MRI-derived Scar Patterns and Associated Ventricular Tachycardias in Nonischemic Cardiomyopathy:

Implications for the Ablation Strategy

Sebastiaan R.D. Piers, MD, Qian Tao, PhD, Carine F.B. van Huls van Taxis, MD, Martin J. Schalij, MD, PhD, Rob J. van der Geest, PhD, Katja Zeppenfeld, MD, PhD

Circulation: Arrhythmia & Electrophysiology 2013;6(5):875-83

ABSTRACT

Background

There are limited data on typical arrhythmogenic substrates and associated ventricular tachycardias (VT) in patients with nonischemic cardiomyopathy (NICM). The substrate location may have implications for the ablation strategy.

Methods and results

Nineteen consecutive patients with NICM (age 58±14years, 79% male, LVEF 41±11%) who underwent contrast-enhanced MRI (CE-MRI) and VT ablation were included. Based on 3D CE-MRI-derived scar reconstructions, 8 patients (42%) had predominant basal anteroseptal scar, 9 (47%) predominant inferolateral scar and 2 (11%) other scar types. Three distinct VT morphologies (≥1 of 3 inducible in 16/19 patients) were associated with underlying scar type. In 9 patients with anteroseptal scar-related VT (8/9 predominant scar, 1/9 non-predominant), ablation target sites (defined as sites with ≥11/12 pacemap, concealed entrainment or VT termination during ablation) were located in the aortic root and/or anteroseptal left ventricular endocardium in 8 (89%) and in the anterior cardiac vein in 1 (11%), with additional target sites at the right ventricular septum in 2 (22%) and at the epicardium in 1 (11%). In contrast, in 8 patients with predominant inferolateral scar-related VT, target sites were located at the epicardium in 5 (63%) and in the endocardial, inferolateral LV in 3 (37%).

Conclusion

Two typical scar patterns (anteroseptal and inferolateral) account for 89% of arrhythmogenic substrates in patients with NICM. Three distinct VT morphologies are highly suggestive for the presence of these scars. Anteroseptal scars were in general most effectively approached from the aortic root or anteroseptal LV endocardium, whereas inferolateral scars frequently required an epicardial approach.

INTRODUCTION

The substrate for ventricular tachycardia (VT) in patients with non-ischemic cardiomyopathy (NICM) is typically located near the base of the left ventricle (LV) close to the valve annuli, with an intramural or subepicardial distribution pattern.[1-3] Isolated septal scars have been reported in approximately 12% of patients,[2] but may be difficult to detect by electroanatomical mapping (EAM),[2,4] thereby underestimating its prevalence. Viable myocardium overlying the substrate may prevent scar detection by bipolar EAM.[2,5] Unipolar voltage mapping has been suggested to have a larger 'field of view' than bipolar voltage mapping, allowing detection of subepicardial scars during endocardial mapping.[6] The exact size of this 'field of view' is however unclear and has not been validated by contrast-enhanced magnetic resonance imaging (CE-MRI), which is considered to be the gold standard to detect scar.

CE-MRI derived 3-dimensional (3D) scar reconstructions may provide insights into the geometry of the arrhythmogenic substrate[4] and its spatial relation to anatomical structures, which may have implications for the procedural strategy, the required access and potential limitations for ablation.

The 12-lead morphology of scar-related VT depends on 3D scar geometry and VT exit site, and may help to identify the substrate in patients in whom CE-MRI is not available. Distinct VT morphologies have been described in selected patients with NICM and isolated septal scars,[2] but not in other scar types.

The aims of the present study were 1) to identify typical MRI-derived scar patterns and the associated 12-lead VT morphologies in consecutive patients with NICM who underwent CE-MRI and VT ablation, 2) to evaluate its implications for the ablation strategy and 3) to analyze the value of bipolar and unipolar endocardial voltage mapping to detect the CE-MRI-derived VT substrate in patients with NICM.

METHODS

Patients

The study sample consisted of 19/21 consecutive patients with NICM who underwent CE-MRI and VT ablation. Two patients with poor CE-MRI image quality were excluded. Patients with coronary artery disease (>50% stenosis, assessed by coronary angiography in all patients), congenital heart disease, hypertrophic, arrhythmogenic right ventricular and restrictive cardiomyopathy, LV noncompaction, (sub)acute myocarditis, cardiac sarcoidosis, tachycardia-induced cardiomyopathy or primary valvular abnormalities were excluded. All patients were treated according to the routine clinical protocol and provided informed consent.

CE-MRI acquisition and processing

Contrast-enhanced MRI was performed on a 1.5 T Gyroscan ACS-NT/Intera MR system (Philips Medical Systems, Best, the Netherlands). A standardized protocol was followed, including cine MRI in long- axis (two- and four-chamber views) and short-axis covering the LV. In addition, the proximal aorta was imaged using a black-blood turbo spin-echo sequence. Contrast-enhanced images were acquired 15 min after bolus injection of gadolinium (Magnevist; Schering, Berlin, Germany; 0.15 mmol/kg) using a 3D turbo-field echo sequence with parallel imaging. The heart was imaged in one or two breath-holds with 20–24 imaging levels (dependent on heart size) in short-axis views. Images were acquired 600–700ms after the R-wave.

Using Mass research software, the centerline of the proximal coronary arteries was manually defined in the black-blood spin-echo image stack. The aortic, endocardial and epicardial contours were semi-automatically detected on short axis views and converted into 3D meshes. Myocardial tissue with 35-50% and ≥50% of maximal signal intensity were considered grey zone and core scar, respectively. The LV endocardial and epicardial meshes were color-coded for scar transmurality in the inner and outer half of the wall, respectively. All meshes were imported into the CARTO system using IPE-software (Figure 1).

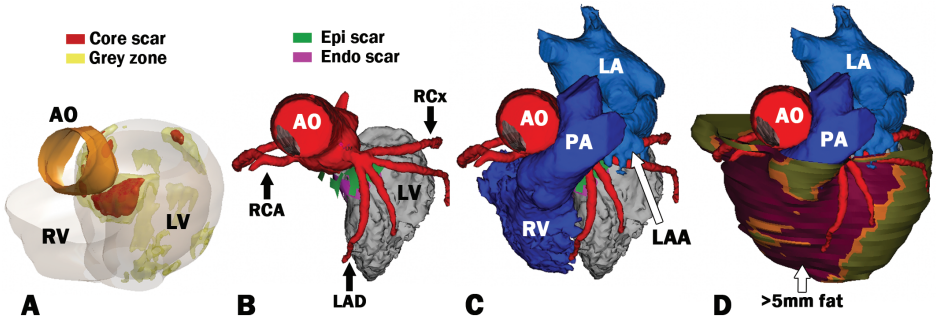


Figure 1. Example of a MRI-derived basal anteroseptal scar
In panel A the core scar is displayed in red, the grey zone in yellow. Based on fused CT- and MRI-derived information, the scar cannot be reached from the epicardium due to overlying coronary arteries (panel B), the pulmonary artery (panel C) and epicardial fat (panel D). In panels B and C, the scar in the endocardial half of the wall is displayed in purple, scar in the epicardial half in green.

CT acquisition and processing

Prior to epicardial ablation electrocardiogram-gated cardiac CT imaging was performed with an intravenous iodinated contrast agent. The endocardial, epicardial and pericardial contours were manually traced on short-axis reformatted CT slices to create 3D meshes color-coded for fat thickness (distance between epicardial and pericardial contours).[7,8] Subsequently, the original CT data and the 3D meshes were imported into the mapping system. These images were used during epicardial VT ablation procedures to avoid RF

applications in the close vicinity of coronary arteries and to provide detailed information on epicardial fat thickness, which may facilitate the interpretation of electrograms and explain ineffective RF applications.[7]

Electrophysiological evaluation

Anti-arrhythmic drugs were discontinued for at least 5 half-lives with the exception of amiodarone (n=2). Programmed electrical stimulation was performed before sedation and opioid administration. The simulation protocol consisted of 3 drive cycle lengths (600, 500 and 400ms) with 1-3 ventricular extrastimuli (≥200ms) from 2 right ventricular (RV) sites and burst pacing (CL≥200ms), repeated with isoproterenol (2-10μg/min) when necessary. Positive endpoint was induction of a sustained monomorphic VT (>30s or requiring termination because of hemodynamic compromise).

VT morphologies

All induced sustained monomorphic VTs were categorized as right or left bundle branch block-like (RBBB or LBBB) morphology (defined as predominant R or S V1), inferior or superior axis (predominant R or S in aVF), left or right axis (predominant R or S in I) and precordial transition (first lead with a predominant R or S for LBBB and RBBB VTs, respectively).

Electroanatomical mapping, real-time image integration and ablation

Epicardial access was obtained through a subxyphoid puncture. Electroanatomical bipolar and unipolar voltage mapping was performed using a 3.5mm irrigated-tip catheter (2mm ring electrode, 1mm interelectrode spacing; NaviStar ThermoCool, Biosense Webster Inc, Diamond Bar, CA, USA) and the CARTO system. Electrograms were filtered at 30-400Hz (bipolar) and 1-240Hz (unipolar). Limited EAM of the aortic root was performed and the position of the left main coronary artery, confirmed by undiluted contrast injection through the mapping catheter, was tagged on the map. The LV was mapped retrogradely focusing on the MRI-derived scar areas. The RV was mapped if indicated. CE-MRI-derived images were aligned with the EAM using the left main landmark. Then, the LV surfaces were aligned with the translation tool until the lowest mean surface registration error was reached. The CT-derived coronary anatomy and epicardial fat meshes were integrated with the EAM in patients who underwent epicardial mapping, as previously described.[8]

Potential re-entry circuit sites targeted for ablation were identified based on activation mapping and entrainment mapping for stable VT. For unstable VT, the area of interest was identified by substrate mapping and pace mapping. Then, VT was reinduced and briefly mapped in an attempt to identify diastolic activity and terminate the VT by ablation. For analyses purposes, ablation target sites were defined as sites with 1) ≥11/12

Table 1. Baseline characteristics and procedural data

	All patients (n=19)	Predominant anteroseptal scar (n=8)	Predominant inferolateral scar (n=9)
Age	58±14	61±12	56±16
Male	15(79%)	7(88%)	7(78%)
LV ejection fraction, %	41±11	40±8	44±15
LV end-diastolic volume, mL	230±73	224±36	237±102
History of atrial flutter/fibrillation	3(16%)	2(25%)	1(11%)
BMI, kg/m^2	26.4±4.2	27.8±5.2	26.2±2.8
Diabetes mellitus	2(11%)	0(0%)	2(22%)
eGFR < 60 mL/min	2(11%)	1(13%)	1(11%)
Number of VTs induced	2(1-3)	3(2-6)	2(1-4)
BBR VT	0(0%)	0(0%)	0(0%)
Unstable VT	14(74%)	5(62%)	7(78%)
Mean CL of induced VTs	298±69	308±75	304±68
LV endocardial mapping	19(100%)	8(100%)	9(100%)
Low bipolar voltage area, cm^2	8.7(3.1-15.0)	9.9(4.1-14.1)	5.1(0.35-15.7)
Low unipolar voltage area, cm^2	14.4(7.1-27.9)	12.9(7.3-27.7)	14.4(0.7-27.5)
Electrogram abnormalities*	11/6/2	5/3/0	5/3/1
Epicardial mapping	11(58%)	3(38%)	7(78%)
Low bipolar voltage area, cm^2	28.4(20.0-41.3)	20.0(16.6-22.7)	34.1(28.4-46.8)
Low unipolar voltage area, cm^2	47.1(16.4-55.9)	16.4(15.0-16.6)	51.6(35.0-55.9)
Electrogram abnormalities*	9/1/1	2/0/1	7/0/0
Epicardial ablation	8(42%)	2(25%)	6(67%)
Procedural duration, minutes	218±83	230±117	225±44
Fluoroscopy time, minutes	49±19	55±26	46±7
Acute outcome			
Complete success	10(53%)	4(50%)	5(56%)
Partial success	6(32%)	3(38%)	3(33%)
Failure	3(16%)	1(13%)	1(11%)

Other scar types in 2 patients are not described separately

*Specific (double, fragmented or late potential)/only other abnormal/none

pace map and/or 2) concealed entrainment suggestive for a central isthmus or exit site and/or 3) VT slowing and termination during ablation.

At the epicardium, ablation was usually withheld when the estimated distance to a coronary artery was <5mm, as assessed by integrated CT-derived coronary anatomy and coronary angiography.[7] High output pacing (10mA, 2ms) was performed to determine the location of the phrenic nerve. Radiofrequency (RF) energy was applied at 30-45W

(maximum temperature 45°C, flow 20-30ml/min, 60s) for endocardial sites and up to 50W (flow 20ml/min) for epicardial sites.

Acute and long-term outcome

After ablation, the entire stimulation protocol was repeated. Isoprenaline was administered if required to induce VT before ablation. Complete procedural success was defined as non-inducibility of any sustained monomorphic VT; partial success as elimination of the clinical VT but inducibility of ≥1 nonclinical VT; failure as inducibility of the clinical VT. Patients were followed at 3, 6 and 12 months and at 6- to 12-monthly intervals thereafter.

Contrast-enhanced MRI-derived 3D scar reconstructions

Based on the short-axis slices, 3D scar reconstructions were created (MATLAB software, version 2009b). For each patient, the MRI-derived scar transmurality (including core and grey zone) was calculated and displayed on a bull's eye image containing the 17 LV segments. Based on the reconstructions, the locations of the predominant (i.e. largest) scar and of additional scars (defined as scars involving ≥25% of a remote segment) were assessed. The scar distribution within the LV wall was determined by calculating the average endocardial and epicardial viable layers for each scar.

After the procedure, all mapping points were superimposed on the MRI-derived 3D scar reconstruction. For each point, a 5mm-diameter transmural cylinder was created and the presence of late enhancement and the thickness of the endocardial viable layer were assessed.

Statistical analysis

Categorical variables are displayed as number (percentage) and continuous variables as mean±SD or median (first-to-third quartile [Q1-to-Q3]). Categorical variables were compared using the Chi-square test or Fisher's exact test. Continuous variables were compared using the Student's t-test when normally distributed, or the Mann-Whitney U test when non-normally distributed. Mapping point-based receiver operating characteristic curve analysis was performed to determine the optimal cut-off values of bipolar and unipolar voltage for scar detection, defined as the values maximizing the sum of sensitivity and specificity. An additional cutoff value with a fixed specificity of 80% was calculated for unipolar voltage. The bipolar and unipolar voltage of mapping points at scars with an endocardial viable layer of 0-2mm, 2-4mm, 4-6mm, 6-8mm, >8mm and non-scar areas were averaged in each patient. Paired T-tests were subsequently performed to analyze the difference between the average voltage at non-scar areas and the average voltage at scar areas with different endocardial viable layers in the same patient. All analyses were performed with SPSS v20.0 (SPSS Inc., Chicago, Illinois). All p-values are two-sided and p-values <0.05 were considered significant.

RESULTS

Patients

Nineteen patients (age 58±14 years, 15 [79%] male, LV ejection fraction 41±11%) underwent VT-ablation with CE-MRI integration. In 11 patients who underwent epicardial mapping, CT-derived coronary anatomy and epicardial fat thickness were also integrated. Baseline characteristics are summarized in Table 1. None of the patients had documented pericarditis or myocarditis. Three patients (16%) had a family history of NICM/sudden cardiac death.

Typical MRI-derived scar patterns

As illustrated by the bull's eye plot color-coded for the average MRI-derived scar transmurality (Figure 2), two typical scar patterns could be identified. One was located in the basal anteroseptal segment (referred to as *anteroseptal scar*) and the other in the basal/mid inferior, inferolateral and/or lateral segments (referred to as *inferolateral scar*). A predominant anteroseptal scar was present in 8/19 patients (42%) and a predominant inferolateral scar in 9 (47%, Figure 3). Of the remaining 2 patients (11%), one had a subepicardial inferoapical scar and the other had a subepicardial scar along the anterior interventricular groove.

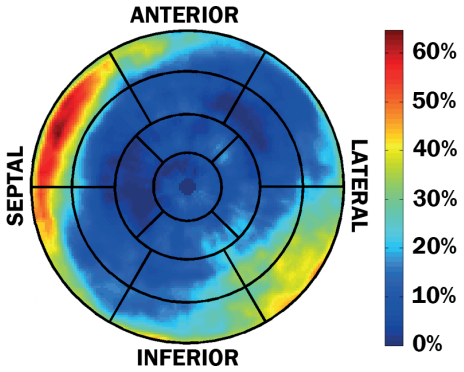


Figure 2. Scar distribution
In each patient the 3D scar reconstruction was used to create a 17-segment bull's eye image displaying the scar transmurality. These data were subsequently averaged to create a single bull's eye image color-coded for the average scar transmurality in all patients, which is displayed continuously from highest (in red) to lowest (in blue).

Two of 8 patients (25%) with a predominant anteroseptal scar also had a smaller inferolateral scar, and 6/9 patients (67%) with a predominant inferolateral scars also had a smaller anteroseptal scar.

Distinct ECG patterns of VTs

A total of 60 VTs were induced (median 2 VTs per patient; Q1-to-Q3, 1–3). Three distinct ECG patterns were observed (Figure 4):

1) RBBB, left/right inferior axis, positive concordance (Panel A) in 12 induced VTs (20%) in 8 patients (42%);
2) LBBB, left/right inferior axis, early (≤V3) precordial transition (Panel B) in 7 induced VTs (12%) in 6 patients (32%);

3) RBBB, right inferior/superior axis, late (≥V5) precordial transition (Panel C) in 6 induced VTs (10%) in 6 patients (32%);

Together, 25 of 60 VTs (42%) had one of these three morphologies. All patients with type 1 or type 2 VTs had anteroseptal scar; all patients with type 3 VTs had inferolateral scar. A less distinct ECG pattern, LBBB VTs with a superior axis and varying transition, was observed in patients with anteroseptal, inferolateral or non-typical scar extending to the inferoseptum. Sixteen of 19 patients (84%) had at least one type 1, 2 or 3 VT. The remaining 3 patients (16%) had extension of the scar on CE-MRI consistent with the VT morphology.

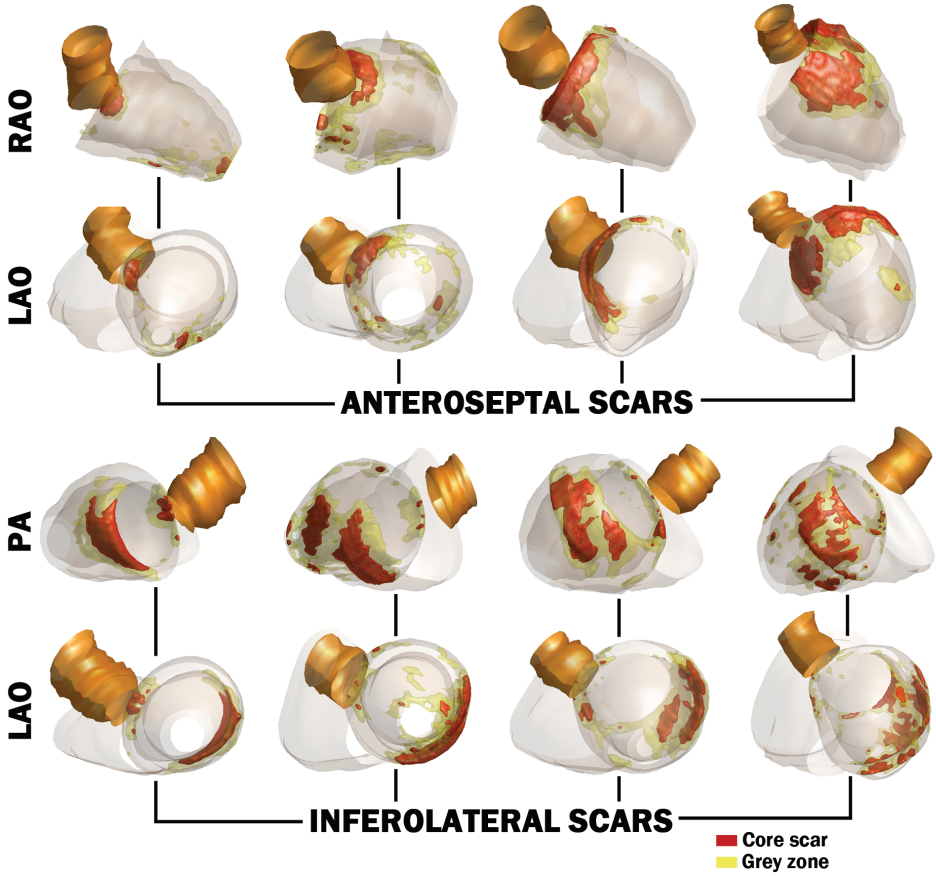


Figure 3. Typical scars

Typical examples of basal anteroseptal scars are shown in right anterior oblique (RAO) and left anterior oblique (LAO) views, typical inferolateral scars in posterior-anterior (PA) and left anterior oblique (LAO) views. Red indicates core scar; yellow, grey zone.

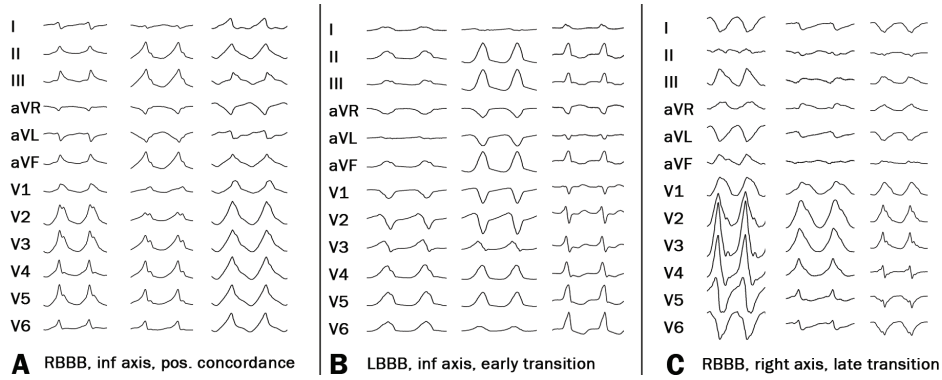


Figure 4. Distinct ECG patterns of ventricular tachycardias
RBBB denotes right bundle branch block; inf, inferior; LBBB, left bundle branch block.

Electroanatomical substrate mapping and ablation target sites

Procedural data are summarized in Table 1. CE-MRI-derived data were successfully integrated in all patients (mean registration error 3.7±0.8mm). Substrate mapping of the LV (all patients, mean 128 points) and the epicardium (11 patients [58%], mean 155 points) was performed focusing on the area of interest as identified by MRI (Table 1 and Figure 5).

A ≥11/12 pacemap was obtained for 31 VTs (52%). Diastolic potentials were identified during 26 VTs (43%) and for 7 VTs (12%) concealed entrainment was suggestive for a central isthmus or exit site (stimulus-QRS 43 – 254ms). Eighteen VTs (30%) slowed and terminated during RF applications after a median of 9 seconds (Q1-to-Q3, 7–13 sec) without premature ventricular contraction. Overall, ablation target sites were identified for 40 VTs (67%). The locations of these target sites are displayed in Figure 6. All target sites were located within 10mm of the CE-MRI-derived scar area.

In 9 patients with basal anteroseptal scar-related VT (predominant in 8), target sites were located in the aortic root and/or basal anteroseptal LV endocardium in 8 (89%) and in the anterior cardiac vein in 1 (11%), with additional target sites at the RV septum in 2 (22%) and at the basal anterior epicardium in 1 (11%).

In contrast, in 8 patients inferolateral scar-related VT (all predominant scars), target sites were located at the inferolateral epicardium in 5 patients (63%) and in the inferolateral endocardial LV in 3 (37%, both endocardial and epicardial target sites in one), with an additional target site at the epicardial RV outflow tract in one. No target sites could be identified in one patient.

Anatomical limitations of mapping and ablation

In patients with a predominant anteroseptal scar, ablation was limited by the proximity of the proximal conduction system in 2 (25%) and by the left main ostium in another 2 (25%). Based on integrated CT- and MRI-derived information, the entire scar could not

be reached from the epicardium due to the RV, pulmonary artery, overlying coronary arteries and/or epicardial fat in 5 patients (63%, Figure 1) and only part of the scar could be

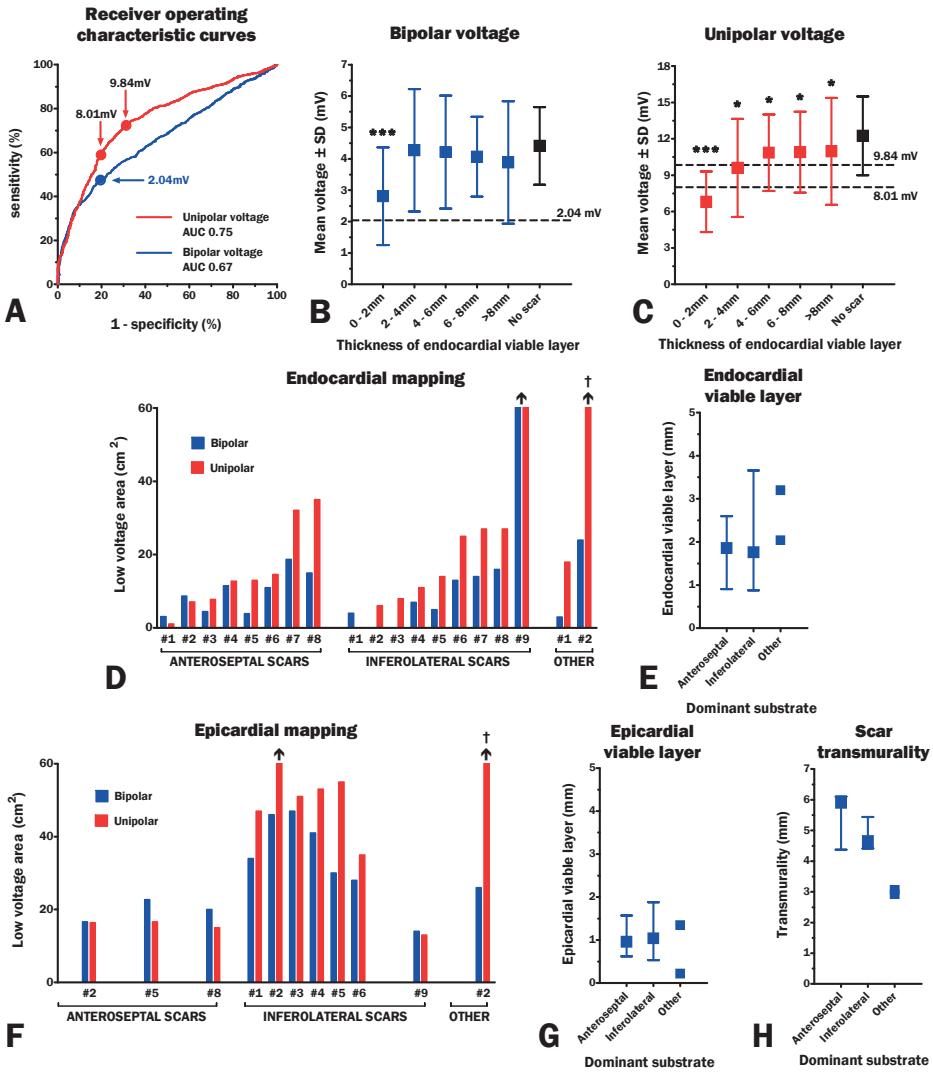


Figure 5. Bipolar vs. unipolar voltage mapping and scar features

Panel A: Receiver operating characteristic curve analysis for bipolar/unipolar voltage and MRI-derived scar. Panel B: Endocardial bipolar voltage is decreased only when the endocardial viable layer is <2mm thick. Panel C: Endocardial unipolar voltage was affected by scar involving the endocardial 4mm and, but less pronounced, by scar >4mm from the endocardium. Panel D: Endocardial low voltage areas. Panel E, G and H: Subendocardial and subepicardial viable layers and scar transmurality. Panel F: Epicardial low voltage areas in patients who underwent epicardial mapping. *** indicates $p < 0.001$ vs. no scar; *, $p < 0.05$ vs. no scar; †, One patient with a relatively thin LV wall (6.3±1.5mm) had low unipolar voltage at the entire endocardium and epicardium. AUC denotes area under the curve.

reached in the remaining 3 patients (37%). In 3 patients with an anteroseptal substrate epicardial mapping and ablation was performed after image integration. The expected epicardial accessibility of the scar was confirmed in these patients (only part of the scar reachable in 2, the entire scar not reachable in one).

In patients with a predominant inferolateral scar and endocardial ablation target sites, endocardial ablation was not limited. Based on integrated CT-derived information, coronary angiography and high-output pacing, RF applications had to be withheld at the epicardium due to the right coronary artery or the obtuse marginal branch in 3/7 patients (43%) and due to phrenic nerve capture in one.

Contrast-enhanced MRI-derived 3D scar reconstructions

A total of 2444 points acquired in the LV were projected on 3D scar reconstructions. Scar was present at 1146 sites (47%). For endocardial bipolar voltage the optimal cut-

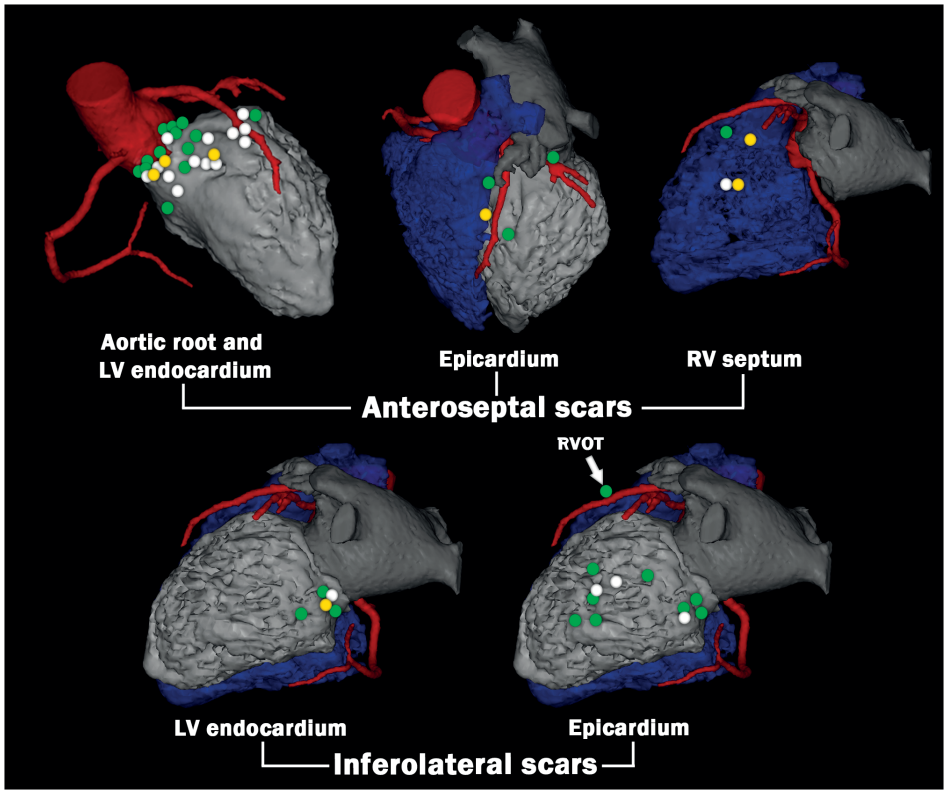


Figure 6. Ablation target sites.
Ablation target sites in all patients projected on the computed tomography-derived anatomy of a single patient. Green points indicate ≥11/12 pace maps; yellow points, concealed entrainment sites suggestive for a diastolic part of the re-entry circuit; white points, VT termination sites. LV denotes left ventricle; RV, right ventricle; RVOT, right ventricular outflow tract.

off value to differentiate between scar and viable myocardium was 2.04mV (AUC 0.67, sensitivity 48%, specificity 81%, Figure 5). For endocardial unipolar voltage the optimal cut-off value was 9.84mV (AUC 0.75, sensitivity 73%, specificity 69%). The specificity could be increased to 80% using a cut-off value of 8.01mV, which resulted in a sensitivity of 59%. Endocardial bipolar voltage was only affected by scar involving the endocardial 2mm, whereas endocardial unipolar voltage was affected by scar involving the endocardial 4mm and, less pronounced, by scar >4mm from the endocardium (Figure 5). Two patients (one with a basal anteroseptal scar and one with an inferolateral scar) had an epicardial scar identified by MRI that significantly exceeded small endocardial bipolar and unipolar low voltage areas (example in Figure 7).

Low bipolar and unipolar voltage areas, thickness of endocardial and epicardial viable layers and average scar transmurality were similar for anteroseptal and inferolateral scars (all p>0.05; Figure 5, panels D-H).

Acute and long-term procedural outcome

Complete success was achieved in 10 patients (53%), partial success in 6 (32%) and ablation failed in 3 (16%). The acute procedural outcome did not differ between patients with a predominant anteroseptal or inferolateral scar (Table 1). Seventeen of 19 patients (90%) were discharged with an implantable cardioverter defibrillator (ICD). During a median 15 (Q1-to-Q3, 11–27) months follow-up, 7/19 patients (37%) had VT recurrence (4/8 with a predominant anteroseptal scar, 2/9 with a predominant inferolateral scar, 1/2 with other scar type). The 6-month VT burden was reduced by ≥75% in 16/19 patients (84%). One patient died due to a lung cancer.

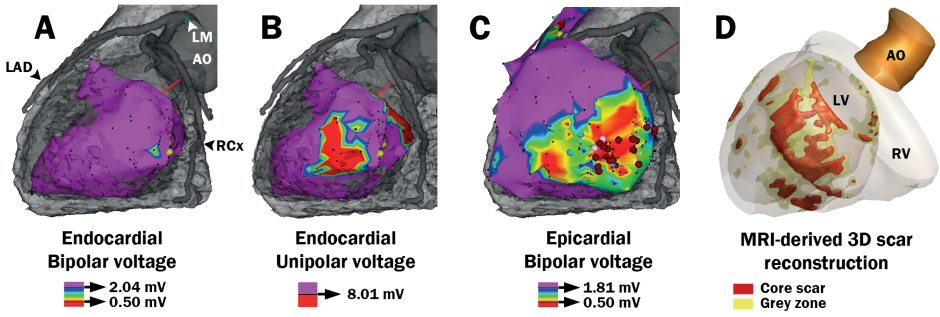


Figure 7. Example of electroanatomical maps and a 3D scar reconstruction

Endocardial bipolar (panel A) and unipolar (panel B) voltage maps, epicardial bipolar voltage map (panel C) with integrated CT-derived anatomy, and the MRI-derived 3D scar reconstruction (panel D). Voltages are color coded as indicated by the color bars. AO indicates aorta; LAD, left anterior descending coronary artery; LM, left main coronary artery; LV, left ventricle; RCx, circumflex coronary artery; RV, right ventricle.

DISCUSSION

In the present study, CE-MRI-derived scar was associated with VT in patients with NICM. Two typical scar patterns (i.e., anteroseptal and/or inferolateral scars) were present in 89% of patients referred for VT ablation. Three distinct 12-lead ECG morphologies of VTs were common and diagnostic for a typical scar pattern. Ablation target sites in patients with a basal anteroseptal scar were mainly identified in the aortic root and the basal anteroseptal LV endocardium, whereas target sites in patients with an inferolateral scar were located at the epicardium in 63% of patients. The typical scar patterns may therefore have implications for the mapping and ablation strategy. Endocardial EAM is insufficient to delineate these scars, as endocardial bipolar voltage was only affected by scar involving the endocardial 2mm, and endocardial unipolar voltage by scar involving the endocardial 4mm and, less pronounced, by scar >4mm from the endocardium.

Typical arrhythmogenic substrates

Prior studies have described arrhythmogenic substrates in NICM, but have not systematically used CE-MRI as a gold standard for scar detection.[2,9] In the current study, the EAM and CE-MRI-derived 3D scar reconstructions allowed a detailed evaluation of the arrhythmogenic substrate.

Importantly, all ablation target sites were located within 10mm of the CE-MRI-derived scar area. A predominant basal anteroseptal scar was present in 42% of patients but often associated with only a small endocardial low bipolar voltage area, difficult to distinguish from a normal low voltage area at the membranous part of the interventricular septum. In this group endocardial target sites could be identified in all but one patient. The ablation was withheld due to the location of the conduction system in one patient and caused expected atrioventricular block in another. Epicardial mapping in the presence of this scar pattern was considered impossible due to or hampered by overlying coronary arteries, fat and the left atrial appendage.

Although basal anteroseptal scars have been described in prior studies and two case reports[2-4,9,10], they are reported to occur in only 11.3% of NICM patients.[2] Based on the current data and two prior studies, these scars may however be difficult to detect by substrate mapping[2,4] and as a result, scar-related VTs may even be mistaken for benign idiopathic outflow tract VTs, which may have important prognostic and therapeutic consequences.[4]

A predominant inferolateral scar was present in 47% of patients but also difficult to detect by endocardial bipolar voltage mapping. Endocardial unipolar voltage mapping allowed improved but still limited scar detection. Epicardial mapping was not limited and epicardial target sites were identified in 63% of these patients. Epicardial ablation was however partly withheld due to coronary arteries and the phrenic nerve.

In the current study, CE-MRI served as a gold standard for LV scar. For both scar patterns endocardial bipolar voltage was only affected by scar involving the endocardial 2mm, whereas endocardial unipolar voltage was affected by scar involving the endocardial 4mm and, less pronounced, by scar >4mm from the endocardium. . Accordingly, the sensitivity for bipolar and unipolar voltage mapping to detect scar in the NICM population is poor with an overall sensitivity of 48% and 59%, respectively. Therefore CE-MRI should be considered in all patients with suspected NICM before VT ablation and ICD implantation.

In only one patient in our study a causative mutation (phospholamban) for NICM has been identified (yet) and none had a history of myocarditis. However, typical septal and/or inferolateral scars have been described in various diseases, such as myocarditis,[11] arrhythmogenic right ventricular cardiomyopathy/dysplasia with LV involvement,[12] laminopathy[13] and Anderson-Fabry disease[14]. Rather than disease specific, these areas may be more vulnerable to various insults resulting in fibrosis and ultimately VT.

Typical 12-lead ECG VT morphologies

At least one of three distinct VT morphologies was observed in 84% of patients and these morphologies were related to the two scar patterns. Documentation of these distinct morphologies may be helpful if CE-MRI is not available. Two typical VT morphologies have been previously described in patients with NICM but only with isolated septal scars, including inferior limb discordance (dominant R in II and dominant S in III, or the opposite) in 16% of VTs, and precordial transition break in V2 (qR/Rs morphology in V1 and V3 but reversal of this in V2) in 24% of VTs.[2] In the current study, each criterion was observed in 5/37 induced VTs (14%) in 2/8 patients (25%) with a predominant anteroseptal scar.

Implications for the procedural strategy

VTs related to basal anteroseptal scar were effectively approached from the aortic root or basal anteroseptal LV endocardium, whereas VTs related to an inferolateral scar often required an epicardial approach. This finding may influence the procedural strategy in patients with NICM and a typical substrate based on imaging or a distinct VT morphology. An initial endocardial approach may be appropriate in patients with a presumed basal anteroseptal substrate. A retrograde approach to the LV may be preferred over an antegrade approach, allowing mapping in the aortic sinus cusps. In patients with an inferolateral scars, epicardial mapping and ablation are likely to be necessary and an initial combined endocardial and epicardial approach may be reasonable.

Limitations

Although the present study demonstrates a clear predilection for scars in the basal anteroseptal and inferolateral segments, there may be nonischemic scar distributions (and associated VT morphologies) that are not identified in this study. The number of patients was limited, as only patients without an implantable device underwent CE-MRI. No ablation target sites could be identified for 33% of VTs, which may be due to intramural circuits or subepicardial circuits in areas covered with fat. Epicardial mapping was not performed in 4 patients with non-complete procedural success because the septal substrate was likely not accessible from the epicardium based on CE-MRI.

CONCLUSION

Basal anteroseptal and inferolateral scars account for 89% of arrhythmogenic substrates in patients with NICM. Typical VT morphologies, observed in 84%, may help to identify the underlying substrate. Basal anteroseptal scars were in general most effectively approached from the aortic root or basal anteroseptal LV endocardium, whereas inferolateral scars frequently required an epicardial approach. These findings are likely to have implications for the procedural strategy in patients with NICM who are referred for VT ablation.

CLINICAL PERSPECTIVE

Ventricular tachycardia ablation in patients with nonischemic left ventricular cardiomyopathy is considered to be chal- lenging, which may partly because of the frequent intramural and subepicardial location of the arrhythmogenic substrate. Relatively little is known about typical scar patterns and its implications for the ablation strategy. In the present study, 19 consecutive patients with nonischemic cardiomyopathy who underwent contrast-enhanced MRI and ventricular tachycardia ablation are described. Two contrast-enhanced MRI–derived scar patterns (ie, basal anteroseptal and inferolateral) accounted for 89% of arrhythmogenic substrates, and 3 distinct 12-lead ECG morphologies of ventricular tachycardias were common and diagnostic for an underlying scar pattern. Basal anteroseptal scars were most effectively approached from the aortic root or basal anteroseptal left ventricular endocardium, and they were usually not well accessible from the epicardium, suggest- ing that an initial endocardial approach may be reasonable in these patients. In patients with inferolateral scars, however, an initial epicardial approach may be considered because epicardial ablation target sites were frequently identified in these patients. Endocardial electroanatomical voltage mapping could identify these scars only to a limited extent, with endocardial bipolar voltage only being affected when the scar involved the endocardial 2 mm and endocardial unipolar voltage when the scar involved the endocardial 4 mm and, less pronounced, by scar >4 mm from the endocardium. These findings provide insights into the arrhythmogenic substrate in patients with nonischemic cardiomyopathy and may have important practi- cal implications for preprocedural planning and intraprocedural substrate identification in patients undergoing ventricular tachycardia ablation.

REFERENCE LIST

1. Nakahara S, Tung R, Ramirez RJ, Michowitz Y, Vaseghi M, Buch E, Gima J, Wiener I, Mahajan A, Boyle NG, Shivkumar K. Characterization of the arrhythmogenic substrate in ischemic and nonischemic cardiomyopathy implications for catheter ablation of hemodynamically unstable ventricular tachycardia. J Am Coll Cardiol 2010;55(21):2355-65.
2. Haqqani HM, Tschabrunn CM, Tzou WS et al. Isolated septal substrate for ventricular tachycardia in nonischemic dilated cardiomyopathy: incidence, characterization, and implications. Heart Rhythm 2011;8(8): 1169-76.
3. Soejima K, Stevenson WG, Sapp JL, Selwyn AP, Couper G, Epstein LM. Endocardial and epicardial radiofrequency ablation of ventricular tachycardia associated with dilated cardiomyopathy: the importance of low-voltage scars. J Am Coll Cardiol 2004; 43(10):1834-42.
4. Tian J, Ahmad G, Mesubi O, Jeudy J, Dickfeld T. Three-dimensional delayed-enhanced cardiac MRI reconstructions to guide ventricular tachycardia ablations and assess ablation lesions. Circ Arrhythm Electrophysiol 2012;5(2):e31-e35.
5. Desjardins B, Morady F, Bogun F. Effect of epicardial fat on electroanatomical mapping and epicardial catheter ablation. J Am Coll Cardiol 2010;56(16):1320-7.
6. Hutchinson MD, Gerstenfeld EP, Desjardins B et al. Endocardial unipolar voltage mapping to detect epicardial ventricular tachycardia substrate in patients with nonischemic left ventricular cardiomyopathy. Circ Arrhythm Electrophysiol 2011;4(1):49-55.
7. van Huls van Taxis CF, Wijnmaalen AP, Piers SR, van der Geest RJ, Schalij MJ, Zeppenfeld K. Real-Time Integration of MDCT-Derived Coronary Anatomy and Epicardial Fat: Impact on Epicardial Electroanatomic Mapping and Ablation for Ventricular Arrhythmias. JACC Cardiovasc Imaging 2013;6(1):42-52.
8. Piers SR, van Huls van Taxis CF, Tao Q, van der Geest RJ, Askar SF, Siebelink HM, Schalij MJ, Zeppenfeld K. Epicardial substrate mapping for ventricular tachycardia ablation in patients with non-ischaemic cardiomyopathy: a new algorithm to differentiate between scar and viable myocardium developed by simultaneous integration of computed tomography and contrast-enhanced magnetic resonance imaging. Eur Heart J 2012;34(8):586-96.
9. Yokokawa M, Good E, Crawford T, Jongnarangsin K, Chugh A, Pelosi F, Jr., Oral H, Morady F, Bogun F. Ventricular tachycardia originating from the aortic sinus cusp in patients with idiopathic dilated cardiomyopathy. Heart Rhythm 2011;8(3):357-60.
10. Yamashina Y, Yagi T, Namekawa A, Ishida A, Sato H, Nakagawa T, Sakuramoto M, Sato E, Yambe T. Reentrant Ventricular Outflow Tract Tachycardia Arising from Focal Scar Detected by Delayed Enhancement Magnetic Resonance Imaging. Pacing Clin Electrophysiol 2012.
11. Mavrogeni S, Spargias C, Bratis C, Kolovou G, Markussis V, Papadopoulou E, Constadoulakis P, Papadimitropoulos M, Douskou M, Pavlides G, Cokkinos D. Myocarditis as a precipitating factor for heart failure: evaluation and 1-year follow-up using cardiovascular magnetic resonance and endomyocardial biopsy. Eur J Heart Fail 2011;13(8):830-7.
12. Corrado D, Basso C, Thiene G et al. Spectrum of clinicopathologic manifestations of arrhythmogenic right ventricular cardiomyopathy/dysplasia: a multicenter study. J Am Coll Cardiol 1997;30(6):1512-20.

13. Holmstrom M, Kivisto S, Helio T et al. Late gadolinium enhanced cardiovascular magnetic resonance of lamin A/C gene mutation related dilated cardiomyopathy. J Cardiovasc Magn Reson 2011;13(30.

14. Moon JC, Sachdev B, Elkington AG, McKenna WJ, Mehta A, Pennell DJ, Leed PJ, Elliott PM. Gadolinium enhanced cardiovascular magnetic resonance in Anderson-Fabry disease. Evidence for a disease specific abnormality of the myocardial interstitium. Eur Heart J 2003; 24(23):2151-5.

Chapter 5

CMR-based Identification of Critical Isthmus Sites of Ischemic and Nonischemic Ventricular Tachycardia

Sebastiaan R.D. Piers, MD, Qian Tao, PhD,
Marta de Riva Silva, MD, Hans-Marc Siebelink, MD, PhD, Martin J. Schalij, MD, PhD,
Rob J. van der Geest, PhD, Katja Zeppenfeld, MD, PhD

JACC: Cardiovascular Imaging 2014;7(8):774-84

ABSTRACT

Objective

This study evaluates whether contrast-enhanced (CE) cardiac magnetic resonance (CMR) can be used to identify critical isthmus sites for ventricular tachycardia (VT) in ischemic and nonischemic heart disease.

Background

Fibrosis interspersed with viable myocytes may cause re-entrant VT. CE-CMR has the ability to accurately delineate fibrosis.

Methods

Patients who underwent VT ablation with CE-CMR integration were included. After the procedure critical isthmus sites (defined as sites with a ≥11/12 pacemap, concealed entrainment or VT termination during ablation) were projected on CMR-derived 3D scar reconstructions. The scar transmurality and signal intensity at all critical isthmus, central isthmus and exit sites were compared to the average of the entire scar. The distance to >75% transmural scar and to the core-border zone (BZ) transition was calculated. The area within 5mm of both >75% transmural scar and core-BZ transition was calculated.

Results

In 44 patients (23 ischemic/21 nonischemic, LVEF 44±12%) a total of 110 VTs were induced (CL 290±67ms). Critical isthmus sites were identified for 78 VTs (71%) based on ≥11/12 pacemap (67 VTs) and/or concealed entrainment (10 VTs) and/or termination (30 VTs). The critical isthmus sites, and in particular central isthmus sites, had high scar transmurality and signal intensity compared to the average of the entire scar. Of the pacemap, concealed entrainment and termination sites 74%, 100% and 84% were within 5mm of >75% transmural scar, and 67%, 100% and 94% were within 5mm of core-BZ transition. The areas within 5mm of both >75% transmural scar and core-BZ transition (median 13% of LV) contained all concealed entrainment sites and 77% of termination sites.

Conclusion

Both in ischemic and nonischemic VT, critical isthmus sites are typically located in close proximity to the CMR-derived core-BZ transition and to >75% transmural scar. These findings suggest that CMR-derived scar characteristics may guide to critical isthmus sites during VT ablation.

INTRODUCTION

The aim of ventricular tachycardia (VT) ablation is to eliminate critical isthmuses, which can be identified by pacemapping, entrainment mapping and termination of VT by ablation. Applying these techniques is limited by the inducibility of multiple and often hemodynamically untolerated VTs, intramural location of some critical isthmuses, epicardial fat, and other factors.

Fibrotic areas interspersed with viable myocytes can form the substrate for reentrant VTs. Contrast-enhanced (CE) cardiac magnetic resonance (CMR) can accurately delineate areas with dense fibrosis and CE-CMR-derived data have been successfully integrated with electroanatomical maps (EAM) during VT ablation with high registration accuracy.[1-7] Integrated CE-CMR scar data may guide to the scar area and uncover intramural and subepicardial scars.[1-4]

Although CE-CMR may help to identify scar areas causing VT, there are limited data on specific CMR-derived scar characteristics at critical isthmus sites, which may be useful to guide ablation. Features of interest are scar transmurality, which has been associated with slow conduction ,[2,4,7,8] and signal intensity (SI), which has been used to identify conducting channels[5,6] and to delineate core scar and border zone (BZ). Importantly, to date no study has analyzed the value of CMR-derived scar characteristics to identify areas containing critical isthmuses, thereby potentially guiding substrate-based VT ablation.

The aims of the present study are: (1) to assess CMR-derived scar characteristics at critical isthmus sites of ischemic and nonischemic VT and (2) to determine the potential value of CMR to delineate areas containing critical isthmus sites for imaging-guided VT ablation.

METHODS

Patients

The study population consisted of 44/48 consecutive patients with prior myocardial infarction (MI, n=23) or nonischemic cardiomyopathy (NICM, n=21) who underwent VT ablation with integration of CE-CMR. Three patients were excluded because of non-interpretable CE-CMR and one because critical isthmus sites could not be reliably identified due to noninducibility of VT.

The diagnosis of prior MI was based on the presence of significant coronary artery disease (≥70% stenosis on coronary angiography) and subendocardial or transmural late gadolinium enhancement (LGE) in a coronary artery perfusion territory. The diagnosis of NICM was based on the exclusion of significant coronary artery disease, congenital heart disease, hypertrophic cardiomyopathy, arrhythmogenic right ventricular cardio-

myopathy, left ventricular noncompaction, restrictive cardiomyopathy, (sub)acute myocarditis, cardiac sarcoidosis, tachycardia-induced cardiomyopathy and primary valvular abnormalities. All patients were treated according to our standard clinical protocol and provided informed consent.

CE-CMR acquisition and processing

Contrast-enhanced CMR was performed on a 1.5T Gyroscan ACS-NT/Intera MR system or on a 3.0T Ingenia MR system (Philips Medical Systems, Best, the Netherlands). A standardized protocol was followed, including cine CMR in long-axis (two- and four-chamber views) and short-axis. In addition, the proximal aorta was imaged using a black-blood turbo spin-echo sequence. Contrast-enhanced images were acquired 15min after bolus injection of gadolinium (Magnevist; Schering, Berlin, Germany; 0.15 mmol/kg) with an inversion-recovery 3D turbo-field echo sequence with parallel imaging. The heart was imaged in one or two breath-holds with 20-24 imaging levels in short-axis views.

Using MASS software (research version 2012; LKEB; Leiden University Medical Centre, the Netherlands), the centerline of the proximal coronary arteries and the luminal boundary of the proximal aorta were manually defined in the black-blood spin-echo images. The endocardial and epicardial contours were semi-automatically detected on the short axis images. The defined geometries of the proximal coronary arteries, aorta and myocardial boundaries were converted into 3D meshes. Scar was defined as myocardium with SI ≥35% of maximal myocardial SI, and subdivided into core scar (>50% of maximal SI) and border zone (BZ, 35-50% of maximal SI) according to the method described by Roes et al.[9]. The vertices of the LV endocardial and epicardial meshes were color-coded for scar transmurality for the inner and outer half of the wall, respectively. All meshes were imported into the CARTO system using CARTOMerge (IPE) software. On the CARTO 3 system scars were also visualized as 3-dimensional structures, which were created using MATLAB software (version 2012a).

Electrophysiological evaluation

Anti-arrhythmic drugs were discontinued for ≥5 half-lives with the exception of amiodarone. Programmed electrical stimulation consisted of 3 drive cycle lengths (600, 500 and 400ms) with 1-3 ventricular extrastimuli (≥200ms) from ≥2 right ventricular sites and burst pacing (cycle length ≥200ms), which was repeated with isoprenaline (2-10μg/min) when necessary. Positive endpoint for stimulation was induction of a monomorphic VT lasting for >30s or requiring termination because of hemodynamic compromise.

Electroanatomical mapping, real-time image integration and ablation

If indicated, epicardial access was first obtained through subxyphoid puncture. Then heparin was administered and EAM was performed using a 3.5mm irrigated-tip

catheter (NaviStar ThermoCool, Biosense Webster Inc, Diamond Bar, CA, USA) and the CARTO system. Limited EAM of the aortic root was performed and the position of the left main coronary artery, confirmed by contrast injection through the mapping catheter, was tagged on the map. CE-CMR-derived images were visually aligned with the EAM using the left main landmark. Then, the LV was mapped retrogradely focusing on the integrated CMR-derived scar. The LV surfaces of CMR and EAM were aligned with the translation tool provided by the mapping system, until the lowest mean surface registration error was reached. Multidetector computed tomography-derived coronary artery anatomy and epicardial fat meshes were integrated with the EAM in patients undergoing epicardial mapping.[4,10]

Potential ablation target sites were identified by activation mapping and entrainment mapping for stable VT. For unstable VT, the area of interest was identified by substrate mapping and detailed pacemapping. To confirm the best pacemap site, pacing was repeated after moving the catheter in all possible directions. With the catheter placed in the area of interest, VT was reinduced and briefly mapped to identify diastolic activity and terminate the VT by ablation, also for hemodynamically unstable VT.

At the epicardium, ablation was usually withheld when the estimated distance to a coronary artery was <5mm, as assessed by integrated multidetector computed tomography-derived coronary anatomy and coronary angiography.[10] High output pacing (10mA, 2ms) was performed to localize the phrenic nerve. Radiofrequency energy was applied at 30-45W (maximum temperature 45°C, flow 20-30ml/min, 60s) for endocardial sites and ≤50W (flow 20ml/min) for epicardial sites.

Acute and long-term outcome

After ablation, the entire programmed electrical stimulation protocol was repeated. Isoprenaline was administered if required to induce VT before ablation. Complete procedural success was defined as non-inducibility of any sustained monomorphic VT; partial success as elimination of the (presumed) clinical VT but persistent inducibility of ≥1 nonclinical VT; failure as persistent inducibility of the (presumed) clinical VT. Patients were followed at 3, 6 and 12 months after ablation and at 6- to 12-monthly intervals thereafter.

Critical isthmus sites

For the current analysis all studies were thoroughly reviewed on the electrophysiology recording system (Prucka Cardiolab recording system, Houston, TX, USA) while the observer was blinded to the electroanatomical maps. Critical isthmus sites were defined by the following criteria:

(1) ≥11/12 pacemap (precise match of major deflections *and* all subtle notches in ≥11/12 leads; site with longest S-QRS delay in case of identical match) and/or

(2) concealed entrainment with post-pacing interval equal to tachycardia cycle length and/or
(3) VT slowing and termination during ablation.

Critical isthmus sites for the same VT could be identified by more than one criterion. Because of differences in accuracy between pacemapping, entrainment and termination, we have stratified the analysis for these different criteria. Critical isthmus sites were further subdivided into central isthmus sites (S-QRS or E-QRS 31-70% of VT cycle length) and exit sites (S-QRS or E-QRS 0-30% of VT cycle length).

The LV endocardial low bipolar (≤1.50mV) and unipolar (≤8.27mV[11]) voltage areas were measured in all patients, and the epicardial low bipolar (≤1.81mV[4]) and unipolar (≤7.95mV[4]) voltage areas were measured in patients with NICM who underwent epicardial mapping. The location of LV endocardial critical isthmus sites with respect to the endocardial low voltage areas was assessed in all patients. The location of LV epicardial critical isthmus sites with respect to epicardial areas with low voltage and abnormal electrograms[4] was assessed in patients with NICM.

Contrast-enhanced CMR-derived 3D scar reconstructions

CMR-derived 3D scar reconstructions and all CMR-based scar parameters were computed using MATLAB software. Examples of scars are displayed in Figures 1 and 2. After the procedure, all mapping points at critical isthmus sites were projected onto the CMR-derived 3D scar reconstructions using MATLAB software (example in Figure 2). Scar transmurality was calculated by dividing scar thickness by wall thickness. The local scar transmurality and SI at a mapping point were calculated as the mean value within a 5mm-radius transmural cylinder around the mapping point. The local scar transmurality and SI at critical isthmus sites were compared to the average scar transmurality and SI in the same patient. The distances from critical isthmus sites to >75% transmural scar and core-BZ transition were calculated. The core-BZ transition was defined as the line where core and BZ meet, projected on the endocardial or epicardial surface.

The following predefined areas were calculated for the endocardium and epicardium in each patient: CMR-derived scar, area within 5mm of >75% transmural scar, area within 5mm of core-BZ transition, and areas within 5mm and 10mm of the core-BZ transition with >75% scar transmurality. The percentage of critical isthmus sites located within these areas was calculated.

CMR-derived overall scar characteristics were calculated, including total scar volume, core volume, BZ volume and areas of ≤50%, 51-75% and >75% transmural scar. The relation between these characteristics and (1) average cycle length of induced VTs, (2) number of induced VTs, (3) inducibility of VT after ablation and (4) VT recurrence was assessed.

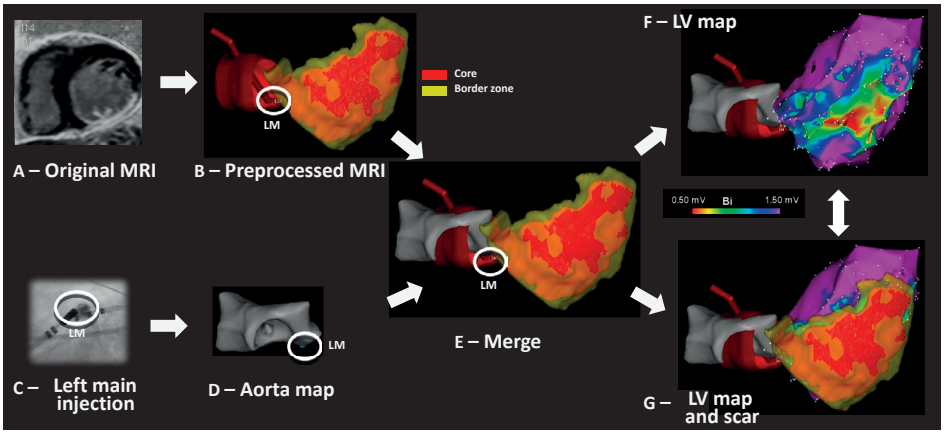


Figure 1. Integration of CMR-derived 3D scar reconstruction with electroanatomical maps
Before the procedure, the original CMR (panel A) is processed to create a three-dimensional scar reconstruction (panel B). During the procedure the position of the left main is confirmed by contrast injection (panel C) and tagged on the map (panel D). The CMR data are subsequently integrated with the electroanatomic map based on the left main landmark (panel E). Left ventricular mapping can then be focused on the CMR-derived scar (panels F and G).
LM indicates left main; LV, left ventricular.

5

Statistical analysis

Categorical variables are displayed as number (percentage) and continuous variables are expressed as mean±standard deviation or median (interquartile range [IQR]). Continuous variables were compared using the Student's *t* test when normally distributed or the Mann-Whitney *U* test when non-normally distributed. For paired variables, the paired *t* test or the Wilcoxon signed-rank-test were used, respectively. The relation between CMR-derived overall scar characteristics and the number of induced VTs and average cycle length of induced VTs was first analyzed by univariate linear regression analysis. The relation with VT inducibility after ablation was analyzed by univariate logistic regression and the relation with VT recurrence by univariate Cox regression. When statistically significant associations were identified in univariate analyses, multivariate analyses were performed to assess the independent associations between the scar characteristics of interest and the VT or outcome parameters. All analyses were performed with SPSS version 20.0 (IBM, Somers, New York, USA). All tests are two-sided and p-values <0.05 were considered significant.

RESULTS

A total of 44 patients (23 post- MI/21 NICM, age 62±13 years, CMR-based LVEF 44±12%) underwent VT ablation with integration of CMR-derived scar (178±76 LV mapping

points; average registration error 3.8±0.6mm, example in Figure 1). Epicardial mapping was performed in 15 patients (13 NICM, 2 post-MI; 174±99 mapping points). Baseline and procedural data are provided in Table 1. A total of 110 distinct VTs (cycle length 290±67ms) could be induced during the procedure. A ≥11/12 pacemap was obtained in 67 VTs (61%; median S-QRS 30ms, IQR 10-48ms). Entrainment was concealed with

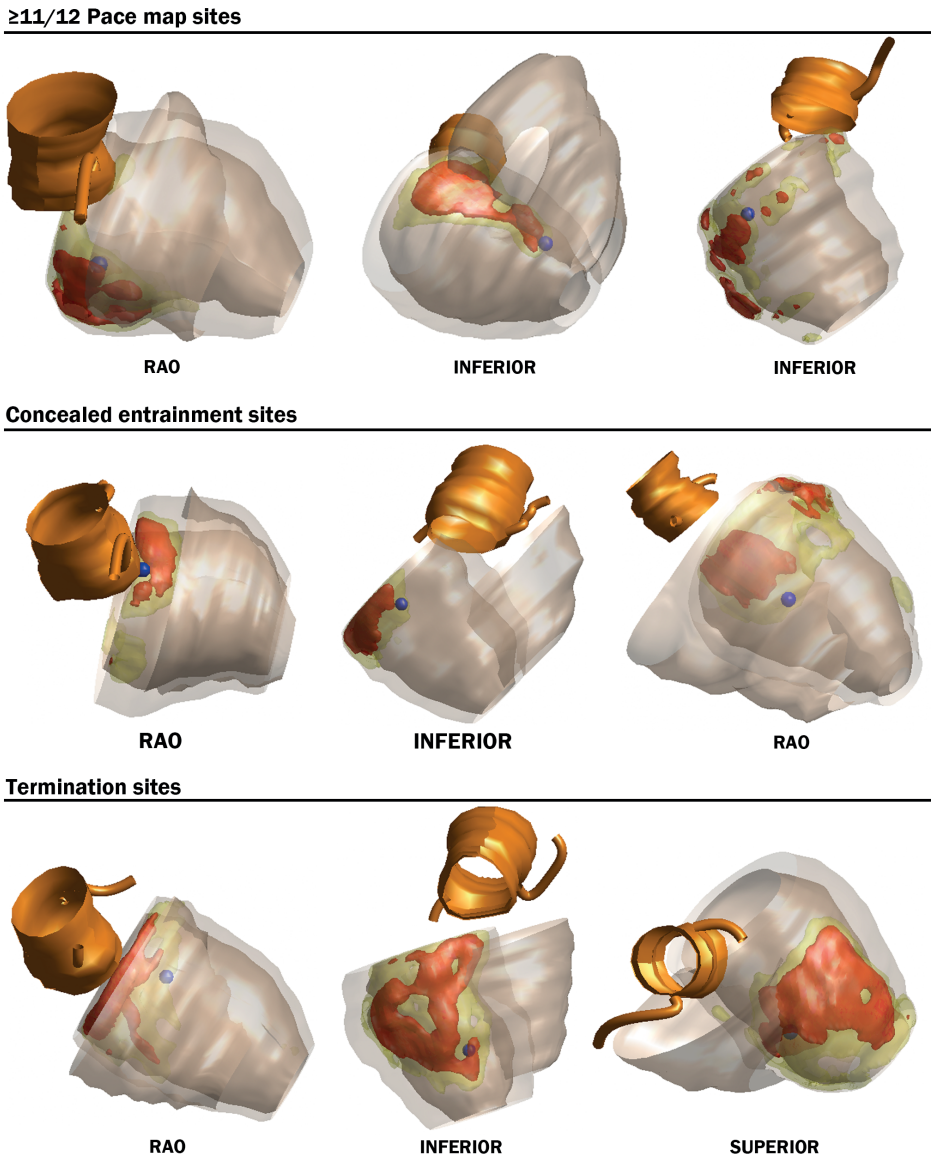


Figure 2. Examples of critical isthmus sites projected on CMR-derived 3D scar reconstructions
RAO indicates right anterior oblique.

Table 1. Baseline, procedural and CMR-derived data.

	All patients (n=44)	Post-infarction (n=23)	NICM (n=21)
Age	62±13	67±9	56±14
Male	37 (84%)	20 (87%)	17 (81%)
NYHA functional class			
I	24 (55%)	12 (52%)	12 (57%)
II	17 (39%)	10 (44%)	7 (33%)
III	3 (7%)	1 (4%)	2 (10%)
LV ejection fraction, %	44±12	45±12	42±11
LV end-diastolic volume, mL	209 (181-253)	203 (174-233)	213 (189-257)
LV end-systolic volume, mL	109 (87-155)	102 (84-134)	124 (89-160)
History of atrial flutter/fibrillation	8 (18%)	5 (22%)	3 (14%)
BMI, kg/m^2	27±5	28±5	27±4
Diabetes mellitus	7 (16%)	5 (22%)	2 (10%)
eGFR <60 mL/min	5 (11%)	3 (13%)	2 (10%)
Number of VTs induced			
1	17 (39%)	12 (52%)	5 (24%)
2	13 (30%)	4 (17%)	9 (43%)
≥3	14 (31%)	7 (31%)	7 (33%)
Hemodynamic stability of VTs			
Only stable VT	12 (27%)	7 (30%)	5 (24%)
Only unstable VT	18 (41%)	8 (35%)	10 (48%)
Stable and unstable VT	14 (32%)	8 (35%)	6 (29%)
Mean cycle length of induced VTs, ms	292±65	292±63	292±68
Pericardial puncture	15 (34%)	2 (9%)	13 (62%)
Radiofrequency energy applications			
Only endocardial	31 (71%)	21 (91%)	10 (48%)
Only epicardial	4 (9%)	1 (4%)	3 (14%)
Endocardial and epicardial	8 (18%)	1 (4%)	7 (33%)
None	1 (2%)	0 (0%)	1 (5%)
Procedural outcome			
Complete success	26 (59%)	15 (65%)	11 (52%)
Partial success	9 (21%)	3 (13%)	6 (29%)
Failure	5 (11%)	1 (4%)	4 (19%)
Indeterminate	4 (9%)	4 (17%)	0 (0%)
Procedural duration, min	201±73	179±51	225±87
Fluoroscopy time, min	44±21	37±16	51±23
CMR scar volume, % of LV wall			
Total scar volume, %	16 (12-22)	18 (12-23)	15 (11-20)
Core scar volume, %	6 (4-9)	7 (4-10)	6 (4-8)
BZ volume, %	10 (7-12)	10 (8-12)	9 (7-13)
CMR scar area, % of endocardial LV			
Area of ≤50% transmural scar, %	15 (12-19)	13 (11-16)	17 (13-24)
Area of 51-75% transmural scar, %	7 (4-10)	9 (5-12)	6 (4-9)
Area of >75% transmural scar, %	6 (3-10)	7 (3-13)	4 (2-7)

BMI indicates body mass index; BZ, border zone; eGFR, estimated glomerular filtration rate; LV, left ventricular; NYHA, New York heart association; VT, ventricular tachycardia

post-pacing interval equaling VT cycle length in 10 VTs (9%; median E-QRS 98ms, IQR 61-133ms). Thirty-one VTs (28%) slowed and terminated during ablation (median E-QRS before ablation 96ms, IQR 37-126ms; median time to termination 9sec, IQR 6-11sec). Based on these findings, critical isthmus sites could be identified in 78 of 110 VTs (71%) at the following locations: LV endocardium (46 VTs, 59%), epicardium (16 VTs, 21%), right ventricular septum (7 VTs, 9%), aortic root (5 VTs, 6%), both aortic root and LV endocardium (2 VTs, 3%), both right ventricular endocardium and epicardium (1 VT, 1%) and anterior cardiac vein (1 VT, 1%). Complete procedural success was achieved in 26 patients (59%), partial success in 9 (21%), failure in 5 (11%), and the acute outcome was indeterminate in 4 (9%) due to non-inducible clinical VT prior to ablation.

Scar transmurality, signal intensity and distance to core-BZ transition at critical isthmus sites

The mapping points at critical isthmus sites were successfully projected on the CE-CMR-derived 3D scar reconstructions (examples in Figure 2). One epicardial VT originated from the right ventricular outflow tract and was excluded from further analyses. Sites with a ≥11/12 pacemap had a scar transmurality of 66±22%, compared with an average scar transmurality in the same patients of 59±12% (p=0.005, Figure 3). The difference in transmurality was larger at concealed entrainment sites (concealed entrainment 76±16% vs. average 62±10%, p=0.024) and termination sites (termination 70±21% vs. average 62±12%, p=0.018).

The scar SI at critical isthmus sites was higher than the average scar SI in the same patients (≥11/12 pacemap 68±24% vs. average 59±16%, p=0.001; concealed entrainment 72±21% vs. average 58±15%, p=0.074; termination 69±21% vs. average 59±15%, p=0.010; Figure 3).

The median distance to >75% transmural scar was 1.5mm (IQR, 0.0-5.6mm) at ≥11/12 pacemaps, 0.0mm (IQR, 0.0-3.0mm) at concealed entrainment sites and 1.8mm (IQR, 0.0-3.8mm) at termination sites (Figure 4). The critical isthmus sites clustered around the core-BZ transition, with a median distance to the transition of 3.7mm (IQR, 1.5-7.0mm) at ≥11/12 pacemaps, 1.9mm (IQR, 0.0-2.6mm) at concealed entrainment sites and 2.5mm (IQR, 1.1-4.2mm) at termination sites.

Scar characteristics at exit and isthmus sites

Based on pacemapping, exit sites could be identified in 60 VTs and central isthmus sites in 6 VTs. Scar transmurality and SI were higher at pacemapping-based central isthmus and exit sites, compared to the average (Figure 5). The differences were more pronounced at central isthmus sites (transmurality 78±14% vs. average 64±8%, p=0.051; SI 77±17% vs. average 59±6%, p=0.012), than at exit sites (transmurality 65±23% vs. average 59±12%, p=0.019; SI 67±25% vs. average 59±17%, p=0.004).

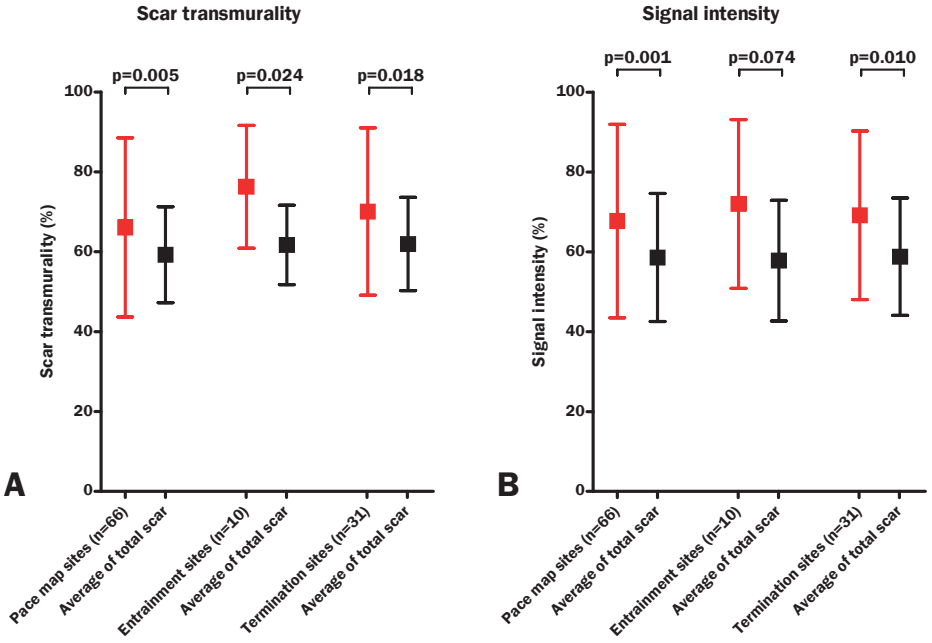


Figure 3. Scar transmurality and signal intensity at critical isthmus sites.
Scar transmurality and SI at critical isthmus sites compared to the average scar transmurality and SI in the same patient. Values are displayed as mean±standard deviation.

Of the 31 termination sites, 16 (52%) were consistent with an exit site and 15 (48%) with a central isthmus site. Scar transmurality was above average at central isthmus sites (75±22% vs. 60±13%, p=0.008), but not at exit sites (66±19% vs. 63±10%, p=0.58). Similarly, SI was above average at central isthmus sites (74±21% vs. 56±13%, p=0.006), but not at exit sites (65±21% vs. 62±15%, p=0.54). The number of concealed entrainment sites was too small for subgroup analyses.

Nonischemic cardiomyopathy vs. post-myocardial infarction

At ≥11/12 pacemaps and termination sites, the CMR-derived scar characteristics (including scar transmurality, SI, distance to >75% transmural scar and distance to core-BZ transition) were not significantly different between patients with NICM or prior MI (all p>0.05, data not shown).

CMR-based identification of critical isthmus sites

The CMR-derived scar area (median 24% of LV, IQR 16-30%) contained 77% of ≥11/12 pacemap sites, 90% of concealed entrainment sites and 90% of termination sites (Figure 6A). The area within 5mm of both >75% transmural scar and core-BZ transition (median

13% of LV, IQR 7-19%) included only 56% of ≥11/12 pacemap sites, but still 100% of concealed entrainment sites and 77% of termination sites.

In post-MI patients the areas within 5mm of >75% transmural scar, within 5mm of the core-BZ transition and the low bipolar voltage areas were limited in size and contained the majority of LV endocardial critical isthmus sites (Figure 6B).

For patients with NICM the areas within 5mm of both >75% transmural scar *and* core-BZ transition (median 13% of LV, IQR 6-19%), and the LV endocardial low unipolar voltage area (median 11% of LV, IQR 2-16%) were comparably small and contained the majority of LV endocardial critical isthmus sites (Figure 6C). The LV epicardial low bipolar

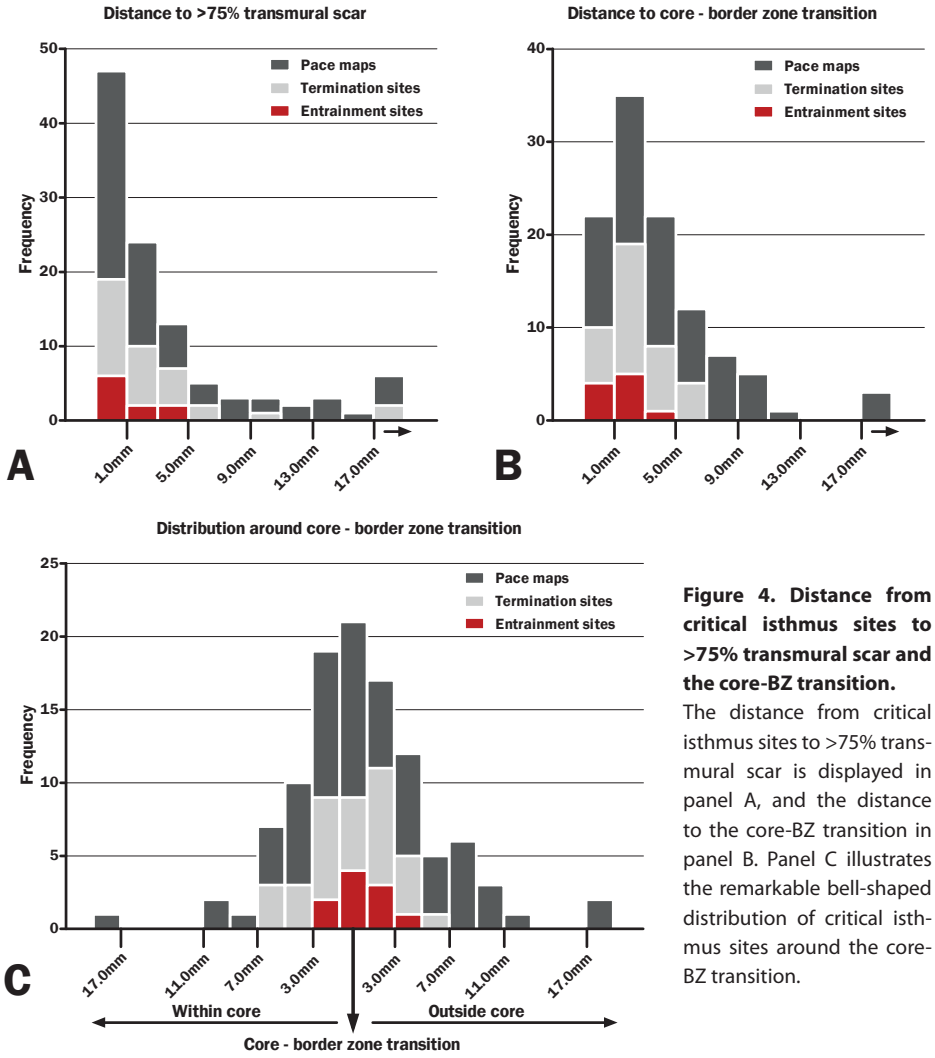


Figure 4. Distance from critical isthmus sites to >75% transmural scar and the core-BZ transition. The distance from critical isthmus sites to >75% transmural scar is displayed in panel A, and the distance to the core-BZ transition in panel B. Panel C illustrates the remarkable bell-shaped distribution of critical isthmus sites around the core-BZ transition.

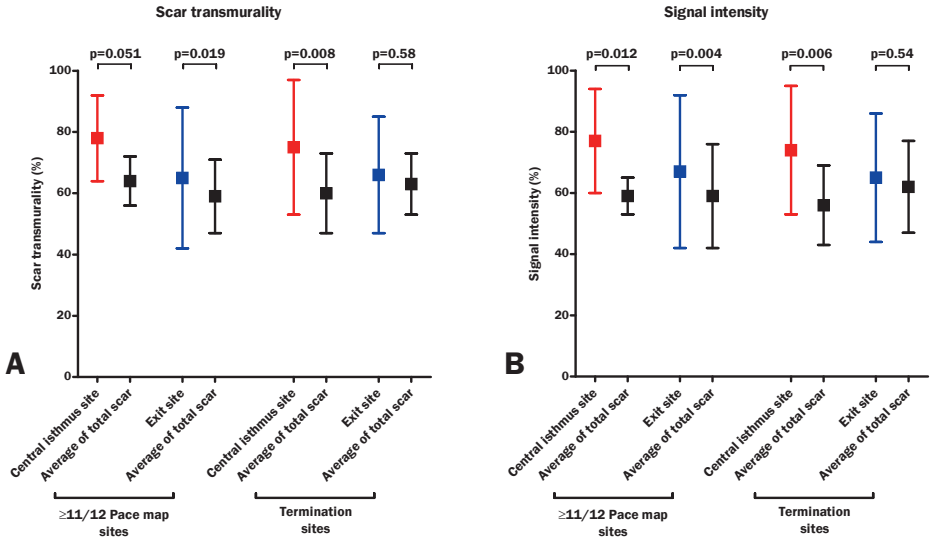


Figure 5. Scar transmurality and signal intensity at central isthmus and exit sites
Scar transmurality and SI at central isthmus and exit sites compared to the average scar transmurality and SI in the same patient. Values are displayed as mean±standard deviation.

and unipolar voltage areas with abnormal electrograms were large (median 27% of LV, IQR 15-41% and median 43% of LV, IQR 25-65%, respectively), while the area within 5mm of both >75% transmural scar *and* core-BZ transition was smaller (median 12% of LV, IQR 6-19%) and contained the majority of epicardial entrainment and termination sites (Figure 6D).

CMR-derived scar characteristics, VT characteristics and outcome

Univariate analysis revealed that total scar, core and BZ volumes, and areas of 51-75% and >75% transmural scar were associated with slower induced VTs (supplemental Table 1). In a multivariate model including scar transmurality areas, only the area of >75% transmural scar remained associated with VT cycle length (+17ms per 5cm^2, 95% confidence interval 7-27ms, p=0.001). In a multivariate model including the core and BZ volumes, only the BZ volume remained associated with VT cycle length (+20ms per 5mL BZ, 95% confidence interval 9-32ms, p=0.001). BZ volume and area of >75% transmural scar were interrelated (R^2 0.50, p<0.001) and became non-significant if both parameters were included in a model. None of the overall scar characteristics were associated with the number of induced VTs, inducibility of VT after ablation, or VT recurrence (all p>0.20, supplemental Tables 2-4).

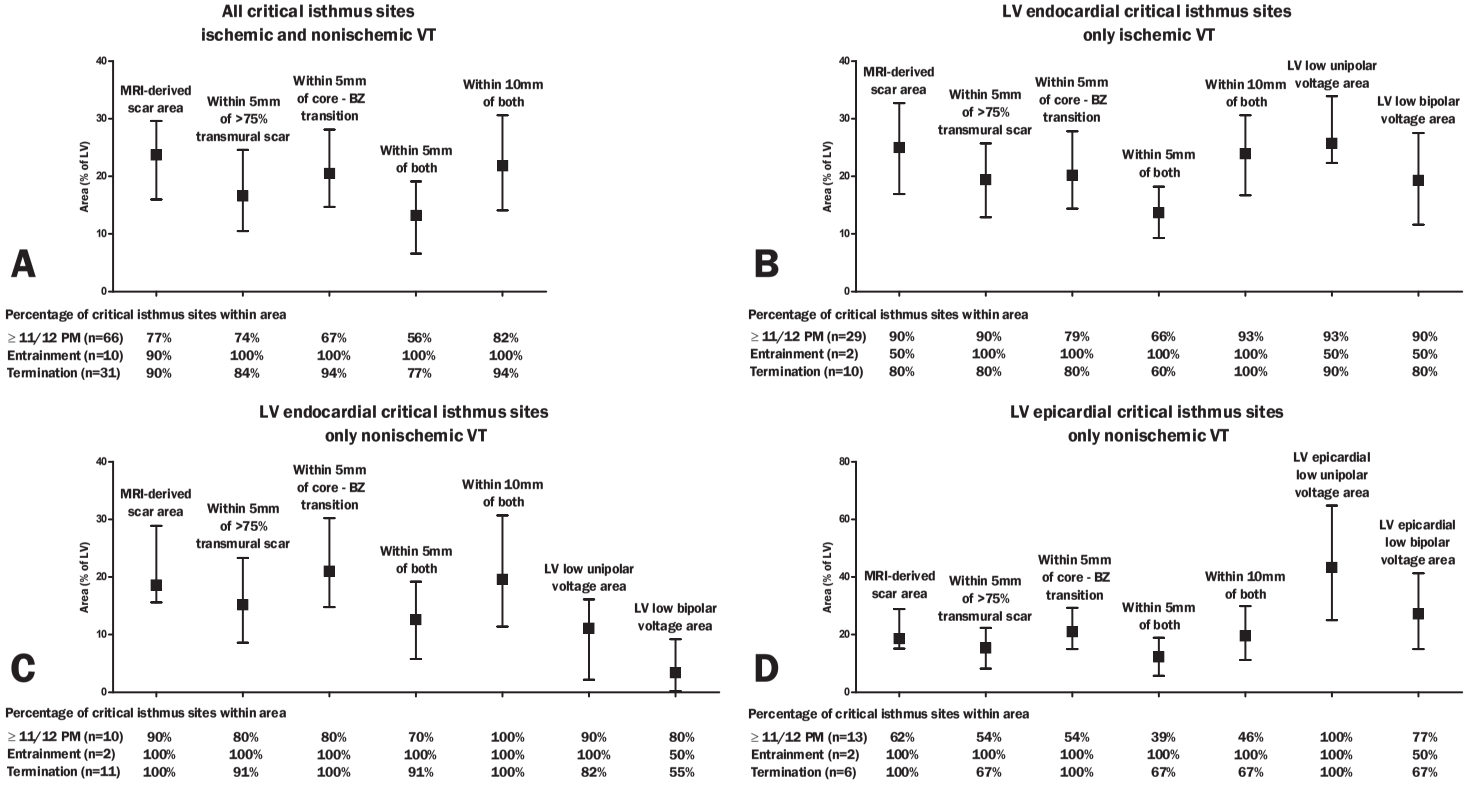


Figure 6. Percentage of critical isthmus sites within specific areas

Values are displayed as median with interquartile range. BZ indicates border zone; LV, left ventricular; PM, pacemap; VT, ventricular tachycardia

DISCUSSION

In the present study critical VT isthmus sites in patients with prior MI or NICM were typically located in close proximity to the CMR-derived core-BZ transition and >75% transmural scar. In particular central isthmus sites had high scar transmurality and signal intensity compared to the average of the entire scar, suggesting that slow conducting pathways are located within relatively dense and transmural scar. The area within 5mm of both >75% transmural scar and the core-BZ transition covered a median of 13% of the LV, but contained all concealed entrainment sites and 77% of VT termination sites, allowing CE-CMR-based delineation of relatively small areas containing critical parts of the reentry circuit. The BZ volume and area of >75% transmural scar were positively correlated with the cycle length of induced VTs, providing further support to the premise that the BZ and >75% transmural scar are associated with slow conduction.

Scar transmurality and signal intensity

The current study comprises the largest series of patients undergoing VT ablation with CE-CMR-integration to date, and provides detailed analyses of CMR-derived scar parameters at VT-related sites. Critical isthmus sites were typically located within, or in close proximity to, >75% transmural scar in post-MI and NICM patients. In one prior study in 23 post-MI patients, 62% of reentrant VT critical sites were identified in regions with >75% transmural scar[8]. Several studies have demonstrated a strong correlation between electrogram prolongation and scar transmurality[2,4,7,8], which is in line with our finding that the area of >75% transmural scar correlated positively with the cycle length of induced VTs. Scar transmurality may therefore be an important aspect of the substrate for reentrant VT.

The scar density at critical isthmus sites is reported in only one study in 9 patients with ischemic VT, in which 71% of VT isthmus sites were located in the infarct core and 29% in the BZ.[7] All critical sites in the BZ were in an area of transmural infarct, with SI slightly lower than the cutoff defining core infarct. In the present study, the remarkable bell-shaped distribution of critical isthmus sites around the core-BZ transition suggests that the 50% of maximal SI threshold may indicate a critical mix between fibrosis and viable myocytes that allows for slow conduction and thereby, reentrant VT.

CMR-derived BZ channels through higher SI scar areas have been correlated with critical isthmus sites.[5,6,12] Notably, in the present study we observed relatively high SI at critical isthmus sites, contradicting the premise that VT isthmuses manifest as relatively low SI channels on CE-CMR.

Prior investigations demonstrated differences in scar features between patients with NICM and prior MI. One study demonstrated a lower LGE SI in patients with atypical LGE patterns, compared to patients with infarct LGE pattern, suggesting a higher scar den-

sity in post-MI patients.[13] A study in 33 patients with NICM or prior MI who underwent VT ablation showed that patients after MI had more pronounced EAM-based conduction delay than patients with NICM.[14] In the current study we could demonstrate that, although overall scar characteristics may be different, CMR-derived scar characteristics at critical isthmus sites were similar between patients with prior MI or NICM.

CMR-based identification of the area of interest

We could demonstrate the added value of CMR-based scar characteristics for identification of areas containing critical isthmus sites during VT ablation. A limited area within 5mm of both >75% transmural scar and core-BZ transition encompassed all concealed entrainment sites and 77% of termination sites, which are considered to be reliable markers for critical isthmus sites. This area may therefore serve as a target area for substrate-guided ablation approaches. Only 56% of ≥11/12 pacemap sites was located in these regions. However, ≥11/12 pacemaps may also be recorded in the vicinity of exit sites and may therefore be less accurate. Importantly, the CMR-derived target area can be displayed and used as a guide for ablation using single landmark-based image integration without extensive electroanatomical substrate mapping.

Limitations

No critical isthmus sites could be identified in 29% of VTs, which may be due to intramural reentry circuits, epicardial reentry circuits in patients who did not undergo epicardial mapping, or epicardial reentry circuits that could not be mapped due to epicardial fat.

Pacemapping is considered to be a less accurate technique for defining critical isthmus sites, in particular if no S-QRS delay is observed. Therefore we have stratified the analysis for different techniques to identify critical isthmus sites and for different E/S-QRS delays.

Scar transmurality and signal intensity were calculated for a 5mm-radius transmural cylinder and therefore, they do not depend on the endocardial or epicardial location. The present data can thus not be used to predict whether an endocardial or epicardial ablation procedure will be successful.

Data from endocardial and epicardial critical isthmus sites were pooled, since the distance to >75% transmural scar and core-BZ transition did not differ between endocardial and epicardial pacemapping-based or termination-based critical isthmus sites in patients with NICM.

Clinical implications

Based on the present findings, CMR may be used to guide to areas that are likely to contain critical isthmus sites. Within these areas, ablation target sites may be further specified (e.g., based on electrogram characteristics or pace-mapping). Importantly, the CMR-derived area of interest is available before extensive substrate mapping and not

limited by intramural or subepicardial location of scars, or by epicardial fat. Moreover, it is relatively small compared to low voltage areas, in particular to epicardial low voltage areas in NICM. VT cycle length was not different between VTs with and without an identifiable critical isthmus site (294±65ms vs. 282±70ms, p=0.40), indicating that both slow and fast VTs are represented in the analysis. CMR may be particularly useful if no or only limited mapping time is available for poorly tolerated fast VT. Future prospective studies are required to assess whether CMR guidance to preselected regions that are likely to contain critical isthmus sites may improve the efficiency and efficacy of VT ablation.

CONCLUSION

In ischemic and nonischemic VT, critical parts of the reentry circuit are typically located in close proximity to >75% transmural scar and the core-BZ transition. The area within 5mm of both >75% transmural scar and core-BZ transition contained all concealed entrainment sites and 77% of termination sites. These findings suggest that CMR-derived scar characteristics may be used to guide to critical isthmus sites during VT ablation.

REFERENCE LIST

1. Bogun FM, Desjardins B, Good E, Gupta S, Crawford T, Oral H, Ebinger M, Pelosi F, Chugh A, Jongnarangsin K, Morady F. Delayed-enhanced magnetic resonance imaging in nonischemic cardiomyopathy: utility for identifying the ventricular arrhythmia substrate. J Am Coll Cardiol 2009;53(13):1138-45.
2. Dickfeld T, Tian J, Ahmad G, Jimenez A, Turgeman A, Kuk R, Peters M, Saliaris A, Saba M, Shorofsky S, Jeudy J. MRI-Guided ventricular tachycardia ablation: integration of late gadolinium-enhanced 3D scar in patients with implantable cardioverter-defibrillators. Circ Arrhythm Electrophysiol 2011;4(2):172-84.
3. Wijnmaalen AP, van der Geest RJ, van Huls van Taxis CF, Siebelink HM, Kroft LJ, Bax JJ, Reiber JH, Schalij MJ, Zeppenfeld K. Head-to-head comparison of contrast-enhanced magnetic resonance imaging and electroanatomical voltage mapping to assess post-infarct scar characteristics in patients with ventricular tachycardias: real-time image integration and reversed registration. Eur Heart J 2011;32(1):104-14.
4. Piers SR, van Huls van Taxis CF, Tao Q, van der Geest RJ, Askar SF, Siebelink HM, Schalij MJ, Zeppenfeld K. Epicardial substrate mapping for ventricular tachycardia ablation in patients with non-ischaemic cardiomyopathy: a new algorithm to differentiate between scar and viable myocardium developed by simultaneous integration of computed tomography and contrast-enhanced magnetic resonance imaging. Eur Heart J 2012;34(8):586-96.
5. Perez-David E, Arenal A, Rubio-Guivernau JL et al. Noninvasive identification of ventricular tachycardia-related conducting channels using contrast-enhanced magnetic resonance imaging in patients with chronic myocardial infarction: comparison of signal intensity scar mapping and endocardial voltage mapping. J Am Coll Cardiol 2011; 57(2):184-94.
6. Andreu D, Berruezo A, Ortiz-Perez JT, Silva E, Mont L, Borras R, de Caralt TM, Perea RJ, Fernandez-Armenta J, Zeljko H, Brugada J. Integration of 3D electroanatomic maps and magnetic resonance scar characterization into the navigation system to guide ventricular tachycardia ablation. Circ Arrhythm Electrophysiol 2011;4(5):674-83.
7. Desjardins B, Crawford T, Good E, Oral H, Chugh A, Pelosi F, Morady F, Bogun F. Infarct architecture and characteristics on delayed enhanced magnetic resonance imaging and electroanatomic mapping in patients with postinfarction ventricular arrhythmia. Heart Rhythm 2009;6(5):644-51.
8. Sasaki T, Miller CF, Hansford R et al. Myocardial structural associations with local electrograms: a study of postinfarct ventricular tachycardia pathophysiology and magnetic resonance-based noninvasive mapping. Circ Arrhythm Electrophysiol 2012;5(6):1081-90.
9. Roes SD, Borleffs CJ, van der Geest RJ et al. Infarct tissue heterogeneity assessed with contrast-enhanced MRI predicts spontaneous ventricular arrhythmia in patients with ischemic cardiomyopathy and implantable cardioverter-defibrillator. Circ Cardiovasc Imaging 2009;2(3):183-90.
10. van Huls van Taxis CF, Wijnmaalen AP, Piers SR, van der Geest RJ, Schalij MJ, Zeppenfeld K. Real-Time Integration of MDCT-Derived Coronary Anatomy and Epicardial Fat: Impact on Epicardial Electroanatomic Mapping and Ablation for Ventricular Arrhythmias. JACC Cardiovasc Imaging 2013;6(1):42-52.
11. Hutchinson MD, Gerstenfeld EP, Desjardins B et al. Endocardial unipolar voltage mapping

to detect epicardial ventricular tachycardia substrate in patients with nonischemic left ventricular cardiomyopathy. Circ Arrhythm Electrophysiol 2011;4(1):49-55.

12. Fernandez-Armenta J, Berruezo A, Andreu D et al. Three-dimensional Architecture of Scar and Conducting Channels Based on High Resolution ce-CMR: Insights for Ventricular Tachycardia Ablation. Circ Arrhythm Electrophysiol 2013;6(3):528-37.
13. Ugander M, Oki AJ, Hsu LY, Kellman P, Greiser A, Aletras AH, Sibley CT, Chen MY, Bandettini WP, Arai AE. Extracellular volume imaging by magnetic resonance imaging provides insights into overt and sub-clinical myocardial pathology. Eur Heart J 2012; 33(10):1268-78.
14. Nakahara S, Tung R, Ramirez RJ, Michowitz Y, Vaseghi M, Buch E, Gima J, Wiener I, Mahajan A, Boyle NG, Shivkumar K. Characterization of the arrhythmogenic substrate in ischemic and nonischemic cardiomyopathy implications for catheter ablation of hemodynamically unstable ventricular tachycardia. J Am Coll Cardiol 2010;55(21):2355-65.

Supplemental Table 1. Relation of CMR features with average cycle length of induced VTs

	Effect size (95%CI)	p
Univariate analysis		
Total scar volume, per 5 mL	+12 ms (5 - 19ms)	0.001
Core scar volume, per 5 mL	+22 ms (6 - 39ms)	0.01
Border zone volume, per 5 mL	+20 ms (9 - 32ms)	0.001
Area of ≤50% transmural scar, per 5 cm^2	-1 ms (-7 - 5)	0.77
Area of 51-75% transmural scar, per 5 cm^2	+19 ms (3 - 35ms)	0.023
Area of >75% transmural scar, per 5 cm^2	+17 ms (7 - 27ms)	0.001
Multivariate model 1		
Core scar volume, per 5 mL	-4 ms (-32 - 24)	0.77
Border zone volume, per 5 mL	+23 ms (3 - 43)	0.027
Multivariate model 2		
Area of ≤50% transmural scar, per 5 cm^2	+1 ms (-6 - 7)	0.86
Area of 51-75% transmural scar, per 5 cm^2	- 1 ms (-28 - 25)	0.91
Area of >75% transmural scar, per 5 cm^2	+18 ms (1 - 34)	0.039
Multivariate model 3		
Border zone volume, per 5 mL	+13 ms (-3 - 29)	0.101
Area of >75% transmural scar, per 5 cm^2	+9 ms (-5 - 22)	0.188

Supplemental Table 2. Relation of CMR features with number of induced VTs

	Effect size (95%CI)	p
Univariate analysis		
Total scar volume, per 5 mL	+0.04 VT (-0.28 - 0.36)	0.81
Core scar volume, per 5 mL	+0.05 VT (-0.68 - 0.77)	0.89
Border zone volume, per 5 mL	+0.08 VT (-0.44 - 0.60)	0.76
Area of ≤50% transmural scar, per 5 cm^2	-0.07 VT (-0.31 - 0.18)	0.60
Area of 51-75% transmural scar, per 5 cm^2	-0.12 VT (-0.82 - 0.57)	0.72
Area of >75% transmural scar, per 5 cm^2	+0.22 VT (-0.22 - 0.66)	0.32

Supplemental Table 3. Relation of CMR features with inducibility of VT after ablation

	Odds ratio (95%CI)	P
Univariate analysis		
Total scar volume, per 5 mL	1.11 (0.87 - 1.41)	0.41
Core scar volume, per 5 mL	1.24 (0.72 - 2.15)	0.44
Border zone volume, per 5 mL	1.18 (0.79 - 1.75)	0.42
Area of ≤50% transmural scar, per 5 cm^2	0.98 (0.81 - 1.19)	0.81
Area of 51-75% transmural scar, per 5 cm^2	1.31 (0.77 - 2.24)	0.32
Area of >75% transmural scar, per 5 cm^2	1.23 (0.87 - 1.72)	0.24

Supplemental Table 4. Relation of CMR features with VT recurrence during follow-up

	Hazard ratio (95%CI)	P
Univariate analysis		
Total scar volume, per 5 mL	0.96 (0.79 - 1.16)	0.67
Core scar volume, per 5 mL	0.73 (0.45 - 1.18)	0.20
Border zone volume, per 5 mL	1.06 (0.77 - 1.46)	0.74
Area of ≤50% transmural scar, per 5 cm^2	0.87 (0.69 - 1.09)	0.22
Area of 51-75% transmural scar, per 5 cm^2	0.93 (0.60 - 1.43)	0.73
Area of >75% transmural scar, per 5 cm^2	0.94 (0.72 - 1.23)	0.66

Part II

From Substrate and VT Features to Therapy and Outcome

Chapter 6

Endocardial or Epicardial Ventricular Tachycardia in Nonischemic Cardiomyopathy?

The Role of 12-lead ECG Criteria in Clinical Practice

Sebastiaan R.D. Piers, MD, Marta de Riva Silva, MD, Gijsbert F.L. Kapel, MD, Serge A. Trines, MD, PhD, Martin J. Schalij, MD, PhD, Katja Zeppenfeld, MD, PhD

Heart Rhythm 2014;11(6):1031-9

ABSTRACT

Background

Specific 12-lead ECG criteria have been reported to predict an epicardial site of origin (SoO) of induced ventricular tachycardias (VTs) in left ventricular nonischemic cardiomyopathy (NICM).

Objectives

This study aimed to (1) determine the value of ECG criteria to predict an epicardial SoO of clinically documented VTs, (2) analyze the effect of VT cycle length (CL) and antiarrhythmic drugs on the accuracy of ECG criteria, and (3) assess interobserver variability.

Methods

In 36 consecutive NICM patients (age 58±16y, 75% male) who underwent combined endocardial/epicardial VT ablation, all clinically documented and induced right bundle-branch block (RBBB) VTs were analyzed for previously reported ECG criteria to determine the SoO, as defined by ≥11/12 pacemap, concealed entrainment, and/or VT termination during ablation.

Results

In 21 patients with clinically documented (25mm/s) RBBB VT, none of the ECG criteria differentiated between patients with and without an epicardial SoO. In induced VTs (100mm/s), 2/4 interval criteria differentiated between an endocardial and epicardial SoO for slow VTs (CL>350ms) and 2/4 criteria in patients on amiodarone, but none for fast VTs (CL≤350ms) or those off amiodarone. The Q-wave in lead I was the most accurate criterion for an epicardial SoO (sensitivity, 88%; specificity, 80%).

In both clinically documented and induced VTs, interobserver agreement was poor for pseudodelta wave and moderate for other criteria.

Conclusion

When applied to clinically documented VTs, no ECG criterion could differentiate between patients with and without an epicardial SoO. Published interval-based ECG criteria do not apply to fast VTs and patients off amiodarone.

INTRODUCTION

In patients with ventricular tachycardia (VT) due to nonischemic cardiomyopathy (NICM), the substrate for VT is frequently—but not always—located intramurally or subepicardially.[1] Endocardial ablation and/or epicardial ablation may therefore be required to abolish VT. Prior studies have demonstrated that 12-lead ECG criteria can identify VTs with an epicardial site of origin (SoO), suggesting a need for epicardial access.[2-4]

Reported ECG criteria have been assessed for relatively slow VTs (average cycle length [CL] >390-400 ms[4,5]) on electrophysiology recording systems with electronic calipers at a sweep speed of 100 mm/s,[2-4] but their accuracy has not been evaluated on 25mm/s 12-lead ECGs of clinically documented VTs, which may be more relevant for planning the ablation approach.

In addition, the effect of VT CL and antiarrhythmic drug (AAD) use on the accuracy of ECG criteria has not been analyzed. In particular, interval criteria that depend on the determination of the VT QRS onset, preceded by an isoelectric interval, and the "earliest fast deflection" in precordial leads may be less accurate for fast VTs and prone to a high interobserver variability, thereby limiting its practical use.

The aims of the present study were to (1) determine the value of the reported ECG criteria when applied to 25 mm/s 12-lead ECGs of clinically documented VTs, (2) analyze the effect of VT CL and AAD use on the accuracy of the ECG criteria, and (3) assess the interobserver variability.

METHODS

Patients

Consecutive patients with NICM who underwent combined endocardial and epicardial VT ablation at the Leiden University Medical Center between 2007 and 2012 were included. The study excluded patients with coronary artery disease (>50% stenosis), congenital heart disease, hypertrophic cardiomyopathy, arrhythmogenic right ventricular cardiomyopathy, left ventricular noncompaction cardiomyopathy, restrictive cardiomyopathy, (sub)acute myocarditis, cardiac sarcoidosis, tachycardia-induced cardiomyopathy, or primary valvular disease. All patients were treated according to the clinical institutional protocol.

In patients undergoing elective VT ablation, AADs were discontinued for ≥5 half-lives, with the exception of amiodarone. Patients were admitted the day before the procedure and monitored with implantable cardioverter defibrillator therapy programmed off to allow recording of 12-lead ECGs of spontaneous VTs. Effort was taken to obtain 12-lead ECGs of all spontaneous VTs.

Electrophysiologic evaluation

Programmed electrical stimulation was performed under conscious sedation or general anesthesia (3 drive CL [600, 500, and 400ms], 1-3 ventricular extrastimuli [coupling interval ≥200ms], 2 right ventricular [RV] sites, and burst pacing, with isoproterenol [2-10μg/min] when necessary). The positive end point for stimulation was induction of a sustained monomorphic VT lasting for >30 seconds or requiring termination because of hemodynamic compromise.

Electroanatomical mapping and ablation

Epicardial access was obtained through a subxiphoid puncture. Electroanatomical mapping (EAM) was performed using a 3.5mm irrigated-tip NaviStar ThermoCool catheter (Biosense Webster Inc., Diamond Bar, CA, USA) and the CARTO™ system. Limited EAM of the aortic root was performed, and the left main coronary artery position, confirmed by undiluted contrast injection through the mapping catheter, was tagged on the map. The left main landmark and the surface registration tool were used to integrate the CT-derived coronary artery anatomy and epicardial fat thickness with the EAM.[6,7] The left ventricle (LV) was mapped retrogradely via the aorta, and the RV was mapped if indicated. After endocardial mapping, epicardial mapping of the region of interest was performed.

Ablation target sites were identified based on activation mapping and entrainment mapping for stable VT. For unstable VT, the area of interest was identified by substrate mapping and pace mapping. Then, VT was reinduced and briefly mapped in an attempt to identify diastolic activity and terminate the VT by ablation. In addition, limited substrate-based ablation was performed, targeting fragmented electrograms and late potentials in areas presumed to be related to VT based on pace, activation and entrainment mapping. Radiofrequency (RF) energy was applied at 30-45W (maximum temperature, 45°C; flow, 20-30 mL/min; 60 seconds) at endocardial sites and up to 50W (flow 20mL/min) at epicardial sites.

VT morphology and ECG criteria

Clinically documented and induced sustained monomorphic VTs were categorized as right or left bundle branch block-like (RBBB or LBBB) morphology (defined as predominant R or S in lead V_1), inferior or superior axis (predominant R or S in lead aVF), left or right axis (predominant R or S in lead I), and by precordial transition (first lead with a predominant R or S for LBBB and RBBB VTs, respectively). The ECG features assessed for all RBBB-like morphology VTs, as previously described[2-4], were:

- ***QRS duration***: interval from the earliest ventricular activation to the offset of the QRS in the precordial leads.
- ***Diastolic interval***: VT CL minus QRS duration.

- ***Pseudodelta wave (PDW)***: interval from the earliest ventricular activation to the onset of the earliest fast deflection in any precordial lead.
- ***Intrinsicoid deflection time in V_2 (IDT)***: interval from the earliest ventricular activation to the peak of the R wave in V_2.
- ***Shortest RS complex (SRS)***: interval from the earliest ventricular activation to the nadir of the first S wave in any precordial lead.
- ***Maximum deflection index (MDI)***: interval from the earliest ventricular activation to the peak of the largest amplitude deflection in each precordial lead (taking the lead with the shortest time) divided by the QRS duration, as described in patients with idiopathic VT.[5]
- ***Q wave in lead I (Q-I)***: initial negative deflection in lead I, occasionally preceded by a short isoelectric segment.
- ***Q waves in inferior leads (Q-INF)***: initial negative deflections in lead II, III, and aVF, occasionally preceded by a short isoelectric segment.
- ***Absence of Q waves in inferior leads (Abs-Q-INF)***: initial positive deflection in lead II, III, or aVF, occasionally preceded by a short isoelectric segment.

Previously published cutoff values were applied (≥34 ms for PDW, ≥85 ms for IDT, ≥121 ms for SRS, and ≥0.45 for MDI).[2] The PDW, IDT, SRS, and MDI are further referred to as "interval" criteria, and the Q-wave criteria are referred to as "morphology" criteria. For the Q-I and Abs-Q-INF criteria, only inferior-axis VTs were analyzed, and for the Q-INF criterion, only superior-axis VTs were analyzed.

Clinical VTs that were documented on a 25mm/s, 10mm/mV 12-lead ECG were analyzed using pens and manual calipers. Induced VTs were analyzed using electronic calipers on an electrophysiologic recording system (Prucka CardioLab EP; GE Healthcare, Waukesha, WI, USA) at a sweep speed of 100mm/s and an amplification of 10mm/mV. All measurements were performed by one observer (SP) and repeated by another independent observer (MRS) to analyze the interobserver reproducibility. Both observers were blinded to the SoO.

Site of origin

The SoO of a VT was defined as a site that was considered as ablation target site, with (1) the best pace map (≥11/12 leads match), (2) entrainment suggestive of an isthmus site (i.e., concealed entrainment with the postpacing interval equaling VT CL), and/or (3) VT slowing and termination during ablation. An induced VT was considered as a clinical VT if the 12-lead ECG showed an exact morphologic match with the clinically documented VT in ≥11/12 leads.

To analyze the value of ECG criteria, VTs with a SoO located at the epicardium or in the cardiac venous system were classified as epicardial VTs and those with a SoO at the LV endocardium as endocardial VTs. The analyses excluded VTs with a SoO located in the aortic sinus cusps and with both endocardial and epicardial sites fulfilling the definition of a SoO.

ECG criteria and the need for an epicardial approach

To assess the value of the ECG criteria in standard 12-lead VT ECGs to predict the requirement for an epicardial approach, the following analyses were performed: (1) the presence of an epicardial SoO was compared between clinical VTs with positive vs negative ECG, (2) the presence of an epicardial SoO of any spontaneous or induced VT was compared between patients with positive vs negative ECG criteria for the clinically documented VT, and (3) the number of epicardial RF applications was compared between patients with positive vs negative ECG criteria to analyze the potential therapeutic consequences of ECG criteria.

Statistics

Statistical analyses were performed with SPSS 20 software (IBM, Armonk, NY, USA). The categoric variables are expressed as number (percentage), and continuous variables as mean ± standard deviation, or median and interquartile range (IQR) where appropriate. Fisher exact tests, χ^2 tests and Mann-Whitney *U* tests were performed where applicable. For each ECG criterion, the sensitivity, specificity, positive predictive value (PPV), and negative predictive value (NPV) were calculated.

To analyze the effect of VT CL and AADs on the accuracy of the ECG criteria, the VTs were categorized according to CL (prespecified as ≤350ms or >350ms) and according to amiodarone use.

The percentage interobserver agreement and the Cohen's Kappa value were calculated for all criteria. The interobserver variability was analyzed by Bland-Altman plots for continuous parameters. The mean bias (mean difference between observer 1 and 2) and the 95% limits of agreement are reported. All *p* values are 2-tailed, and a value of $p < 0.05$ was considered to be statistically significant.

RESULTS

Baseline characteristics

A total of 36 NICM patients (age, 58±16 years; LV ejection fraction, 42±14%) underwent combined endocardial and epicardial VT ablation (Table 1); of these, 13 (36%) had VT recurrence after prior endocardial ablation, 6 (17%) were rescheduled for combined endocardial and epicardial VT ablation after a failed endocardial procedure, and the remaining 17 (47%) had no prior VT ablation.

Clinically documented VTs

Before ablation, 34 distinct VTs in 25 patients were documented on 12-lead ECGs (examples in Figure 1). Of these VTs, 18 (53%) were recorded in our center and 16 (47%) in

Table 1. Baseline and procedural data

	N=36
Age, years	58±16
Male	27 (75%)
LV ejection fraction, %	42±14
LV end-diastolic volume, mL	162±48
History of atrial flutter/fibrillation	8 (22%)
eGFR < 60 mL/min/1.73m^2	2 (6%)
Anti-arrhythmic drugs	
Class I	5 (14%)
Class II	20 (56%)
Class III–Sotalol	8 (22%)
Class III–Amiodarone	16 (44%)
Class IV	0 (0%)
Number of VTs induced	3 (1–4)
BBR VT	1 (3%)
Unstable induced VT	27 (75%)
Mean CL of induced VTs, ms	346±74
Endocardial RF applications	25 (69%)
Epicardial RF applications	22 (61%)
Acute outcome	
Complete success	11 (31%)
Partial success	16 (44%)
Failure	9 (25%)

BBR, bundle-branch re-entry; CL, cycle length; LV, left ventricular; eGFR, estimated glomerular filtration rate; RF, radiofrequency energy; VT, ventricular tachycardia

other centers. Six VTs (18%) were documented while the patient was on a class I AAD, 6 (18%) on sotalol, 20 (59%) on amiodarone, and 1 (3%) on a class IV AAD. Four patients (12%) were on 2 AADs, 25 (74%) on 1 ADD, and 5 (15%) were off AADs.

Mapping and ablation

A total of 111 distinct VTs (CL 342±89ms) were induced in 34 patients; of these, 66 VTs (59%) in 32 patients (94%) had RBBB-like morphology and were further analyzed. A SoO could be identified for 45 of these 66 VTs (68%) in 28 of 32 patients (88%). A ≥11/12 pace map was obtained for 34 VTs (52%), with a median S-QRS interval of 40ms (IQR, 15–65ms). Entrainment was concealed, and the postpacing interval was equal to the VT CL in 3 VTs (5%), with S-QRS intervals of 9%, 17%, and 46% of VT CL. During ablation, 21 VTs (32%) slowed and terminated without a premature ventricular contraction, with a median E-QRS percentage of VT CL before ablation of 24% (IQR 14%–35%) and median

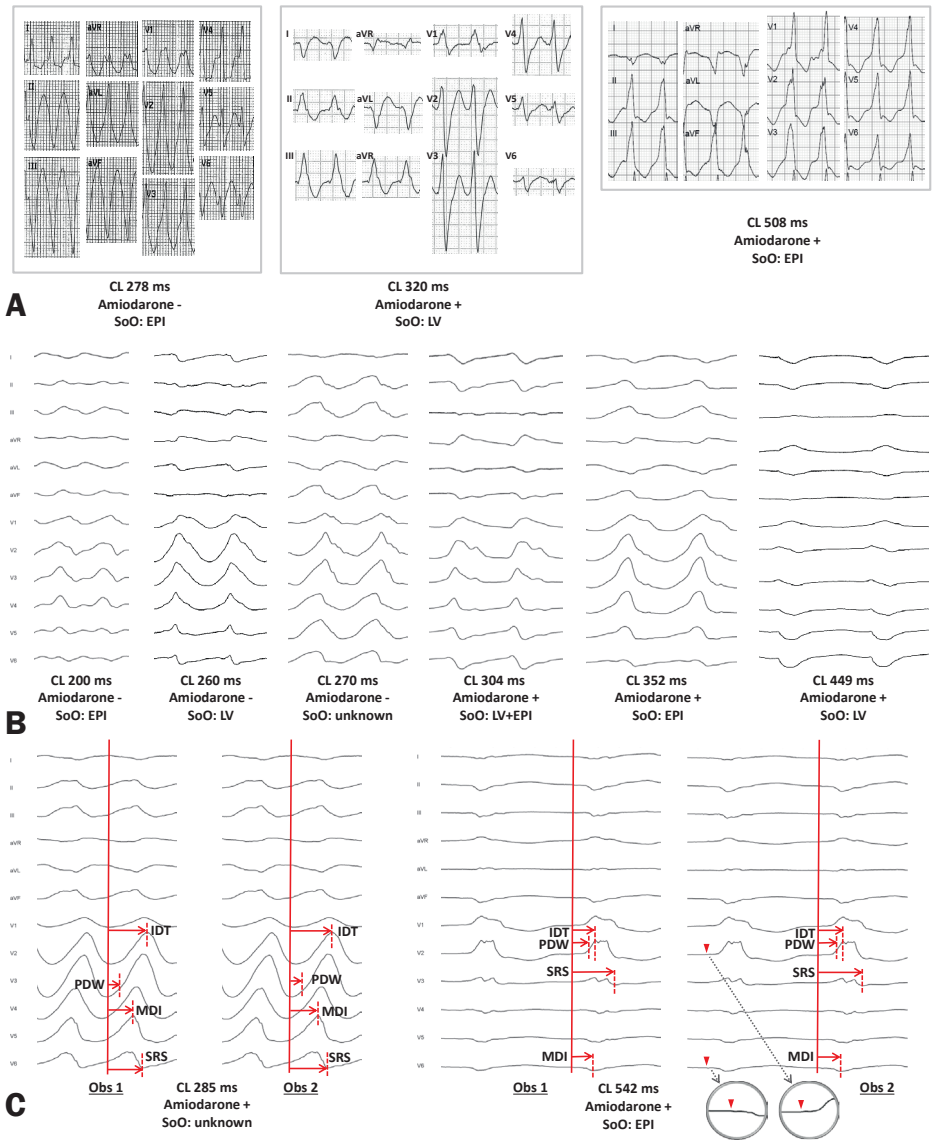


Figure 1. Examples of induced and clinically documented VTs

Panel A: Examples of clinically documented spontaneous VTs displayed at 25 mm/s. Panel B: Examples of induced VTs displayed at 100 mm/s. Panel C: Measurements of observers 1 and 2 for one fast and one slow VT. For the fast VT, the onset of the QRS complex is defined differently by observer 1 and 2, affecting all interval criteria. For the slow VT, a slurred onset of the QRS complex is observed (indicated with triangles), which may be difficult to detect if VT is faster, with a potential overlap with the preceding T-wave. CL, cycle length; SoO, site of origin.

termination time of 11 seconds (IQR, 8–29 seconds). The SoOs were classified as epicardial in 15 patients (54%), as endocardial in 6 (21%), and as endocardial and epicardial SoO in 7 (25%). Epicardial ablation was performed in 22 patients (61%).

ECG criteria applied to clinically documented VTs

Of 66 induced RBBB VTs, 19 (29%) corresponded to a clinically documented VT. Twelve of these 19 clinical VTs (63%) had a SoO at the LV epicardium, 3 (11%) at the LV endocardium, 1 (4%) in the LV and at the epicardium (termination In the LV, best pacemap at the epicardium), and 1 (4%) in the aortic sinus cusps. No SoO could be identified for 2 VTs (7%). The 15 VTs with a SoO categorized as LV endocardial or epicardial were further analyzed.

When applied to the clinically documented VTs, none of the interval criteria differed between endocardial and epicardial VTs (Table 2). The value of the Q-wave criteria could not reliably be assessed due to the limited number of endocardial and epicardial VTs in the inferior and superior axes subgroups.

The percentage of patients with an epicardial SoO of at least 1 RBBB VT was not significantly different between patients with positive or negative ECG criteria for the clinical VTs (Table 2). Depending on the applied criterion, 33% to 100% of patients with a negative criterion for the clinically documented VT had at least 1 epicardial RBBB VT necessitating an epicardial approach.

The number of epicardial RF applications tended to be higher in patients with positive vs negative criteria for clinical VTs, which was statistically significant for the Q-I criterion (Table 2), suggesting that the substrate may be more amenable to epicardial ablation in patients with a Q-wave in lead I during VT.

ECG criteria applied to induced VTs

For induced RBBB VTs, the SoO were located at the epicardium for 26 of 66 VTs (39%), at the endocardial LV for 11 VTs (17%), at the epicardium and at the endocardial LV for 4 VTs (6%), in the aortic root for 2 VTs (3%), and in the anterior cardiac vein for 2 VTs (3%). No SoO could be identified for the remaining 21 VTs (32%). The 39 VTs with a SoO categorized as LV endocardial or epicardial were further analyzed.

When measured in these induced VTs (examples in Figure 1), the PDW (p=0.040), IDT (p=0.008), SRS (p=0.022), and MDI (p=0.034), but not the QRS duration (p=0.32), differed significantly between endocardial and epicardial VTs (Figure 2). Of interest, the ECG criteria were similar for epicardial VTs and VTs of unknown origin (all p>0.05, interval criteria displayed in Figure 2). The most accurate ECG criteria to distinguish epicardial from endocardial VTs were Q-I for inferior-axis VTs (sensitivity, 88%; specificity, 80%) and Q-INF for superior-axis VTs (sensitivity, 73%; specificity, 67%). The diagnostic accuracy of all criteria is displayed in Figure 3.

Table 2. ECG criteria and the need for an epicardial approach

	Presence of an epicardial SoO of clinically documented VT if… (per VT)			Presence of an epicardial SoO of any clinically documented or induced VT if… (per patient)			Number of epicardial RF applications if… (per patient)		
	Criterion positive	Criterion negative	p	Criterion positive	Criterion negative	p	Criterion positive	Criterion negative	P
PDW ≥34 ms	3/3 (100%)	9/12 (75%)	1.00	4/5 (80%)	12/16 (75%)	1.00	8 (1-23)	8 (0-12)	0.77
IDT ≥85 ms	11/13 (85%)	1/2 (50%)	0.37	14/17 (82%)	2/4 (50%)	0.23	8 (1-17)	5 (0-11)	0.34
SRS ≥121 ms	11/13 (85%)	1/2 (50%)	0.37	14/17 (82%)	2/4 (50%)	0.23	10 (1-17)	4 (0-9)	0.20
MDI ≥0.45	7/8 (88%)	5/7 (71%)	0.57	9/11 (82%)	7/10 (70%)	0.64	11 (0-21)	5 (0-9)	0.20
Q-I*	1/2 (50%)	6/6 (100%)	0.25	4/4 (100%)	7/11 (64%)	0.52	12 (10-24)	0 (0-8)	0.043
Abs-Q-INF*	7/8 (88%)	N/A	N/A	10/12 (83%)	1/3 (33%)	0.15	8 (0-12)	0 (0-28)	0.66
Q-INF†	3/4 (75%)	2/3 (67%)	1.00	3/5 (60%)	4/4 (100%)	0.44	11 (1-26)	9 (7-18)	0.81

Abs-Q-INF, absence of Q-waves in inferior leads; IDT, intrinsicoid deflection time in V2; MDI, maximum deflection index; PDW, pseudodelta wave; Q-I, Q-wave in lead I; Q-INF, Q-wave in inferior leads; RF, radiofrequency energy; SoO, site of origin; SRS, shortest RS complex; VT, ventricular tachycardia.

*Only for inferior-axis VTs.

†Only for superior-axis VTs.

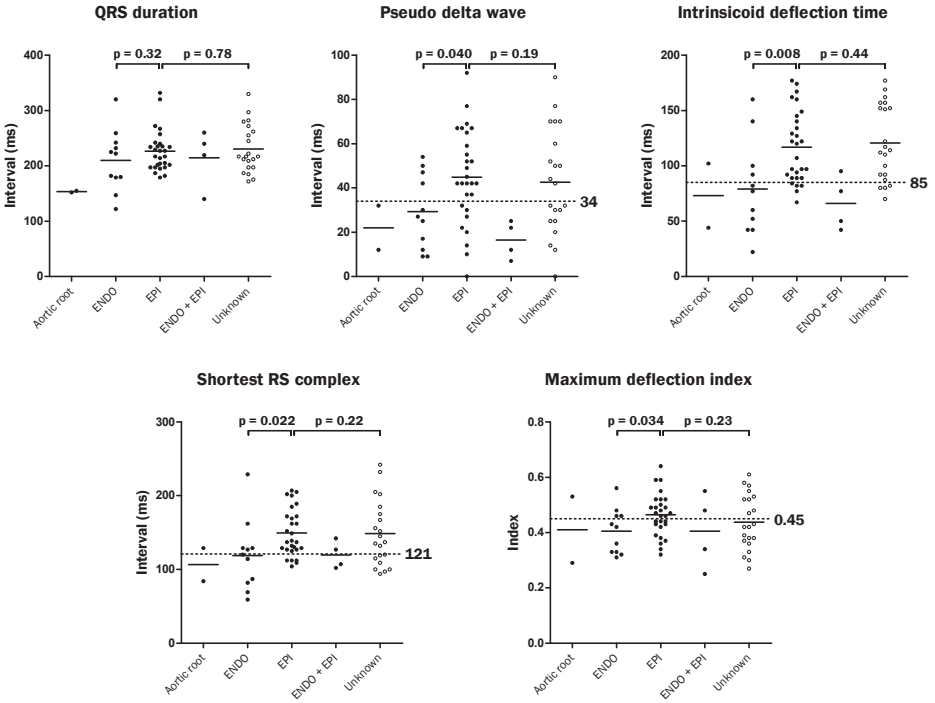


Figure 2. Interval criteria according to the site of origin of induced VTs

Effect of VT cycle length

For induced slow VTs (CL ≥350ms, n=16), the QRS duration, IDT and the SRS were significantly longer for epicardial VTs compared with endocardial VTs (Table 3). A trend was observed for a longer PDW and MDI. However, for fast VTs (CL <350ms, n=23), none of the interval criteria differed significantly between endocardial and epicardial VTs. The QRS duration was similar for slow and fast VTs (235±43 vs 213±41ms, p=0.19), but the diastolic interval was significantly longer in slow VTs than in fast VTs (median, 228ms [IQR, 174-302ms] vs 58ms [IQR, 27-92ms], p<0.001).

Effect of amiodarone use

For the 15 induced VTs in patients on amiodarone, the IDT and SRS were significantly longer in epicardial VTs than in endocardial VTs. The QRS duration, PDW and MDI also tended to be longer in epicardial VTs (Table 4). For the 24 VTs in patients off amiodarone, however, none of the interval criteria could distinguish epicardial from endocardial VTs. The QRS duration was similar in patients on and off amiodarone (228±53ms vs 218±36ms, p=0.62); however, compared with patients off amiodarone, patients on amiodarone had a significantly longer CL (422±91 ms vs 306±89ms, p<0.001) and median diastolic interval (205 ms [IQR 80-285ms] vs 62 ms [IQR 42-114ms], p=0.002).

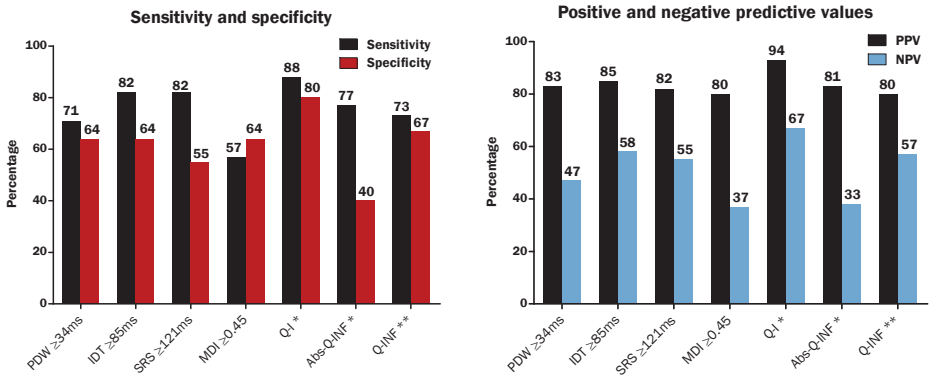


Figure 3. Accuracy of ECG criteria applied to induced VTs

NPV, negative predictive value; PPV, positive predictive value.

* Only for inferior-axis VTs ** Only for superior-axis VTs

Table 3. Effect of VT cycle length on the accuracy of ECG criteria in induced VTs

	Slow VT (CL ≥350ms, n=16)		Fast VT (CL <350ms, n=23)	
	Epicardial vs. endocardial VTs (n=11 vs. n=5)	*p*	Epicardial vs. endocardial VTs (n=17 vs. n=6)	*p*
QRS, ms	247±45 vs. 208±26	0.038	214±25 vs. 212±75	0.92
PDW, ms	55±22 vs. 31±18	0.052	38±19 vs. 28±17	0.20
IDT, ms	130±38 vs. 61±19	0.002	108±26 vs. 94±52	0.81
SRS, ms	175±28 vs. 118±18	<0.001	133±23 vs. 119±65	0.32
MDI	0.46±0.08 vs. 0.39±0.07	0.12	0.47±0.07 vs. 0.42±0.09	0.16
Q-I, %*	7/8 (88%) vs. 1/3 (33%)	0.15	8/9 (89%) vs. 0/2 (0%)	0.055
Abs-Q-INF, %*	7/8 (88%) vs. 1/3 (33%)	0.15	6/9 (67%) vs. 2/2 (100%)	1.00
Q-INF, %†	2/3 (67%) vs. 1/2 (50%)	1.00	6/8 (75%) vs. 1/4 (25%)	0.22

Abbreviations as in Table 2. *Only for inferior-axis VTs †Only for superior-axis VTs

Table 4. Effect of amiodarone on the accuracy of ECG criteria in induced VTs

	VTs on amiodarone (n=15)		VTs off amiodarone (n=24)	
	Epicardial vs. endocardial VTs (n=8 vs. n=7)	*p*	Epicardial vs. endocardial VTs (n=20 vs. n=4)	*p*
QRS, ms	242±43 vs. 211±61	0.12	220±34 vs. 208±52	0.79
PDW, ms	53±24 vs. 28±17	0.054	42±20 vs. 32±18	0.39
IDT, ms	123±37 vs. 71±34	0.009	114±31 vs. 94±57	0.63
SRS, ms	176±25 vs. 127±51	0.040	139±29 vs. 104±45	0.16
MDI	0.48±0.10 vs. 0.40±0.07	0.072	0.46±0.07 vs. 0.42±0.11	0.48
Q-I, %*	4/5 (80%) vs. 1/3 (33%)	0.46	11/12 (92%) vs. 0/2 (0%)	0.033
Abs-Q-INF, %*	5/5 (100%) vs. 2/3 (67%)	0.11	8/12 (67%) vs. 2/2 (100%)	1.00
Q-INF, %†	2/3 (67%) vs. 2/4 (50%)	1.00	6/8 (75%) vs. 0/2 (0%)	0.13

Abbreviations as in Table 2. *Only for inferior-axis VTs †Only for superior-axis VTs

Because the subgroups of endocardial and epicardial VTs with inferior and superior axes were small, the effects of VT CL and amiodarone on the Q-wave criteria could not be reliably analyzed.

Interobserver variability of ECG criteria

Bland-Altman plots of interval criteria measurements are provided in Supplemental Figures 1 and 2. The mean bias for the interval criteria was high, and the 95% limits of agreement were wide for induced VTs and, in particular, for the clinically documented VTs (Table 5). The interobserver agreement for clinically documented and induced VTs was poor for the PDW, SRS, and MDI, but moderate or good for IDT, Q-I, and Q-INF.

Table 5. Interobserver variability and agreement

	Clinically documented VTs (n=27)					Induced VTs (n=66)				
	Mean±SD or %	Mean bias	95% limits of agreement	Interobserver agreement, %	Cohen's Kappa	Mean±SD or %	Mean bias	95% limits of agreement	Interobserver agreement, %	Cohen's Kappa
QRS, ms	265±51	43	-33–119	NA	NA	222±44	27	-41–96	NA	NA
PDW, ms	18±15	27	-88–34	44%	0.08	39±22	4	-48–55	68%	0.37
IDT, ms	132±54	24	-62–110	85%	0.51	107±39	7	-42–56	82%	0.61
SRS, ms	172±56	25	-88–139	74%	0.38	141±40	19	-48–86	74%	0.51
MDI	0.46±0.11	0.02	-0.20–0.24	63%	0.26	0.44±0.09	0.02	-0.18–0.23	68%	0.36
Q-I*	31%	NA	NA	77%	0.42	66%	NA	NA	74%	0.44
Abs-Q-INF*	0%	NA	NA	100%	1.00	23%	NA	NA	86%	0.53
Q-INF†	50%	NA	NA	93%	0.86	48%	NA	NA	84%	0.68

Abbreviations as in Table 2.

*Only for inferior-axis VTs (induced VTs, n=35; clinically documented VTs, n=13).

†Only for superior-axis VTs (induced VTs, n=31; clinically documented VTs, n=14).

DISCUSSION

The clinical VT documentation in the present study demonstrated that the suggested ECG criteria could not reliably identify NICM patients who needed an epicardial approach. When applied to induced VTs on 100 mm/s electrophysiology recording system tracings, some ECG criteria proved useful for the identification of epicardial VTs, but not for all VT subgroups. Two of 4 interval criteria differed between induced endocardial and epicardial slow VTs (CL >350ms) and 2 of 4 criteria in patients on amiodarone, but none when applied to fast VTs (CL ≤350ms) or in patients off amiodarone. The Q-wave in lead I (Q-I) was the most accurate criterion. In clinically documented and induced VTs, the interobserver agreement was poor for the PDW but moderate for IDT, Q-I, and Q-INF.

ECG criteria applied to clinically documented VTs: the need for an epicardial approach

Applying ECG criteria to the 12-lead VT ECG for the identification of a potential epicardial SoO has been considered to be useful for selection of patients who may benefit from epicardial ablation.[2-4] To assist preprocedural planning, ECG criteria are typically applied to clinically documented VTs. However, this approach may have important limitations. First, measurements need to be performed on 25mm/s 12-lead ECGs, which may be less accurate than on 100mm/s recordings as used in the electrophysiology laboratory.

Second, not clinically documented VTs are frequently induced, which may originate from other parts of the scar and need to be targeted if noninducibility is pursued. In the current study, at least 1 VT originated from the epicardium in 79% of patients with induced RBBB VTs.

Third, 12-lead ECG morphology and thereby ECG criteria are particularly influenced by the VT exit site; however, the VT may be abolished by ablation at any part of the reentry circuit.

Based on the present data we conclude that, although potentially useful as a guide to the area of interest for VTs induced during the procedure, the ECG criteria do probably not allow identification of patients who are likely to benefit from an epicardial approach.

ECG criteria applied to induced VTs

When applied to induced VTs, most of the ECG criteria had a high PPV, indicating that an epicardial SoO may be likely when criteria are positive. All criteria have moderate and often even poor NPV, indicating that induced VTs may still originate and be targeted from the epicardium if the ECG criteria are negative. Interestingly, the ECG criteria did not differ between epicardial VTs and VTs of unknown origin, which is in line with prior observations,[4] perhaps suggesting that most of these VTs may also be of epicardial origin. Thick layers of epicardial fat and the coronary arteries may have prevented the identification of some epicardial SoO.

In NICM, the effect of the VT CL and AADs on the accuracy of ECG criteria has not been analyzed. The initial reports on ECG criteria have included VTs with a mean CL of >400ms[4] and 390ms.[5] However, in patients with NICM currently considered for VT ablation, fast VTs are frequently induced (CL 342±89ms in this study and CL 346±74ms in a recent report[8]), and therefore, evaluation of the accuracy of ECG criteria for fast VTs is important. All criteria rely on an accurate identification of the onset of the QRS complex, which may be particularly difficult to define when the QRS is broad, in the absence of an isoelectric interval, and when there is overlap with a previous T-wave, which is commonly observed in fast VTs. In the present study, the IDT and SRS differed between endocardial and epicardial slow (CL >350ms), but not fast, VTs (CL ≤350ms). The IDT and SRS also differed between endocardial and epicardial VTs in patients with amiodarone,

but not in patients without amiodarone. Although the number of RBBB inferior-axis VTs was limited, the Q-I criterion appeared not to be affected by VT CL or amiodarone use. The diastolic interval was significantly shorter in fast VTs and in patients off amiodarone, which may hamper determination of the QRS onset. Owing to the limited number of VTs, the independent effects of VT CL and amiodarone use could not be analyzed.

Interobserver agreement

Only one study in postmyocardial infarction patients reported interobserver agreement of ECG criteria for epicardial VTs.[9] The interobserver agreement in the present study was particularly poor for the PDW criterion, as has been observed in postmyocardial infarction patients,[9] and for the MDI, which relies on an accurate identification of the QRS onset, QRS offset, and maximum deflection in all precordial leads. In contrast, the IDT relies only on the identification of the onset of the QRS and the well-defined peak of the R wave in V_2, perhaps explaining the relatively high interobserver agreement. The Q-wave criteria are typically easier to assess, with moderate to good interobserver agreement, but may be less clear when the onset of the QRS is difficult to define or when a putative initial R wave is very small.

Limitations

The number of patients and VTs was too small for analysis in some subgroups. Owing to inclusion of patients after endocardial ablation failure, it may be expected that the number of NICM patients with an epicardial SoO will be overrepresented. However, among the 32 patients with inducible RBBB VT, 9 of 14 patients (64%) who had not undergone prior ablation had an epicardial SoO compared with 13 of 18 patients (72%) who had undergone prior endocardial ablation (p=0.71).

The SoO could be identified for only 68% of induced RBBB VTs, with ≥1 identified SoO in 88% of patients with inducible RBBB VTs, which may be explained by the strict definition of a SoO, intramural reentry circuits, epicardial SoOs covered with epicardial fat, fast VTs without a reasonable pacemap, and other reasons.

Limb leads are typically placed on the torso in the electrophysiology lab, while the clinically documented VT may be recorded with the leads placed on the extremities. The resulting differences in extremity lead vectors may affect Q-waves, but were not analyzed in the present study.

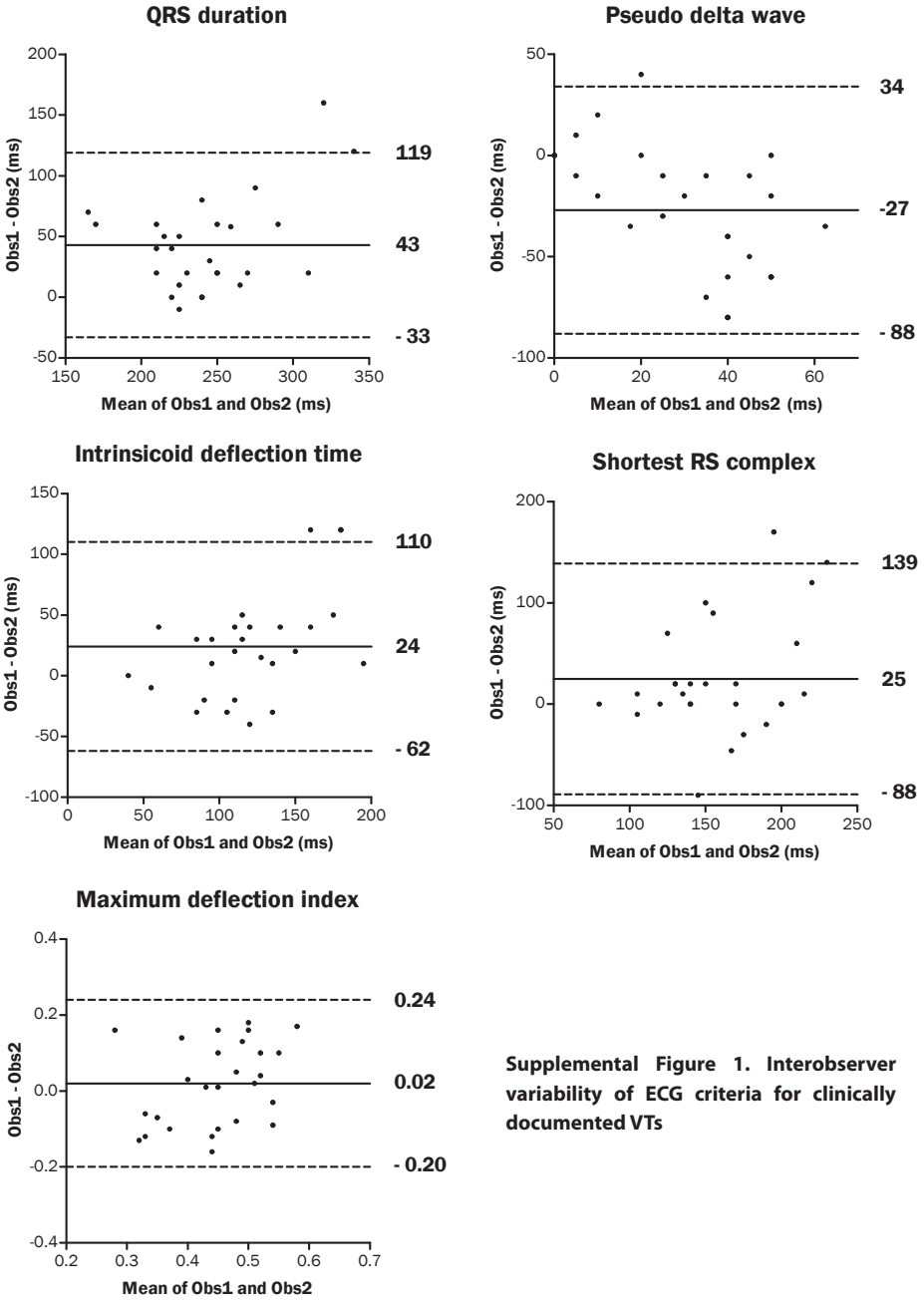
CONCLUSION

When applied to 25mm/s ECGs of clinically documented VTs, none of the ECG criteria could differentiate between patients with and without epicardial VTs. These data sug-

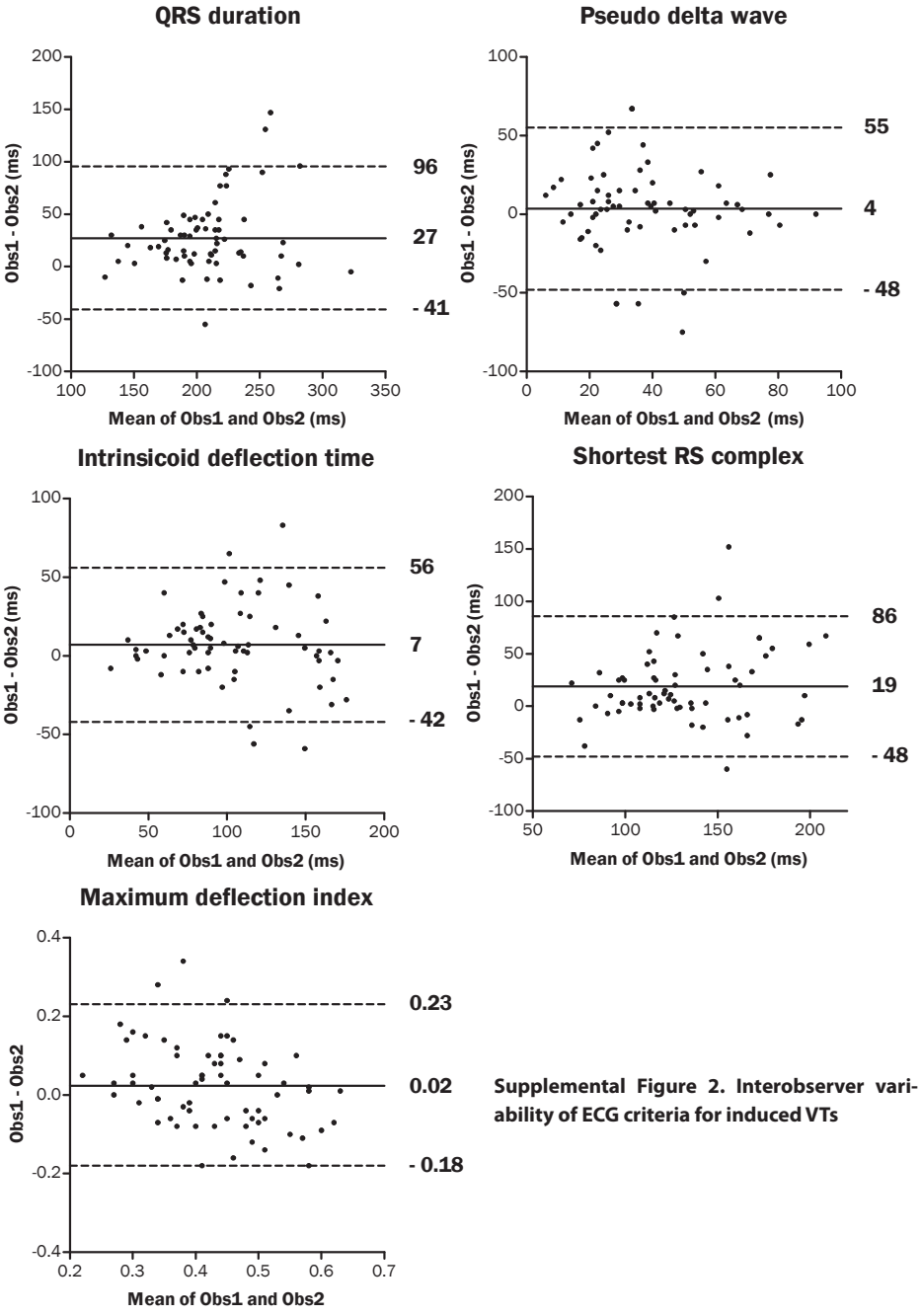
gest that the ECG criteria do not allow identification of patients who are likely to benefit from a primary epicardial ablation approach. The VT CL and the use of AADs affect the accuracy of ECG criteria in induced VTs.

REFERENCE LIST

1. Nakahara S, Tung R, Ramirez RJ, Michowitz Y, Vaseghi M, Buch E, Gima J, Wiener I, Mahajan A, Boyle NG, Shivkumar K. Characterization of the arrhythmogenic substrate in ischemic and nonischemic cardiomyopathy implications for catheter ablation of hemodynamically unstable ventricular tachycardia. J Am Coll Cardiol 2010;55(21):2355-65.
2. Valles E, Bazan V, Marchlinski FE. ECG criteria to identify epicardial ventricular tachycardia in nonischemic cardiomyopathy. Circ Arrhythm Electrophysiol 2010;3(1):63-71.
3. Bazan V, Gerstenfeld EP, Garcia FC, Bala R, Rivas N, Dixit S, Zado E, Callans DJ, Marchlinski FE. Site-specific twelve-lead ECG features to identify an epicardial origin for left ventricular tachycardia in the absence of myocardial infarction. Heart Rhythm 2007;4(11):1403-10.
4. Berruezo A, Mont L, Nava S, Chueca E, Bartholomay E, Brugada J. Electrocardiographic recognition of the epicardial origin of ventricular tachycardias. Circulation 2004; 109(15):1842-7.
5. Daniels DV, Lu YY, Morton JB, Santucci PA, Akar JG, Green A, Wilber DJ. Idiopathic epicardial left ventricular tachycardia originating remote from the sinus of Valsalva: electrophysiological characteristics, catheter ablation, and identification from the 12-lead electrocardiogram. Circulation 2006;113(13):1659-66.
6. Piers SR, van Huls van Taxis CF, Tao Q, van der Geest RJ, Askar SF, Siebelink HM, Schalij MJ, Zeppenfeld K. Epicardial substrate mapping for ventricular tachycardia ablation in patients with non-ischaemic cardiomyopathy: a new algorithm to differentiate between scar and viable myocardium developed by simultaneous integration of computed tomography and contrast-enhanced magnetic resonance imaging. Eur Heart J 2012;34(8):586-96.
7. van Huls van Taxis CF, Wijnmaalen AP, Piers SR, van der Geest RJ, Schalij MJ, Zeppenfeld K. Real-Time Integration of MDCT-Derived Coronary Anatomy and Epicardial Fat: Impact on Epicardial Electroanatomic Mapping and Ablation for Ventricular Arrhythmias. JACC Cardiovasc Imaging 2013;6(1):42-52.
8. Piers SR, Leong DP, van Huls van Taxis CF, Tayyebi M, Trines SA, Pijnappels DA, Delgado V, Schalij MJ, Zeppenfeld K. Outcome of Ventricular Tachycardia Ablation in Patients with Nonischemic Cardiomyopathy: The Impact of Noninducibility. Circ Arrhythm Electrophysiol 2013; 6(3):513-21.
9. Martinek M, Stevenson WG, Inada K, Tokuda M, Tedrow UB. QRS characteristics fail to reliably identify ventricular tachycardias that require epicardial ablation in ischemic heart disease. J Cardiovasc Electrophysiol 2012;23(2):188-93.



Supplemental Figure 1. Interobserver variability of ECG criteria for clinically documented VTs



Supplemental Figure 2. Interobserver variability of ECG criteria for induced VTs

Chapter 7

Influence of Steroid Therapy on the Incidence of Pericarditis and Atrial Fibrillation Following Percutaneous Epicardial Mapping and Ablation for Ventricular Tachycardia

Sebastiaan RD Piers, MD, Katia Dyrda, MD, MSc, Carine F. van Huls van Taxis, MD, Martin J Schalij, MD, PhD, Katja Zeppenfeld, MD, PhD

Sebastiaan R.D. Piers and Katia Dyrda share first authorship on this manuscript

Circulation: Arrhythmia & Electrophysiology 2014;7(4):671-6

ABSTRACT

Background

This study evaluates the influence of 3 therapeutic approaches on the incidence of pericarditis and atrial fibrillation (AF) following percutaneous epicardial mapping and ablation for ventricular tachycardia (VT).

Methods and Results

Eighty-five consecutive procedures (2006 to 2011) were retrospectively reviewed. After the first 17 procedures (20.0%), no steroids were administered. For the subsequent 30 (35.3%), systemic steroids were administered intravenously or orally (IV/PO) while the last 38 (44.7%) were followed by intrapericardial steroid injection.

Compared to no steroids, the incidence of pericarditic chest pain was significantly reduced by intrapericardial steroids (58.8% vs. 21.1%, p=0.006), but not by IV/PO steroids (58.8% vs. 43.4%, p=0.31). There was no significant difference in the incidence of pericarditic ECG with steroids (36.8, 30.0%, and 41.2% for intrapericardial, IV/PO and none, respectively). There was a non-significant reduced incidence of chest pain with ECG changes with steroids (13.2%, 10.0%, and 29.4% for intrapericardial, IV/PO and none, respectively). Radiofrequency applications (65.9% of procedures), did not affect the incidence of pericarditic ECG changes, pericarditic chest pain or pericarditis (all p>0.05). In 7 (8.3%) patients with no prior history of AF, AF was documented a median 36 hours post procedure. Patients with pericarditic ECG tended to be at greater risk of AF (16.7 vs. 3.6%, p=0.091)

Conclusion

There is a high incidence of pericarditic chest pain and ECG changes following epicardial VT mapping and ablation. Pericarditic chest pain is significantly decreased by intrapericardial steroids. Procedure-related AF is relatively frequent and tends to occur more commonly with pericarditic ECG changes.

INTRODUCTION

Catheter ablation of ventricular tachycardia (VT) is increasingly employed for both idiopathic and scar-related etiologies.[1] In particular, in patients with nonischemic cardiomyopathy, the substrate for VTs is often located intramurally or subepicardially and may require a percutaneous, transpericardial approach. In virtually all patients who undergo an epicardial procedure, pericarditis occurs to a variable extent as a result of local inflammation.[4] This can manifest clinically from mild pericarditis to hemorrhagic pericardial effusion and, rarely, cardiac tamponade.[4] If symptoms occur, patients may be treated with oral anti-inflammatory nonsteroidal and corticosteroid agents. Data on the pharmacokinetic profile of intrapericardially delivered agents has proven favorable suggesting that targeted local concentrations can be reached with minimal systemic concentrations (therefore reducing the potential risk of systemic side effects).[4] Intrapericardial corticosteroids and Hyaluronic Acid have been successfully used to treat recurrent noninfectious pericarditis[5-8] and to prevent adhesions after open-chest cardiac surgery.[9, 10] The intrapericardial instillation of 2 mg/kg of triamcinolone acetate after epicardial radiofrequency ablation was demonstrated to successfully prevent the occurrence of postprocedure pericarditis and adhesions in porcine animal.[4] Prevention of adhesions may be important given the potential need to re-obtain access to the pericardial space due to recurrence of arrhythmia.

The occurrence of new onset atrial fibrillation (AF) after epicardial VT ablation was recently reported to be 19.5% within 7 days.[13] In that study, all patients who developed AF had symptoms of pericarditis. Of note, episodes of AF after epicardial VT ablation may be accompanied by the risk for thromboembolic complications, as oral anticoagulation is relatively contraindicated due to the risk for pericardial bleeding.

This study was thus designed to evaluate the influence of 3 therapeutic approaches on the incidence of pericarditis and AF following percutaneous epicardial mapping and ablation for VT.

METHODS

A total of 85 consecutive procedures in which epicardial mapping or mapping and radiofrequency ablation was performed for VT between 2006 and 2011 were retrospectively reviewed. All patients were treated according to our standard clinical protocol and provided informed consent.

Access to the pericardial space

Prior to the procedure, oral anticoagulation was discontinued. On the day of the procedure, all forms of heparin were withheld. Local anesthesia with conscious sedation was the standard approach for procedural analgesia. Femoral venous and arterial access was obtained and a quadripolar catheter was positioned at the right ventricular (RV) apex. The pericardial space was then entered via a transthoracic percutaneous subxyphoid puncture with a 17-gauge Tuohy needle. Under fluoroscopic guidance, contrast media was injected as the needle was advanced to the pericardium. Once access into the pericardial space was obtained, a guidewire was passed through the needle, over which a 6F introducer sheath was advanced. A 6F pigtail catheter was then introduced into the epicardial space to protect the sheath and the guidewire was removed. Intravenous heparin was then administered to allow for safe endocardial mapping and ablation.

Mapping and Ablation Procedure

Prior to epicardial mapping, detailed endocardial mapping was performed to determine the epicardial area of interest in order to restrict epicardial mapping and minimize potentially painful manipulations. A 3.5mm irrigated-tip catheter (NaviStar ThermoCool, Biosense Webster Inc, Diamond Bar, CA, USA) was then inserted after replacing the 6F by an 11cm 8F introducer sheath (Cordis) and was maneuvered within the pericardial space for cardiac mapping and ablation. A 63 cm, 8.5F sheath (SLO St-Jude Medical) and subsequently a steerable 71 cm 8.5F sheath (Agilis NxT, medium curl, St-Jude Medical) was used in later procedures. The radiofrequency (RF) ablation generator used was the Stockert generator (Biosense-Webster Inc). Epicardial applications were delivered up to 50W, flow rate 20ml/min with a temperature limit of 45°C, and delivered for up to 60 seconds each. Fluid was removed after a maximum of 5 RF applications corresponding to an estimated amount of 100cc.

Administration of Anti-inflammatory Agents

The therapeutic approach evolved over time from no steroid therapy to systemic steroids to intrapericardial steroids without overlap between the groups. At the end of the first 17 procedures (20.0%), no steroids were administered. For the subsequent 30 (35.3%), systemic steroids were administered intravenously or orally (IV/PO) at a dose of 1mg per kg per day for 3 consecutive days. The last 38 (44.7%) procedures were followed by complete fluid removal and intrapericardial steroid injection, consisting of triamcinolone acetate (2mg/kg), which was injected in the pericardial space via a pigtail catheter and left in-situ by capping the pigtail. The pigtail was not placed under vacuum. Non-steroidal anti-inflammatory drugs (NSAIDS), in the form of diclofenac 50 mg every 8 hours, were offered on an as-needed basis to all patients who did not have contraindications.

Postablation Care and Evaluation

Standard post-operative monitoring was performed in all patients, consisting of the first 24 hours in the coronary care unit and at least another 48 hours on the ward. Electrocardiograms (ECGs) were obtained immediately following the procedure and subsequently every 12 hours until discharge. Trans-thoracic echocardiography was performed prior to pigtail removal, and again 12 and 24 hours after pigtail removal.

Anticoagulation, where indicated, was restarted after removal of the pigtail catheter. In patients who developed AF, an early cardioversion at < 24 hours of AF duration was favored in order to avoid the need for anticoagulation. Otherwise, for persistent AF, anticoagulation was initiated ≥24 hours after pigtail removal.

Pericarditis definition

Pericarditis was defined as typical pericarditic chest pain (pleuritic, improved with sitting upright) with acute pericarditic ECG changes (new widespread ST elevation or PR depression).

Statistical analysis

Statistical analyses were performed with SPSS version 20 (IBM, Somers, New York, USA). The continuous variables were expressed as number (percentage), mean ± SD or median (interquartile range) where appropriate. Chi-square tests, Fisher's exact tests, Student's t tests and Mann-Whitney U tests were performed where applicable. To analyze the effect of steroid treatment on pericarditic chest pain, pericarditic ECG changes and pericarditis, overall chi-square tests were performed to compare the three treatment groups. Then, two one-by-one comparisons were performed, applying the Bonferroni correction for multiple comparisons so that a p-value of $p < 0.025$ was considered to be statistically significant. For all other tests, a p-value of $p < 0.05$ was considered to be statistically significant.

RESULTS

Eighty-five epicardial procedures were reviewed which were performed in 76 patients. Seven patients required a second epicardial procedure (4 of 7 within 2 weeks after the first procedure) and of those 7 patients, 2 underwent a third epicardial procedure 67 and 84 days after the second procedure. The patient characteristics are presented in Table 1. Only 8 procedures (9.4%) were performed under general anesthesia.

Epicardial mapping alone was performed in 29 (34.1%) while 56 (65.9%) underwent mapping and ablation. A non-steerable long sheath (SR0 or SL0) was used in 22 cases (25.9%) while an Agilis sheath was used in 42 cases (49.4%). In the mapping only group,

Table 1. Patient characteristics

	All patients (n=85)	No Steroids (n=17)	Systemic Steroids (n=30)	Intra-Pericardial Steroids (n=38)
Age (years)	58 ±17	56 ±21	58 ±17	59 ±15
Male, n (%)	67 (79%)	16 (94,1%)	22 (73,3%)	29 (76,3%)
LVEF(%)	42 ±13	46 ±13	40 ±15	41 ±12
VT related to				
Ischemic CMP, n (%)	13 (15,3%)	1 (5,9%)	6 (20,0%)	6 (15,8%)
DCM, n (%)	32 (37,6%)	8 (47,1%)	12 (40,0%)	12 (31,6%)
Other structural heart disease, n (%)	26 (30,6%)	5 (29,4%)	8 (26,6%)	13 (34,2%)
Idiopathic VT, n (%)	14 (16,5%)	3 (17,6%)	4 (13,3%)	7 (18,4%)
Beta-blocker therapy, n (%)	45 (52,9%)	8 (47,1%)	18 (60,0%)	19 (50,0%)
Amiodarone, n (%)	32 (37,6%)	6 (35,3%)	13 (43,3%)	13 (34,2%)
Other AAD, n (%)	38 (44,7%)	5 (29,4%)	15 (50,0%)	18 (47,4%)

ADD: anti-arrhythmic drug; CMP: cardiomyopathy; DCM: dilated cardiomyopathy; LVEF: left ventricular ejection fraction; VT: ventricular tachycardia

epicardial ablation was not performed due to anatomical limitations (coronary arteries or thick fat layer), or because no epicardial ablation target site for VT could be identified.

In the first 17 procedures (20.0%), no steroids were administered. In the subsequent 30 (35.3%), systemic steroids were administered IV or PO while in the last 38 (44.7%), intrapericardial steroids were given. On the ward, 62% of patients received NSAIDS for a variety of complaints including chest pain, pain at the pigtail insertion site but also headaches, back pain and others. The distribution of NSAIDS was the following: 4 of 17 patients (24%) received NSAIDS who had received no steroids, 28 of 30 patients (93%) received NSAIDs who had received systemic steroids, and, 21 of 38 patients (55%) received NSAIDs who had received intrapericardial steroids ($p < 0.001$).

Pericarditis occurred after 15.3% of procedures. Pericarditic ECG changes alone, or typical pericarditic chest pain alone, were diagnosed in 20.0% and 21.2%, respectively. There was no age difference between the patients who developed pericarditis and those who did not, with mean ages of 57.6±17.3 vs. 58.9±15.1 years respectively (p=0.474). Clinical chest pain developed within 12 hours of the procedure while the ECG changes occurred within 20 hours at the latest.

The results of the influence of steroid therapy on the incidence of pericarditis are presented in figure 1. The incidence of pericarditic chest pain was significantly reduced if patients received intrapericardial steroids (21.1%) compared to no steroids (58.8%) (p=0.006). Systemic steroids administration did not significantly reduce the incidence of pericarditic chest pain (43.4% vs. 58.8% for patients receiving IV/PO steroids or no steroids, respectively, p=0.31). There was no significant difference in the incidence of pericarditic ECG with steroid therapy (36.8%, 30.0%, and 41.2% for intrapericardial, IV/

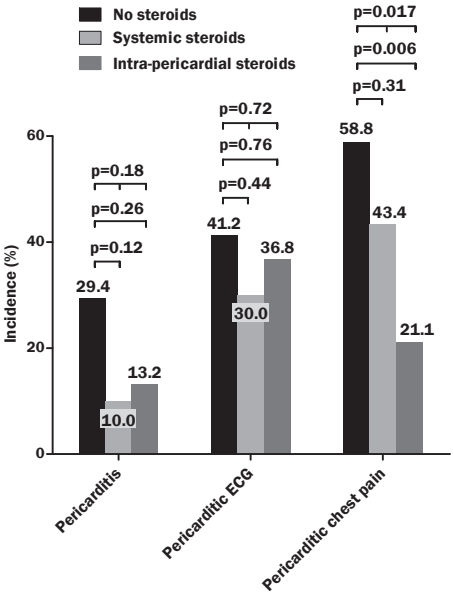


Figure 1. Impact of steroid therapy on the incidence of pericarditis

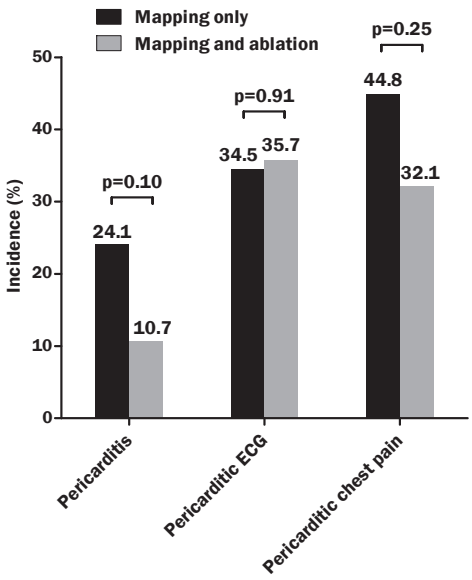


Figure 2. Influence of mapping and ablation on the incidence of pericarditis

PO or none, respectively). There was a non-significant reduced incidence of chest pain with ECG changes with steroids (13.2%, 10.0%, and 29.4% for intrapericardial, IV/PO or none, respectively. Results were similar when only first procedures were analyzed.

There was no statistical difference between mapping alone and mapping with ablation in the incidence of pericarditic chest pain (44.8 vs. 32.1%, p=0.249), pericarditic ECG (34.5 vs 35.7%, p=0.910), or both chest pain and ECG changes (24.1 vs. 10.7%, p=0.103) as demonstrated in Figure 2.

The details relating to procedure duration are displayed in Table 2 including procedure duration from time of sheath insertion to sheath removal (median 4h:01min, IQR 3h:20min – 4h:40min), procedural duration from pericardial puncture to pigtail placement (median 3h:08min, IQR 2h:15min – 4h:02min) and procedure duration from start of epicardial mapping to pigtail placement (median 2h:00min, IQR 1h:14min – 2h:40min).

Table 2. Procedural length

	All patients
Procedure duration from sheath placement to sheath removal	4h:01min (3h:20min – 4h:40min)
Duration from pericardial puncture to pigtail placement	3h:08min (2h:15min – 4h:02min)
Duration from start epicardial mapping to pigtail placement	2h:00min (1h:14min – 2h:40min)
Fluoroscopy time	47 min (32 – 56 min)

Variables are expressed as median (interquartile range).

There was no difference comparing the above three duration times between patients with vs. without chest pain, with vs. without pericarditic ECG changes, and with vs. without both chest pain and pericarditic ECG changes.

A pigtail catheter was left in the pericardial space less than 3 hours in 8% of patients while 44% patients had the pigtail for greater or equal to 24 hours. Patients with a pigtail for ≥24 hours more often had chest pain (51% vs. 25%, p=0.012), but less often ECG changes (19% vs. 48%, p=0.006) as shown in Table 3.

Table 3. Influence of the presence of a pigtail catheter on the incidence of pericarditis

	Pigtail ≥24 hours	Pigtail < 24 hours	p
Chest pain	19/37 (51%)	12/48 (25%)	0.012
ECG changes	7/37 (19%)	23/48 (48%)	0.006
Chest pain and ECG changes	4/37 (11%)	9/48 (19%)	0.31

A total of 13 patients developed a post-procedural pericardial effusion or tamponade with a mean effusion of 12 +/- 7 mm by transthoracic echocardiography, observed 18 +/- 14 hours after the procedure. The effusion was noted at first echo in 8 of 13 patients, at second echo in 4 patients (20, 20, 20 and 19 hours after procedure) and at third echo in 1 patient (50 hours after procedure, but < 5mm).

In 7 (8.3%) patients with no prior history of AF, procedure-related AF was documented (paroxysmal in 4 and persistent in 3, requiring cardioversion). The median time to new AF was 36 hours (IQR 19 – 60 hours). For the persistent cases, 2 underwent rapid cardioversion while the last was anticoagulated for 6 weeks prior to cardioversion. Patients who developed new onset AF were older than the patients who did not, with ages of 64.7±7.6 vs. 57.2±17.3 years (p=0.016). Patients with a pericarditic ECG tended to be at greater risk of developing AF (16.7 vs. 3.6%, p=0.091). There were no complications associated with the episodes of AF. One patient had a recurrence of paroxysmal AF 18 months after resolution of the pericarditis.

The median length of stay in hospital post-procedure was 5 days (IQR 3 – 8 days). There was no statistically significant increase in the hospital stay duration due to the incidence of pericarditic chest pain (median 5 days, IQR 3 – 9 days vs. median 5 days, IQR 3 – 7 days, p = 0.75), pericarditic ECG (median 5 days, IQR 3 – 8 days vs. median 4 days, IQR 3 – 8 days, p = 0.98) or of pericarditis (median 5 days, IQR 3 – 9 days vs. median 5 days, IQR 3 – 8 days, p = 0.88).

In 7 patients, repeat epicardial access was required for a total of 9 procedures. In only one case, epicardial access to the area of interest could not be re-obtained. The patient thus underwent surgical dissection of adhesions and cryoablation. This patient had received oral steroids after his first 2 procedures. Of the 6 patients who underwent

unimpeded repeat procedures, one had received no steroid, 3 had received oral steroids while 2 had received intrapericardial steroids after the first procedure.

Figure 3 demonstrates pericardial adhesions as photographed in the operating room. Interestingly, although an inflammatory process clearly took place, this patient never reported chest pain and the ECG never demonstrated ECG changes typical of pericarditis.

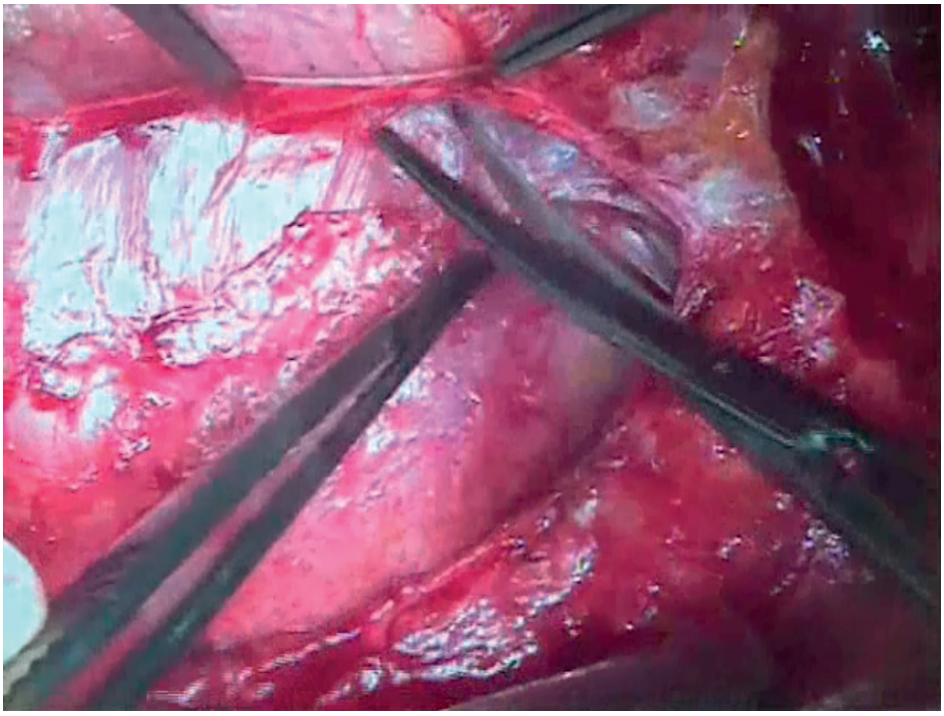


Figure 3. Dissection of epicardial adhesions during surgery

Complications

In total, 5 patients experienced a bleeding complication which can be further described as follows: 1 case (1.2%) of groin hematoma and 4 cases (4.7%) of moderate to severe pericardial bleeding (>80cc) occurring acutely in 2 and delayed in 2. For the acute bleeding cases, one occurred following epicardial puncture (without evidence of RV puncture) and resolved within 20 minutes while the second was due to RV puncture. In the first of the delayed bleeding cases, an echo performed due to clinical deterioration with shortness of breath demonstrated tamponade 13 hours post procedure in a patient who had accidentally been administered low-molecular weight heparin. The second case of delayed bleeding cases occurred in a patient on heparin and dual-antiplatelet therapy due to recent coronary artery stenting and was noted 4.75 hours post procedure on an echo performed due to low blood pressure and poor diuresis. The bleeding persisted for

the following 48 hours. Both were managed with percutaneous drainage. There were no procedure-related deaths.

There were no adverse consequences from the use of IP triamcinolone more specifically, no infection or myocardial perforation. The patients who underwent redo procedures did so, either as a planned staged approach due to extensive disease and lengthy first ablation procedure or, following VT recurrence more than a month after the first ablation procedure.

DISCUSSION

The prophylactic instillation of 2 mg/kg of intrapericardial corticosteroids has been demonstrated to effectively prevent inflammatory adhesions in a porcine model of post procedural pericarditis after epicardial mapping and ablation.[4] To date, the impact of intrapericardial steroid administration after epicardial mapping and ablation has not been studied in humans. In the present study, it is demonstrated for the first time that the use of intrapericardial steroids portends an important clinical benefit by significantly reducing the incidence of pericarditic chest pain. This is a valuable clinical gain as it is associated with increased patient satisfaction. The clinical benefits of the use of intrapericardial steroids may stem from the mode of delivery, the pharmacokinetics and metabolism of the drug and, the duration of exposure to the drug. Triamcinolone is an intermediate acting, liver metabolized glucocorticoid. Triamcinolone acetate is the more potent type of triamcinolone, being about eight times as effective as prednisone. The drug thus delivered directly and left in the pericardial space can be absorbed locally. In addition, in this work the drug was left in-situ rather than being simply flushed through the epicardial space.

Intrapericardial instillation of steroids has also been used in other clinical settings including recurrent idiopathic pericarditis and uremic pericarditis where studies have consistently demonstrated safety. In the present series, a therapeutic dose of intrapericardial triamcinolone 2mg/kg was thus chosen. Importantly, there were no adverse consequences from the use of IP triamcinolone more specifically, no infection or myocardial perforation.

Two recently published studies have reported a widely varying incidence of chest pain after mapping and/or ablation in the epicardium.[11,12] The first reported chest pain in almost all patients,[11] whereas the second reported a 21% incidence with 1 out of 6 participating centers using systemic steroids routinely and another 1 out of 6 participating centers using intrapericardial infusion of steroids routinely[12]. The etiology of the pain in some cases was felt to be related, not only to the epicardial mapping and ablation, but also to the friction of the pigtail left in the pericardium for continuous drainage.[12]

In our series, we report an incidence of chest pain of 36.5% (21.2% chest pain only and 15.3% chest pain with ECG changes). Some of the difference in the reported numbers may arise from the difficulty in accurately assessing the quality of the pain retrospectively. In addition, similarly to our approach, the centers included in the above series used a conscious sedation approach, where the analgesic drugs and dosages administered varied and thus provided a varying degree of post-procedural pain control. Also, the type of ablation catheter and sheaths varied from center to center. Furthermore, the use of NSAIDs was not uniform, where in one series it ranged from being left to the discretion of the physician to being prescribed almost routinely for a week[11]. Nevertheless, in the series where steroids were used,[12] including but not only intrapericardial steroids, a lower incidence of chest pain was reported.

With respect to AF, the incidence of 8.3% reported in the present series sits within the range previously quoted in the literature. Already in 1976, the incidence of AF in a cohort of 100 patients with pericarditis was reported to be 5%.[14] An incidence of 19.5% was reported for new onset AF within 7 days of procedure in a recent series of 41 patients undergoing epicardial VT ablation.[13] In that series, patients developing AF were significantly younger than those without AF whereas our study demonstrated the opposite. They also described lack of amiodarone therapy as a risk factor for procedurally related new onset AF. Interestingly, in the data presented here, none of the patients who developed new onset AF were receiving amiodarone therapy for VT nor did they receive it post-procedurally for AF prevention. On a more concordant note, in their series, all patients with new onset AF had clinical symptoms of pericarditis while in the present data there was a trend towards AF occurring more commonly in patients with pericarditic ECG changes. In addition, 85.7% of the patients with new onset AF in the present series had both mapping and ablation performed. The diverging results between the 2 studies can be in large part explained by the small number of patients developing procedure-related AF in the present series.

Limitations

No randomization was performed, however, the therapeutic approaches in the current study were applied non-selectively in consecutive patients. The findings are therefore highly suggestive for an effect of intrapericardial steroids on pericarditic chest pain after epicardial mapping and/or ablation. As this is a retrospective study, it is difficult to ascertain from the charts whether patients requested NSAIDs only after the onset of chest pain. The use of NSAIDs however may have had an influence on clinical variables such as pericarditic ECG changes, even if the NSAIDs were started after the onset of chest pain. The dose of steroids was unchanged over time and as a result, the most effective dose of steroids for the prevention of pericarditic chest pain could not be determined. Although the number of procedures in this study was relatively large, some subgroup

analyses were still limited by the sample size. In addition, given that the introduction of the Agilis sheath was contemporary to the introduction of intrapericardial steroids, the relative impact of each variable on the incidence of pericarditis cannot be further determined. However, as the steerable Agilis sheath is assumed to be more traumatic than a non-steerable sheath, the impact of the intrapericardial steroid on the reduction of clinical pericarditic chest pain may be even underestimated.

CONCLUSION

There is a high incidence of pericarditic chest pain and, of pericarditic ECG following percutaneous epicardial access for VT mapping and ablation. Complaints of pericarditic chest pain are significantly decreased by the administration of intrapericardial steroids, but not IV/PO steroids. Procedure-related AF is relatively frequent and tends to occur more commonly in patients with pericarditic ECG changes.

CLINICAL PERSPECTIVE

Catheter ablation for ventricular tachycardia is increasingly used and may require a percutaneous, epicardial approach. Complications of an epicardial approach include, among others, pericarditis and atrial fibrillation. This study was thus designed to evaluate the influence of steroid therapy, delivered systemically or intrapericardially versus the absence of steroids, on the incidence of pericarditis and atrial fibrillation after percutaneous epicardial mapping and ablation for ventricular tachycardia. The results demonstrate a high incidence of pericarditic chest pain and ECG changes after epicardial ventricular tachycardia mapping and ablation. Pericarditic chest pain is significantly decreased by the use of intrapericardial steroids. Procedure- related atrial fibrillation is relatively frequent and tends to occur more commonly with pericarditic ECG changes. There were no adverse consequences from the use of intrapericardial triamcinolone. The administration of intrapericardial triamcinolone does thus provide clinical benefits, specifically greater patient comfort, and may be considered for routine use after epicardial ventricular tachycardia ablation procedures.

REFERENCE LIST

1. Sacher F, Tedrow UB, Field ME, Raymond J-M, Koplan BA, Epstein LM, Stevenson WG. Ventricular tachycardia ablation evolution of patients and procedures over 8 years. *Circ Arrhythm Electrophysiol*. 2008;1(3):153-161.
2. Cesario DA, Vaseghi M, Boyle NG, Fishbein MC, Valderrabano M, Narasimhan C, Wiener I, Shivkumar K. Value of high-density endocardial and epicardial mapping for catheter ablation of hemodynamically unstable ventricular tachycardia. *Heart Rhythm*. 2006;3(1):1-10.
3. Roberts-Thomson KC, Seiler J, Steven D, Inada K, Michaud GF, John RM, Koplan BA, Epstein LM, Stevenson WG, Tedrow UB. Percutaneous access of the epicardial space for mapping ventricular and supraventricular arrhythmias in patients with and without prior cardiac surgery. *J Cardiovasc Electrophysiol*. 2010;21(4):406-411.
4. D'Avila A, Neuzil P, Thiagalingam A, Gutierrez P, Aleong R, Ruskin JN, Reddy VY. Experimental efficacy of pericardial instillation of anti-inflammatory agents during percutaneous epicardial catheter ablation to prevent postprocedure pericarditis. *J Cardiovasc Electrophysiol*. 2007;18(11): 1178-1183.
5. Buselmeier TJ, Simmons RL, Najarian JS, Kjellstrand CM. Intrapericardial steroids in uremic pericarditis. *Lancet*. 1977;2(8032): 301-302.
6. Grubb SR, Cantley LK, Jones DL, Carter WH. Iatrogenic cushings-syndrome after intra-pericardial corticosteroid-therapy. *Ann Intern Med*. 1981;95(6):706-707.
7. Maisch B, Ristic AD, Pankuweit S. Intrapericardial treatment of autoreactive pericardial effusion with triamcinolone - the way to avoid side effects of systemic corticosteroid therapy. *Eur Heart J*. 2002;23(19):1503-1508.
8. Medani CR, Ringel RE. Intrapericardial triamcinolone hexacetonide in the treatment of intractable uremic pericarditis in a child. *Pediatr Nephrol*. 1988;2(1):32-33.
9. Mitchell JD, Lee R, Neya K, Vlahakes GJ. Reduction in experimental pericardial adhesions using a hyaluronic-acid bioabsorbable membrane. *Eur J Cardiothorac Surg*. 1994; 8(3):149-152.
10. Seeger JM, Kaelin LD, Staples EM, Yaacobi Y, Bailey JC, Normann S, Burns JW, Goldberg EP. Prevention of postoperative pericardial adhesions using tissue-protective solutions. *J Surg Res*. 1997;68(1):63-66.
11. Sacher F, Roberts-Thomson K, Maury P, Tedrow U, Nault I, Steven D, Hocini M, Koplan B, Leroux L, Derval N, Seiler J, Wright MJ, Epstein L, Haissaguerre M, Jais P, Stevenson WG. Epicardial ventricular tachycardia ablation a multicenter safety study. *J Am Coll Cardiol*. 2010;55(21):2366-2372.
12. Della Bella P, Brugada J, Zeppenfeld K, Merino J, Neuzil P, Maury P, Maccabelli G, Vergara P, Baratto F, Berruezo A, Wijnmaalen AP. Epicardial ablation for ventricular tachycardia: a European multicenter study. *Circ Arrhythm Electrophysiol*. 2011;4(5): 653-659.
13. Mahapatra S LD, Bhamidipati CM, McDaniel G, Kamath S, Bunch TJ, Ailawadi G. Incidence, risk factors, and consequences of new-onset atrial fibrillation following epicardial ablation for ventricular tachycardia. *Europace*. 2011;13(4):548-554.
14. Spodick D. Arrhythmias during acute pericarditis. A prospective study of 100 consecutive cases. *JAMA*. 1976;235(1):39-41

Chapter 8

Outcome of Ventricular Tachycardia Ablation in Patients with Nonischemic Cardiomyopathy: The Impact of Noninducibility

Sebastiaan R.D. Piers, MD, Darryl P. Leong, MBBS, MPHMD, PhD, Carine F.B. van Huls van Taxis, MD, Mohammad Tayyebi, MD, Serge A. Trines, MD, PhD, D.A. Pijnappels, PhD, Victoria Delgado, MD, PhD, Martin J. Schalij, MD, PhD, Katja Zeppenfeld, MD, PhD

Circulation: Arrhythmia & Electrophysiology 2013;6(3):513-21

ABSTRACT

Background

Ablation failure and recurrence rates after ventricular tachycardia (VT) ablation in nonischemic cardiomyopathy (NICM) are high and the optimal procedural endpoint is not well defined. This study assessed the outcome after ablation, the impact of noninducibility and other potential predictors of VT recurrence.

Methods and Results

Forty-five patients with NICM (60±16 years, LVEF 44±14%) accepted for VT ablation were included. Epicardial mapping was performed in 29 (64%). A median of 2 (first-to-third quartile, 2–4) VTs (cycle length [CL] 342±77ms) were induced per patient. After ablation, the complete programmed electrical stimulation protocol (3 drive CL, 3 extrastimuli ≥200ms, burst, ≥2 sites) was repeated. Complete success (non-inducibility of any monomorphic VT) was achieved in 17 patients (38%), partial success (elimination of clinical VT, persistent inducibility of non-clinical VT) in 17 patients (38%), and failure (persistent inducibility of clinical VT) in 11 patients (24%). During 25±15 months follow-up VT occurred in 24 patients (53%), but the 6-month VT burden was reduced by ≥75% in 79%. Recurrence rates were low after complete procedural success (18%), but high after both partial success (77%) and failure (73%). Non-complete procedural success was the strongest predictor of VT recurrence (hazard ratio 8.20, 95% confidence interval 2.37-28.43, p=0.001).

Conclusions

Although 53% of patients had VT during follow-up, the 6-month VT burden was decreased by ≥75% in 79%. Recurrence rates are low after complete procedural success, but high after both partial success and failure. Non-complete procedural success was the strongest predictor of VT recurrence.

INTRODUCTION

In patients with left ventricular (LV) non-ischemic cardiomyopathy (NICM) several aspects of ventricular tachycardia (VT) ablation require elucidation.

First, the procedural endpoint is not well defined. Although non-inducibility of VT by programmed electrical stimulation (PES) is frequently used as an endpoint, data supporting its predictive value for VT recurrence are mainly derived from patients after myocardial infarction (MI)[1,2] who are likely to have different substrates, higher procedural success and lower VT recurrence rates.[1,3] In addition, studies in post-MI patients are inconsistent, perhaps due to different induction protocols, incomplete application of protocols and differences between patient populations.[1,2,4-6] Data on the value of PES as a procedural endpoint in NICM are limited to two small series.[3,7] Recently, alternative endpoints have been proposed such as elimination of abnormal bipolar electrograms or late potentials consistent with slow conduction[4,8], late potentials are however less frequently found in patients with NICM than in post-MI patients.[3]

Second, risk factors for VT recurrence in NICM are not established. Risk stratification may allow an individually tailored treatment strategy. A conservative approach may be appropriate in patients at low risk, whereas patients at high risk may require either more extensive ablation or concomitant drug therapy.

Third, the role of VT ablation early in the therapeutic course (e.g. for a first VT, symptomatic ATP or a single ICD shock) is unclear in NICM patients. The indication for VT ablation in patients with structural heart disease has changed over time.[9] Recent recommendations apply to all patients with structural heart disease, although evidence is limited and based on trials conducted in post-MI patients.[10,11] The risk-benefit ratio of VT ablation early in the therapeutic course may be different in patients with NICM, in whom VT ablation is reported to be less effective[1,3] and may more often requires epicardial ablation, which is associated with a higher procedural risks.[12,13]

The aims of the current study are fourfold: 1) to determine the outcomes of VT ablation in NICM, 2) to assess the value of PES as a procedural endpoint, 3) to identify predictors of acute and long-term outcome, 4) to evaluate the role of VT ablation early in the therapeutic course in NICM.

METHODS

Patients

The study population consisted of 45 consecutive NICM patients who underwent VT ablation at the Leiden University Medical Centre between 1/2007 and 6/2011, including patients in whom no radiofrequency (RF) energy was delivered. All patients had systolic

impairment and evidence of scar in the LV based on contrast-enhanced MRI and/or electroanatomical mapping. Patients with significant coronary artery disease (>50% stenosis, assessed by coronary angiography in all patients), congenital heart disease, hypertrophic cardiomyopathy, arrhythmogenic right ventricular cardiomyopathy, left ventricular noncompaction, restrictive cardiomyopathy, (sub)acute myocarditis, cardiac sarcoidosis, toxic cardiomyopathy, tachycardia-induced cardiomyopathy or primary valvular abnormalities were excluded. All patients were treated according to the routine clinical protocol and provided informed consent.

Clinical presentation and procedural strategy

In patients presenting with incessant VT, ≥2 implantable cardioverter defibrillator (ICD) shocks or multiple VT recurrences after prior endocardial ablation, VT ablation was classified as 'late in the therapeutic course'. In these patients, epicardial mapping was always attempted if endocardial ablation did not result in complete success. In patients presenting with a first VT, symptomatic ATP or a single ICD shock, VT ablation was classified as 'early in the therapeutic course'. In these patients, epicardial mapping was not attempted in case of 1) prior surgery, 2) a septal or basal anterior substrate likely not reachable from the epicardium due to coronary arteries and/or a basal fat layer, 3) only remaining non-clinical very fast VT (cycle length [CL] ≤250ms), 4) patient preference.

Ventricular tachycardia induction

The procedure was performed under conscious sedation (n=43) or general anesthesia (n=2); anti-arrhythmic drugs (AADs) were discontinued for ≥5 half-lives with the exception of amiodarone (n=19; 42%). In patients who were not under general anesthesia, PES was performed before sedation and opioid administration. PES consisted of three drive CLs (600, 500 and 400ms) with 3 ventricular extrastimuli (≥200ms) from ≥2 right ventricular sites and burst pacing. Positive endpoint was induction of sustained monomorphic VT lasting >30s or requiring termination because of hemodynamic compromise. Isoprenaline was used if the (presumptive) clinical VT could not be induced. Induced VTs were regarded clinical if the 12-lead ECG matched that of a spontaneous VT, or presumptive clinical when the CL matched that of an ICD-recorded VT (difference <30ms).

Electroanatomical mapping and ablation

Electroanatomical LV endocardial mapping was performed retrogradely during pacing or sinus rhythm using a 3.5mm, irrigated-tip catheter and an electroanatomical mapping system (NaviStar ThermoCool and CARTO XP™, Biosense Webster Inc, Diamond Bar, CA, USA). Epicardial mapping was performed through a subxyphoid puncture. Electrograms were filtered at 30-400Hz (bipolar) and 1-240Hz (unipolar). Endocardial areas with low bipolar voltage (≤1.50mV) or low unipolar voltage (≤8.27mV[14]), and epicardial areas

with low bipolar voltage (≤1.81mV[15]) and low unipolar voltage areas (≤7.95mV[15]) were considered abnormal and consistent with scar if ≥1cm^2 in size and accompanied by double potentials, fragmented electrograms, late potentials or other prolonged electrograms ≥50ms.[15] Substrates were classified as septal if they were predominantly located in one of the anteroseptal or inferoseptal segments. Endocardial and epicardial ablation target sites were identified based on the combination of substrate, pace, activation and entrainment mapping for stable VT, and based on substrate and pace mapping for unstable VT (defined as VTs requiring prompt termination[9]). At the epicardium, ablation was usually withheld when the estimated distance to a coronary artery was <5mm, as assessed by integrated CT-derived coronary anatomy and coronary angiography.[16] High output pacing (10mA, 2ms) was performed to determine the location of the phrenic nerve. RF energy was applied at 30-45W (maximum temperature 45ºC, flow 20-30mL/min, 60s) for endocardial sites and ≤50W (flow 20mL/min) for epicardial sites.

Acute procedural outcome and reasons for non-complete procedural success

After the last RF application, the entire PES protocol was repeated in each patient. Isoprenaline was administered if required to induce VT before ablation. Complete procedural success was defined as non-inducibility of any sustained monomorphic VT regardless of VT CL; partial success as elimination of the (presumptive) clinical VT but persistent inducibility of ≥1 nonclinical VT; failure as persistent inducibility of the (presumptive) clinical VT.

Reasons for non-complete procedural success (partial success and failure) were categorized as 1) vicinity of coronary arteries and/or epicardial fat, 2) proximity of the His bundle, 3) pericardial adhesions, 4) prolonged low cardiac output after electrical cardioversion, 5) no identifiable target site for fast clinical VT, 6) multiple cardioversions for non-clinical fast VT with hemodynamic collapse, 7) patient preference for medical therapy.

Follow-up

ICDs were offered to all patients regardless of acute procedural outcome. ICDs were typically programmed to include 3 zones: monitor zone (150-188bpm, ATP if indicated), fast VT zone (188-210bpm, ATP and shock), VF zone (>210bpm, if available ATP during charging, and shock). Patients were followed at 3, 6 and 12 months after ablation and at 6- to 12-monthly intervals thereafter. Recordings were analyzed by two experienced observers. Recurrence was defined as any VT treated with ATP or shock and any sustained VT occurring in the monitor zone, including VTs that occurred before discharge from the hospital. In patients without an ICD, VT recurrence was defined as sustained VT documented on a 24h Holter ECG or any complaints suggestive for VT. The reduction of

VT burden was calculated as follows: 1 – (# of VT episodes in period post-ablation / # of VT episodes in same period pre-ablation).

Disease progression

To analyze the effect of disease progression on VT recurrence, the LV end-diastolic volume (LVEDV) and LV ejection fraction (LVEF) were assessed by transthoracic echocardiography before the procedure and during follow-up. The annual changes in LVEDV and LVEF were calculated as follows: (value last echocardiogram – value baseline echocardiogram)/time interval in years.

Statistical analysis

Categorical variables are displayed as number (percentage) and continuous variables are expressed as mean±SD when normally distributed or median (first-to-third quartile [Q1-to-Q3]) when non-normally distributed. Categorical variables were compared using the χ^2 test or the Fisher's exact test when the expected value in any cell was below 5. Continuous variables were compared using the Student's *t* test when normally distributed or the Mann-Whitney *U* test when non-normally distributed. The VT burden before and after ablation was compared using the Wilcoxon signed-rank test. Survival curves were estimated by the Kaplan-Meier method and compared by the log-rank test. Univariable logistic regression and Cox regression analysis were performed to identify predictors of acute procedural success and predictors of VT recurrence, respectively. Start of cardiac resynchronization therapy (CRT) during follow-up was included as a time-dependent covariate. Multivariable analyses were not performed due to the limited number of patients and events. Probability values are all 2-sided and, if not otherwise specified, a probability value <0.05 was considered statistically significant. Analyses were performed using SPSS 20.0 software (SPSS Inc, Chicago, Ill).

RESULTS

Patients

Forty-five consecutive patients with NICM (76% male, age 60±16 years) were included after failure of 1.8±1.0 AADs. Twelve patients (27%) had previously undergone endocardial VT ablation, 2 of them at another center. Baseline characteristics are displayed in Table 1, the procedural strategy in Figure 1.

Procedure

A median of 2 (Q1-to-Q3, 2–4) VTs with a mean CL of 342±77ms was induced per patient. Clinical VTs (mean CL 363±98ms) were induced in 43 patients (96%) and only non-clinical

VT in 2 patients (4%), which was based on the 12 lead ECG in 36 patients (80%) and on ICD recordings in 9 patients (20%). In only one patient isoprenaline administration was required to induce the clinical VT before ablation (2%). Bundle branch re-entry (BBR) VT was induced in 3 patients (7%).

Table 1. Baseline characteristics.

	n=45
Male	34 (76%)
Age, years	60±16
NYHA classification	
I	17 (38%)
II	13 (29%)
III or IV	15 (33%)
LV ejection fraction, %	44±14
LV end-diastolic volume, mL	171±70
History of atrial flutter/fibrillation	14 (31%)
History of hypertension	16 (36%)
Body mass index, kg/m^2	27±5
Diabetes mellitus	5 (11%)
Estimated GFR	
30-60 mL/min	6 (13%)
<30 mL/min	4 (9%)
VT burden 6 months (episodes)	7 (3 - 25)
VT burden 12 months (episodes)	8 (3 - 31)
Incessant VT	5 (11%)
VT storm[9]	17 (38%)
ICD shocks in last 12 months	
0	23 (51%)
1	9 (20%)
≥2	13 (29%)
Electrical storm in last 12 months	8 (18%)
Clinical VTs >1 morphology	13 (29%)
Cycle length of clinical VT(s)	363±98
Failed anti-arrhythmic drugs	
Class I	9 (20%)
β-blocker	33 (73%)
Sotalol	15 (33%)
Amiodarone	22 (49%)
Calcium-antagonist	2 (4%)
ICD before ablation	30 (67%)
Prior endocardial VT ablation	12 (27%)

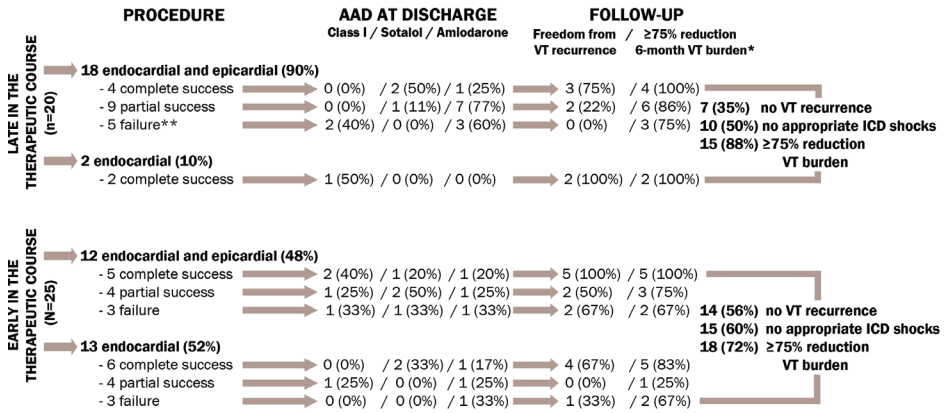


Figure 1. Procedural strategy

* In patients who have ≥6 months follow-up. ** Despite intraoperative cryoablation in 2 patients

Endocardial mapping was performed in all patients, percutaneous epicardial mapping in 29 patients (64%) and intraoperative epicardial mapping in 2 patients (4%, in one both percutaneous and intraoperative). Abnormal low bipolar or low unipolar voltage areas were present in all patients who underwent both endocardial and epicardial substrate mapping. Neither RF catheter ablation, nor intraoperative cryoablation was performed in 2 patients (4%) because no target site could be identified. Procedural data are summarized in Table 2.

Acute procedural outcome and reasons for non-complete success

Complete success was achieved in 17 patients (38%), partial success in 17 (38%) and failure in 11 (24%, including the 2 patients in whom neither RF nor cryoablation was performed). In 2 patients the clinical VT was abolished but the final induction protocol could not be completed due to prolonged low cardiac output after non-clinical VT induction; partial success was achieved in both.

The reasons for non-complete procedural success were proximity of coronary arteries and/or epicardial fat in 5 (18%), the proximity of the His bundle in 2 (7%), adhesions due to prior surgery in 1 (4%), prolonged low cardiac output after cardioversion in 2 (7%), no identifiable target site for fast clinical VT in 5 (18%), multiple cardioversions due to non-clinical fast VT with hemodynamic collapse in 11 (39%) and patient preference for medical therapy in 2 patients (7%).

Seven patients did not undergo epicardial mapping despite non-complete procedural success, because of prior surgery in one, a basal septal substrate likely not reachable from the epicardium based on contrast-enhanced MRI in one, patient preference in one and only remaining very fast non-clinical VT in the setting of ablation early in the therapeutic course in 4 patients.

Table 2. Procedural data.

	n=45
Number of VTs induced	
1	10 (22%)
2	16 (36%)
≥3	19 (42%)
Bundle branch re-entry VT	3 (7%)
Hemodynamic stability of VTs	
Only stable VT	14 (31%)
Only unstable VT	11 (24%)
Stable and unstable VT	20 (44%)
Cycle length of induced VTs (ms)	
Shortest	294±69
Mean	342±77
Longest	395±116
Pericardial puncture	29 (64%)
Endocardial substrate mapping	42 (93%)
Bipolar voltage area ≤1.50mV	29/42 (69%)
Unipolar voltage area ≤8.27mV	39/42 (93%)
Epicardial substrate mapping	27 (60%)
Bipolar voltage area ≤1.81mV	23/27 (85%)
Unipolar voltage area ≤7.95mV	23/27 (85%)
Predominantly septal substrate	19/42 (45%)
Substrate location/extent involves	
Any basal segment	40/42 (95%)
Any mid segment	25/42 (56%)
Any apical segment	12/42 (27%)
Radiofrequency energy applications	
Only endocardial	22 (49%)
Only epicardial	2 (4%)
Endocardial and epicardial	18 (40%)
None	3 (7%)
Intra-operative cryoablation	2 (4%)
Procedural duration (min)	206±86
Fluoroscopy time (min)	45±21

Predictors of acute procedural outcome

A higher age (odds ratio [OR] 1.78, p=0.01) and lower creatinine clearance (OR 1.28 per 10 mL/min decrease, p=0.03) were associated with non-complete procedural success (Figure 2). A trend was observed for lower LVEF (OR 1.52 per 10% decrease, p=0.09) and induction of unstable VT (OR 3.26, p=0.08).

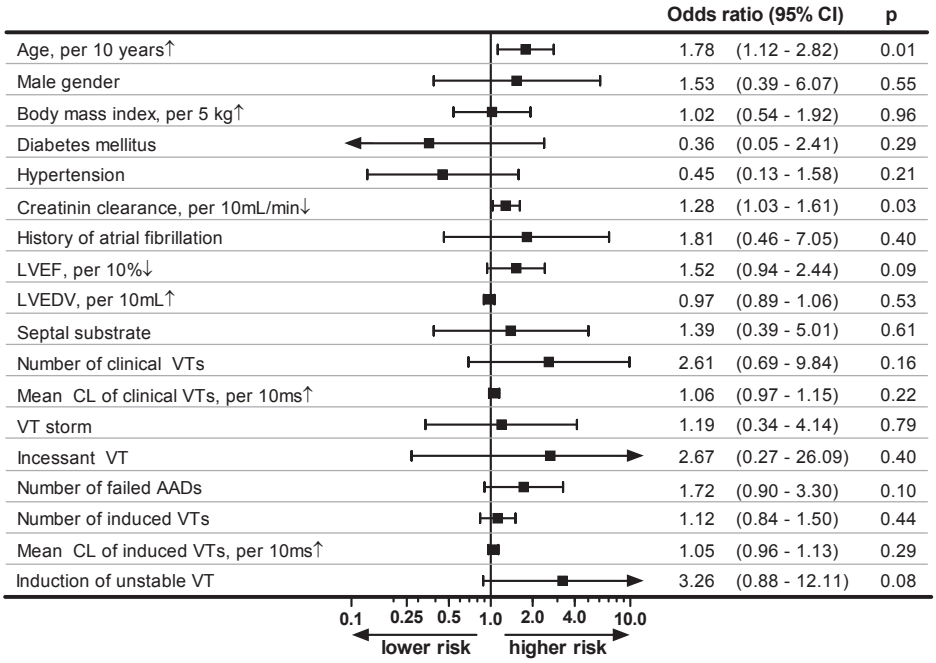


Figure 2. Predictors of non-complete procedural success
CI denotes confidence interval. CL, Cycle length

Complications

One patient developed a pseudo-aneurysm of the femoral artery. Acute pericardial bleeding >80mL occurred in 2/29 patients (7%) who underwent pericardial puncture. One patient (3%) who accidentally received heparin developed tamponade after the procedure managed by drainage.

VT recurrence during follow-up

All but 4 patients were discharged with an ICD; 8 patients (18%) were discharged on class I AADs, 29 (64%) on β-blocker, 10 (22%) on sotalol and 17 (38%) on amiodarone. During median 24 (Q1-to-Q3, 12–37) months follow-up (no patient lost to follow-up; at least 6 months follow-up in 42 patients, remaining 3 patients died within 6 months) 24 patients (53%) had VT recurrence, 20 (44%) received ≥1 ICD shock and 6 patients (13%) experienced an episode of electrical storm (defined as ≥3 appropriate ICD shocks within 24 hours). Only 1/8 patients with electrical storm before ablation had electrical storm recurrence.

The 6-month VT burden was reduced by ≥75% in 33/42 patients (79%) with at least 6 months follow-up (Figure 3). The 6-month VT burden was reduced equally in patients with and without an ICD before ablation (78% vs. 80% of patients ≥75% reduction,

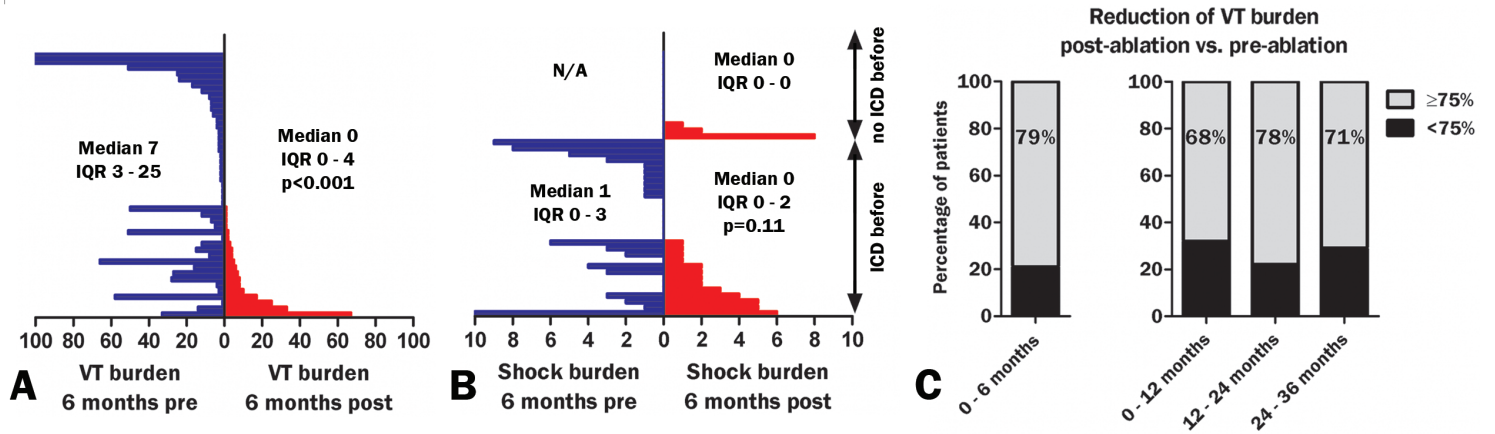


Figure 3. Reduction of ventricular tachycardia and shock burden after ablation

Panel A: All 45 patients are sorted according to 6-month ventricular tachycardia (VT) burden during follow-up on the right side of the y-axis (red bars), with the corresponding 6-month VT burden before ablation on the left side of the y-axis (blue bars). The VT burden is truncated at 100. Panel B: All 45 patients are sorted according to 6-month appropriate shock burden. Patients with (n=30) and without (n=15) an implantable cardioverter defibrillator (ICD) before ablation are displayed separately in the lower and upper parts of the graph, as indicated. The shock burden is truncated at 10. Panel C: Percentage of patients with ≥75% reduction of VT burden.

p>0.05). The 12-month VT burden was reduced by ≥75% in 68%, 78% and 71% of patients in the first, second and third year after ablation, respectively.

Eleven of 24 patients (46%) with VT recurrence had ≥1 fast VT (CL≤300ms) and 20/24 patients (83%) with VT recurrence received ≥1 appropriate ICD shock. A median of 23% (Q1-to-Q3, 5–64%) of all VTs per patient required a shock for termination.

Impact of noninducibility

Only 3/17 patients (18%) with complete procedural success had VT recurrence, compared with 13/17 patients (77%) with partial procedural success and 8/11 patients (73%) with procedural failure (Figure 4). The 6-month VT burden was reduced by ≥75% in 94%, 67% and 70%, respectively. Importantly, 6/11 patients (55%) with induction of a very fast VT (CL≤250ms) at the end of the procedure had VT recurrence, including 2/3 patients (67%) with persistent inducibility of clinical very fast VT and 4/8 patients (50%) with inducibility of non-clinical very fast VT.

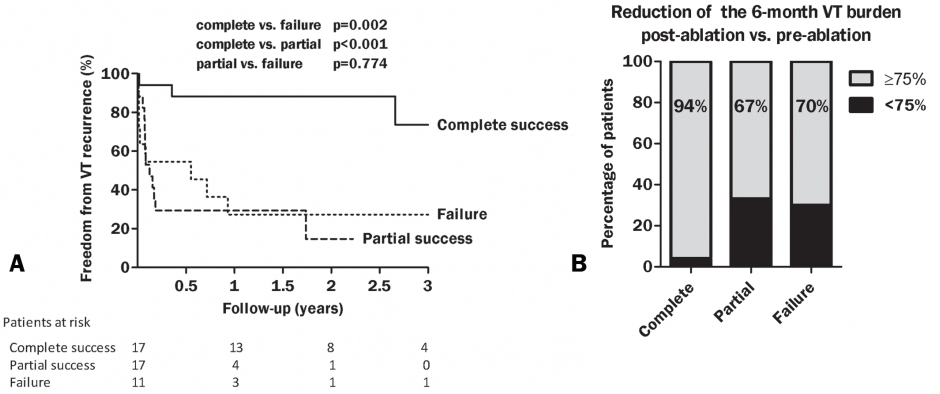


Figure 4. Ventricular tachycardia recurrence and reduction of the 6-month VT burden according to acute procedural outcome

Predictors of VT recurrence

Non-complete procedural success (hazard ratio [HR] 8.20, p=0.001), lower LVEF (HR 1.61 per 10% decrease, p=0.004), VT storm (HR 2.50, p=0.03), a higher number of failed AADs (HR 1.62, p=0.01) and a longer mean CL of induced VTs (HR 1.08 per 10ms increase, p=0.02) were identified as predictors of VT recurrence (Figure 5). A trend was observed for the number of induced VTs (HR 1.08 per VT, p=0.09).

Disease progression and VT recurrence

Disease progression was assessed by repeat echocardiography up to 19±9 months after baseline echocardiography in the 21/42 patients (50%) with at least 6 months follow-up.

The LVEF decreased by a median of 1.4% (Q1-to-Q3, -3.0–4.5%) and the LVEDV increased by a median of 10mL (Q1-to-Q3, -10–26mL) per year. In 5 patients (24%) the LVEF decreased by ≥5%/year, all had VT recurrence (100%). In 11 patients (31%) the LVEDV increased by ≥10mL/year, 7 had VT recurrence (64%).

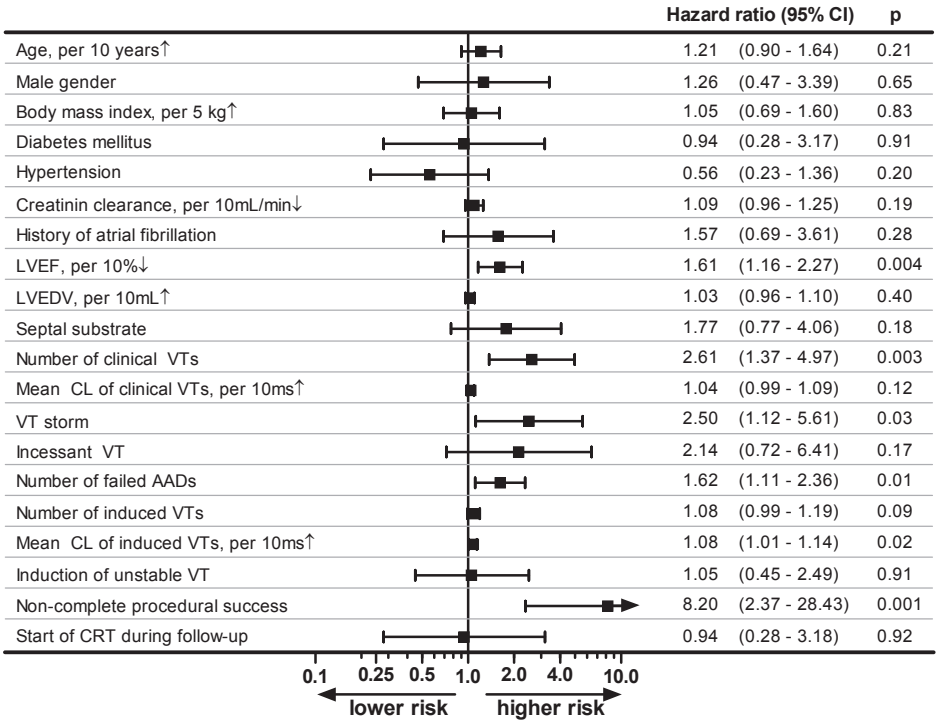


Figure 5. Predictors of ventricular tachycardia recurrence
CI denotes confidence interval; CRT, cardiac resynchronization therapy

VT ablation early in the therapeutic course

Epicardial mapping was performed in 12/25 patients (48%, Figure 1) who underwent VT ablation early in the therapeutic course (i.e. for a first VT, symptomatic ATP or a single ICD shock). Complete success was achieved in 11 (44%), partial success in 8 (32%) and ablation failed in 6 (24%). The procedure was complicated by a pseudo-aneurysm of the femoral artery in 1 patient (4%) and tamponade after the procedure in another (4%). During a median follow-up of 24 months (Q1-to-Q3, 13–37 months), 14 patients (56%) were free from VT and 15 (60%) were free from appropriate ICD shocks. Twelve of 25 patients (48%) were both off amiodarone and without recurrent VT during follow-up.

The acute success rate and VT recurrence rate were not significantly different between patients undergoing ablation early in the therapeutic course and the other patients (p=0.58 and p=0.17, Figure 1).

Repeat ablation

Repeat VT ablation was performed in 8/45 patients (18%) 11±11 months after the index procedure because of incessant VT and/or ≥1 appropriate ICD shock. Seven had prior partial success and one complete success. Pericardial puncture was performed in 4 (50%), but was unsuccessful due to adhesions in 2 patients who underwent epicardial mapping at baseline, despite intravenous steroids after the procedure. Complete procedural success was achieved in 3/8 patients (38%), partial success in 4 (50%) and failure in 1 (13%). During a mean follow-up of 17±13 months, 4 patients (50%) had VT recurrence and 2 (25%) received one appropriate ICD shock. Three of 6 patients (50%) with ≥6 months follow-up had ≥75% reduction of the 6-month VT burden.

Mortality during follow-up

Six patients (13%) died during follow-up. The cause of death was terminal heart failure (n=2), incessant VT in the setting of progressive heart failure (n=2), respiratory insufficiency after cardiac surgery (n=1) and cancer (n=1). Two patients (4%) underwent cardiac transplantation.

DISCUSSION

The main findings of this study can be summarized as follows: 1) although VT occurs in 53% of NICM patients after ablation, the 6-month VT burden was substantially reduced in 79%, 2) complete procedural success, defined as non-inducibility of any VT after the last RF application, was associated with low VT recurrence rates, whereas partial success and procedural failure were both associated with high recurrence rates, 3) non-complete procedural success, a lower LVEF, a higher number of clinical VTs, VT storm, a higher number of failed AADs and a higher mean CL of induced VTs are predictors of VT recurrence and 4) after VT ablation early in the therapeutic course, 56% of NICM patients remain free from VT recurrence.

Prior reports

To our knowledge, this series of NICM patients undergoing VT ablation and complete PES after the last RF delivery is the largest reported to date. Patients had a higher LVEF than patients in prior studies (44% vs. 27-34%[3,7,13,17-20]), had less frequently an ICD before ablation (67% vs. 71-100%[3,7,13,17-20]) and were less often on amiodarone (42% vs. 43-88%[3,13,17-20]), suggesting that VT ablation was employed at an earlier stage, which is in line with recently extended indications for VT ablation.[9]

Complete procedural success was achieved in 38% of patients, which is lower than some prior studies[7,17,18] but similar to others.[3,13,21] However, the currently reported recur-

rence rate of 53% during median 24 (Q1-to-Q3, 12–37) months follow-up is, considering differences in follow-up duration, favorable when compared to two studies employing epicardial mapping in the majority of patients[3,13] and similar to one study with epicardial mapping in all patients.[17] An overview of studies analyzing outcome of VT ablation in NICM is provided in a supplemental Table.

Noninducibility as a procedural endpoint

The majority of available data on the predictive value of non-inducibility is derived from post-MI patients.[1,2,4-6] NICM patients may however have a different arrhythmogenic substrate.[3,22] Of interest, 96% of our patients were inducible for the clinical VT, suggesting the presence of a fixed substrate. The small number of patients under general anesthesia and the fact that initial PES was performed before sedative and opioid administration may also have contributed to this finding.

Only 2 small prior studies (including 13 and 16 patients) have analyzed the value of PES at the end of VT ablation procedures in patients with NICM.[3,7] In the present study PES was performed after the last RF application in all 45 patients. Perhaps due to the consistent application of the induction protocol, patients remained more often inducible for non-clinical and in particular fast VTs, and therefore partial success may have been achieved more frequently compared to prior studies (supplemental Table). Prolonged depression of cardiac output prevented completion of the induction protocol in only 2 patients, which may be partly due to the higher LVEF and our strategy to perform substrate mapping and only limited mapping during VT in all patients independent of VT CL.

Both partial procedural success and failure were associated with high VT recurrence rates, indicating that partial success may not be superior to ablation failure. Importantly, 55% of patients with induction of a very fast VT (CL≤250ms) after ablation had VT recurrence, suggesting that induction of these VTs after ablation is not a non-specific finding. However, the latter does not necessarily imply that very fast, nonclinical VTs should always be targeted. Persistent inducibility of very fast VTs may be a marker for a more complex or functional arrhythmogenic substrate less amenable to VT ablation. This is in line with the observation that 83% of patients required one or more ICD shocks to terminate ≥1 VT which may be due to ATP failure or short VT CL. Further studies are needed to assess whether additional ablation can abolish these nonclinical, usually rapid VTs and improve long-term outcomes after ablation.

Predictors of acute procedural success and VT recurrence

Higher age was strongly associated with non-complete procedural success, also after adjustment for epicardial access, LVEF and AADs (data not shown), perhaps due to a

different substrate in older patients. Interestingly, although age was associated with non-complete procedural success, it seemed not to predict VT recurrence.

All patients with a significantly decreasing LVEF and 64% of patients with a significantly increasing LVEDV had VT recurrence during follow-up, perhaps indicating that patients with deteriorating LV function and dimensions may be at high risk for VT recurrence. Previous studies in post-MI patients demonstrated that a lower LVEF[6,23], a higher number of induced VTs[23,24], a higher number of clinical VTs[6] and acute procedural failure[6] are associated with VT recurrence. The current study suggests that most of these factors also apply to patients with NICM. Different substrates may however result in comparable clinical features, such as lower LVEF, and to date little is known about the VT substrates in NICM. Therefore, more studies are needed to identify potentially different substrates and their impact on VT occurrence. So far, PES after the last RF application is the strongest predictor of VT recurrence and may therefore be an important tool to identify patients who may need additional ablation, epicardial mapping and/or enhanced drug therapy.

VT ablation early in the therapeutic course

This is the first study reporting on the results of VT ablation in NICM patients presenting with a first VT, symptomatic ATP or a single ICD shock. Importantly, no complication resulted in serious sequelae. Fifty-six percent had no VT recurrence and 60% were free from ICD shocks during follow up. Twelve of 25 patients (48%) were off amiodarone and without recurrent VT during follow-up. These findings suggest that VT ablation may be considered for indications such as a first VT, symptomatic ATP or a single ICD shock in NICM patients and perhaps even be considered as an alternative to life-long amiodarone therapy, particularly in young patients. The risks of VT ablation should be weighed carefully against the risks of medical therapy, which persist during follow-up and may include serious side effects. When considering epicardial ablation, the risk of pericardial adhesions preventing future pericardial access should also be taken into account, which may occur even after administration of intrapericardial steroids.

Limitations

Non-complete procedural success may have been caused by lack of epicardial access in 7 patients (16%). One patient preferred not to undergo epicardial mapping and in the remaining 6 patients the potential benefits were considered not to outweigh the risks based on the clinical presentation. In a significant proportion of patients an ICD was implanted only after the procedure and therefore, ICD therapy for non-sustained VT after the procedure may have led to an underestimation of the reduction of VT burden. Echocardiography was performed in 50% of patients who survived ≥6 months after ablation and therefore, the relation between LVEF decrease and LVEDV increase and VT recurrence should be interpreted with caution.

CONCLUSION

Although VT recurs in 53% of the patients during follow-up, the 6-month VT burden is reduced by ≥75% in 79% of patients. Noninducibility may be an appropriate endpoint in patients with NICM, as recurrence rates are low after complete procedural success, but high after both partial success and failure. Importantly, induction of very fast VT after ablation appears not to be a non-specific finding. Non-complete procedural success, a lower LVEF, VT storm, a higher number of clinical VTs, a higher number of failed AADs and a higher mean CL of induced VTs are predictors of VT recurrence. After ablation for a first VT, symptomatic ATP or a single ICD shock, 56% of NICM patients remain free from VT recurrence.

CLINICAL PERSPECTIVE

There are limited data on ventricular tachycardia (VT) ablation in patients with nonischemic left ventricular cardiomyopathy, in particular, on the procedural end point. The present study comprised 45 patients with nonischemic cardiomyopathy who underwent VT ablation. The complete programmed electric stimulation protocol was consistently applied after the last radiofrequency energy application in each patient, resulting in noninducibility of any VT in 38%, induction of nonclinical VT in another 38%, and inducibility of the clinical VT in 24%. Although VT recurred in approximately half of the patients during follow-up, the VT burden was substantially reduced in the majority. In 25 patients VT ablation was performed because of a first VT, symptomatic ATP, or a single implantable cardioverter defibrillator shock; 56% of these patients remained free from VT during follow-up, suggesting that catheter ablation may also be considered early in the therapeutic course. Programmed electric stimulation after ablation seemed to provide important prognostic information. Noninducibility of any VT was associated with a very low recurrence rate during long-term follow-up, whereas persistent inducibility of clinical or nonclinical VT was associated with a poor prognosis. Induction of very fast VT, which has previously been considered a nonspecific finding, also seemed to be associated with a high recurrence rate. Inducibility of VT after ablation was the strongest predictor of VT recurrence. These data support the role of programmed electric stimulation to assess the procedural end point in patients with nonischemic cardiomyopathy and may, therefore, significantly aid clinicians who perform VT ablation in this population.

REFERENCE LIST

1. Carbucicchio C, Santamaria M, Trevisi N, Maccabelli G, Giraldi F, Fassini G, Riva S, Moltrasio M, Cireddu M, Veglia F, Della BP. Catheter ablation for the treatment of electrical storm in patients with implantable cardioverter-defibrillators: short- and long-term outcomes in a prospective single-center study. Circulation 2008;117(4):462-9.
2. Della Bella P, De Ponti R., Uriarte JA, Tondo C, Klersy C, Carbucicchio C, Storti C, Riva S, Longobardi M. Catheter ablation and antiarrhythmic drugs for haemodynamically tolerated post-infarction ventricular tachycardia; long-term outcome in relation to acute electrophysiological findings. Eur Heart J 2002;23(5):414-24.
3. Nakahara S, Tung R, Ramirez RJ, Michowitz Y, Vaseghi M, Buch E, Gima J, Wiener I, Mahajan A, Boyle NG, Shivkumar K. Characterization of the arrhythmogenic substrate in ischemic and nonischemic cardiomyopathy implications for catheter ablation of hemodynamically unstable ventricular tachycardia. J Am Coll Cardiol 2010;55(21):2355-65.
4. Jais P, Maury P, Khairy P et al. Elimination of local abnormal ventricular activities: a new end point for substrate modification in patients with scar-related ventricular tachycardia. Circulation 2012;125(18): 2184-96.
5. Stevenson WG, Wilber DJ, Natale A et al. Irrigated radiofrequency catheter ablation guided by electroanatomic mapping for recurrent ventricular tachycardia after myocardial infarction: the multicenter thermocool ventricular tachycardia ablation trial. Circulation 2008;118(25):2773-82.
6. Della Bella P, Riva S, Fassini G, Giraldi F, Berti M, Klersy C, Trevisi N. Incidence and significance of pleomorphism in patients with postmyocardial infarction ventricular tachycardia. Acute and long-term outcome of radiofrequency catheter ablation. Eur Heart J 2004;25(13):1127-38.
7. Arya A, Bode K, Piorkowski C, Bollmann A, Sommer P, Gaspar T, Wetzel U, Husser D, Kottkamp H, Hindricks G. Catheter ablation of electrical storm due to monomorphic ventricular tachycardia in patients with nonischemic cardiomyopathy: acute results and its effect on long-term survival. Pacing Clin Electrophysiol 2010;33(12):1504-9.
8. Vergara P, Trevisi N, Ricco A, Petracca F, Baratto F, Cireddu M, Bisceglia C, Maccabelli G, Della BP. Late Potentials Abolition as an Additional Technique for Reduction of Arrhythmia Recurrence in Scar Related Ventricular Tachycardia Ablation. J Cardiovasc Electrophysiol 2012.
9. Aliot EM, Stevenson WG, Almendral-Garrote JM et al. EHRA/HRS Expert Consensus on Catheter Ablation of Ventricular Arrhythmias: developed in a partnership with the European Heart Rhythm Association (EHRA), a Registered Branch of the European Society of Cardiology (ESC), and the Heart Rhythm Society (HRS); in collaboration with the American College of Cardiology (ACC) and the American Heart Association (AHA). Heart Rhythm 2009;6(6):886-933.
10. Kuck KH, Schaumann A, Eckardt L, Willems S, Ventura R, Delacretaz E, Pitschner HF, Kautzner J, Schumacher B, Hansen PS. Catheter ablation of stable ventricular tachycardia before defibrillator implantation in patients with coronary heart disease (VTACH): a multicentre randomised controlled trial. Lancet 2010;375(9708): 31-40.
11. Reddy VY, Reynolds MR, Neuzil P, Richardson AW, Taborsky M, Jongnarangsin K, Kralovec S, Sediva L, Ruskin JN, Josephson ME. Prophylactic catheter ablation for the prevention of defibrillator therapy. N Engl J Med 2007;357(26):2657-65.

12. Sacher F, Roberts-Thomson K, Maury P et al. Epicardial ventricular tachycardia ablation a multicenter safety study. J Am Coll Cardiol 2010;55(21):2366-72.
13. Schmidt B, Chun KR, Baensch D, Antz M, Koektuerk B, Tilz RR, Metzner A, Ouyang F, Kuck KH. Catheter ablation for ventricular tachycardia after failed endocardial ablation: epicardial substrate or inappropriate endocardial ablation? Heart Rhythm 2010; 7(12):1746-52.
14. Hutchinson MD, Gerstenfeld EP, Desjardins B et al. Endocardial unipolar voltage mapping to detect epicardial ventricular tachycardia substrate in patients with nonischemic left ventricular cardiomyopathy. Circ Arrhythm Electrophysiol 2011;4(1):49-55.
15. Piers SR, van Huls van Taxis CF, Tao Q, van der Geest RJ, Askar SF, Siebelink HM, Schalij MJ, Zeppenfeld K. Epicardial substrate mapping for ventricular tachycardia ablation in patients with non-ischaemic cardiomyopathy: a new algorithm to differentiate between scar and viable myocardium developed by simultaneous integration of computed tomography and contrast-enhanced magnetic resonance imaging. Eur Heart J 2012;34(8):586-96.
16. van Huls van Taxis CF, Wijnmaalen AP, Piers SR, van der Geest RJ, Schalij MJ, Zeppenfeld K. Real-Time Integration of MDCT-Derived Coronary Anatomy and Epicardial Fat: Impact on Epicardial Electroanatomic Mapping and Ablation for Ventricular Arrhythmias. JACC Cardiovasc Imaging 2013;6(1):42-52.
17. Cano O, Hutchinson M, Lin D et al. Electroanatomic substrate and ablation outcome for suspected epicardial ventricular tachycardia in left ventricular nonischemic cardiomyopathy. J Am Coll Cardiol 2009; 54(9):799-808.
18. Haqqani HM, Tschabrunn CM, Tzou WS et al. Isolated septal substrate for ventricular tachycardia in nonischemic dilated cardiomyopathy: incidence, characterization, and implications. Heart Rhythm 2011;8(8): 1169-76.
19. Hsia HH, Callans DJ, Marchlinski FE. Characterization of endocardial electrophysiological substrate in patients with nonischemic cardiomyopathy and monomorphic ventricular tachycardia. Circulation 2003; 108(6):704-10.
20. Soejima K, Stevenson WG, Sapp JL, Selwyn AP, Couper G, Epstein LM. Endocardial and epicardial radiofrequency ablation of ventricular tachycardia associated with dilated cardiomyopathy: the importance of low-voltage scars. J Am Coll Cardiol 2004; 43(10):1834-42.
21. Tokuda M, Tedrow UB, Kojodjojo P, Inada K, Koplan BA, Michaud GF, John RM, Epstein LM, Stevenson WG. Catheter ablation of ventricular tachycardia in nonischemic heart disease. Circ Arrhythm Electrophysiol 2012;5(5):992-1000.
22. Yokokawa M, Tada H, Koyama K, Ino T, Hiramatsu S, Kaseno K, Naito S, Oshima S, Taniguchi K. The characteristics and distribution of the scar tissue predict ventricular tachycardia in patients with advanced heart failure. Pacing Clin Electrophysiol 2009; 32(3):314-22.
23. Kosmidou I, Inada K, Seiler J, Koplan B, Stevenson WG, Tedrow UB. Role of repeat procedures for catheter ablation of postinfarction ventricular tachycardia. Heart Rhythm 2011;8(10):1516-22.
24. Tung R, Josephson ME, Reddy V, Reynolds MR. Influence of clinical and procedural predictors on ventricular tachycardia ablation outcomes: an analysis from the substrate mapping and ablation in Sinus Rhythm to Halt Ventricular Tachycardia Trial (SMASH-VT). J Cardiovasc Electrophysiol 2010;21(7):799-803.

Supplemental Table 1. Studies analyzing outcome of VT ablation in nonischemic cardiomyopathy

First author and year of publication	Hsia[19] 2003	Soejima[20] 2004	Cano[17] 2009	Nakahara[3] 2010	Schmidt[13] 2010	Arya[7] 2010	Haqqani[18] 2011	Current study
Population	Only endocardial	Only LVEF≤50%	All endo-epicardial	-	All endo-epicardial	Electrical storm	Isolated septal substrate	-
Number of patients	19	28	22	16	16	13	31	45
Age	61±16	54±14	56±13	59±11	57±11	57±18%	59±12	60±16
LV ejection fraction (%)	34±11	30±11	30±13	27±12	32±8	33±9	30±14	44±14
Failed antiarrhythmic drugs	-	-	All ≥1	All ≥1	2±2	All ≥2	All ≥1	1.8±1.0
ICD before	84%	71%	95%	94%	81%	100%	84%	67%
Prior ablations	-	7%	mean 1.8	38%	100%	-	32%	27%
Pericardial access	0%	29%	100%	75%	94%	24%	45%	64%
Anesthesia during epicardial mapping	NA	-	General	General	-	-	CS or general	96% CS, 4% General
VTs induced per patient	3±1	2.9±1.7	mean 3.3	2.6±1.6	1.9±1.7	range 1 – 4	mean 4.9	2 (2 - 4)
Mean cycle length (ms)	373±91	-	392±109	421±88	409±94	384±75	396±90	342±77
Amiodarone at time of procedure	63%	43%	59%	88%	69%	-	74%	42%
Complete success	74%	61%	67%	44%	38%	62%	66%	38%
Partial success	26%	14%	33%	44%	38%	38%	20%	38%
Failure		25%		13%	24%	0%	14%	24%
Follow-up duration in months	22±12	9±9	18±7	15±13	median 12	median 23	20±28	median 24
VT recurrence rate	58%	36%	29%	50%	47%	38%	32%	53%
VT recurrence rate per year	32%	48%	19%	40%	47%	20%	19%	27%

The table includes all studies including ≥10 patients with nonischemic cardiomyopathy who underwent VT ablation.
CS denotes conscious sedation; LV, left ventricle; ICD, implantable cardioverter defibrillator; VT, ventricular tachycardia

Chapter 9

Early Reperfusion Therapy Affects Inducibility, Cycle Length and Occurrence of Ventricular Tachycardia Late After Myocardial Infarction

Sebastiaan R.D. Piers, Adrianus P. Wijnmaalen, C. Jan Willem Borleffs, Carine F.B. van Huls van Taxis, Joep Thijssen, Johannes B. van Rees, Suzanne C. Cannegieter, Jeroen J. Bax, Martin J. Schalij, Katja Zeppenfeld

Sebastiaan R.D. Piers and Adrianus P. Wijnmaalen share first authorship on this manuscript

Circulation: Arrhythmia & Electrophysiology 2011;4(2):195-201.

ABSTRACT

Background

This study aimed to evaluate the impact of early reperfusion during acute myocardial infarction (MI) on ventricular tachycardia (VT) inducibility, inducible VT cycle length (CL) and occurrence of spontaneous VT late after MI.

Methods and results

Five-hundred-six patients (440 male, 63±11yr) with prior MI who underwent electrophysiology study before implantation of an implantable cardioverter defibrillator for primary or secondary prevention were assessed. Patients were classified according to the reperfusion strategy {reperfusion (thrombolysis (n=44) or percutaneous coronary intervention (n=65)) vs. no reperfusion (n=397)} during acute MI. Monomorphic sustained VT was inducible in 351 (69%) patients. Inducibility in reperfused and non-reperfused patients was similar in primary prevention patients (56% vs.58%) but significantly higher for non-reperfused patients in secondary prevention patients (56% vs.79%, p=0.001). Induced VTCL was shorter (247±40 vs.287±63, p<0.001) and very fast VT (CL≤250 ms) was more often induced in reperfused patients (71% vs.47%, p=0.001). In primary prevention patients, non-reperfusion was associated with a doubled risk for first spontaneous VT during follow-up.

Conclusion

There are important differences in VT inducibility, induced VTCL and occurrence of spontaneous VT in the chronic infarct healing phase between patients with and without successful reperfusion during acute MI. These findings suggest differences in the chronic arrhythmogenic substrate.

INTRODUCTION

Survivors of acute myocardial infarction (MI) may be at risk for reentrant ventricular tachycardia (VT) originating from infarct scar.[1] In the past decades, early reperfusion therapies such as thrombolysis and primary percutaneous coronary intervention (PCI) have significantly improved outcome after acute MI.[2] Early reperfusion during MI results in myocardial salvage and improved ventricular function but also influences size, transmurality and geometry of myocardial fibrosis, which may function as a substrate for ventricular arrhythmias.[3-7] A fixed substrate may lead to reentrant tachycardias reproducible induced during electrophysiology study (EPS) and more than 90% of patients with sustained VT late after MI had the arrhythmia induced in the lab.[8] However, these data were derived before the widespread availability of reperfusion therapy and the role for EPS in patients late after reperfused MI is less clear. Mapping studies demonstrated that the 3-dimensional geometry of the infarcted area may determine VT reentry circuit characteristics.[9-12] In a small group of patients referred for treatment of VT late after MI, we previously demonstrated that early reperfusion affects the electroanatomical VT substrate.[13] In addition, cycle length (CL) of spontaneous and induced VTs was shorter in patients who underwent early reperfusion as compared to non-reperfused patients.

The aim of the present study was to evaluate the effect of early reperfusion during acute MI on VT inducibility, induced VTCL and the occurrence of spontaneous VT during follow-up in a larger population of patients with prior MI in one coronary territory who underwent EPS before implantable cardioverter defibrillator (ICD) treatment.

METHODS

Patients

Since 1996, information on all patients who received an ICD at the Leiden University Medical Center was prospectively collected in the departmental Cardiology Information System (EPD-Vision®, Leiden University Medical Center). Patient's history, baseline characteristics and results of studies before ICD-implantation were recorded. For the current study, all consecutive patients (1) with a prior MI in a single coronary territory and documented reperfusion strategy during the index MI; (2) without evidence of reversible ischemia assessed by coronary angiogram and nuclear imaging at the time of evaluation, and (3) who underwent EPS before ICD implantation were included. Patients with documented spontaneous monomorphic VT or ventricular fibrillation (VF) in the absence of a reversible cause were considered as secondary prevention ICD recipients and asymptomatic patients with left ventricular ejection fraction (LVEF) <40% without

prior documentation of a sustained ventricular arrhythmia primary prevention ICD recipients.[14-16]

All coronary angiograms performed in reperfused patients within 6 months before EPS were reviewed by an interventional cardiologist to evaluate the late patency of the infarct related artery. Patients with ≤ TIMI II flow of the infarct related artery were excluded from analysis. All patients were followed at our institute.

Myocardial infarction

The presence of prior MI was assessed using the definition for MI, as defined by the Task Force for the Redefinition of Myocardial Infarction.[17] Either acute MI had to be documented, or evidence of prior MI had to be present, based on any of the following criteria: 1) development of new pathological Q-waves with or without symptoms; 2) imaging evidence of a region of loss of viable myocardium that is thinned and fails to contract, in the absence of a non-ischemic cause; 3) pathological findings of a healed or healing MI.[17]

MI was considered to be present in more than one coronary artery region if the criteria for acute or prior MI were met for more than one of the regions provided by the three main coronary arteries.

The treatment of prior MI was assessed using the patients' medical charts. Patients were categorized as reperfused when TIMI flow grade 3 was achieved within 9 hours after onset of symptoms. Reperfused patients were subdivided into patients who had underwent primary PCI (defined as angioplasty and/or stenting without prior or concomitant fibrinolytic therapy)[18] and patients who had received thrombolytic therapy. All other patients were categorized as non-reperfused.

Electrophysiology study

Electrophysiological studies to test inducibility of VT were performed according to the current international guidelines.[19] Patients were studied in the post absorptive, non-sedated state. Antiarrhythmic drugs were discontinued for 5 half-lives, with the exception of amiodarone. EPS consisted of up to three basic drive cycle lengths (600, 500 and 400ms) with up to three ventricular extrastimuli and burst pacing from the right ventricular apex and right ventricular outflow tract. The positive endpoint of EPS was reproducible induction of a sustained monomorphic VT (SMVT).[19] Arrhythmias induced by anti-tachycardia pacing (ATP) to terminate the induced VT were not included in the analysis.

Ventricular arrhythmia during electrophysiology study

Ventricular arrhythmias were categorized according to the EHRA/HRS consensus document.[20] SMVT was defined as continuous VT with a similar QRS configuration from beat

to beat lasting for more than 30 seconds or requiring an intervention for termination. Separately scored arrhythmia not considered diagnostic for the presence of fixed reentry circuits and therefore non-specific were polymorphic VT, defined as VT with continuously changing QRS configuration from beat to beat and VF.[19]

For each patient, the mean CL of all induced SMVTs was calculated. Patients with missing data on one or more CLs were excluded from all analyses involving VTCL. Monomorphic VTs were categorized into the following four pre-defined subgroups according to CL: ≤250, 251-286, 287-320 and >320 ms (corresponding to a rate of ≥240, 240-210, 210-188 and <188bpm, respectively). A very fast VT was defined as a VT with CL ≤250 ms.

Implantable cardioverter defibrillator settings and follow-up

Defibrillators were programmed as follows: a ventricular arrhythmia monitor zone was programmed in all patients (150-188bpm). Ventricular arrhythmias faster than 188bpm were initially attempted to be terminated with two bursts of ATP followed by a defibrillator shock, if appropriate. In the case of a ventricular arrhythmia faster than 210bpm, device shocks were the initial therapy. Atrial arrhythmia detection was set to >170bpm with supraventricular tachycardia discriminators enabled. Settings were adapted, only when clinically indicated (i.e. hemodynamic well tolerated VT at high rate; VT in the monitor zone).

Patient follow-up was scheduled every three-six months. Device interrogation printouts were checked for appropriate and inappropriate ICD therapy (ATP or shocks). Therapies were classified as appropriate when they occurred in response to VT or VF and as inappropriate when triggered by sinus or supraventricular tachycardia, T-wave oversensing, or electrode dysfunction.

In both primary and secondary prevention ICD recipients, the correlation between treatment of acute MI and the occurrence of first spontaneous monomorphic VT during follow-up was assessed.

Statistical analysis

Dichotomous and categorical data are displayed as numbers and percentages. Continuous data are expressed as mean ± standard deviation or median and interquartile range where appropriate. Patients were grouped according to acute MI treatment. Different groups were compared for 1) inducibility of SMVT, 2) mean CL of induced SMVTs, 3) inducibility of very fast VT (CL ≤250ms), and 4) the occurrence of first spontaneous VT during follow-up in primary and secondary prevention ICD patients. Data were analyzed by means of the Chi-square test, the Student's t-test or the Mann-Whitney U-test as appropriate. For the Student's t-test, equal variances were assumed if Levene's test for equality of variances showed a p-value >0.05. Univariate relationships between baseline parameters and the mean CL of induced VTs were analyzed with linear regression analy-

sis. For each variable, the effect on the mean CL with a 95% confidence interval (95%-CI) was calculated. Variables with a p-value <0.10 were further evaluated in a multivariate model, using backward stepwise selection. At each step, the least significant variable was discarded from the model, until all variables in the model reached a p-value <0.25.

The cumulative incidence of first spontaneous VT during follow-up in primary and secondary prevention ICD patients was analyzed by method of Kaplan-Meier. The effect of acute MI treatment on the risk of spontaneous VT was assessed in a Cox regression model. As with linear regression analysis, first, univariate analyses were performed and variables with a p-value <0.10 were further evaluated in a multivariate model, using backward stepwise selection. At each step, the least significant variable was discarded from the model, until all variables in the model reached a p-value <0.25.

All analyses were performed with SPSS for Windows, version 17.0 (SPSS, Chicago, IL). P-values are all two-sided and for all tests, a p-value <0.05 was considered statistically significant.

RESULTS

Patients

Since 1996, 996 patients with prior MI in one coronary artery region received an ICD at the Leiden University Medical Center. Of these patients, 511 had a documented reperfusion strategy and underwent EPS before ICD implantation and after exclusion of reversible ischemia. Five patients (1%) were excluded due to lack of late patency of the infarct related artery. The remaining 506 patients (87% male, age 63 ± 11 years) comprised the studied sample. The presenting and documented arrhythmia was SMVT in 221 patients (44%) and VF in 113 (22%); 172 patients (34%) had no prior sustained arrhythmia. The majority of patients had a depressed left ventricular ejection fraction (36 ± 13%). Mean QRS duration was 115 ± 29 ms and mean creatinin clearance was 79 ± 39mL/min. Medication during EPS included amiodarone in 22% and ACE-inhibitors or ATII-antagonists in 75% of patients. Baseline characteristics are summarized in Table 1.

Myocardial infarction treatment

One-hundred-nine (22%) of 506 patients were treated with reperfusion therapy during the acute MI and 397 (78%) were not reperfused. Of the 109 reperfused patients, 65 (13%) underwent primary PCI and 44 (9%) received thrombolytic therapy. Before electrophysiological evaluation, the infarct-related artery was patent in 97 (89%), collaterally perfused in 11 (10%) and bypassed in one (1%) of the initially reperfused patients. In non-reperfused patients, the infarct-related artery was patent in 140 (35%), occluded in 116 (29%), collaterally perfused in 88 (22%) and bypassed in 53 (13%). Patients who were

reperfused were younger than non-reperfused patients (59 ±11 vs. 65 ±10, p<0.001), presented less often with SMVT (22% vs. 49%, p<0.001) and had a shorter interval between MI and electrophysiological evaluation (median 1.6, IQR 0.2 – 5.9 vs. median 10.5, IQR 2.1 – 17.5, p<0.001). In addition, reperfused patients had an anterior MI more frequently (72% vs. 52%, p<0.001), a shorter QRS-duration (median 100, IQR 90 – 120 vs. median 110, IQR 100 – 138, p=0.001), were less often treated with amiodarone (12% vs. 25%, p=0.001) but were more likely to receive beta-blockers (53% vs. 40%, p=0.014).

Table 1. Baseline Characteristics.

	All Patients (n=506)	Nonreperfused (n=397)	Reperfused (n=109)	*P* Value
Male sex	440 (87%)	341 (86%)	99 (91%)	0.176
Age, y	65 (57–71)	66 (58–73)	60 (51–68)	<0.001
Presenting arrhythmia				<0.001
Sustained VT	221 (44%)	197 (50%)	24 (22%)	
Ventricular fibrillation	113 (22%)	94 (24%)	19 (17%)	
No sustained arrhythmia	172 (34%)	106 (27%)	66 (61%)	
Location of MI				<0.001
Anterior	285 (56%)	206 (52%)	79 (72%)	
Nonanterior	221 (44%)	191 (48%)	30 (28%)	
Years from MI to EPS	7.5 (0.9–15.0)	10.5 (2.1–17.5)	1.6 (0.2–5.9)	<0.001
LVEF, %	36±13	35±13	37±13	0.180
NYHA classification				0.555
I	227 (45%)	172 (43%)	55 (50%)	
II	201 (40%)	164 (41%)	37 (34%)	
III	72 (14%)	56 (14%)	16 (15%)	
IV	6 (1%)	5 (1%)	1 (1%)	
QRS duration, ms	110 (94–130)	110 (100–138)	100 (90–120)	0.001
Renal clearance, mL/min*	79±39	77±41	85±27	0.066
Documented AF or atrial flutter	89 (18%)	69 (17%)	20 (18%)	0.823
Current smoking	126 (25%)	94 (24%)	32 (29%)	0.253
Amiodarone	111 (22%)	98 (25%)	13 (12%)	0.004
β-blocker	217 (43%)	159 (40%)	58 (53%)	0.014
ACE inhibitor or ARB	380 (75%)	291 (73%)	89 (82%)	0.070

ACE indicates angiotensin-converting enzyme; AF, atrial fibrillation; ARB, angiotensin receptor blocker; ICD, implantable cardioverter-defibrillator; LVEF, left ventricular ejection fraction; MI, myocardial infarction; NYHA, New York Heart Association; EPS, electrophysiological study; and VT ventricular tachycardia.
Data are expressed as No. (percentages), mean±SD, or median (interquartile range).
* Renal clearance was determined with the formula of Cockroft-Gault.

Inducibility of ventricular arrhythmia

In 422 patients (83%), at least one ventricular arrhythmia was inducible: SMVT was induced in 351 (69%) patients, 45 of them were also inducible for polymorphic VT or VF. In 71 (14%) patients, only polymorphic VT or VF was induced. Inducibility of SMVT consisted of only one VT morphology in 222 (63%) and two or more different morphologies in 129 (37%) patients. Inducibility for SMVT was similar in reperfused and non-reperfused patients without prior documentation of sustained VT or VF (56% vs 58%, p=ns). However, in the secondary prevention group inducibility for SMVT was significantly lower in reperfused patients as compared to non-reperfused patients (56% vs 79%, p=0.001).

Ventricular tachycardia cycle length

In 37 (11%) out of 351 patients with inducible SMVT, one or more induced VTCL was unknown, these patients were excluded from VTCL analyses. In the remaining 314 patients, the mean CL was 280 ± 61 ms (Table 2). In 161 (51%) patients, at least one monomorphic fast VT (CL ≤ 250) was induced.

Table 2. Difference of Mean Cycle Length of Induced Monomorphic Ventricular Tachycardias by *t* Tests.

	n	Mean CL	Difference* (95% CI)	*P* Value
All patients	314	280±61	NA	NA
Nonreperfused	258	287±63	NA	NA
Reperfused	56	247±40	40 (27–53)	<0.001
Thrombolysis	23	260±37	27 (2–53)	0.038
Primary PCI	33	238±40	49 (27–70)	<0.001

CI indicates confidence interval; CL, cycle length; NA, not applicable; and PCI, percutaneous coronary intervention.

* When compared with nonreperfused patients.

Reperfused patients had a shorter mean CL of the induced VT than non-reperfused patients (247 ± 40ms vs. 287 ± 63ms, p<0.001, Table 2). This difference was even more pronounced when patients who underwent primary PCI were compared to non-reperfused patients (238 ± 40ms vs. 287 ± 63ms, p<0.001). Patients treated with thrombolysis also had a significantly shorter mean CL than non-reperfused patients, but the difference was smaller (260 ± 37ms vs. 287 ± 63ms, p=0.038). After exclusion of patients on amiodarone during EPS the induced VTCL remained significantly shorter in reperfused patients (244 ± 40ms vs. 274 ± 58ms, p<0.001). Of importance, reperfused patients were more often inducible for very fast VT (CL ≤ 250ms) than non-reperfused patients (71% vs. 47%, p=0.001, Figure 1). The difference was mainly attributable to patients treated with primary PCI, while patients treated with thrombolysis had a similar percentage of very fast VT, as compared to non-reperfused patients. Univariate and subsequent

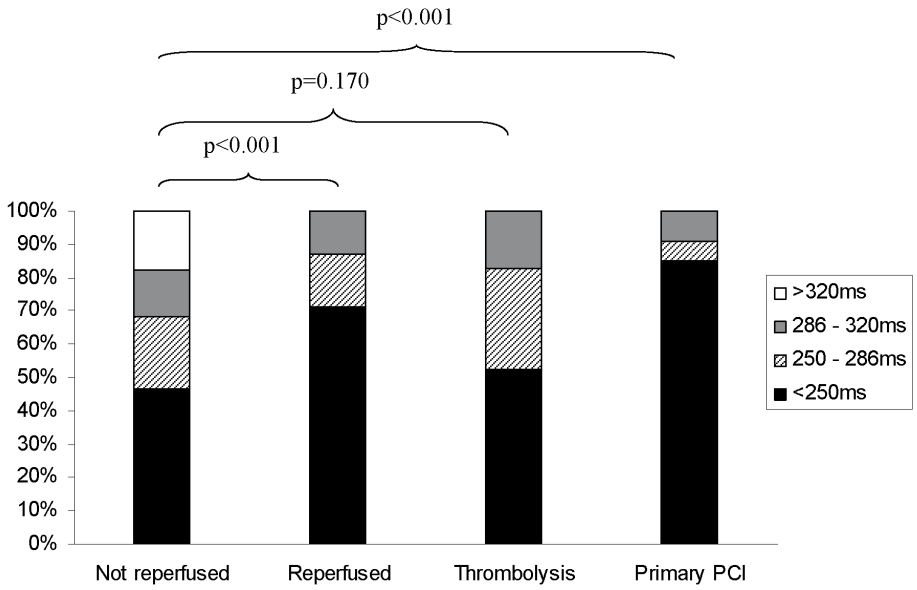


Figure 1.
Cycle length of the fastest induced monomorphic ventricular tachycardia, categorized into 4 subgroups. Percentages are for all patients with induced monomorphic ventricular tachycardia in the specific group. PCI indicates percutaneous coronary intervention.

multivariate analysis identified the following five variables as independently affecting the mean CL of induced VTs: no reperfusion, QRS > 120 ms, presenting arrhythmia, use of amiodarone and age. After adjustment, no reperfusion at MI was correlated with 17 ms (95%-CI 0-34 ms, p=0.048) increase in VT CL at EPS (Figure 2).

Spontaneous ventricular tachycardia

The 172 primary prevention ICD recipients were followed for a median of 28 months (IQR 11 – 45). During follow-up, spontaneous VT, triggering appropriate ICD therapy was observed in 51 (30%) patients. The cumulative incidence of first appropriate therapy was 13% (95% CI 8-18%) at one year, 22% (95% CI 15-28%) at two years, and 30% (95% CI 22-39%) at three years follow-up.

The three year cumulative incidence of first appropriate device therapy was 36% (95% CI 26-47%) in non-reperfused patients and 18% (95% CI 7-29%) in reperfused patients (Figure 3). Cox regression modeling demonstrated that non-reperfused patients exhibited a more than doubled risk for spontaneous VT (hazard ratio 2.2, 95% CI 1.2- 4.3, p=0.010).

The 334 secondary prevention ICD recipients were followed for a median of 37 months (IQR 9 – 68). Spontaneous VT occurred in 170 (51%) patients. The three year cumulative incidence of first appropriate device therapy was 38% (95% CI 32-44%) in

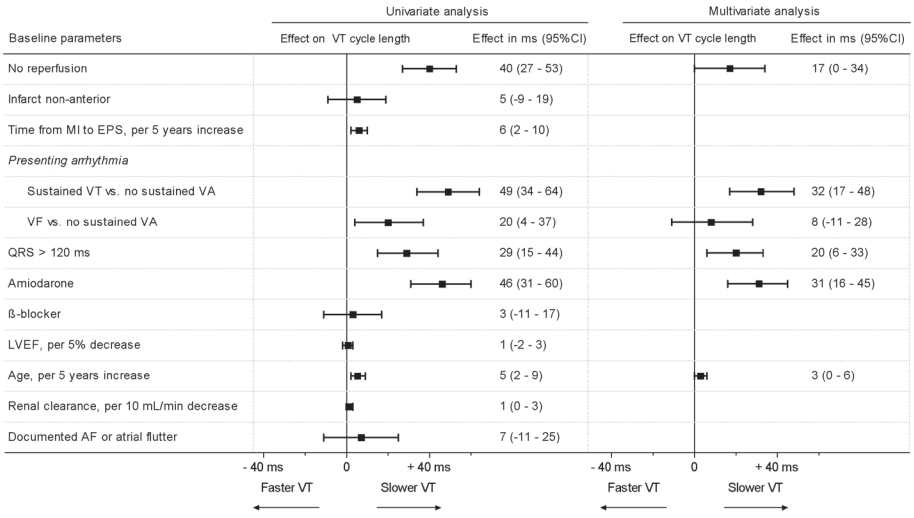


Figure 2.
Forest plot of the effect of baseline parameters on the mean cycle length of induced monomorphic ventricular tachycardias (VT). For example, in multivariate analysis, patients who did not receive reperfusion therapy at the index myocardial infarction on average had a 17-ms (95% confidence interval [CI], 0 to 34 ms) longer Vt cycle length (ie, a slower Vt), as compared with patients who did receive reperfusion therapy. AF indicates atrial fibrillation; LVEF, left ventricular ejection fraction; EPS, electrophysiology study; VA, ventricular arrhythmia; and VF, ventricular arrhythmia.

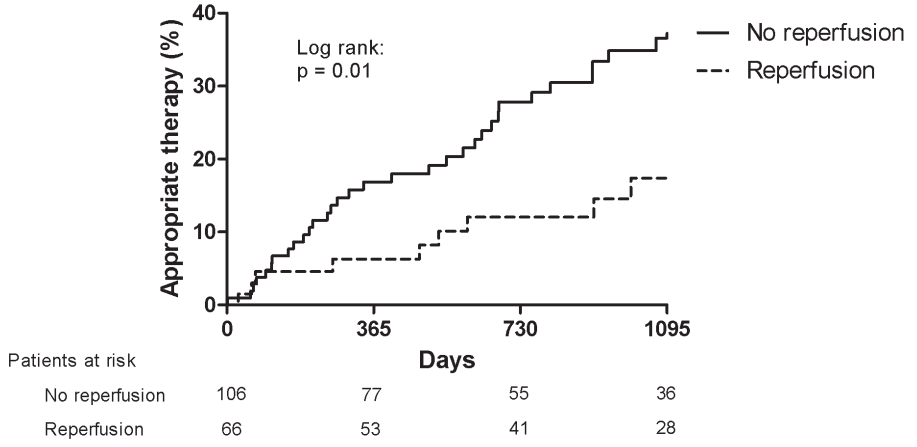


Figure 3.
Kaplan-Meier curve for the occurrence of first appropriate implantable cardioverter-defibrillator therapy in patients with primary-prevention implantable cardioverter-defibrillator with reperfusion versus no reperfusion at prior acute myocardial infarction.

non-reperfused patients and 26% (95% CI 12-39%) in reperfused patients (Figure 4). In this population with prior sustained ventricular arrhythmia, MI treatment did not significantly correlate with the occurrence of spontaneous VT during follow-up (hazard ratio 1.4, 95% CI 0.9-2.3).

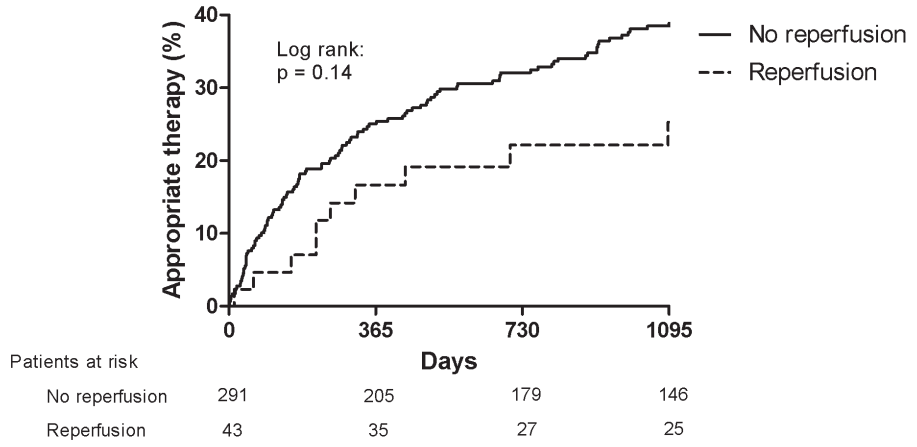


Figure 4.
Kaplan-Meier curve for the occurrence of first appropriate implantable cardioverter-defibrillator therapy in patients with secondary-prevention implantable cardioverter-defibrillator with reperfusion versus no reperfusion at prior acute myocardial infarction.

DISCUSSION

Early reperfusion therapy for acute MI has dramatically increased over the last decenniums and is likely to influence the chronic arrhythmogenic substrate for reentrant tachycardias after infarct healing.

The current study evaluates the effects of early reperfusion during acute MI on VT inducibility, induced VT CL and occurrence of spontaneous VT late after the index MI. Reperfused patients who presented with sustained VT or VF were less likely inducible for monomorphic VT as compared to non-reperfused patients. Reperfused and non-reperfused patients without prior sustained arrhythmia had comparable VT induction rates; however reperfused patients were less likely to experience spontaneous VT during follow-up. Among inducible patients VTCL of induced VTs was significantly shorter and inducible VT was more often very fast VT (CL ≤ 250 ms) in reperfused patients. These differences were even more pronounced in patients treated with primary PCI as compared to thrombolytic therapy. After adjustment for potential confounders, treatment of the index MI appeared to have an independently significant effect on the mean CL of induced VTs.

Early reperfusion during MI and inducibility of VT

Former studies performed before the widespread availability of reperfusion therapy have demonstrated that in patients with coronary artery disease VT was inducible in 92% of patients who presented with sustained VT and in 83% of patients who presented with cardiac arrest due to VF.[8] Accordingly, 79% of the non-reperfused patients in our study who presented with sustained VT or VF were inducible for monomorphic VT. In contrast, in only 56% of reperfused patients with documented VT or VF monomorphic VT was inducible. Although all patients had a chronic substrate as spontaneous arrhythmias occurred in the absence of a reversible cause the sensitivity of an EPS for substrate assessment after reperfusion therapy seems to be low. This finding is of clinical importance if EPS is performed for the evaluation of patients who present with unexplained syncope due to non-documented VT or during ablation procedures of VT if non-inducibility of monomorphic VT is considered as endpoint for ablation.

Acute reperfusion has resulted in a lower prevalence of spontaneous and induced ventricular arrhythmias in the acute phase of MI..[4, 21-23] In small series, 9-48% of patients receiving thrombolysis were inducible for ventricular arrhythmias as compared to 88-100% of patients without reperfusion therapy.[24, 25] However, the arrhythmogenic substrate causing late ventricular arrhythmias may develop over time. In our series, EPS was performed in the chronic healing phase of MI. Of interest, non-reperfused and reperfused patients without prior spontaneous arrhythmia showed high inducibility rates of 58% and 56%, respectively. However, during follow-up the three year cumulative incidence of appropriate device therapy was 36% in non-reperfused patients and only 17% in reperfused patients. This finding suggest that despite the presence of an arrhythmogenic substrate the value of EPS to predict VT occurrence is lower in reperfused patients as compared to non-reperfused patients.

Effect of early reperfusion and inducible VTCL

Early reperfusion during MI results in myocardial salvage and reduced mortality during follow-up.[3] Histological studies in patients and animal models of acute MI have shown that the duration of coronary artery occlusion is proportionally correlated to the size and transmural extent of myocardial scar.[4, 5, 26] Scar size and geometry are important determinants for the reentrant circuit geometry and may contribute to occurrence and cycle length of VT.[9, 27]

We recently demonstrated that reperfused patients referred for ablation of recurrent VT late after MI appeared to have smaller and less confluent electroanatomical scars with thick layers of surviving myocardium found at histology. Interestingly, the CL of spontaneous and induced VTs was shorter in reperfused than in non-reperfused patients likely due to the observed differences in scar geometry after reperfusion therapy.[13] The association between acute reperfusion therapy and shorter inducible VTCL was con-

firmed and extended, as the present study is conducted in a large population of post-MI patients also including patients without previously documented ventricular arrhythmia. In addition, we adjusted for all baseline characteristics that affect induced VTCL.

Limitations

Our study was performed in a selected population of ICD recipients with prior MI and low LVEF, who are not representative for the general population with prior MI. In addition, our cutoff of 9 hours for early reperfusion is arbitrarily chosen. Furthermore, we studied induced VTs, and our findings do not necessarily apply to spontaneous VTs. However, in the previous study by Wijnmaalen et al., spontaneous VTs were taken into account and similar differences were found, as compared to induced VTs. Finally, therapy for acute MI was not randomly assigned and time from MI to EPS differs between groups, which could have resulted in selection bias. However, since primary PCI has been shown to be the preferred treatment for acute MI, a study in which patients would be randomly assigned to primary PCI, thrombolysis or conservative treatment is ethically unacceptable and therefore, selection bias is now inevitable in studying the effects of reperfusion. To correct for it, we adjusted for baseline characteristics using linear regression and could demonstrate that reperfusion independently affects the CL of induced VTs.

CONCLUSION

There are important differences in VT inducibility, induced VTCL and occurrence of spontaneous VT in the chronic phase of MI between patients with and without successful reperfusion during acute MI. Reperfused patients who present with sustained VT/VF are less likely inducible for monomorphic VT. Despite similar VT induction rates in patients without prior documented sustained arrhythmias, reperfused patients are at lower risk for spontaneous VT. However, early reperfusion is associated with faster induced VT.

These findings suggest important differences in the chronic arrhythmogenic substrate after reperfusion, which gives rise to faster VT and which might be less reliably assessable by EPS.

CLINICAL PERSPECTIVE

Early reperfusion during myocardial infarction (MI) results in myocardial salvage and improved ventricular function, but it also influences the specific dimensions and geometry of myocardial fibrosis and thus the propensity for ventricular arrhythmia occurring late after MI. Recently, it has been demonstrated that reperfusion is associated with smaller, less confluent myocardial scars that appear to give rise to faster spontaneous and induced ventricular tachycardias (VTs) in patients referred for VT ablation late after MI. The present study comprised a large population of post-MI patients referred for electrophysiological evaluation and implantation of implantable defibrillators, without previously documented ventricular arrhythmia. In this population, reperfusion during MI affects inducibility, spontaneous occurrence, and cycle length of VTs. Monomorphic VT was inducible in only 56% of reperfused patients as compared with 79% of nonreperfused patients with documented VT or ventricular fibrillation. Reperfused and nonreperfused patients without prior sustained arrhythmia had comparable VT induction rates, but reperfused patients were less likely to have spontaneous VT during follow-up, suggesting that the value of electrophysiological study to predict VT occurrence is lower in reperfused patients as compared with nonreperfused patients. Finally, induced VTs were faster in reperfused patients. These findings probably reflect a different chronic arrhythmogenic substrate in reperfused patients, manifest by faster VTs and less reliably assessed by electrophysiological study.

REFERENCE LIST

1. Josephson M, Wellens HJ. Implantable defibrillators and sudden cardiac death. Circulation 2004;109(22):2685-91.
2. Heidenreich PA, McClellan M. Trends in treatment and outcomes for acute myocardial infarction. 1975-1995. Am J Med 2001;110(3):165-74.
3. The effects of tissue plasminogen activator, streptokinase, or both on coronary-artery patency, ventricular function, and survival after acute myocardial infarction. The GUSTO Angiographic Investigators. N Engl J Med 1993;329(22):1615-22.
4. Miyazaki S, Fujiwara H, Onodera T, Kihara Y, Matsuda M, Wu DJ, Nakamura Y, Kumada T, Sasayama S, Kawai C. Quantitative analysis of contraction band and coagulation necrosis after ischemia and reperfusion in the porcine heart. Circulation 1987;75(5): 1074-82.
5. Reimer KA, Lowe JE, Rasmussen MM, Jennings RB. The wavefront phenomenon of ischemic cell death. 1. Myocardial infarct size vs duration of coronary occlusion in dogs. Circulation 1977;56(5):786-94.
6. Tarantini G, Cacciavillani L, Corbetti F, Ramondo A, Marra MP, Bacchiega E, Napodano M, Bilato C, Razzolini R, Iliceto S. Duration of ischemia is a major determinant of transmurality and severe microvascular obstruction after primary angioplasty. a study performed with contrast-enhanced magnetic resonance. J Am Coll Cardiol 2005; 46(7):1229-35.
7. Thiele H, Kappl MJ, Linke A, Erbs S, Boudriot E, Lembcke A, Kivelitz D, Schuler G. Influence of time-to-treatment, TIMI-flow grades, and ST-segment resolution on infarct size and infarct transmurality as assessed by delayed enhancement magnetic resonance imaging. Eur Heart J 2007;28(12):1433-9.
8. Prystowsky EN, Miles WM, Evans JJ, Hubbard JE, Skale BT, Windle JR, Heger JJ, Zipes DP. Induction of ventricular tachycardia during programmed electrical stimulation. analysis of pacing methods. Circulation 1986;73(2 Pt 2):II32-II38.
9. Ciaccio EJ, Ashikaga H, Kaba RA, Cervantes D, Hopenfeld B, Wit AL, Peters NS, McVeigh ER, Garan H, Coromilas J. Model of reentrant ventricular tachycardia based on infarct border zone geometry predicts reentrant circuit features as determined by activation mapping. Heart Rhythm 2007;4(8):1034-45.
10. Marchlinski FE, Callans DJ, Gottlieb CD, Zado E. Linear ablation lesions for control of unmappable ventricular tachycardia in patients with ischemic and nonischemic cardiomyopathy. Circulation 2000;101(11): 1288-96.
11. Verma A, Marrouche NF, Schweikert RA, Saliba W, Wazni O, Cummings J, Abdul-Karim A, Bhargava M, Burkhardt JD, Kilicaslan F, Martin DO, Natale A. Relationship between successful ablation sites and the scar border zone defined by substrate mapping for ventricular tachycardia post-myocardial infarction. J Cardiovasc Electrophysiol 2005;16(5):465-71.
12. Peters NS, Coromilas J, Severs NJ, Wit AL. Disturbed connexin43 gap junction distribution correlates with the location of reentrant circuits in the epicardial border zone of healing canine infarcts that cause ventricular tachycardia. Circulation 1997; 95(4):988-96.
13. Wijnmaalen AP, Schalij MJ, von der Thüsen JH, Klautz RJM, Zeppenfeld K. Early reperfusion during acute myocardial infarction affects ventricular tachycardia characteristics and the chronic electroanatomical and histological substrate. Circulation 2010; 121(17):1887-1895.

14. Bardy GH, Lee KL, Mark DB, Poole JE, Packer DL, Boineau R, Domanski M, Troutman C, Anderson J, Johnson G, McNulty SE, Clapp-Channing N, et al. Amiodarone or an implantable cardioverter-defibrillator for congestive heart failure. N Engl J Med 2005; 352(20):225-37.

15. Buxton AE, Lee KL, Fisher JD, Josephson ME, Prystowsky EN, Hafley G. A randomized study of the prevention of sudden death in patients with coronary artery disease. Multicenter Unsustained Tachycardia Trial Investigators. N Engl J Med 1999;341(25): 1882-90.

16. Moss AJ, Zareba W, Hall WJ, Klein H, Wilber DJ, Cannom DS, Daubert JP, Higgins SL, Brown MW, Andrews ML. Prophylactic implantation of a defibrillator in patients with myocardial infarction and reduced ejection fraction. N Engl J Med 2002; 346(12):877-83.

17. Thygesen K, Alpert JS, White HD. Universal definition of myocardial infarction. Eur Heart J 2007;28(20):2525-38.

18. Van de Werf F, Bax J, Betriu A, Blomstrom-Lundqvist C, Crea F, Falk V, Filippatos G, Fox K, Huber K, Kastrati A, Rosengren A, Steg PG, et al. Management of acute myocardial infarction in patients presenting with persistent ST-segment elevation. the Task Force on the Management of ST-Segment Elevation Acute Myocardial Infarction of the European Society of Cardiology. Eur Heart J 2008;29(23):2909-45.

19. Zipes DP, Camm AJ, Borggrefe M, Buxton AE, Chaitman B, Fromer M, Gregoratos G, Klein G, Moss AJ, Myerburg RJ, Priori SG, Quinones MA, et al. ACC/AHA/ESC 2006 guidelines for management of patients with ventricular arrhythmias and the prevention of sudden cardiac death. a report of the American College of Cardiology/American Heart Association Task Force and the European Society of Cardiology Committee for Practice Guidelines (Writing Committee to Develop Guidelines for Management of Patients With Ventricular Arrhythmias and the Prevention of Sudden Cardiac Death). J Am Coll Cardiol 2006;48(5):e247-e346.

20. Aliot EM, Stevenson WG, mendral-Garrote JM, Bogun F, Calkins CH, Delacretaz E, Della BP, Hindricks G, Jais P, Josephson ME, Kautzner J, Kay GN, et al. EHRA/HRS Expert Consensus on Catheter Ablation of Ventricular Arrhythmias. developed in a partnership with the European Heart Rhythm Association (EHRA), a Registered Branch of the European Society of Cardiology (ESC), and the Heart Rhythm Society (HRS); in collaboration with the American College of Cardiology (ACC) and the American Heart Association (AHA). Heart Rhythm 2009;6(6):886-933.

21. de Chillou C, Sadoul N, Bizeau O, Feldmann L, Gazakure E, Ismail M, Magnin-Poull I, Blankoff I, Aliot E. Prognostic value of thrombolysis, coronary artery patency, signal-averaged electrocardiography, left ventricular ejection fraction, and Holter electrocardiographic monitoring for life-threatening ventricular arrhythmias after a first acute myocardial infarction. Am J Cardiol 1997;80(7):852-8.

22. Hohnloser SH, Franck P, Klingenheben T, Zabel M, Just H. Open infarct artery, late potentials, and other prognostic factors in patients after acute myocardial infarction in the thrombolytic era: A prospective trial. Circulation 1994;90(4):1747-56.

23. Hohnloser SH, Klingenheben T, Zabel M, Schopperl M, Mauss O. Prevalence, characteristics and prognostic value during long-term follow-up of nonsustained ventricular tachycardia after myocardial infarction in the thrombolytic era. J Am Coll Cardiol 1999;33(7):1895-902.

24. Kersschot IE, Brugada P, Ramentol M, Zehender M, Waldecker B, Stevenson WG,

Geibel A, De ZC, Wellens HJ. Effects of early reperfusion in acute myocardial infarction on arrhythmias induced by programmed stimulation: a prospective, randomized study. J Am Coll Cardiol 1986;7(6):1234-42.

25. Sager PT, Perlmutter RA, Rosenfeld LE, McPherson CA, Wackers FJ, Batsford WP. Electrophysiologic effects of thrombolytic therapy in patients with a transmural anterior myocardial infarction complicated by left ventricular aneurysm formation. J Am Coll Cardiol 1988;12(1):19-24.
26. Matsuda M, Fujiwara H, Onodera T, Tanaka M, Wu DJ, Fujiwara T, Hamashima Y, Kawai C. Quantitative analysis of infarct size, contraction band necrosis, and coagulation necrosis in human autopsied hearts with acute myocardial infarction after treatment with selective intracoronary thrombolysis. Circulation 1987;76(5):981-9.
27. Ciaccio EJ, Costeas C, Coromilas J, Wit AL. Static relationship of cycle length to reentrant circuit geometry. Circulation 2001;104(16):1946-51.

Chapter 10

Myocardial Scar Predicts Monomorphic VT but not Polymorphic VT or VF in Non-ischemic Dilated Cardiomyopathy

Sebastiaan R.D. Piers*, Kimberly Everaerts†, Rob J. van der Geest‡, Mark R. Hazebroek†, Hans-Marc Siebelink*, Laurent A.F.G. Pison†, Martin J. Schalij*, Sebastiaan C.A.M. Bekkers†, Stephane Heymans†§, Katja Zeppenfeld*

* Department of Cardiology, Leiden University Medical Centre, Leiden, The Netherlands
† Department of Cardiology, University Medical Centre Maastricht, Maastricht, The Netherlands
‡ Division of Image Processing, Leiden University Medical Centre, Leiden, The Netherlands
§ Netherlands Heart Institute (ICIN), Utrecht, The Netherlands.

Heart Rhythm 2015;12(10):2106-14.

ABSTRACT

Background

The relation between myocardial scar and different types of ventricular arrhythmias in patients with non-ischemic dilated cardiomyopathy (NIDCM) is unknown.

Objectives

To analyze the effect of myocardial scar, assessed by late gadolinium enhancement (LGE)-CMR, on the occurrence and type of ventricular arrhythmia in patients with NIDCM.

Methods

Consecutive patients with NIDCM who underwent LGE-CMR and ICD implantation at two centers were included. LGE was defined by signal intensity ≥35% of maximal signal intensity, subdivided into core and border zone (≥50% and 35-50% of maximal signal intensity, respectively), and categorized according to (non)basal location and transmurality. ICD recordings and ECGs were reviewed to determine the occurrence and type of ventricular arrhythmia during follow-up.

Results

Of 87 patients (age 56±13 years, 62% male, LVEF 29±12%), 55 (63%) had LGE (median 6.3g, interquartile range 0.0–13.8g). During a median follow-up of 45 months, monomorphic VT occurred in 18 (21%) patients, and polymorphic VT/VF in 10 (11%). LGE predicted monomorphic VT (Log-rank, $p<0.001$), but not polymorphic VT/VF (Log-rank, $p=0.40$). The optimal cut-off value for LGE to predict monomorphic VT was 7.2g (area under curve 0.84). Features associated with monomorphic VT were core extent, basal location, and area with 51-75% LGE transmurality.

Conclusions

Myocardial scar assessed by LGE-CMR predicts monomorphic VT, but not polymorphic VT/VF in NIDCM. The risk for monomorphic VT is particularly high when LGE shows a basal transmural distribution and a mass ≥7.2g. Importantly, patients without LGE on CMR remain at risk for potentially fatal polymorphic VT/VF.

INTRODUCTION

The presence of myocardial scar, as assessed by late gadolinium enhancement (LGE)-CMR, is an independent predictor of appropriate ICD therapy, sudden cardiac death and all-cause mortality in patients with non-ischemic dilated cardiomyopathy (NIDCM).[1-4] Ventricular arrhythmias do however occur in patients without LGE and may be caused by a different underlying substrate.[1,2,4]

Sustained monomorphic ventricular tachycardias (VTs) in patients with NIDCM undergoing catheter ablation are often due to scar-related fixed re-entry. Slow-conducting parts of these re-entry circuits are found in regions with myocardial scar, as demonstrated by integrating LGE-CMR data with 3D electroanatomical maps during VT ablation.[5-8] Several mechanisms for monomorphic VT have however been proposed[9] and the association between LGE and monomorphic VT has never been systematically analyzed in the general population of patients with NIDCM.

In contrast to sustained monomorphic VT, polymorphic VT and VF are thought to be related to multiple wavelet re-entry or a mother rotor fractionating to daughter wave fronts, resulting in continuously changing activation.[10] Although normal myocardium can sustain VF, different cardiac fibrosis patterns may contribute to the initiation and maintenance of polymorphic VT/VF.

The aims of the present study were (1) to analyze the effect of myocardial scar, as assessed by LGE-CMR, on the occurrence and type of ventricular arrhythmias in patients with NIDCM and (2) to evaluate the predictive value of LGE presence, extent and characteristics, for monomorphic VT.

METHODS

Patients

All patients with NIDCM who underwent LGE-CMR before ICD implantation at Leiden University Medical Centre (n=46) and Maastricht University Medical Centre (n=41), the Netherlands, between 2004 and 2012 were included. Patients who were implanted at the Maastricht University Medical Centre but followed at another center were excluded. The diagnosis of NIDCM was based on World Heart Organization definitions[11] and on CMR findings, requiring increased LV end-diastolic volume index and decreased LV ejection fraction (LVEF) compared with published 95% reference ranges normalized for gender, age and body surface area.[12] Significant coronary artery disease (≥70% stenosis in a major coronary artery) was excluded by coronary angiography or MDCT in all patients. Patients with sarcoidosis, amyloidosis or subendocardial LGE in a coronary artery perfusion territory were excluded.

The Dutch Central Committee on Human-related Research (CCMO) allows use of anonymous data without prior approval of an institutional review board provided that the data is acquired for patient care. All data used for this study was acquired for clinical purposes and handled anonymously.

LGE-CMR acquisition

CMR was performed on a 1.5T Gyroscan ACS-NT/Intera MR system (Philips Medical Systems, Best, the Netherlands) at the two centers. A standardized protocol was followed, including cine imaging in long-axis (two- and four-chamber) views, and in short-axis view covering the complete LV.

Approximately 15 minutes after bolus injection of gadolinium (Magnevist; Schering, Berlin, Germany; 0.15 mmol/kg) a look-locker sequence was acquired in short axis orientation at mid-ventricular level. T1-weighted LGE images were acquired with an inversion-recovery 3D turbo-field echo sequence with parallel imaging. Typical scan parameters were: average TR/TE 3.7/2.4ms, Flip angle 15°, FOV 400mm, matrix 256×206, acquired and reconstructed voxel size 1.56x1.94x5mm. The inversion time was optimized to null normal appearing myocardium. The heart was imaged in long-axis two- and four-chamber views (between 5-10 slices), and short-axis views (between 20-24 slices). Signal outside the field of view was suppressed using two saturation slabs to avoid fold-over artifacts.

CMR image analysis

All CMR analyses were performed using Mass software (research version 2012; LKEB; Leiden University Medical Centre, the Netherlands). The LV and RV end-diastolic and end-systolic endocardial contours were traced on cine images to calculate LV mass, end-diastolic volumes, end-systolic volumes and ejection fractions. Volumes and LV mass were indexed to body surface area.

To measure post-contrast T1-values, LV endocardial and epicardial contours were semi-automatically traced on look-locker images. Signal intensity was plotted against time and fitted to an exponential curve to obtain T1-values for the six midventricular segments, according to the American Heart Association (AHA) 17-segment model. The overall T1-value was defined as the average of these T1-values, excluding segments with LGE, to analyze the effects of myocardial scar and diffuse fibrosis separately. Similar to the method reported by Gai et al.[13], T1-values were normalized to a heart rate of 60 bpm using the following formula: T1 corrected = T1 uncorrected + α*(60–heart rate), where α equals -3.409, i.e. the slope of the regression line of heart rate vs. T1 of nonenhanced segments. Shorter T1 values indicate more diffuse myocardial fibrosis.[14]

Myocardial scar was assessed while the observer was blinded to clinical data and outcome, and was only considered to be present if LGE was visible in 2 orthogonal views. LGE was defined by signal intensity ≥35% of maximal myocardial signal intensity,

and subdivided into core (≥50% of maximal signal intensity) and border zone (35-50% of maximal signal intensity).[15] To assess the predictive value of LGE location, intensity and transmurality for monomorphic VT, the following parameters were calculated using Mass research software:

1. Extent of LGE (≥35% of maximal signal intensity, in grams) in basal and nonbasal segments (American Heart Association segments 1-6 and 7-17, respectively);
2. Extent of LGE (in grams) according to pre-defined signal intensity categories (30-40%, 40-50%, 50-60%, 60-70% and >70% of maximal signal intensity)
3. Endocardial surface area of myocardial regions with LGE (≥35% of maximal signal intensity, in cm^2) according to pre-defined transmurality categories (1-25%, 26-50%, 51-75% and 76-100% transmurality).

ICD programming and follow-up

ICDs were typically programmed to include 3 zones: monitor zone (150-188bpm, antitachycardia pacing [ATP] if clinically indicated), fast VT zone (188-210bpm, ATP and shock), VF zone (>210bpm, if available ATP during charging, and shock). Patients were followed at 6-monthly intervals. Intracardiac recordings were analyzed by an experienced observer who was blinded to clinical and CMR data when reviewing the recordings. The combined endpoint of any ventricular arrhythmia consisted of monomorphic VT and polymorphic VT/VF. Monomorphic VT was defined as VT with ≤30ms beat-to-beat variation in cycle length and stable far-field electrogram morphology, lasting >30 seconds or treated with ATP and/or shock. Polymorphic VT/VF was defined as any ventricular arrhythmia with >30ms beat-to-beat variation in cycle length and unstable far-field electrogram morphology, lasting >30 seconds or treated with ATP and/or shock. If ICD recordings and/or 12-lead ECGs were not available for some of the episodes, the missing episodes were considered to be of the same type as the documented episodes provided that the cycle length was similar. When ICD recordings and/or 12-lead ECGs were missing for all episodes, patients were excluded from all analysis involving the type of arrhythmia.

Statistical analysis

Categorical variables are displayed as number (percentage) and compared using the χ^2 test or the Fisher's exact test. Continuous variables are expressed as mean ± standard deviation or median (interquartile range [IQR]), and compared using the Student's *t* test or the Mann-Whitney *U* test when appropriate. The LGE extent in basal and nonbasal segments was compared using the Wilcoxon signed rank test.

Kaplan Meier survival analysis and Cox proportional hazard analysis were performed to identify predictors for arrhythmic events during follow-up. Multivariable Cox proportional hazard analyses were performed to analyze the independent predictive value of LGE and

specific LGE features, adjusting for other predictors with a p-value<0.10 in univariable analyses and for other LGE features of interest, respectively. A maximum of 1 variable per ~10 endpoints was included in the models. Receiver operating characteristic curve analysis was performed to determine the optimal cut-off values of LGE for prediction of monomorphic VT, which were defined as the values maximizing the sum of sensitivity and specificity. All analyses were performed with SPSS version 20.0 (IBM, Somers, New York, USA). All tests are two-sided and p-values<0.05 were considered significant.

RESULTS

Patients

Of the 87 patients (age 56±13 years, 62% male), 64 (74%) underwent ICD implantation for primary prevention, 10 (11%) after presentation with sustained monomorphic VT and 13 (15%) after out-of-hospital cardiac arrest with VF as the initial recorded rhythm (OHCA-VF)(Table 1). Forty-six patients (53%) were implanted with a cardiac resynchronization therapy-defibrillator.

CMR parameters and presenting arrhythmia

Patients presenting with OHCA-VF and in particular patients presenting with sustained monomorphic VT had lower LV end-diastolic and end-systolic volume indexes and higher LVEF, compared to primary prevention patients (Table 1).

Overall, LGE was present in 55 patients (63%, examples in Figure 1A-F), with a median LGE extent of 6.3 g (IQR, 0.0–13.8). LGE was observed in 9 of 10 patients (90%) presenting with sustained monomorphic VT and in only 4 of 13 patients (31%) with OHCA-VF, compared to 42 of 64 primary prevention patients (66%). The LGE extent was substantially higher in patients presenting with sustained monomorphic VT compared with primary prevention patients. In contrast, patients presenting with OHCA-VF tended to have less LGE than primary prevention patients.

The corrected T1 did neither differ between groups (Table 1) nor between patients with and without LGE (340±64 vs. 336±50, respectively, p=0.78).

Ventricular arrhythmias during follow-up

One patient (1%) was lost to follow-up after ICD implantation. During a median follow-up of 45 months (IQR, 23–67 months), 392 episodes of ventricular arrhythmia occurred in 28 patients (32%) (examples in Figure 1G-H). The ICD tracings or 12-lead ECGs could be reviewed for 298 episodes (76%), with at least one reviewed episode in 26 of 28 patients (93%). Of the 2 remaining patients, one had a dislocated RV lead and was resuscitated because of OHCA-VF, with VF as the first recorded rhythm, and the other had one single

episode with ATP, with no available tracings. These 2 patients were excluded from all analysis involving the type of arrhythmia.

Monomorphic VT occurred in 18 patients (median 5, IQR 3–23 episodes per patient; mean cycle length 308±47ms). At least one episode was terminated by ATP in 15 patients

Table 1. Baseline characteristics according to presenting arrhythmia

	All patients (n=87)	Primary prevention (n=64)	SMVT (n=10)	p†	OHCA (n=13)	p†
Age	56±13	56±13	61±12	0.30	51±15	0.20
Male	54(62%)	37(58%)	8(80%)	0.30	9(69%)	0.44
NYHA functional class						
I	28(32%)	11(17%)	7(70%)	**0.001**	10(77%)	**< 0.001**
II	32(37%)	26(41%)	3(30%)		3(23%)	
III-IV	27(31%)	27(42%)	0(0%)		0(0%)	
History of AF/atrial flutter	14(16%)	12(19%)	0(0%)	0.20	2(15%)	1.00
History of hypertension	25(29%)	18(28%)	3(30%)	1.00	4(31%)	1.00
Diabetes mellitus	6(7%)	4(6%)	2(20%)	0.18	0(0%)	1.00
eGFR, mL/min/1.73m^2	72±24	69±22	74±12	0.51	86±31	**0.027**
QRS duration, ms	132±32	130±31	128±35	0.84	142±31	0.21
LV volumes and function						
LVEDV, mL	288 (231–358)	318 (248–376)	219 (180–241)	**0.001**	244 (213–302)	**0.033**
LVESV, mL	209 (145–279)	228 (170–309)	119 (102–147)	**< 0.001**	150 (128–197)	**0.004**
LVEF, %	29±12	25±11	44±7	**< 0.001**	37±11	**0.001**
LV mass, g	147 (111–176)	150 (114–177)	135 (102–155)	0.31	138 (93–194)	0.45
RV volumes and function						
RVEDV, mL	158 (129–204)	153 (129–208)	160 (126–192)	0.90	166 (133–182)	0.83
RVESV, mL	80 (57–118)	80 (57–125)	75 (54–129)	0.68	71 (55–84)	0.16
RVEF, %	47±15	44±15	49±14	0.40	56±11	**0.004**
T1 corrected	339±59	335±54	341±79	0.80	355±74	0.27
LGE						
LGE presence	55(63%)	42(66%)	9(90%)	0.16	4(31%)	**0.019**
LGE extent						
Total LGE, g	6.3 (0.0–13.8)	5.8 (0.0–12.8)	16.6 (9.5–24.3)	**0.007**	0.0 (0.0–10.9)	0.14
Core, g	2.8 (0.0–5.8)	2.6 (0.0–4.8)	10.0 (5.6–15.3)	**0.002**	0.0 (0.0–3.3)	0.094
Border zone, g	3.0 (0.0–7.7)	2.5 (0.0–7.6)	5.9 (4.0–10.0)	0.070	0.0 (0.0–7.6)	0.14

Data are expressed as number (percentage), mean ± standard deviation or median (interquartile range). AF indicates atrial fibrillation; BMI, body mass index; eGFR, estimated glomerular filtration rate; LGE, late gadolinium enhancement; LV, left ventricular; LVEDV, LV end-diastolic volume; LVEF, LV ejection fraction; LVESV, LV end-systolic volume; NYHA, New York Heart Association; OHCA, out-of-hospital cardiac arrest; RV, right ventricular; SMVT, sustained monomorphic ventricular tachycardia. † vs. primary prevention.

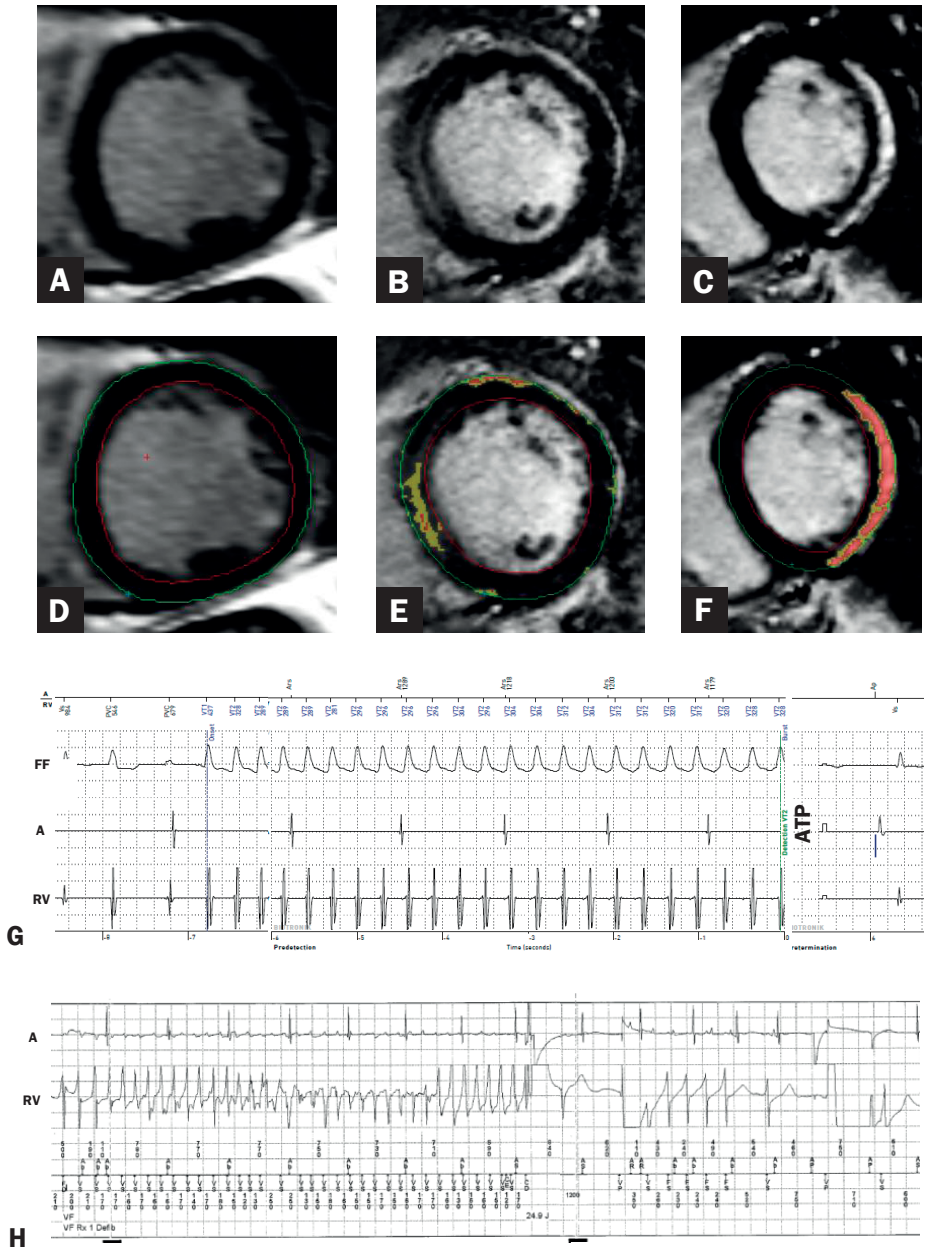


Figure 1. Examples of LGE-CMR and ventricular arrhythmias

Examples of a patient without LGE (panels A&D), small amount of LGE (panels B&E) and extensive LGE (panels C&F). Red indicates LGE core and yellow border zone. Monomorphic VT was related to LGE and frequently terminated by antitachycardia pacing (panel G), whereas polymorphic VT/VF was not related to LGE and typically terminated by an ICD shock (panel H).

(83%) and ≥1 episode by an ICD shock in 9 (50%). Seven patients (39%) had ≥1 episode lasting >30 seconds in the monitor zone or below detection rate.

Polymorphic VT/VF occurred in 10 patients (one episode in 8 patients (80%), 2 and 4 episodes in the remaining 2 patients). Nine of 10 patients (90%) only had episodes terminated by an ICD shock, while one patient had 4 episodes of polymorphic VT that stopped after a single burst of ATP.

Of note, only 2 patients had both monomorphic VT and polymorphic VT/VF – the other 26 patients with ventricular arrhythmias during follow-up had only one type of ventricular arrhythmia.

Predictors of different types of ventricular arrhythmia during follow-up

Predictors of monomorphic VT and polymorphic VT/VF were remarkably different. The presence of myocardial scar, as assessed by LGE-CMR, predicted the occurrence of monomorphic VT ($p<0.001$), but not of polymorphic VT/VF ($p=0.41$) (Figure 2, Table 2, Supplemental Table 1). Accordingly, the total LGE extent was a strong predictor of monomorphic VT ($p<0.001$), but not of polymorphic VT/VF ($p=0.66$).

Monomorphic VT was also predicted by male gender, presentation with sustained monomorphic VT, hypertension, diabetes mellitus, LVEF and corrected T1 values. The LGE extent remained an independent predictor for monomorphic VT when adjusted for each of these parameters separately (Supplemental Table 2), and also when only primary prevention patients were analyzed (Supplemental Table 3 and supplemental Figure 1).

The only predictor of polymorphic VT/VF during follow-up was presentation with OHCA-VF (Table 2). Of importance, LV and RV volumes and function, and LGE presence and extent were not associated with the occurrence of polymorphic VT/VF.

The combined endpoint of any ventricular arrhythmia was predicted by the presence and extent of LGE, male gender, hypertension, diabetes mellitus, LVEF and corrected T1 values (Figure 3, Table 2, Supplemental Table 1). The LGE extent remained an independent predictor when adjusted for each of these parameters separately, except diabetes mellitus (Supplemental Table 2), which may be due to the small number of patients with diabetes mellitus.

Myocardial scar characteristics and monomorphic VT

Receiver operating characteristic curve analysis of the association between the total LGE, core and border zone extent and monomorphic VT during follow-up yielded areas under the curve of 0.84, 0.86 and 0.78, respectively. The optimal cut-off values for prediction of monomorphic VT were 7.2g for total LGE extent (sensitivity 94%, specificity 67%), 3.0g for core (sensitivity 94%, specificity 64%) and 2.3g for border zone (sensitivity 100%, specificity 58%). Patients with LGE <7.2g were at very low risk for monomorphic VT (Figure 2) and at relatively low risk for any ventricular arrhythmia during follow-up (Figure 3).

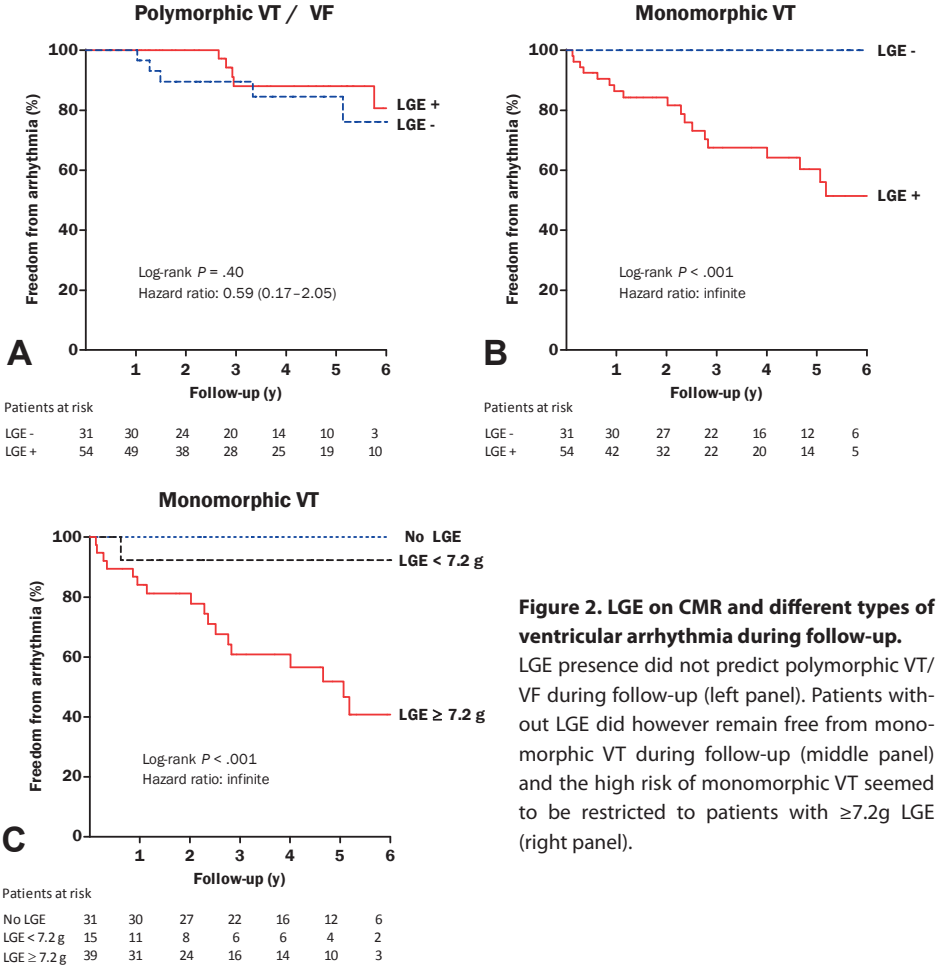


Figure 2. LGE on CMR and different types of ventricular arrhythmia during follow-up. LGE presence did not predict polymorphic VT/VF during follow-up (left panel). Patients without LGE did however remain free from monomorphic VT during follow-up (middle panel) and the high risk of monomorphic VT seemed to be restricted to patients with ≥7.2g LGE (right panel).

The LGE extent was larger in basal segments than in nonbasal segments (basal median 2.0g (IQR 0.0-7.7g), vs. nonbasal median 1.1g (IQR, 0.0-4.0g), p=0.011). The LGE extent in basal segments was a stronger predictor for monomorphic VT than the extent in nonbasal segments (Table 3). When both were included in a single model, only the LGE extent in basal segments remained an independent predictor of monomorphic VT (Supplemental Table 4).

When subdivided into 5 signal intensity categories, categories with LGE >60% of maximal signal intensity carried stronger prognostic information than categories with LGE 30-60% of maximal signal intensity (Table 3). When the two categories of LGE 30-60% and >60% of maximal signal intensity were included in a single model, only LGE >60% of maximal signal intensity remained associated with monomorphic VT (Supplemental Table 4).

Table 2. Predictors of ventricular arrhythmia during follow-up

Univariate analyses	Any ventricular arrhythmia		Monomorphic VT		Polymorphic VT/VF	
	Hazard ratio (95% CI)	P	Hazard ratio (95% CI)	p	Hazard ratio (95% CI)	p
Age, per 5 years↑	1.03 (0.90–1.19)	0.65	1.17 (0.96–1.42)	0.13	0.88 (0.71–1.10)	0.27
Male gender	3.59 (1.24–10.35)	**0.018**	2.89 (0.83–9.99)	0.094	4.42 (0.56–34.92)	0.16
Presenting arrhythmia						
OHCA vs. none	2.29 (0.82–6.39)	0.12	0.68 (0.08–5.43)	0.71	7.77 (1.90–31.69)	**0.004**
SMVT vs. none	6.54 (2.75–15.54)	**< 0.001**	11.52 (4.22–31.42)	**< 0.001**	3.01 (0.55–16.51)	0.21
Symptomatic heart failure	0.66 (0.31–1.40)	0.28	0.62 (0.24–1.57)	0.31	0.55 (0.16–1.89)	0.34
History of AF / atrial flutter	1.04 (0.39–2.74)	0.94	0.98 (0.28–3.40)	0.98	0.47 (0.06–3.76)	0.48
History of hypertension	2.36 (1.11–5.02)	**0.025**	4.81 (1.86–12.47)	**0.001**	1.04 (0.26–4.07)	0.96
Diabetes mellitus	7.27 (2.56–20.60)	**< 0.001**	12.29 (3.94–38.34)	**< 0.001**	1.70 (0.21–13.43)	0.62
eGFR, per 10mL/min/1.73m^2↓	1.04 (0.88–1.22)	0.69	1.06 (0.87–1.31)	0.56	0.91 (0.71–1.16)	0.45
QRS duration, per 10ms↑	0.93 (0.82–1.05)	0.23	0.94 (0.81–1.09)	0.41	0.89 (0.72–1.11)	0.30
Class III AAD at discharge	1.36 (0.55–3.36)	0.51	1.47 (0.48–4.46)	0.50	0.47 (0.06–3.71)	0.47
LV volumes and function						
LVEDV index, per 10mL/m^2↑	1.00 (0.93–1.06)	0.91	0.93 (0.83–1.04)	0.18	0.98 (0.87–1.10)	0.70
LVESV index, per 10mL/m^2↑	0.99 (0.92–1.06)	0.71	0.90 (0.80–1.02)	0.086	0.97 (0.87–1.09)	0.64
LVEF, per 10%↓	0.74 (0.54–1.01)	0.054	0.55 (0.36–0.83)	**0.005**	0.85 (0.51–1.41)	0.52
LV mass index, per 10g/m^2↑	0.88 (0.73–1.07)	0.20	0.89 (0.72–1.11)	0.31	0.75 (0.51–1.10)	0.14
RV volumes and function						
RVEDV index, per 10mL/m^2↑	1.04 (0.94–1.16)	0.45	1.04 (0.91–1.18)	0.59	1.04 (0.87–1.24)	0.65
RVESV index, per 10mL/m^2↑	1.01 (0.90–1.14)	0.83	0.99 (0.85–1.15)	0.92	1.00 (0.82–1.23)	0.98
RVEF, per 10%↓	1.01 (0.79–1.30)	0.92	0.94 (0.68–1.29)	0.68	0.94 (0.61–1.45)	0.78
T1 corrected, per 50ms↓	0.65 (0.45–0.93)	**0.020**	0.58 (0.37–0.92)	**0.020**	1.22 (0.66–2.26)	0.53
LGE						
LGE presence	2.71 (1.10–6.69)	**0.031**	∞	**< 0.001**	0.59 (0.17–2.05)	0.41
LGE extent						
Total LGE, per 10g↑	1.47 (1.10–1.97)	**0.010**	1.90 (1.35–2.67)	**< 0.001**	0.87 (0.48–1.59)	0.66
Core, per 10g↑	2.38 (1.34–4.22)	**0.003**	4.28 (2.15–8.51)	**< 0.001**	0.74 (0.22–2.49)	0.63
Border zone, per 10g↑	1.79 (1.03–3.10)	**0.039**	2.59 (1.38–4.86)	**0.003**	0.80 (0.26–2.48)	0.70

Abbreviations as in Table 1. When events only occurred in one subgroup, hazard ratios were infinite(∞) and p-values were derived from Kaplan-Meier analyses.

Finally, the area with 51-75% transmural LGE was a particularly strong predictor for monomorphic VT, whereas the area with 1-25% transmural LGE was not significantly associated with monomorphic VT (Table 3). Only the area of 51-75% transmural LGE remained an independent predictor when adjusted for each of the other transmurality categories (Supplemental Table 4).

Table 3. Specific LGE characteristics predicting monomorphic VT

Univariate analyses	Amount of LGE	Predictive value for monomorphic VT	
	Median (IQR)	Hazard ratio (95% CI)	p
LGE location †			
LGE in basal segments, g	2.0 (0.0–7.7)	3.82 (2.11–6.93)†	**< 0.001**
LGE in nonbasal segments, g	1.1 (0.0–4.0)	2.17 (1.13–4.17)†	**0.020**
LGE according to % of maximal signal intensity			
>70%, g	0.6 (0.0–1.8)	1.55 (1.29–1.85)	**< 0.001**
60-70%, g	0.7 (0.0–1.6)	1.66 (1.28–2.13)	**< 0.001**
50-60%, g	1.2 (0.0–2.4)	1.29 (1.11–1.50)	**0.001**
40-50%, g	1.8 (0.0–4.3)	1.21 (1.07–1.36)	**0.003**
30-40%, g	2.9 (0.0–7.0)	1.12 (1.03–1.21)	**0.006**
LGE transmurality areas ‡			
76-100%, cm^2	1.6 (0.0–7.0)	1.05 (1.01–1.10)	**0.029**
51-75%, cm^2	1.6 (0.0–4.6)	1.22 (1.11–1.34)	**< 0.001**
26-50%, cm^2	3.4 (0.0–9.5)	1.09 (1.02–1.16)	**0.007**
1-25%, cm^2	4.8 (0.0–12.1)	1.04 (0.99–1.08)	0.092

† per 10g † ‡ based on total LGE (≥35% of maximal SI)

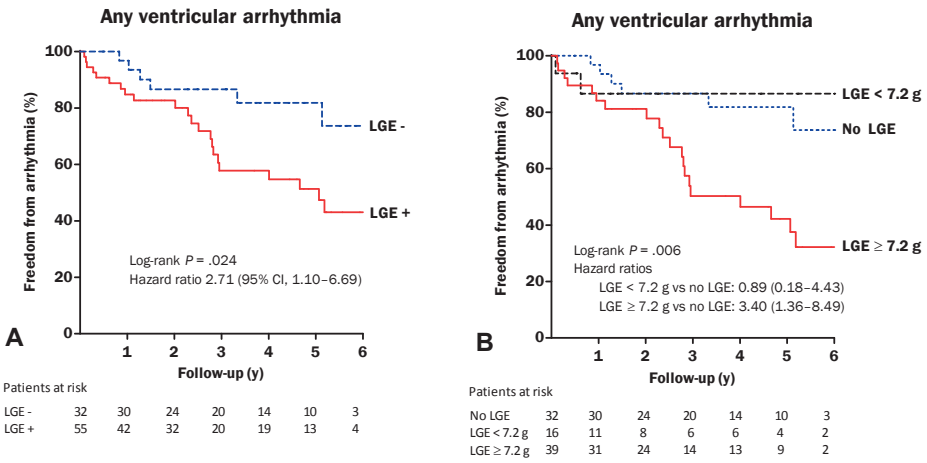


Figure 3. LGE on CMR and any ventricular arrhythmia during follow-up.
LGE presence predicted any ventricular arrhythmia during follow-up. The risk for ventricular arrhythmia was only increased in patients with ≥7.2g LGE.

DISCUSSION

In this study we analyzed the impact of myocardial scar, assessed by LGE-CMR, on different types of ventricular arrhythmias in NIDCM. We found that LGE was an important predictor for monomorphic VT, but not for polymorphic VT/VF. The optimal cut-off value for the extent of LGE to predict monomorphic VT was 7.2g. Patients with LGE extent <7.2g were at very low risk for monomorphic VT. Specific LGE characteristics associated with a high risk for monomorphic VT were LGE extent in basal segments, extent with >60% of maximal signal intensity and area with 51-75% transmural scar. Of importance, patients without LGE remain at risk for potentially lethal polymorphic VT/VF, and the only predictor for polymorphic VT/VF was a history of OHCA-VF.

Myocardial scar and type of ventricular arrhythmia

The presence of LGE on CMR has been reported to predict combined arrhythmic endpoints.[2-4,16] The present study is the first to analyze the predictive value of clinical and CMR parameters separately for monomorphic VT and polymorphic VT/VF. Patients presenting with sustained monomorphic VT had a substantially larger extent of LGE compared to patients without prior arrhythmias. Remarkably, the smallest LGE extent was observed in patients after OHCA-VF and accordingly, the predictive value of LGE for ventricular arrhythmias during follow-up was entirely explained by LGE predicting monomorphic VT, but not polymorphic VT/VF. This strong association between LGE and monomorphic VT is supported by studies on integration of CMR-derived data during VT ablation in patients with non-ischemic LV cardiomyopathy.[5,7,8]

The optimal cut-off for LGE extent to predict monomorphic VT was 7.2g. Patients with <7.2g LGE were at very low risk for monomorphic VT. Prior studies have identified 4–6.1% LGE as the optimal cut-off value for different combined endpoints (cardiovascular death and appropriate ICD therapy[1]; all-cause mortality and hospitalization for cardiovascular event;[4] cardiac death, hospitalization for decompensated heart failure and appropriate ICD discharge[16]). To the best of our knowledge, none has analyzed cut-off values for prediction of arrhythmic endpoints.

When LGE extent was analyzed separately in basal or nonbasal segments, the basal LGE extent appeared to be a stronger predictor for monomorphic VT. This finding is consistent with VT ablation studies reporting predominantly basal substrates for monomorphic VT in non-ischemic LV cardiomyopathy.[8] Similar to observations in post-infarct patients, basal scars and mitral/aortic annuli may serve as un-excitable barriers that can define parts of the re-entry circuit of monomorphic VT.

Other LGE features strongly associated with monomorphic VT were >60% of maximal signal intensity and 51-75% transmurality. This is in line with our prior findings during VT ablation procedures, demonstrating that the critical VT isthmus sites are typically

located close to the core-border zone transition (i.e., the 50% of maximal signal intensity cut-off value) and to >75% transmural scar.[17] These more specific LGE features may facilitate identification of NIDCM patients at risk for monomorphic VT.

Diffuse fibrosis and ventricular arrhythmias

The present study also analyzed post-contrast T1 values, which have been shown to correlate with the amount of diffuse fibrosis in biopsy specimens.[14] T1 values were similar between patients presenting with sustained monomorphic VT, OHCA-VF and no prior ventricular arrhythmias. In the latter group T1 values did not predict any type of ventricular arrhythmia during follow-up. Prior studies using endomyocardial biopsy specimens could also neither demonstrate a correlation between fibrosis content and history of ventricular arrhythmias,[18] inducible sustained monomorphic VT,[19] and LGE on CMR,[20] nor between the amount of interstitial tissue and arrhythmic events during follow-up.[21] Of interest, some data suggest that the microscopic pattern of fibrosis, rather than the amount may be important for arrhythmias.[22] Future studies are required to evaluate whether T1 mapping may contribute to the identification of specific arrhythmogenic substrates.

Predicting polymorphic VT/VF

Although we could identify clinical and CMR characteristics with predictive value for monomorphic VT, the only predictor for polymorphic VT/VF was a history of OHCA-VF. Neither LV and RV volumes and function, nor LGE presence and extent were associated with polymorphic VT/VF. It therefore appears that polymorphic VT/VF cannot be predicted with the same methods/parameters that apply for monomorphic VT. More insights are required into the substrate and related mechanisms of polymorphic VT/VF in patients with NIDCM to identify predictors for these arrhythmias, which may include parameters that are beyond the scope of imaging techniques.

Limitations

Not all patients with NIDCM underwent CMR before ICD implantation, and although patient characteristics were similar to prior studies in patients with NIDCM undergoing CMR and ICD implantation,[1,3] we cannot exclude a selection bias. T1 measurement is considered to be a marker for diffuse fibrosis, but is validated only to a limited extent by histology in patients with NIDCM.[14] The LGE core, but not the border zone definition has been validated by histopathology in NIDCM.[2] Also, core and border zone may not be comparable between patients after myocardial infarction and NIDCM due to differences in maximal LGE signal intensity. The present study did not allow differentiation between VTs based on scar-related re-entry or other mechanisms such as triggered activity. Follow-up was relatively long (median 45 months), but the sample size was limited and the multivariable models therefore had to be restricted to 2-3 variables.

CONCLUSIONS

The present study provides evidence that different types of ventricular arrhythmias are due to different underlying substrates in patients with NIDCM. The presence and extent of LGE on CMR identifies patients who are at risk for monomorphic VT, but not those at risk for potentially fatal polymorphic VT/VF. Only patients with a significant amount of myocardial scar (i.e., ≥7.2g) appeared to be at high risk for monomorphic VT. In addition, specific LGE features (extent in basal segments, LGE with >60% of maximal signal intensity, LGE area with 51-75% transmurality) further indicate a predisposition for monomorphic VT. Although patients without LGE are at relatively low risk for ventricular arrhythmias during follow-up, they still remain at risk for potentially fatal polymorphic VT/VF.

Acknowledgements

The research leading to these results has received funding given to SH from the European Union Commission's Seventh Framework program under grant agreement N° 305507 (HOMAGE), N° 305507 (FIBROTARGETS) and N° 261409 (MEDIA) and N° 278249 (EU MASCARA) and the Marie-Curie Industry Academy Pathways and Partnerships (CARDIOMIR) N°285991, FP7-Health-2013-Innovations-1 N° 602156 (HECATOS).

CLINICAL PERSPECTIVES

Myocardial scar, assessed by LGE-CMR, has been shown to predict appropriate ICD therapy and sudden cardiac death in patients with NIDCM. However, ventricular arrhythmias encompass monomorphic VT, polymorphic VT and VF which may be related to different underlying substrates. The present study is the first to evaluate the relation between myocardial scar and different types of arrhythmia in NIDCM. Importantly, it is demonstrated that LGE predicts monomorphic VT, but not polymorphic VT/VF. Specific LGE features (including mass ≥ 7.2g, basal location, higher signal intensity, and area with 51-75% transmurality) were associated with a high risk for monomorphic VT. Although patients without LGE were at relatively low risk for ventricular arrhythmias, they still remained at risk for polymorphic VT/VF. Despite the availability of advanced measures of LV and RV volumes and function and of LGE indices, the only predictor for polymorphic VT/VF was a history of out-of-hospital cardiac arrest.

These novel insights may have important implications for risk stratification and therapeutic interventions. The risk for monomorphic VT in patients with NIDCM can be predicted by the presence, location and geometry of LGE on CMR, which may be useful for selection of patients that benefit from VT ablation at the time of ICD implantation. It is important to recognize that patients without LGE remain at risk for potentially fatal polymorphic VT/VF. More insights are required into the substrate and mechanisms of the different ventricular arrhythmias in patients with NIDCM to also identify those at risk for polymorphic VT/VF.

REFERENCE LIST

1. Neilan TG, Coelho-Filho OR, Danik SB et al.: CMR quantification of myocardial scar provides additive prognostic information in nonischemic cardiomyopathy. JACC Cardiovasc Imaging 2013;9:944-54.
2. Gulati A, Jabbour A, Ismail TF et al.: Association of fibrosis with mortality and sudden cardiac death in patients with nonischemic dilated cardiomyopathy. JAMA 2013;9: 896-908.
3. Iles L, Pfluger H, Lefkovits L, Butler MJ, Kistler PM, Kaye DM, Taylor AJ: Myocardial fibrosis predicts appropriate device therapy in patients with implantable cardioverter-defibrillators for primary prevention of sudden cardiac death. J Am Coll Cardiol 2011;7:821-8.
4. Assomull RG, Prasad SK, Lyne J, Smith G, Burman ED, Khan M, Sheppard MN, Poole-Wilson PA, Pennell DJ: Cardiovascular magnetic resonance, fibrosis, and prognosis in dilated cardiomyopathy. J Am Coll Cardiol 2006;10:1977-85.
5. Bogun FM, Desjardins B, Good E, Gupta S, Crawford T, Oral H, Ebinger M, Pelosi F, Chugh A, Jongnarangsin K, Morady F: Delayed-enhanced magnetic resonance imaging in nonischemic cardiomyopathy: utility for identifying the ventricular arrhythmia substrate. J Am Coll Cardiol 2009;13:1138-45.
6. Fernandez-Armenta J, Berruezo A, Andreu D et al.: Three-dimensional Architecture of Scar and Conducting Channels Based on High Resolution ce-CMR: Insights for Ventricular Tachycardia Ablation. Circ Arrhythm Electrophysiol 2013;3:528-37.
7. Piers SR, van Huls van Taxis CF, Tao Q, van der Geest RJ, Askar SF, Siebelink HM, Schalij MJ, Zeppenfeld K: Epicardial substrate mapping for ventricular tachycardia ablation in patients with non-ischaemic cardiomyopathy: a new algorithm to differentiate between scar and viable myocardium developed by simultaneous integration of computed tomography and contrast-enhanced magnetic resonance imaging. Eur Heart J 2012;8:586-96.
8. Piers SR, Tao Q, van Huls van Taxis CF, Schalij MJ, van der Geest RJ, Zeppenfeld K: Contrast-Enhanced MRI-Derived Scar Patterns and Associated Ventricular Tachycardias in Nonischemic Cardiomyopathy: Implications for the Ablation Strategy. Circ Arrhythm Electrophysiol 2013;5:875-83.
9. Delacretaz E, Stevenson WG, Ellison KE, Maisel WH, Friedman PL: Mapping and radiofrequency catheter ablation of the three types of sustained monomorphic ventricular tachycardia in nonischemic heart disease. J Cardiovasc Electrophysiol 2000;1:11-7.
10. Gelzer AR, Koller ML, Otani NF, Fox JJ, Enyeart MW, Hooker GJ, Riccio ML, Bartoli CR, Gilmour RF, Jr.: Dynamic mechanism for initiation of ventricular fibrillation in vivo. Circulation 2008;11:1123-9.
11. Richardson P, McKenna W, Bristow M et al.: Report of the 1995 World Health Organization/International Society and Federation of Cardiology Task Force on the Definition and Classification of cardiomyopathies. Circulation 1996;5:841-2.
12. Maceira AM, Prasad SK, Khan M, Pennell DJ: Normalized left ventricular systolic and diastolic function by steady state free precession cardiovascular magnetic resonance. J Cardiovasc Magn Reson 2006; 3:417-26.
13. Gai N, Turkbey EB, Nazarian S, van der Geest RJ, Liu CY, Lima JA, Bluemke DA: T1 mapping of the gadolinium-enhanced myocardium: adjustment for factors affecting interpatient comparison. Magn Reson Med 2011;5:1407-15.

14. Iles L, Pfluger H, Phrommintikul A, Cherayath J, Aksit P, Gupta SN, Kaye DM, Taylor AJ: Evaluation of diffuse myocardial fibrosis in heart failure with cardiac magnetic resonance contrast-enhanced T1 mapping. J Am Coll Cardiol 2008;19:1574-80.
15. Roes SD, Borleffs CJ, van der Geest RJ et al.: Infarct tissue heterogeneity assessed with contrast-enhanced MRI predicts spontaneous ventricular arrhythmia in patients with ischemic cardiomyopathy and implantable cardioverter-defibrillator. Circ Cardiovasc Imaging 2009;3:183-90.
16. Lehrke S, Lossnitzer D, Schob M et al.: Use of cardiovascular magnetic resonance for risk stratification in chronic heart failure: prognostic value of late gadolinium enhancement in patients with non-ischaemic dilated cardiomyopathy. Heart 2011;9: 727-32.
17. Piers SR, Tao Q, de Riva SM, Siebelink HM, Schalij MJ, van der Geest RJ, Zeppenfeld K: CMR-Based Identification of Critical Isthmus Sites of Ischemic and Nonischemic Ventricular Tachycardia. JACC Cardiovasc Imaging 2014;8:774-84.
18. Boulaksil M, Winckels SK, Engelen MA et al.: Heterogeneous Connexin43 distribution in heart failure is associated with dispersed conduction and enhanced susceptibility to ventricular arrhythmias. Eur J Heart Fail 2010;9:913-21.
19. Lo YS, Billingham M, Rowan RA, Lee HC, Liem LB, Swerdlow CD: Histopathologic and electrophysiologic correlations in idiopathic dilated cardiomyopathy and sustained ventricular tachyarrhythmia. Am J Cardiol 1989;16:1063-6.
20. Schalla S, Bekkers SC, Dennert R, van Suylen RJ, Waltenberger J, Leiner T, Wildberger J, Crijns HJ, Heymans S: Replacement and reactive myocardial fibrosis in idiopathic dilated cardiomyopathy: comparison of magnetic resonance imaging with right ventricular biopsy. Eur J Heart Fail 2010;3: 227-31.
21. Grimm W, Rudolph S, Christ M, Pankuweit S, Maisch B: Prognostic significance of morphometric endomyocardial biopsy analysis in patients with idiopathic dilated cardiomyopathy. Am Heart J 2003;2:372-6.
22. Kawara T, Derksen R, de Groot JR, Coronel R, Tasseron S, Linnenbank AC, Hauer RN, Kirkels H, Janse MJ, de Bakker JM: Activation delay after premature stimulation in chronically diseased human myocardium relates to the architecture of interstitial fibrosis. Circulation 2001;25:3069-75.

Supplemental Table 1. Baseline characteristics and ventricular arrhythmias during follow-up.

	No arrhythmia (n=59)	Monomorphic VT (n=18)		Polymorphic VT/VF (n=10)	
			p*		p*
Age	55±14	60±9	0.17	52±13	0.45
Male gender	30 (51%)	15 (83%)	**0.014**	9 (90%)	**0.035**
Presenting arrhythmia					
OHCA	8 (14%)	1 (6%)	0.68	4 (40%)	0.064
SMVT	1 (2%)	9 (50%)	**< 0.001**	2 (20%)	0.053
Symptomatic heart failure	43 (73%)	10 (56%)	0.17	5 (50%)	0.16
History of AF / atrial flutter	9 (15%)	3 (17%)	1.00	1 (10%)	1.00
History of hypertension	13 (22%)	11 (61%)	**0.002**	3 (30%)	0.69
Diabetes mellitus	1 (2%)	5 (28%)	**0.002**	1 (10%)	0.27
eGFR, mL/min/1.73m^2	73±22	67±20	0.31	75±36	0.90
QRS duration, ms	134±32	129±33	0.57	125±27	0.41
Class III AAD at discharge	8 (14%)	4 (22%)	0.46	1 (10%)	1.00
LV volumes and function					
LVEDV index, 10mL/m^2	154 (123–176)	124 (100–165)	0.056	128 (116–195)	0.71
LVESV index, 10mL/m^2	113 (82–139)	72 (61–103)	**0.008**	74 (66–160)	0.38
LVEF, %	27±11	37±13	**0.001**	33±13	0.18
LV mass index, g/m^2	75 (60–93)	68 (62–81)	0.77	67 (49–91)	0.41
RV volumes and function					
RVEDV index, mL/m^2	77 (64–95)	81 (70–115)	0.33	98 (72–103)	0.19
RVESV index, mL/m^2	39 (28–59)	41 (31–58)	0.66	42 (33–54)	0.61
RVEF, %	46±16	49±12	0.58	48±16	0.73
T1 corrected, ms	332±55	362±78	0.082	322±62	0.64
LGE					
LGE presence	33 (56%)	18 (100%)	**0.001**	5 (50%)	0.75
LGE extent					
Total LGE, g	2.3 (0.0–10.2)	15.8 (9.7–24.3)	**< 0.001**	6.9 (0.0–15.7)	0.60
Core, g	1.0 (0.0–3.8)	9.4 (3.8–14.5)	**< 0.001**	2.0 (0.0–9.3)	0.67
Border zone, g	0.8 (0.0–6.6)	6.9 (4.7–10.7)	**< 0.001**	2.6 (0.0–9.8)	0.72

Data are expressed as number (percentage), mean ± standard deviation or median (interquartile range). AF indicates atrial fibrillation; eGFR, estimated glomerular filtration rate; LGE, late gadolinium enhancement; LV, left ventricular; LVEDV, LV end-diastolic volume; LVEF, LV ejection fraction; LVESV, LV end-systolic volume; OHCA, out-of-hospital cardiac arrest; RV, right ventricular; SMVT, sustained monomorphic ventricular tachycardia.

* vs. no arrhythmia

Supplemental Table 2. Extent of LGE adjusted for other predictors of any ventricular arrhythmia and monomorphic VT

Multivariate analyses	Any ventricular arrhythmia		Monomorphic VT	
	Hazard ratio (95% CI)	p	Hazard ratio (95% CI)	p
Model 1				
Total LGE, per 10g ↓	1.42 (1.05–1.93)	0.023	1.87 (1.32–2.66)	< 0.001
Male gender	3.24 (1.12–9.39)	0.030	2.46 (0.71–8.53)	0.16
Model 2				
Total LGE, per 10g ↓	1.36 (1.00–1.85)	0.049	1.63 (1.14–2.32)	0.007
History of hypertension	1.87 (0.84–4.14)	0.12	3.26 (1.18–8.96)	0.022
Model 3				
Total LGE, per 10g ↓	1.25 (0.90–1.74)	0.18	1.52 (1.03–2.25)	0.035
Diabetes mellitus	4.80 (1.44–16.01)	0.011	5.49 (1.43–21.18)	0.013
Model 4				
Total LGE, per 10g ↓	1.52 (1.12–2.05)	0.007	2.08 (1.42–3.03)	< 0.001
LVEF, per 10% ↓	0.72 (0.53–0.98)	0.034	0.55 (0.37–0.80)	0.002
Model 5				
Total LGE, per 10g ↓	1.46 (1.08–1.98)	0.014	1.97 (1.35–2.86)	< 0.001
T1 corrected, per 50ms ↓	0.65 (0.45–0.93)	0.018	0.57 (0.37–0.90)	0.016

LGE indicates late gadolinium enhancement; LVEF, LV ejection fraction.

Supplemental Table 3. Predictors of any ventricular arrhythmia and monomorphic VT in primary prevention patients.

Univariate analyses	Any ventricular arrhythmia		Monomorphic VT	
	Hazard ratio (95% CI)	p	Hazard ratio (95% CI)	P
Age, per 5 years ↓	1.04 (0.84–1.28)	0.74	1.17 (0.85–1.60)	0.33
Male gender	9.87 (1.29–75.53)	0.028	5.11 (0.63–41.55)	0.13
Symptomatic heart failure	1.52 (0.34–6.78)	0.59	1.76 (0.22–14.34)	0.60
History of AF / atrial flutter	1.47 (0.46–4.69)	0.52	1.23 (0.25–6.14)	0.80
History of hypertension	4.40 (1.52–12.75)	0.006	∞	< 0.001
Diabetes mellitus	18.69 (4.08–85.69)	< 0.001	41.69 (6.79–256.14)	< 0.001
eGFR, per 10mL/min/1.73m^2 ↓	1.30 (1.00–1.68)	0.052	1.27 (0.90–1.80)	0.18
QRS duration, per 10ms ↓	0.91 (0.76–1.09)	0.32	1.02 (0.82–1.28)	0.85
Class III AAD at discharge	1.36 (0.38 - 4.88)	0.64	0.71 (0.09 - 5.78)	0.75
LV volumes and function				
LVEDV index, per 10mL/m^2 ↓	1.06 (0.99–1.13)	0.11	1.01 (0.90–1.13)	0.85
LVESV index, per 10mL/m^2 ↓	1.06 (0.99–1.14)	0.098	1.00 (0.90–1.13)	0.94
LVEF, per 10% ↓	1.23 (0.72–2.10)	0.44	0.81 (0.42–1.55)	0.53
LV mass index, per 10 g/m^2 ↓	1.10 (0.89–1.37)	0.37	1.06 (0.80–1.41)	0.67
RV volumes and function				
RVEDV index, per 10mL/m^2 ↓	1.05 (0.91–1.21)	0.51	1.04 (0.85–1.25)	0.73
RVESV index, per 10mL/m^2 ↓	1.05 (0.92–1.20)	0.47	1.01 (0.83–1.23)	0.89
RVEF, per 10% ↓	1.23 (0.87–1.73)	0.24	1.03 (0.66–1.63)	0.89
T1 corrected, per 50ms ↓	0.79 (0.47–1.32)	0.37	0.78 (0.40–1.55)	0.48
LGE				
LGE presence	2.41 (0.67–8.66)	0.18	∞	0.024
LGE extent				
Total LGE, per 10g ↓	1.46 (0.97–2.22)	0.072	1.84 (1.12–3.03)	0.016
Core, per 10g ↓	2.14 (0.88–5.20)	0.094	3.43 (1.19–9.91)	0.023
Border zone, per 10g ↓	1.98 (0.95–4.13)	0.069	2.96 (1.22–7.17)	0.016

AF indicates atrial fibrillation; eGFR, estimated glomerular filtration rate; LGE, late gadolinium enhancement; LV, left ventricular; LVEDV, LV end-diastolic volume; LVEF, LV ejection fraction; LVESV, LV end-systolic volume; RV right ventricular; RVEF, RV ejection fraction.

Supplemental Table 4. Specific LGE characteristics predicting monomorphic VT – multivariable models.

Multivariable analyses	Monomorphic VT	
	Hazard ratio (95% CI)	p
Model 1: LGE in basal and nonbasal segments		
Basal segments, per 10g	3.95 (1.88–8.32)	< 0.001
Nonbasal segments, per 10g	0.93 (0.35–2.46)	0.88
Model 2: Signal intensity categories		
>60% of maximal SI, per g	1.36 (1.16–1.61)	< 0.001
30–60% of maximal SI, per g	0.97 (0.91–1.04)	0.40
Model 3: Transmurality categories (A)		
51–75% transmural LGE, per cm^2	1.25 (1.12–1.40)	< 0.001
1–25% transmural LGE, per cm^2	0.98 (0.93–1.03)	0.45
Model 4: Transmurality categories (B)		
51–75% transmural LGE, per cm^2	1.31 (1.11–1.55)	0.001
26–50% transmural LGE, per cm^2	0.94 (0.84–1.06)	0.31
Model 5: Transmurality categories (C)		
51–75% transmural LGE, per cm^2	1.22 (1.09–1.37)	0.001
76–100% transmural LGE, per cm^2	1.00 (0.93–1.07)	0.95

LGE indicates late gadolinium enhancement; SI, signal intensity.

Chapter 11

Critical QRS Prolongation after Premature Stimulation is Associated with Polymorphic Ventricular Tachycardia in Nonischemic Cardiomyopathy: Results from the Leiden Nonischemic Cardiomyopathy Study

Sebastiaan R.D. Piers[1], Saïd F.A. Askar[1], Jeroen Venlet[1], Gijsbert F.L. Kapel[1], Marta de Riva Silva[1], Jan J.D.H. Jongbloed[2], J. Peter van Tintelen[2,3], Martin J. Schalij[1], Daniël A. Pijnappels[1], Katja Zeppenfeld[1]

[1] Department of Cardiology, Leiden University Medical Center, the Netherlands

[2] Department of Genetics, University of Groningen, University Medical Center Groningen, the Netherlands

[3] Department of Clinical Genetics, Academic Medical Center, University of Amsterdam, the Netherlands

Accepted for publication in Heart Rhythm

ABSTRACT

Background

Progressive activation delay after premature stimulation has been associated with ventricular fibrillation in nonischemic cardiomyopathy (NICM). The purpose of this study was to (1) investigate prolongation of the paced QRS duration (QRSd) after premature stimulation as a marker of activation delay in NICM, (2) assess its relation to induced ventricular arrhythmias, and (3) analyze its underlying substrate by late gadolinium enhancement CMR (LGE-CMR) and endomyocardial biopsy.

Methods and results

Forty patients with NICM (age 57±14years, 83% male, LVEF 30±13%) were prospectively enrolled in the Leiden Nonischemic Cardiomyopathy Study and underwent a comprehensive evaluation including LGE-CMR, electrophysiological study (EPS) and endomyocardial biopsy. Twenty patients without structural heart disease served as controls for EPS. After the 400 ms drive train and progressively premature stimulation, the maximum increase in QRSd was larger in NICM than in controls (35±18ms vs. 23±12ms, p=0.005) and the coupling interval window with QRSd prolongation was wider (47±23ms vs. 31±14ms, p=0.005). The maximum paced QRSd exceeded the ventricular refractory period allowing for pacing before the QRS offset in 20/39 NICM patients vs. 1/20 controls (p<0.001). In NICM, QRSd prolongation was associated with polymorphic VT inducibility (16/39 patients), and was related to long thick strands of fibrosis in biopsies, but not to focal enhancement on LGE-CMR (all p>0.05).

Conclusions

QRSd is a simple parameter to quantify activation delay after premature stimulation and its prolongation is associated with the inducibility of polymorphic VT and with the pattern of myocardial fibrosis in biopsies.

Clinical Trial Registration—clinicaltrials.gov. Identifier: NCT01940081.

INTRODUCTION

Implantable cardioverter defibrillator (ICD) therapy can terminate, but does not prevent potentially life-threatening ventricular arrhythmias. Although progress has been made to treat monomorphic ventricular tachycardia (VT), therapies that prevent polymorphic VT and ventricular fibrillation (VF) in nonischemic cardiomyopathy (NICM) are lacking. Improved understanding and identification of the underlying substrate for these arrhythmias may allow personalized risk stratification and development of tailored treatment.

Activation delay following premature stimulation has been associated with a history of VF in patients with various non-coronary heart diseases based on intracardiac recordings from the right ventricle (RV).[1] Total biventricular activation delay may be quantified by measuring paced QRS duration (QRSd) on surface ECGs, which is easy to apply and may better reflect activation delay in left dominant myocardial disease.

The purpose of this study was to (1) investigate prolongation of the paced QRSd following decremental premature stimulation as a marker of activation delay in NICM, (2) assess its relation to induced ventricular arrhythmias, and (3) analyze its association with the extent and distribution of fibrosis in endomyocardial biopsy specimens and on late gadolinium enhancement CMR (LGE-CMR).

METHODS

Patients

The Leiden Cardiomyopathy Study is a single-center, prospective cohort study designed to analyze the substrate and mechanisms of ventricular arrhythmias in NICM (ClinicalTrials.gov Identifier: NCT01940081). From October 2011, patients 18-80 years old with NICM and documented sustained ventricular arrhythmia, suspected sustained ventricular arrhythmia (e.g. because of out-of-hospital cardiac arrest, palpitations or syncope) or considered to be at intermediate or high risk for ventricular arrhythmias were enrolled. A high risk for ventricular arrhythmias was defined as a left ventricular ejection fraction (LVEF) ≤ 35%; an intermediate risk as LVEF ≤ 50% and late enhancement on LGE-CMR. Exclusion criteria were inability to understand the nature and risks of the study procedures, pregnancy, inability to comply with the protocol due to hemodynamic instability, and other cardiomyopathies (e.g. prior myocardial infarction, sarcoidosis, infiltrative cardiac disease such as amyloidosis, Chagasic cardiomyopathy, arrhythmogenic right ventricular cardiomyopathy, hypertrophic cardiomyopathy, non-compaction cardiomyopathy and congenital heart disease).

Patients underwent a comprehensive evaluation including transthoracic echocardiography, LGE-CMR, 24-hour Holter monitoring, exercise testing, blood sampling for NT-proBNP levels, an invasive electrophysiological study, endomyocardial biopsy, iodine-123 metaiodobenzylguanidine (MIBG) scan and genetic analysis of 55 cardiomyopathy-related genes. Targeted next generation sequencing of these 55 genes, a list of which is provided in the Supplemental Methods, was performed analyzing 151 bp paired-end reads on an Illumina MiSeq sequencer, as previously described.[2] The (likely) pathogenicity of single nucleotide polymorphisms and small indels was based on the nature and location of the variant, conservation of the affected amino acid residue(s) and the surrounding region, frequency of the variant in (healthy) population databases, its predicted pathogenicity according to multiple available prediction programs, the scientific literature and/or variant databases.

Premature ventricular contraction (PVC) or VT ablation and ICD implantation were performed if clinically indicated. The study protocol was approved by the local ethics committee and by the appropriate national ethics committee. All patients provided written informed consent.

The control group for electrophysiologic study measurements consisted of 20 patients referred for catheter ablation of atrioventricular nodal reentrant tachycardia or a concealed bypass tract in the absence of structural heart disease, who underwent routine electrophysiological study according to our institutional protocol.

LGE-CMR acquisition

In patients who had not undergone LGE-CMR previously, CMR was performed on a 1.5T Gyroscan ACS-NT/Intera MR system, or on a 3.0T Ingenia MR system (both Philips Medical Systems, Best, the Netherlands). A standardized protocol was followed, including cine images in long-axis (two- and four-chamber) and short-axis views covering the complete LV. Approximately 15 minutes after bolus injection of gadolinium (Magnevist; Schering, Berlin, Germany; 0.15 mmol/kg) a look-locker sequence was acquired in short axis orientation at mid-ventricular level. T1-weighted LGE images were acquired with an inversion-recovery 3D turbo-field echo sequence with parallel imaging. The inversion time was optimized to null normal appearing myocardium. The heart was imaged in long-axis two- and four-chamber views (between 5-10 slices), and short-axis views (between 20-24 slices). Signal outside the field of view was suppressed using two saturation slabs to avoid fold-over artifacts.

In patients who had already undergone CMR previously, the scan was acquired on various systems, but always included cine acquisitions in long-axis (two- and four-chamber) and short-axis views, covering the complete left ventricle (LV). LGE images were acquired in long-axis (two- and four-chamber) and short-axis views. CMR was not performed in patients with an implanted device.

LGE-CMR analysis

All CMR analyses were performed using MASS software (research version 2012; LKEB; Leiden University Medical Center, the Netherlands). The LV and RV end-diastolic and end-systolic endocardial contours were traced on short-axis cine images to calculate the LV end-diastolic and end-systolic volumes, LVEF, LV mass, RV end-diastolic and end-systolic volumes, and RV ejection fraction. The LV and RV volumes and the LV mass were indexed to body surface area.[3] Myocardial scar was only considered to be present if LGE was visible in 2 orthogonal views. LGE was defined by signal intensity ≥35% of maximal myocardial signal intensity, and subdivided into core (≥50% of maximal signal intensity) and border zone (35-50% of maximal signal intensity).[4]

Electrophysiological study

Anti-arrhythmic drugs were discontinued for at least 5 half-lives, if possible. Programmed electrical stimulation consisted of 3 drive trains of 8 beats (S1) (cycle lengths (CL) 600, 500 and 400ms) with 1-3 ventricular extrastimuli and burst pacing at twice diastolic threshold from the RV apex and the RV outflow tract using the distal electrode pair of a quadripolar catheter. The first extrastimulus (S2) was applied at a coupling interval identical to the CL of the drive train, followed by a coupling interval (CI) of 350ms, which was then progressively decreased by steps of 10ms until the ventricular effective refractory period (VERP) was reached. Consecutive extrastimuli (S3 and S4) and burst pacing were applied from a coupling interval of 350ms down to 200ms. Polymorphic VT was defined by ≥5 consecutive ventricular beats at ≥ 120 bpm with continuously changing QRS morphology,[5,6] and was regarded as sustained if lasting > 30s or requiring termination because of hemodynamic compromise. Sustained monomorphic VT was defined by similar beat-to-beat QRS morphology and duration >30s or the requirement for termination because of hemodynamic compromise. If no sustained ventricular arrhythmia was induced, stimulation was repeated with isoprenaline (2-10µg/min).

In the control group for electrophysiology study measurements, drive trains of 600 and 400 ms with single extrastimuli were applied from the RV apex as part of the routine electrophysiological study protocol. All studies were recorded on an electrophysiology recording system for offline analysis, with a sweeping speed of 200 mm/second and bipolar electrograms filtered at 30-500 Hz (Prucka Cardiolab recording system, Houston, Texas).

Electrophysiological study analysis

The paced QRSd was measured from the pacing artifact to the latest offset of the QRS in any lead (examples in Figure 1) using electronic calipers. For the 600ms and 400ms drive trains with single extrastimuli from the RV apex, QRSd restitution curves were constructed and the following parameters were derived:

(1) CI at onset of QRSd prolongation (CI_{onset}): the CI of the first premature extrastimulus that results in a ≥5 ms increase in QRSd compared to the previous step.
(2) CI window with QRSd prolongation: the interval between CI_{onset} and the VERP.
(3) Maximal ΔQRSd: maximum increase in QRSd after premature stimulation.
(4) Critical QRSd prolongation: the QRSd that exceeds the length of the VERP, which allows to pace before the offset of the QRS (calculated as QRSd-VERP).
(5) Critical CI ($CI_{critical}$) window: the CI window at which the paced QRSd exceeds the length of the VERP.

Examples of QRS restitution curves and calculations of the derived parameters are displayed in Figure 1.

Endomyocardial biopsy

After the electrophysiological study, endomyocardial biopsies were obtained – immediately thereafter, two were stored in liquid nitrogen and one specimen was fixed in 4% formaldehyde and embedded in paraffin. Cross-sections were cut at 4 μm and stained with picro-Sirius Red to evaluate collagen content and collagen distribution patterns. Mayer's haematoxylin was used to counterstain cell nuclei. Using a fluorescent microscope, high-resolution photomicrographs were taken with a digital camera (Nikon Eclipse, Nikon Europe, Badhoevedorp, the Netherlands) and analyzed using dedicated software (ImageJ 1.49c, National Institutes of Health, USA). All staining and subsequent analyses were performed by an independent investigator blinded to all clinical and procedural data. Fibrosis content was quantified by calculating the collagen area percentage. Distribution of fibrosis was categorized according to predefined patterns:

1) Interstitial: collagen strand thickness exceeds 10% of the width of adjacent cardiomyocytes without interrupting myocardial fiber continuity.
2) Short thin strands: dispersed presence of two or more fibrotic areas smaller than the width of five cardiomyocytes that disrupt myocardial fiber continuity.
3) Long thick strands: one or more fibrotic areas exceeding the width of five cardiomyocytes that disrupt the myocardial fiber continuity.

Underlying substrate of QRS prolongation

The relation between QRSd restitution curve parameters and the following parameters was analyzed: 1) CMR-derived LV and RV volumes and ejection fraction, 2) LGE on CMR, 3) NT-proBNP levels, 4) collagen area percentages in biopsy specimens, 5) pattern of fibrosis in biopsy specimens and 6) the presence of a pathogenic or likely pathogenic mutation.

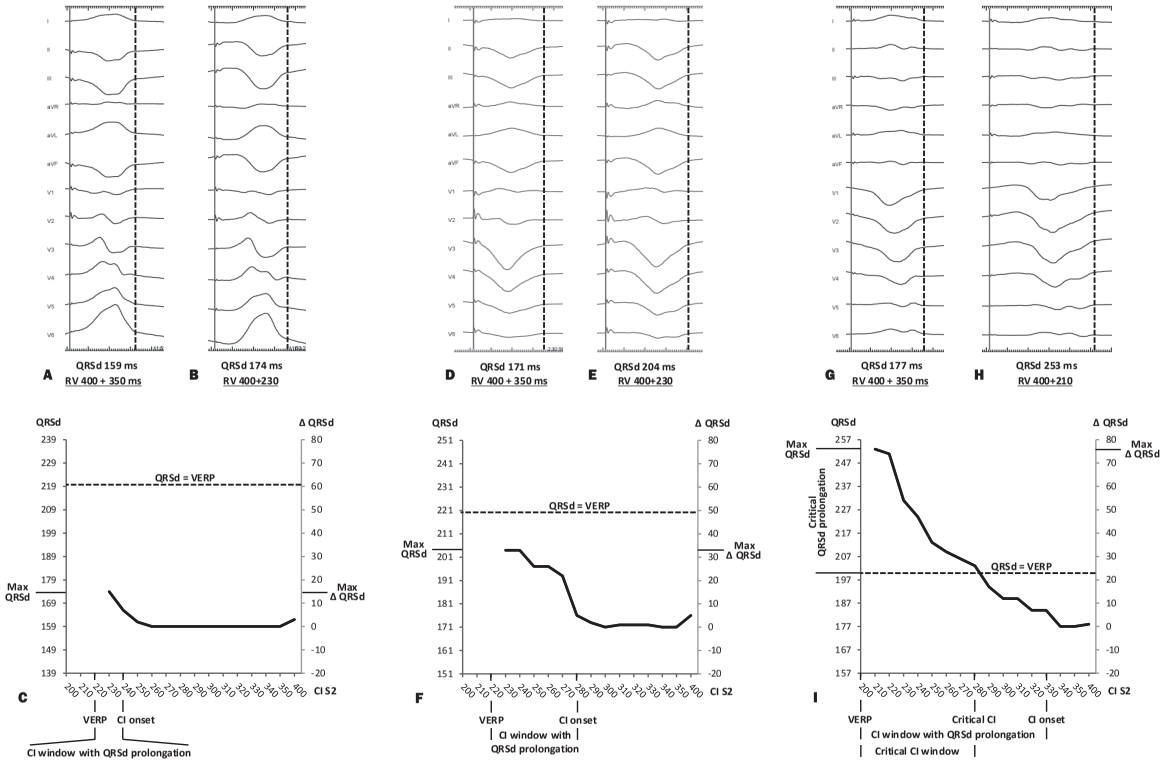


Figure 1. Examples of QRS duration restitution curves and derived parameters

QRS duration measurements and restitution curves in a control without structural heart disease after premature stimulation (panels A-C), on a patient with cardiomyopathy and more pronounced QRSd prolongation, but without *critical* QRSd prolongation (panels D-F), and in a patient with cardiomyopathy and marked *critical* QRSd prolongation after premature stimulation (panels G-I). In this patient the maximal QRSd exceeds the VERP (indicated by horizontal dashed line) and therefore S2 can be applied within the QRS complex of S1. CI indicates coupling interval; VERP, ventricular effective refractory period.

Statistical analysis

Categorical variables are displayed as number (percentage) and continuous variables are expressed as mean ± standard deviation or median (interquartile range, IQR). Categorical variables were compared using the χ^2 test or the Fisher's exact test. Continuous variables were compared using the Mann-Whitney *U* test because of the limited sample size. For paired variables the Wilcoxon signed-rank-test was used. The association between QRS restitution curve parameters and patient characteristics was analyzed by univariate linear regression analyses. For this purpose, NT-proBNP levels were log-transformed because of the skewed distribution. All analyses were performed with SPSS version 20.0 (IBM, Somers, New York, USA). All tests are two-sided and probability values <0.05 were considered significant.

RESULTS

Patients

Between October 2011 and August 2013, 40 patients (age 57 ± 14 years, 83% male) were enrolled in the Leiden Nonischemic Cardiomyopathy Study. Baseline characteristics are summarized in Table 1. Eight patients (20%) had documented sustained ventricular arrhythmia, 6 (15%) had suspected sustained ventricular arrhythmia, and 26 (65%) were considered to be at intermediate or high risk for ventricular arrhythmia. Cine CMR was performed in 36 patients (90%), while the remaining 4 (10%) had an implanted device and underwent echocardiography. Based on combined CMR and echo data the LVEF was reduced in all patients and the LV end-diastolic volume index was increased in 34 patients (85%) compared with published reference ranges normalized for gender, age and body surface area.[7] LGE was observed in 26 of 34 (77%) patients with LGE images and the median LGE mass was 8.8 g (IQR, 1.1–19.3 g). CMR and biopsy data are summarized in Table 2. Genetic analysis of 55 cardiomyopathy-related genes was performed in all but one patient and revealed a pathogenic or likely pathogenic mutation in 19 (49%) – details are listed in supplemental Table 1.

QRSd prolongation in NICM patients and controls

Both in NICM and in controls, the QRSd increased after premature stimulation (examples in Figure 1). Differences between NICM patients and controls were more pronounced after the 400 ms drive train than after the 600 ms drive train (supplemental Figure 1 and supplemental Table 2) and therefore, the 400 ms drive train was used for further analyses. After the 400 ms drive train, the onset of QRSd prolongation occurred at longer CI (CI_{onset}) in NICM compared to controls (275±23 vs. 235±16 ms, p<0.001, Figure 2), the CI window with QRSd prolongation was wider (47±23 vs. 31±14 ms, p=0.005), and the

Table 1. Baseline characteristics

	n=40
Age, years	57 ± 14
Male	33 (83%)
BMI, kg/m^2	27 ± 4
Diabetes mellitus	6 (15%)
Hypertension	10 (25%)
NYHA functional class	
I	7 (18%)
II	20 (50%)
III or IV	13 (33%)
History of AF / atrial flutter	16 (40%)
ECG	
Heart rate, bpm	73 ± 13
PR interval, ms	182 ± 32
QRS duration, ms	129 ± 34
eGFR, mL/min/1.73m^2	86 ± 25
NT-proBNP, pg/mL	932 (499 - 1773)
Exercise test (n=29)	
Peak oxygen consumption, mL/kg/min	20 ± 6
Peak oxygen consumption, % of predicted	80 ± 22
AAD during electrophysiology study	
Class I	0 (0%)
Sotalol	1 (3%)
Amiodarone	2 (5%)
Device at discharge	
CRT-defibrillator	20 (50%)
Implantable cardioverter-defibrillator	13 (33%)
None	7 (18%)
Genetic screening (n=39)	
Pathogenic or likely pathogenic mutation	19/39 (49%)

Variables are expressed as number (percentage), mean ± standard deviation, or median (interquartile range). AAD indicates anti-arrhythmic drugs; AF, atrial fibrillation; BMI, body mass index; CRT, cardiac resynchronization therapy; eGFR, estimated glomerular filtration rate; NYHA, New York Heart Association

maximum Δ QRSd was larger (35±18 vs. 23±12 ms, p=0.005). Critical QRS prolongation (i.e., QRSd exceeding VERP, which allowed to apply an extrastimulus within the paced QRS complex) was observed in 20 of 39 patients with NICM (51%) compared with only one of 20 controls (5%, p<0.001) (Figure 1 panels G-I, Figure 2, example Figure 3). The critical CI window, with QRSd exceeding VERP, ranged from 10 to 130 ms in NICM, compared with only one case with a critical CI window of 10 ms in controls (p<0.001, Figure

Table 2. CMR and biopsy data

Parameter	Value
CMR - cine images (n=36)	
LVEDV, mL	303 ± 90
LVEDV index, mL/m^2	147 ± 42
LVESV, mL	221 ± 93
LVESV index, mL/m^2	107 ± 44
LVEF, %	30 ± 13
LV mass, g	143 ± 34
LV mass index, g/m^2	70 ± 16
RVEDV, mL	189 ± 45
RVEDV index, mL/m^2	92 ± 19
RVESV, mL	105 ± 39
RVESV index, mL/m^2	51 ± 18
RVEF, %	46 ± 11
CMR - LGE images (n=34)	
LGE presence	26/34 (77%)
LGE total, g	8.8 (1.1 - 19.3)
Core mass, g	3.3 (0.4 - 8.7)
Border zone mass, g	4.9 (0.6 - 13.4)
Endomyocardial biopsy (n=23)	
Collagen area percentage, %	33 (19 - 42)
Collagen distribution type	
Interstitial	8/23 (35%)
Short thin strands	7/23 (30%)
Long thick strands	8/23 (35%)

Variables are expressed as number (percentage), mean ± standard deviation, or median (interquartile range). LGE denotes late gadolinium enhancement; LVEDV, LV end-diastolic volume; LVEF, LV ejection fraction; LVESV, LV end-systolic volume; RVEDV, RV end-diastolic volume; RVEF, RV ejection fraction; RVESV, RV end-systolic volume.

2). Results were similar when excluding the 3 cardiomyopathy patients who were on class III anti-arrhythmic drugs.

QRSd prolongation and inducibility of polymorphic VT

The programmed electrical stimulation protocol could be successfully completed, or resulted in reproducible induction of sustained ventricular arrhythmias in 39 of 40 NICM patients (98%). Sustained monomorphic VT was induced in 11 of 39 patients (28%) and polymorphic VT ≥ 5 beats in 16 of 39 (41%) (Figure 3). The longest polymorphic VT was induced with triple extrastimuli in all 16 patients. None of the baseline characteristics were associated with polymorphic VT inducibility (Table 3).

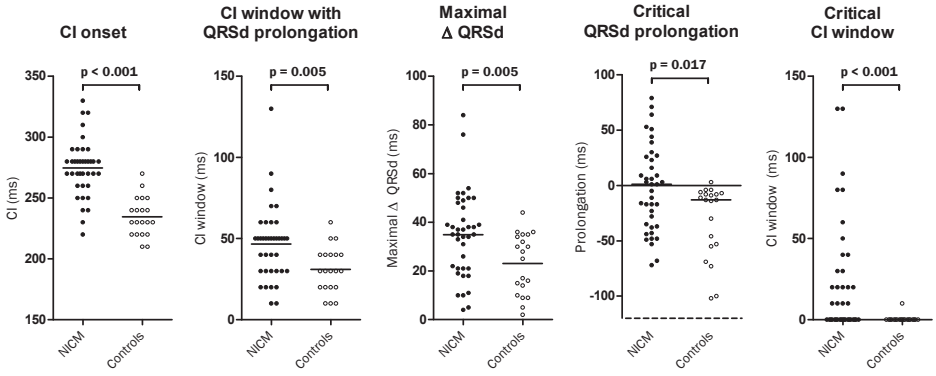


Figure 2. QRS duration prolongation in nonischemic cardiomyopathy and controls
The QRS duration restitution curve parameters based on 400 ms drive trains with single extrastimuli differed significantly between patients with cardiomyopathy and controls.

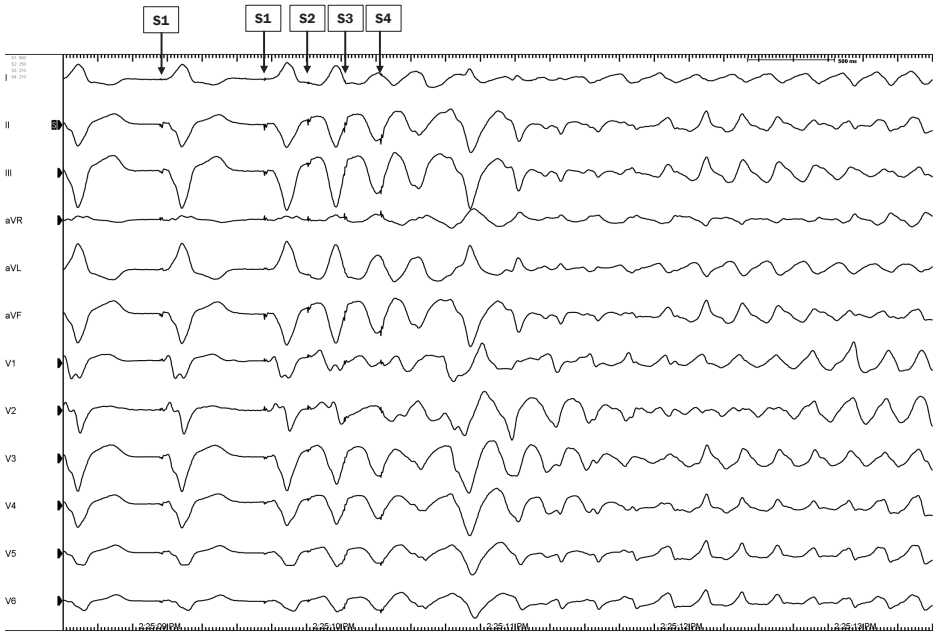


Figure 3. Example of pacing within the QRS complex and induction of polymorphic VT
During application of triple extrastimuli after a 400 ms drive train, the QRS complex prolongs after premature stimulation. S3 and S4 are applied within the paced preceding QRS complexes, resulting in the induction of polymorphic VT.

In contrast, four of five QRSd restitution curve parameters were associated with the inducibility of polymorphic VT (Figure 4 and supplemental Table 3). The CI at onset of QRS prolongation was similar in patients with vs. without inducible polymorphic VT (276 ± 20 ms vs 274 ± 26 ms, p=0.92), but the CI window with QRSd prolongation was wider

Table 3. Baseline characteristics and inducible polymorphic VT

	PVT (n=16)	No PVT (n=23)	P
Age, years	60 ± 13	56 ± 13	0.40
Male	13 (81%)	19 (83%)	1.00
BMI, kg/m^2	27 ± 4	28 ± 4	0.47
Diabetes mellitus	9 (56%)	7 (30%)	0.11
Hypertension	4 (25%)	6 (26%)	1.00
NYHA functional class III or IV	4 (25%)	9 (39%)	0.36
History of AF / atrial flutter	2 (13%)	4 (17%)	1.00
eGFR, mL/min/1.73m^2	87 ± 24	86 ± 27	1.00
NT-proBNP, pg/mL	1058 (487 - 2232)	872 (498 - 1646)	0.64
ECG			
Heart rate	72 ± 15	73 ± 12	0.77
PR interval	188 ± 33	181 ± 31	0.49
QRS duration	126 ± 32	133 ± 36	0.69
Exercise test			
Peak oxygen consumption, mL/kg/min	19 ± 7	20 ± 5	0.65
Peak oxygen consumption, % of predicted	81 ± 28	80 ± 16	0.91
Genetic screening			
Pathogenic or likely pathogenic mutation	8/16 (50%)	10/22 (46%)	0.78
MRI - cine images			
LVEDV index, mL/m^2	136 ± 44	153 ± 41	0.27
LVEF, %	35 ± 15	27 ± 12	0.19
LV mass index, g/m^2	67 ± 7	71 ± 19	0.51
RVEDV index, mL/m^2	96 ± 22	89 ± 18	0.63
RVEF, %	41 ± 13	49 ± 10	0.057
MRI - LGE images			
LGE presence	11/13 (85%)	15/20 (75%)	0.68
LGE total, g	15.0 (4.3 - 22.7)	8.2 (0.4 - 22.6)	0.32
LGE core, g	5.5 (1.9 - 11.1)	2.9 (0.1 - 8.4)	0.41
LGE BZ, g	7.7 (2.4 - 14.0)	4.3 (0.2 - 14.0)	0.39
Endomyocardial biopsy specimens			
Collagen area percentage, %	22 (10 - 39)	38 (23 - 51)	0.093
Interstitial fibrosis	3/10 (30%)	4/12 (33%)	
Short thin strands	2/10 (20%)	5/12 (42%)	0.42
Long thick strands	5/10 (50%)	3/12 (25%)	

PVT denotes polymorphic ventricular tachycardia. Other abbreviations as in tables 1 and 2.

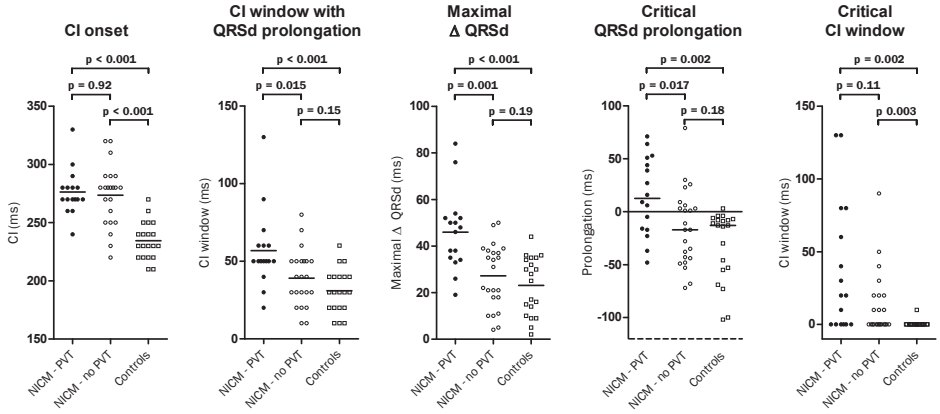


Figure 4. QRS duration prolongation and inducibility of polymorphic VT
Three QRS duration restitution curve parameters were associated with the inducibility of polymorphic VT in patients with cardiomyopathy.

(57 ± 25 ms vs. 39 ± 18 ms, p=0.015) and the maximum Δ QRSd was larger (46 ± 17 ms vs 27 ± 14 ms, p=0.001). The critical QRS prolongation was significantly longer, allowing to pace further within the QRS (15 ± 37 ms vs -15 ± 36 ms, p=0.017) and the critical CI window tended to be wider, thereby allowing to pace within the QRS over a wider range of CIs (median 20 ms, IQR 0-75 ms vs. median 0 ms, IQR 0-20 ms, p=0.11).

CMR-derived data, NT-proBNP levels and genetics: relation to QRSd prolongation

Larger end-diastolic LV volume indexes were associated with a wider CI window with QRSd prolongation, and larger end-systolic LV volume indexes and lower LVEF were associated with a smaller maximal Δ QRSd, but neither was associated with any of the other QRSd restitution curve parameters (Supplemental Table 4). The extent of LGE (total LGE, core and border zone), NT-proBNP levels and the presence of a (likely) pathogenic mutation were not associated with any QRSd restitution curve parameter (all p>0.05).

Extent and distribution of fibrosis in biopsy specimens and association with QRSd prolongation

Endomyocardial biopsy was performed in 24 patients (60%; LV in 23 patients, RV side of septum in 1 patient); no biopsies were obtained in the remaining 16 patients (40%) because of a potential risk for complications or patient's preference. One set of biopsies was excluded due to poor quality. In the remaining 23 patients, the median collagen area percentage was 33% (IQR, 19 – 42%) and the collagen distribution type was interstitial in 8 (35%), short thin strands in 7 (30%) and long thick strands in 8 (35%) (examples in Figure 5). The density of fibrosis quantified as area percentages was weakly

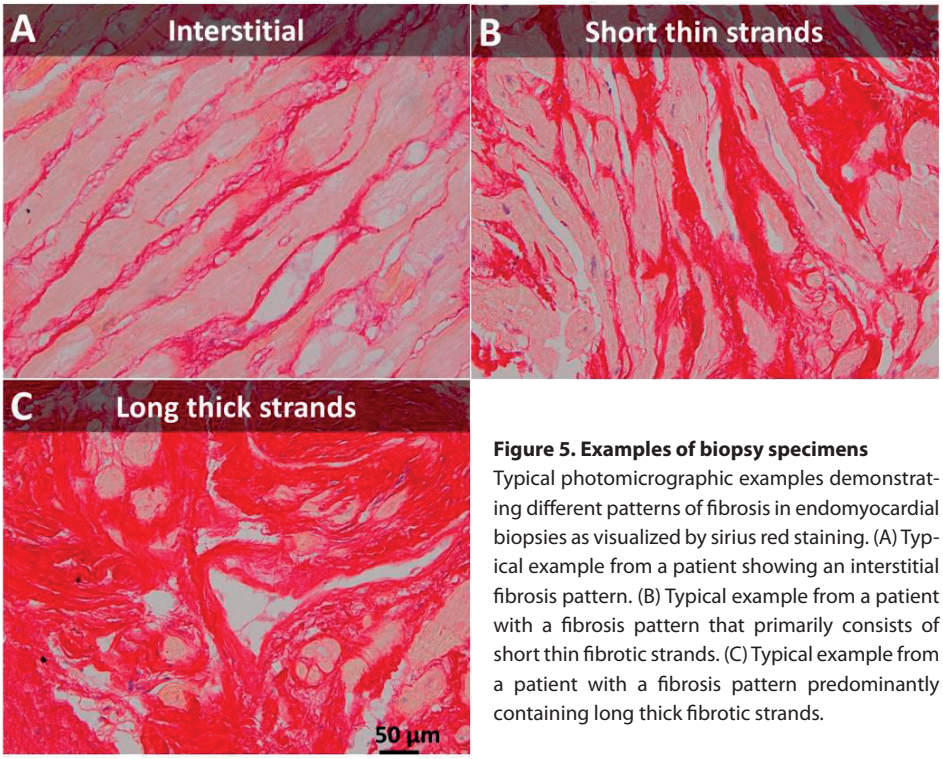


Figure 5. Examples of biopsy specimens
Typical photomicrographic examples demonstrating different patterns of fibrosis in endomyocardial biopsies as visualized by sirius red staining. (A) Typical example from a patient showing an interstitial fibrosis pattern. (B) Typical example from a patient with a fibrosis pattern that primarily consists of short thin fibrotic strands. (C) Typical example from a patient with a fibrosis pattern predominantly containing long thick fibrotic strands.

associated with a smaller maximal increase in QRSd but not with any other parameter of QRSd prolongation (Supplemental Table 4). However, long thick strands of fibrosis were associated with a wider CI window with QRSd prolongation, and with a wider critical CI window with the ability to pace within QRSd.

DISCUSSION

The key findings of this study are: (1) In patients with NICM and in controls, the paced QRSd increased after premature stimulation, (2) in NICM, the QRSd started to increase earlier, at longer CI than in controls, the maximum increase in QRSd was larger and the paced QRSd frequently exceeded the VERP (i.e., critical QRS prolongation), which allowed to apply an extrastimulus within the paced QRS complex, (3) the CI window with QRSd prolongation, the maximal ΔQRSd, and critical QRS prolongation were associated with the inducibility of polymorphic VT in NICM, (4) not the density of fibrosis but the presence of long thick strands of fibrosis was associated with a wider CI window of progressive QRS prolongation and a wider critical CI window at which the QRSd exceeds VERP, which may indicate a substrate for polymorphic VT or VF, and (5) none of the QRSd

restitution curve parameters was related to the presence or extent of LGE on CMR, NT-pro BNP levels, nor the presence of (likely) pathogenic mutations.

Quantification of activation delay after premature stimulation

Activation delay after premature stimulation has previously been quantified and related to VF in humans with various cardiac diseases, in particular hypertrophic cardiomyopathy, by applying stimulation protocols sequentially from 4 different RV catheters.[1] Left ventricular activation could not be assessed as no catheters were placed in the LV. Of interest, both normal and abnormal electrogram responses were frequently observed at the different positions of the 4 RV catheters, suggesting that conduction delay may not be uniform and therefore, multiple recording sites may be required. In contrast, the paced QRSd is easily available, can be measured during a standard programmed electrical stimulation protocol, does not require multiple intracardiac catheters and reflects both RV and LV activation.

Activation delay and polymorphic VT

In the current study we could demonstrate that the CI window with QRSd prolongation, the maximum Δ QRSd and critical QRS prolongation were associated with the inducibility of polymorphic VT. In contrast, none of the baseline characteristics, including CMR-derived volumes, ejection fraction and LGE, NT-proBNP levels and the presence of a (likely) pathogenic mutation, were associated with polymorphic VT inducibility.

A larger CI window with QRSd prolongation may increase the likelihood that a spontaneous PVC is discontinuously propagated, resulting in progressive activation delay, wave break and increased dispersion of repolarization. The maximal Δ QRSd may be considered as a marker of the cumulative activation delay throughout the heart after the shortest-coupled (VERP + 10 ms) premature stimulus. Prolonged and pronounced activation delay may reflect non-uniform anisotropic conduction which, together with dispersion of repolarization, may predispose for polymorphic VT and VF.[8]

These findings are consistent with a prior study using extensive stimulation protocols and multiple RV catheters in patients with various non-coronary heart diseases (but only 5 patients with dilated cardiomyopathy), which demonstrated that the maximum increase in RV intracardiac electrogram duration was larger, but also that the S1S2 coupling intervals at which the electrograms started to increase were longer in patients with a history of VF.[1] In a retrospective study in consecutive patients with and without structural heart disease who underwent EPS for various reasons, activation delay, measured from the distal stimulation electrodes to proximal electrodes located at 35 mm distance, was substantially longer in patients with vs. without inducible VF.[9] Finally, in a retrospective study conducted in borderline NICM patients with LVEF >50% and LV end-diastolic dimension < 65 mm, 15 patients resuscitated from polymorphic VT/VF had

longer paced QRSd after S3 (at CI 10 ms above VERP) compared to patients without documented ventricular arrhythmias.[10]

Substrate and mechanisms of activation delay and polymorphic VT

The QRSd restitution curve parameters that were associated with the inducibility of polymorphic VT did not correlate with CMR-derived volumes, ejection fraction or LGE, and were not related to larger fibrosis area percentages on biopsy, but tended to be related to long thick strands of fibrosis in biopsy. This is in line with two studies in explanted hearts from patients with end-stage heart failure, which suggested that activation delay after premature stimulation may be related to the presence of long fibrotic strands.[11,12] In one of these studies, even large amounts of diffusely distributed, short-stranded fibrosis only marginally affected conduction velocity, whereas large fibrotic strands appeared to serve as inexcitable barriers with consecutive conduction delay, supporting that the geometry rather than the total amount of fibrosis creates a potential substrate for arrhythmias.[12] The authors elegantly demonstrated how such barriers may contribute to activation delay, namely by increased path length, transverse instead of longitudinal conduction, wave front curvature and reduced conduction velocity.[12] In addition, activation delay caused by long strands of fibrosis may promote wave break and thereby predispose for polymorphic VT/VF.[13] Of interest, treatment with eplerenone, losartan, or both could reduce the development of age-related interstitial and patchy fibrosis in adult mice.[14] Importantly, only the reduction of patchy fibrosis correlated with reduced inducibility of ventricular arrhythmias based on anisotropic reentry, further supporting the link between type of fibrosis and arrhythmogeneity.

Other potential mechanisms of activation delay after premature stimulation have been described in patients with various structural heart disease.[15] In particular early applied extrastimuli that capture at an earlier and less repolarized level of the preceding beat correlated with delayed propagation. Mechanisms are not necessarily mutually exclusive and the observed critical QRS prolongation may be dependent on the combination of different underlying structural and functional changes resulting in an increased vulnerability for polymorphic VT.

Clinical implications

Activation delay after premature stimulation, which was associated with ventricular arrhythmias in the present and in prior studies, can be easily quantified by any clinical electrophysiologist by measuring the QRSd after 400 ms drive trains with single extrastimuli. The protocol and calculation of the suggested parameters can be performed in a couple of minutes and can be obtained non-invasively in patients with pacemakers or implantable cardioverter-defibrillators. Whether QRSd restitution curve parameters

predict spontaneous ventricular arrhythmias requires further studies with larger sample sizes and long follow-up duration.

Limitations

The number of subjects is small. As this study focused on identifying electrophysiological parameters associated with a predisposition towards polymorphic VT, several factors such as dispersion of repolarization after premature stimulation not caused by activation delay,[8] connexin 43 expression, distribution and co-localization with N-cadherin[11] were not analyzed. Also, the current study did not analyze the association between activation delay and spontaneous polymorphic VT/VF as such analyses require larger patient cohorts and long follow-up.

CONCLUSION

Premature stimulation in patients with NICM causes progressive activation delay, which can be easily quantified by measuring the QRSd after a 400 ms drive train with single extrastimuli. The CI window with QRSd prolongation was wider in patients with NICM than in controls, the maximum increase in QRSd was larger, and a pronounced critical QRS prolongation was demonstrated allowing for extrastimuli being applied within the QRS complex. These 3 phenomena, which are easily assessed during a 3-minute stimulation protocol, were associated with the inducibility of polymorphic VT. QRSd prolongation after premature stimulation tended to be related to long thick strands of fibrosis, but not to overall fibrosis area percentages in biopsy specimens, supporting the link between the geometry of fibrosis and arrhythmogeneity. Measuring the QRSd may be a simple tool to quantify progressive activation delay after premature stimulation as a risk factor for polymorphic VT/VF.

REFERENCE LIST

1. Saumarez RC, Chojnowska L, Derksen R, Pytkowski M, Sterlinski M, Huang CL, Sadoul N, Hauer RN, Ruzyllo W, Grace AA. Sudden death in noncoronary heart disease is associated with delayed paced ventricular activation. Circulation. 2003;107:2595-600.
2. Sikkema-Raddatz B, Johansson LF, de Boer EN, Almomani R, Boven LG, van den Berg MP, van Spaendonck-Zwarts KY, van Tintelen JP, Sijmons RH, Jongbloed JD, Sinke RJ. Targeted next-generation sequencing can replace Sanger sequencing in clinical diagnostics. Hum Mutat. 2013;34:1035-42.
3. Mosteller RD. Simplified calculation of body-surface area. N Engl J Med. 1987;317: 1098.
4. Roes SD, Borleffs CJ, van der Geest RJ, Westenberg JJ, Marsan NA, Kaandorp TA, Reiber JH, Zeppenfeld K, Lamb HJ, de RA, Schalij MJ, Bax JJ. Infarct tissue heterogeneity assessed with contrast-enhanced MRI predicts spontaneous ventricular arrhythmia in patients with ischemic cardiomyopathy and implantable cardioverter-defibrillator. Circ Cardiovasc Imaging. 2009;2:183-90.
5. Grimm W, Christ M, Maisch B. Long runs of non-sustained ventricular tachycardia on 24-hour ambulatory electrocardiogram predict major arrhythmic events in patients with idiopathic dilated cardiomyopathy. Pacing Clin Electrophysiol. 2005;28 Suppl 1: S207-S210.
6. Wellens HJ, Brugada P, Stevenson WG. Programmed electrical stimulation of the heart in patients with life-threatening ventricular arrhythmias: what is the significance of induced arrhythmias and what is the correct stimulation protocol? Circulation. 1985;72: 1-7.
7. Maceira AM, Prasad SK, Khan M, Pennell DJ. Normalized left ventricular systolic and diastolic function by steady state free precession cardiovascular magnetic resonance. J Cardiovasc Magn Reson. 2006; 8:417-26.
8. Yuan S, Blomstrom-Lundqvist C, Pehrson S, Pripp CM, Wohlfart B, Olsson SB. Dispersion of repolarization following double and triple programmed stimulation. A clinical study using the monophasic action potential recording technique. Eur Heart J. 1996;17:1080-91.
9. Avitall B, McKinnie J, Jazayeri M, Akhtar M, Anderson AJ, Tchou P. Induction of ventricular fibrillation versus monomorphic ventricular tachycardia during programmed stimulation. Role of premature beat conduction delay. Circulation. 1992;85: 1271-8.
10. Schueller PO, Hennersdorf MG, Strauer BE. Sudden death is associated with a widened paced QRS complex in noncoronary cardiac disease. J Interv Card Electrophysiol. 2006; 15:125-30.
11. Glukhov AV, Fedorov VV, Kalish PW, Ravikumar VK, Lou Q, Janks D, Schuessler RB, Moazami N, Efimov IR. Conduction remodeling in human end-stage nonischemic left ventricular cardiomyopathy. Circulation. 2012;125:1835-47.
12. Kawara T, Derksen R, de Groot JR, Coronel R, Tasseron S, Linnenbank AC, Hauer RN, Kirkels H, Janse MJ, de Bakker JM. Activation delay after premature stimulation in chronically diseased human myocardium relates to the architecture of interstitial fibrosis. Circulation. 2001;104:3069-75.
13. Derksen R, van Rijen HV, Wilders R, Tasseron S, Hauer RN, Rutten WL, de Bakker JM. Tissue discontinuities affect conduction velocity restitution: a mechanism by which structural barriers may promote wave break. Circulation. 2003;108:882-8.

14. Stein M, Boulaksil M, Jansen JA, Herold E, Noorman M, Joles JA, van Veen TA, Houtman MJ, Engelen MA, Hauer RN, de Bakker JM, van Rijen HV. Reduction of fibrosis-related arrhythmias by chronic renin-angiotensin-aldosterone system inhibitors in an aged mouse model. Am J Physiol Heart Circ Physiol. 2010;299: H310-H321.

15. Koller BS, Karasik PE, Solomon AJ, Franz MR. Relation between repolarization and refractoriness during programmed electrical stimulation in the human right ventricle. Implications for ventricular tachycardia induction. Circulation. 1995;91:2378-84.

Supplemental Table 1. Genetic screening results

Gene with likely pathogenic or pathogenic mutation	Frequency
LMNA	5 (12.8%)
TTN	4 (10.3%)
SCN5A	2 (5.1%)
MYH6	2 (5.1%)
LDB3	1 (2.6%)
PKP2	1 (2.6%)
PLN	1 (2.6%)
CALR3	1 (2.6%)
DES	1 (2.6%)
Multiple*	1 (2.6%)
None	20 (51.3%)

* 3 mutations: DSP, MYPN and MYH7

Supplemental Table 2. Comparison of 600 ms and 400 ms drive trains between NICM and controls

	NICM	Controls	p (Mann-Whitney)
Regular 12-lead ECG, 25 mm/second			
QRSd	129 ± 34	90 ± 12	< 0.001
EPS - drive train 600 ms from RV apex			
QRSd during drive train	195 ± 18	157 ± 12	< 0.001
QRSd after extrastimulus 350 ms	191 ± 25	147 ± 14	< 0.001
QRSd plateau	191 ± 25	148 ± 13	< 0.001
CI at onset of QRSd prolongation	311 ± 17	262 ± 15	< 0.001
Local VERP	259 ± 25	228 ± 26	< 0.001
CI window with QRSd prolongation	54 ± 23	34 ± 20	0.003
Maximal QRSd	229 ± 28	176 ± 15	< 0.001
Maximal Δ QRSd	38 ± 20	29 ± 12	0.21
Critical QRSd prolongation	-28 (-56 – -8)	-51 (-77 – -28)	0.053
Critical CI window	0 (0 – 0)	0 (0 – 0)	0.41
EPS - drive train 400 ms from RV apex			
QRSd during drive train	192 ± 23	153 ± 13	< 0.001
QRSd after extrastimulus 350 ms	192 ± 26	150 ± 15	< 0.001
QRSd plateau	191 ± 27	149 ± 15	< 0.001
CI at onset of QRSd prolongation	275 ± 23	235 ± 16	< 0.001
Local VERP	228 ± 23	204 ± 21	< 0.001
CI window with QRSd prolongation	47 ± 23	31 ± 14	0.005
Maximal QRSd	226 ± 31	172 ± 18	< 0.001
Maximal Δ QRSd	35 ± 18	23 ± 12	0.005
Critical QRSd prolongation	+1 (-37 – +26)	-13 (-55 – -7)	0.017
Critical CI window	10 (0 – 30)	0 (0 – 0)	< 0.001

Variables are expressed as mean ± standard deviation or median (interquartile range).
CI indicates coupling interval; EPS, electrophysiology study; QRSd, QRS duration; RV, right ventricle; VERP, ventricular effective refractory period

Supplemental Table 3. QRSd prolongation and inducibility of polymorphic VT

	Polymorphic VT	No Polymorphic VT	p (Mann-Whitney)
Regular 12-lead ECG, 25 mm/second			
QRSd	126 ± 32	133 ± 36	0.69
RVA - Drive train 600 ms with 1 extrastimulus			
QRSd during drive train	193 ± 15	197 ± 20	0.63
QRSd after extrastimulus 350 ms	188 ± 15	194 ± 32	0.85
QRSd plateau	188 ± 15	194 ± 32	0.85
CI at onset of QRSd prolongation	308 ± 18	314 ± 17	0.34
Local VERP	252 ± 23	266 ± 25	0.11
CI window with QRSd prolongation	60 ± 23	48 ± 23	0.14
Maximal QRSd	234 ± 24	225 ± 31	0.23
Maximal Δ QRSd	45 ± 21	31 ± 17	0.058
Critical QRSd prolongation	-18 (-44 – +10)	-38 (-73 – -11)	0.13
Critical CI window	0 (0 – 20)	0 (0 – 0)	0.18
RVA - Drive train 400 ms with 1 extrastimulus			
QRSd during drive train	190 ± 17	193 ± 27	0.88
QRSd after extrastimulus 350 ms	189 ± 19	194 ± 31	0.53
QRSd plateau	188 ± 19	193 ± 32	0.68
CI at onset of QRSd prolongation	276 ± 20	274 ± 26	0.92
Local VERP	219 ± 19	235 ± 23	0.061
CI window with QRSd prolongation	57 ± 25	39 ± 18	0.015
Maximal QRSd	234 ± 26	220 ± 34	0.030
Maximal Δ QRSd	46 ± 17	27 ± 14	0.001
Critical QRSd prolongation	+13 (-17 – +49)	-17 (-44 – +6)	0.017
Critical CI window	20 (0 – 75)	0 (0 – 20)	0.11

Variables are expressed as mean ± standard deviation or median (interquartile range). Abbreviations as in supplemental Table 1.

Supplemental Table 4. Parameters affecting QRSd prolongation

All RV 400 train	Effect on CI at onset QRSd prolongation, ms		Effect on CI window with QRSd prolongation, ms		Effect on maximal Δ QRSd, ms		Effect on critical QRSd prolongation, ms		Effect on critical CI window, ms	
	(95% CI)	p	(95% CI)	p	(95% CI)	p	(95% CI)	p	(95% CI)	p
CMR - cine images (n=36)										
LVEDV index, per 10 mL/m^2 ↑	2.2 (0.3 - 4.0)	**0.023**	-0.1 (-2.1 - 1.9)	0.92	-1.0 (-2.4 - 0.5)	0.19	-0.9 (-3.8 - +2.0)	0.54	0.5 (-2.0 - 3.0)	0.68
LVESV index, per 10 mL/m^2 ‹ ↑	1.6 (-0.2 - 3.4)	0.076	-0.7 (-2.6 - 1.1)	0.44	-1.4 (-2.7 - 0.0)	**0.044**	-1.4 (-4.1 - +1.4)	0.32	0.1 (-2.3 - 2.5)	0.93
LVEF, per 10 % ↓	2.4 (-3.9 - 8.7)	0.45	-4.4 (-10.4 - 1.7)	0.15	-5.7 (-10.0 - -1.4)	**0.011**	-5.6 (-14.6 - +3.5)	0.22	-2.4 (-10.2 - 5.4)	0.54
RVEDV index, per 10 mL/m^2 ↑	1.5 (-2.9 - 6.0)	0.49	1.1 (-3.3 - 5.4)	0.62	0.1 (-3.2 - 3.4)	0.93	0.0 (-6.4 - +6.3)	0.99	0.7 (-4.7 - 6.2)	0.79
RVESV index, per 10 mL/ ↑	0.4 (-4.3 - 5.1)	0.86	-0.5 (-5.1 - 4.1)	0.84	0.5 (-3.1 - 4.0)	0.79	+0.8 (-6.0 - +7.6)	0.81	-0.2 (-6.1 - 5.6)	0.93
RVEF, per 10% ↓	-0.9 (-8.5 - 6.7)	0.82	-2.3 (-9.7 - 5.1)	0.54	0.9 (-4.8 - 6.5)	0.76	+2.1 (-8.9 - +13.0)	0.70	-2.1 (-11.5 - 7.2)	0.64
CMR - LGE images (n=34)										
Total LGE mass, per 10 g ↑	-3.8 (-9.2 - 1.5)	0.15	0.5 (-5.1 - 6.0)	0.86	-1.0 (-4.9 - 3.0)	0.63	+0.4 (-7.7 - +8.4)	0.93	-1.5 (-8.4 - 5.5)	0.67
Core mass, per 10 g ↑	-8.2 (-17.6 - 1.2)	0.086	1.3 (-8.7 - 11.2)	0.80	-0.7 (-7.8 - 6.5)	0.85	+2.3 (-12.1 - +16.7)	0.75	-1.3 (-13.7 - 11.2)	0.83
Border zone mass, per 10 g ↑	-5.4 (-16.7 - 5.8)	0.33	0.4 (-11.0 - 11.9)	0.94	-3.2 (-11.3 - 5.0)	0.44	-1.5 (-18.1 - +15.1)	0.86	-4.5 (-18.7 - 9.8)	0.52
Laboratory										
Log NT-proBNP	6.2 (-0.3 - 12.7)	0.060	1.1 (-5.4 - 7.6)	0.73	-0.8 (-5.9 - 4.3)	0.76	-1.1 (-12.3 - +10.1)	0.84	3.6 (-6.5 - 13.8)	0.47
Biopsy (n=23)										
Collagen area percentage, per 10% ↑	-0.4 (-5.5 - 4.7)	0.87	-4.7 (-10.3 - 0.9)	0.096	-4.4 (-8.5 - -0.3)	**0.036**	-7.4 (-15.9 - +1.0)	0.081	-3.6 (-12.6 - 5.4)	0.42
Collagen distribution pattern										
Long strands vs. interstitial	12.9 (-11.8 - 37.5)	0.28	18.6 (-10.9 - 48.0)	0.20	3.8 (-22.9 - 30.5)	0.76	+15.1 (-29.0 - +59.4)	0.47	35.9 (-12.2 - 84.0)	0.13
Long strands vs. short strands	4.3 (-26.9 - 35.5)	0.77	41.4 (12.7 - 70.1)	**0.008**	15.5 (-11.4 - 42.5)	0.24	+35.4 (-18.3 - +89.2)	0.18	44.5 (-6.9 - 96.9)	0.084
Long strands vs. others	8.6 (-13.8 - 31.0)	0.43	30.0 (6.7 - 53.3)	**0.014**	9.7 (-9.9 - 29.2)	0.31	+25.3 (-13.6 - +64.1)	0.19	40.2 (3.7 - 76.6)	**0.032**
Genetics (n=39)										
Pathogenic or likely pathogenic mutation	11.1 (-4.6 - 26.7)	0.16	1.5 (-14.1 - 17.0)	0.85	2.7 (-9.1 - 14.6)	0.64	+3.7 (-22.1 - +29.4)	0.77	6.7 (-16.9 - 30.4)	0.57

Effect in ms (95%) is displayed.

Chapter 12

Summary, conclusions and future perspectives:

Towards more effective, individualized substrate-based therapies for ventricular arrhythmias

Summary, conclusions and future perspectives: Towards more effective, individualized substrate-based therapies for ventricular arrhythmias

In the general introduction of this thesis (**chapter 1**) it is stated that improved understanding of different types of ventricular arrhythmias, underlying substrates and mechanisms is the key to more accurate risk stratification and development of more effective, individualized and substrate-based therapies.

Part I of this thesis focuses on image integration during VT ablation. The reported applications, potential advantages and limitations are reviewed in **chapter 2**. Imaging modalities that have been applied include multidetector computed tomography (MDCT), late gadolinium enhancement magnetic resonance imaging (LGE-MRI), intracardiac echocardiography (ICE) and nuclear imaging modalities. The majority of studies have focused on the integration of MDCT and LGE-MRI in post-myocardial infarction patients; MDCT because of its relatively high spatial resolution, and LGE-MRI as current non-invasive gold standard for visualization of fibrosis. To date, image integration has been used to uncover and delineate the arrhythmogenic substrate,[1-10] to guide the procedural strategy,[11,12] to avoid ablation in close proximity of coronary arteries,[13,14] to visualize epicardial fat tissue[9,13] and to analyze ablation lesions.[15,16] Although image integration has provided important insights into the substrate for VT, to date it has not been demonstrated that it is cost-effective, reduces total radiation exposure, shortens procedure and mapping time and, most importantly, improves the safety and acute and long-term outcome after VT ablation. Prospective randomized studies comparing imaging-guided VT ablation with standard VT ablation in the setting of different cardiac diseases are required to determine whether this promising technology translates into improved results.

Substrate mapping is indispensable during VT ablation, mainly due to the frequent inducibility of hemodynamic unstable VT. At the epicardium substrate mapping may be hampered by fat tissue, which attenuates bipolar electrogram amplitudes,[13,17] and as a result, it may be difficult to differentiate between scar, myocardium and epicardial fat. Previous studies have demonstrated the feasibility and accuracy of integration of MRI-derived scar data with endocardial electroanatomical maps,[2,7,10,16] and of MDCT-derived epicardial fat with epicardial electroanatomical maps.[13,17] In **chapter 3**, these image integration techniques are combined in a series of 10 patients with NICM who underwent endocardial and epicardial VT ablation. It is demonstrated that bipolar voltage ≤1.81mV and unipolar voltage ≤7.95mV are the optimal cutoff values to distinguish scar from viable myocardium in epicardial regions devoid of fat. However, both bipolar and unipolar voltages are reduced by epicardial fat. Specific electrogram morphologies were not affected by fat, but were present at only one quarter of all scar sites. An algorithm

was constructed to improve differentiation between scar, viable myocardium and fat. These findings provide important insights into epicardial substrate mapping in patients with NICM, which is essential for successful VT ablation.

Chapter 4 describes typical scar patterns and associated VT morphologies in a series of 19 consecutive patients with NICM who underwent VT ablation. In 17 of 19 patients, either a basal anteroseptal or inferolateral scar was observed. Both scar patterns were associated with specific VT 12-lead ECG morphologies. In the 9 patients with anteroseptal scar-related VT, the ablation target sites were mainly located in the aortic root and/or anteroseptal LV endocardium, and in only one case at the epicardium. Of the 8 patients with inferolateral scar-related VT however, 5 had epicardial ablation target sites. The anteroseptal LV is usually difficult to reach during epicardial VT ablation due to the proximal coronary arteries, epicardial fat and the left atrial appendage.[13,18] Epicardial access to the inferolateral LV is typically not or only partly limited by epicardial fat, although the coronary arteries and the variable course of the phrenic nerve need to be considered. These findings are likely to be important for clinicians who consider epicardial VT ablation in patients with NICM. After publication of this study, other investigators have replicated and extended our findings in a larger patient cohort, demonstrating that patients with predominant anteroseptal scar types are at higher risk for VT recurrence during follow-up.[19]

Chapter 5 analyzes the scar characteristics at critical isthmus sites of VTs in patients after myocardial infarction or with nonischemic cardiomyopathy (NICM), aiming to improve our understanding of the substrate for VT, and to analyze the value of MRI-based areas of interest to guide VT ablation. Analysis of scar features at critical VT isthmus sites revealed that critical isthmus sites are characterized by relatively high scar transmurality and signal intensity, compared to the average values for the entire scar, which was particularly evident for the central isthmus sites. The vast majority of critical isthmus sites were located within close proximity (i.e., 5 mm) of >75% transmural scar, and the transition between core and border zone. It is concluded that MRI-derived scar features may be used to guide VT ablation. Other investigations also suggest an association between scar transmurality and electrogram prolongation[7,9,20,21] and VT isthmuses.[21] The relation between scar transmurality and VT in NICM patients is further supported by the study described in chapter 10, which demonstrated that the area of 50-75% scar transmurality carried important prognostic information in patients with NICM undergoing ICD implantation.

Overall, the integration of CT- and MRI-derived data has led to important insights into the substrate for sustained monomorphic VT. Practically, integration of MRI-derived data helps to identify and delineate the substrate, and to lead to areas that contain parts of the reentry circuit. Novel MRI techniques such as T1 mapping, which allows calculation of exact extracellular volumes, and wideband inversion pulses, which allows acquisi-

tion of high-quality contrast-enhanced MRI images in patients with devices,[22,23] may be applied to further enhance the added value of MRI during VT ablation procedures. Ultimately, randomized controlled trials need to be performed to assess the effect of MRI integration on procedural duration, complications and outcomes.

In **part II** of this thesis, the substrate, mechanisms and treatment for different types of ventricular arrhythmias are analyzed in patients with ischemic and nonischemic heart disease.

Chapter 6 focuses on the identification of VTs with an epicardial site of origin in patients with NICM. Although several investigators have previously reported that 12-lead ECG criteria allow differentiation between endocardial and epicardial VTs,[24-26] the ECG criteria were only evaluated on electrophysiology recording systems with electronic calipers at a sweep speed of 100 mm/s. To guide pre-procedural planning, the ECG criteria would however have to be applied to standard 25mm/s 12-lead ECGs of clinically documented VTs. The current study analyzed the value of ECG criteria for identification of VTs with an epicardial site of origin in 36 patients who underwent combined endocardial and epicardial VT ablation. When applied to standard 25mm/s 12-lead ECGs, none of the criteria could accurately differentiate between endocardial or epicardial VTs. When applied to 100mm/s tracings, part of the ECG criteria could distinguish epicardial from endocardial VTs, but only in slow VTs and in patients on amiodarone. The latter may be explained by the fact that the majority of ECG criteria rely on accurate identification of the QRS onset, which may be difficult to define in fast VTs in patients off amiodarone. These data suggest that when applied to standard 12-lead ECGs, the ECG criteria do not allow identification of patients who are likely to benefit from a primary epicardial ablation approach. LGE-MRI-derived substrate features may be more reliable to guide the procedural strategy in patients undergoing VT ablation.[11]

If epicardial mapping and ablation are performed, post-procedural pericarditic chest pain and pericarditic ECG changes may occur. In **chapter 7** we analyzed the effect of intrapericardial and systemic steroids on post-procedural pericarditic chest pain and ECG changes in a series of 85 patients who underwent epicardial mapping and ablation for VT. Over the years, the post-procedural management has evolved from no steroids, to systemic steroids, and finally to intrapericardial steroids. Pericarditic chest pain occurred in 59%, 43% and 21% of patients, respectively (overall p=0.017; no steroids vs intrapericardial steroids, p=0.006), and ECG changes in 41%, 30% and 37%, respectively (overall p=0.72), suggesting that intrapericardial steroids may reduce pericarditic chest pain, but not ECG changes after epicardial mapping and ablation. Although not randomly allocated, therapies were applied unselectively in consecutive patients, and the observed effects were large, suggesting a true beneficial effect of intrapericardial

steroids on pericarditic chest pain after epicardial mapping and ablation. A randomized study would however be required to definitively prove its efficacy.

There is limited data on the outcome after VT ablation in patients with NICM, and in particular on the value of programmed electrical stimulation to assess the acute procedural outcome. **Chapter 8** describes and analyzes the acute and long-term outcomes after VT ablation in a contemporary series of 45 patients with NICM. At the end of the procedure, a programmed electrical stimulation protocol was consistently applied and completed in all patients to assess the acute procedural outcome. Complete success was achieved in 38% of patients, partial success in another 38% and failure in 24%. Although 53% of patients had VT during an average of two years follow-up, the 6-month VT burden was reduced by ≥ 75% in 79% of patients. Non-complete success was the strongest predictor of VT recurrence, with recurrences in only 18% after complete success, compared with 77% after partial success and 73% after procedural failure. Importantly, the inducibility of non-clinical, usually fast VTs after successful ablation of the clinical VT was associated with high recurrence rates, and should therefore not be regarded as a non-specific finding. This does however not necessarily imply that fast, nonclinical VTs should always be targeted – persistent inducibility of fast VTs may also be a marker for a more complex or functionally determined arrhythmogenic substrate, which may be less amenable to VT ablation. Further studies are needed to assess whether targeting of these nonclinical, usually rapid VTs improves long-term outcomes after ablation. More generally, it is unclear whether and to what extent high VT recurrence rates are attributable to the timing of the procedure, not identified or not reachable substrates, insufficient lesion formation or lesion recovery, arrhythmogenic substrates that evolve over time, progressive heart failure, or other factors that are currently poorly understood. Future observational and experimental studies should aim to assess the effects of these and other factors (e.g., early referral, procedural strategy, ablation techniques, optimization of medical and device therapy) on procedural outcome.

Chapter 9 evaluates the impact of early reperfusion therapy on the inducibility and cycle length of VTs, and on the occurrence of VTs late after myocardial infarction. In a prior study in patients who were referred for treatment of VT, spontaneous and induced VTs were faster in reperfused patients, who typically had a patchy electroanatomic scar pattern, as opposed to a more confluent scar pattern in nonreperfused patients.[27] The present study aimed to analyze the effects of reperfusion therapy on ventricular arrhythmias in a large cohort of 506 post-infarction patients who underwent an electrophysiology study before ICD implantation for primary or secondary prevention. Inducibility of VT was comparable between primary prevention patients with and without reperfusion therapy (56% and 58%, respectively), but higher in secondary prevention patients without reperfusion therapy compared to those who had underwent reperfusion therapy (79% versus 56%, respectively, p=0.001). The absence of reperfusion therapy

was independently associated with a slower CL of induced VTs. In primary prevention patients, nonreperfused patients had a more than twofold increased risk for appropriate ICD therapy during follow-up. Thus, the application of reperfusion therapies at the time of acute myocardial infarction is an important determinant of the occurrence and characteristics of late ventricular arrhythmias. These findings improve our understanding of contemporary changes in arrhythmogenic substrates due to the widespread application of reperfusion therapies for acute myocardial infarction. Whether these changes are (partly) attributable to scar transmurality, which is associated with VT (chapter 5) and in general larger in nonreperfused patients, remains to be elucidated.

Not only in patients after myocardial infarction, but also in NICM patients accurate prediction of arrhythmic events is desirable, and would allow preventive treatment in those who are at risk. Prior studies have typically aimed to identify predictors for appropriate ICD therapy, sudden cardiac death, all-cause mortality or combined endpoints. Different types of ventricular arrhythmias may however have different underlying substrates and related predictors. Sustained monomorphic VT in NICM is considered to be the manifestation of a stable reentry circuit, whereas polymorphic VT and VF are thought to be related to one or more unstable reentry circuits or rotors. **Chapter 10** aimed to analyze the impact of myocardial scar on the occurrence and type of ventricular arrhythmia in patients with NICM, and to assess the predictive value of specific patterns of fibrosis for monomorphic VT. At the Maastricht en Leiden University Medical Centers, LGE-MRI was performed before ICD implantation in 87 patients with NICM. The presence, characteristics and extent of myocardial scar were assessed on LGE-MRI images. ICD recordings and 12-lead ECGs were reviewed to determine the occurrence and type of ventricular arrhythmia during follow-up. Importantly, the presence of myocardial scar predicted monomorphic VT, but not polymorphic VT/VF. The risk for monomorphic VT was particularly high when the LGE extent was ≥ 7.2 grams, whereas patients with < 7.2 grams LGE were at low risk for monomorphic VT, but remained at risk for potentially fatal polymorphic VT/VF. Features that were associated with high risk for monomorphic VT were core extent, location in basal segments and area with 51-75% transmurality. Thus, the current study demonstrates that patients at risk for monomorphic VT can be identified by LGE-MRI, which may have important implications for risk stratification and therapeutic interventions in patients with NIDCM. If patients at risk for polymorphic VT/VF can also be more accurately identified in the future, a randomized controlled trial should be performed to reassess the benefit of ICD implantation on all-cause mortality, quality of life and costs in patients who are considered at low risk for both monomorphic VT and polymorphic VT/VF.

Chapter 11 focuses on the substrate and mechanisms of polymorphic VT/VF in NICM. In order to improve our understanding of the substrate and mechanisms of ventricular arrhythmias in NICM, we designed and initialized the Leiden Nonischemic Cardiomy-

opathy Study in 2011. In this prospective cohort study patients are comprehensively analyzed by LGE-MRI, echocardiography, 24-hour Holter monitoring, exercise testing, blood sampling, an invasive electrophysiological study, endomyocardial biopsy, an MIBG scan and genetic analysis of 55 cardiomyopathy-related genes. The first results of this study are presented in chapter 11, which focuses on the substrate and mechanisms of polymorphic VT and VF. Prediction of these arrhythmias is challenged due to various potential causes, ranging from conduction and repolarization abnormalities to electrolyte imbalances.[28-31] One phenomenon that has been related to VF in patients with NICM is progressive activation delay after premature stimulation.[30] In the current study, we measured the paced QRS duration after premature stimulation as a simple marker of activation delay after premature stimulation in 40 patients with NICM and 20 healthy controls. The QRS duration started to increase at longer coupling intervals in NICM compared with controls, and the maximum increase was larger. In patients with NICM, the local refractory period at the pacing site was frequently shorter than the maximal paced QRS duration, which allowed to pace and capture within the previous QRS complex, with the potential to initiate a second, different activation wave front. This phenomenon was related to the inducibility of polymorphic VT and was associated with long thick strands of fibrosis in biopsy specimens. This study suggest that progressive activation delay may be quantified by measuring the QRS duration during a standard electrophysiological study, and that activation delay correlates with electrical instability. A future research project within the Leiden Nonischemic Cardiomyopathy Study aims to analyze whether progressive activation delay after premature stimulation predicts spontaneous polymorphic VT and VF during follow-up.

CONCLUSIONS

In patients undergoing VT ablation, image integration improves preprocedural planning, substrate identification and delineation, and can guide to areas containing critical isthmus sites. In patients with prior myocardial infarction or NICM, the presence, extent and features of myocardial scar determine the occurrence and characteristics of monomorphic VT. Progressive activation delay after premature stimulation is associated with the inducibility of polymorphic VT in NICM.

The studies described in this thesis contribute to an improved understanding of the substrate and mechanisms of ventricular arrhythmias in ischemic and nonischemic heart disease, which is the most important prerequisite for the development of effective, individualized and substrate-based therapies for ventricular arrhythmias in the future.

REFERENCE LIST

1. Andreu D, Berruezo A, Ortiz-Perez JT, Silva E, Mont L, Borras R, de Caralt TM, Perea RJ, Fernandez-Armenta J, Zeljko H, Brugada J. Integration of 3D electroanatomic maps and magnetic resonance scar characterization into the navigation system to guide ventricular tachycardia ablation. Circ Arrhythm Electrophysiol 2011;4(5):674-83.
2. Bogun FM, Desjardins B, Good E, Gupta S, Crawford T, Oral H, Ebinger M, Pelosi F, Chugh A, Jongnarangsin K, Morady F. Delayed-enhanced magnetic resonance imaging in nonischemic cardiomyopathy: utility for identifying the ventricular arrhythmia substrate. J Am Coll Cardiol 2009;53(13):1138-45.
3. Cochet H, Komatsu Y, Sacher F et al. Integration of merged delayed-enhanced magnetic resonance imaging and multidetector computed tomography for the guidance of ventricular tachycardia ablation: a pilot study. J Cardiovasc Electrophysiol 2013; 24(4):419-26.
4. Piers SR, Dyrda K, Tao Q, Zeppenfeld K. Bipolar ablation of ventricular tachycardia in a patient after atrial switch operation for dextro-transposition of the great arteries. Circ Arrhythm Electrophysiol 2012;5(2): e38-e40.
5. Codreanu A, Odille F, Aliot E, Marie PY, Magnin-Poull I, Andronache M, Mandry D, Djaballah W, Regent D, Felblinger J, de CC. Electroanatomic characterization of post-infarct scars comparison with 3-dimensional myocardial scar reconstruction based on magnetic resonance imaging. J Am Coll Cardiol 2008;52(10):839-42.
6. Piers SR, Tao Q, de Riva SM, Siebelink HM, Schalij MJ, van der Geest RJ, Zeppenfeld K. CMR-Based Identification of Critical Isthmus Sites of Ischemic and Nonischemic Ventricular Tachycardia. JACC Cardiovasc Imaging 2014.
7. Dickfeld T, Tian J, Ahmad G, Jimenez A, Turgeman A, Kuk R, Peters M, Saliaris A, Saba M, Shorofsky S, Jeudy J. MRI-Guided ventricular tachycardia ablation: integration of late gadolinium-enhanced 3D scar in patients with implantable cardioverter-defibrillators. Circ Arrhythm Electrophysiol 2011;4(2):172-84.
8. Perez-David E, Arenal A, Rubio-Guivernau JL et al. Noninvasive identification of ventricular tachycardia-related conducting channels using contrast-enhanced magnetic resonance imaging in patients with chronic myocardial infarction: comparison of signal intensity scar mapping and endocardial voltage mapping. J Am Coll Cardiol 2011; 57(2):184-94.
9. Piers SR, van Huls van Taxis CF, Tao Q, van der Geest RJ, Askar SF, Siebelink HM, Schalij MJ, Zeppenfeld K. Epicardial substrate mapping for ventricular tachycardia ablation in patients with non-ischaemic cardiomyopathy: a new algorithm to differentiate between scar and viable myocardium developed by simultaneous integration of computed tomography and contrast-enhanced magnetic resonance imaging. Eur Heart J 2012;34(8):586-96.
10. Wijnmaalen AP, van der Geest RJ, van Huls van Taxis CF, Siebelink HM, Kroft LJ, Bax JJ, Reiber JH, Schalij MJ, Zeppenfeld K. Head-to-head comparison of contrast-enhanced magnetic resonance imaging and electroanatomical voltage mapping to assess post-infarct scar characteristics in patients with ventricular tachycardias: real-time image integration and reversed registration. Eur Heart J 2011;32(1):104-14.
11. Andreu D, Ortiz-Perez JT, Boussy T, Fernandez-Armenta J, de Caralt TM, Perea RJ, Prat-Gonzalez S, Mont L, Brugada J, Berruezo A. Usefulness of contrast-enhanced cardiac magnetic resonance in identifying

the ventricular arrhythmia substrate and the approach needed for ablation. Eur Heart J 2014;35(20):1316-26.

12. Piers SR, Tao Q, van Huls van Taxis CF, Schalij MJ, van der Geest RJ, Zeppenfeld K. Contrast-Enhanced MRI-Derived Scar Patterns and Associated Ventricular Tachycardias in Nonischemic Cardiomyopathy: Implications for the Ablation Strategy. Circ Arrhythm Electrophysiol 2013.
13. van Huls van Taxis CF, Wijnmaalen AP, Piers SR, van der Geest RJ, Schalij MJ, Zeppenfeld K. Real-Time Integration of MDCT-Derived Coronary Anatomy and Epicardial Fat: Impact on Epicardial Electroanatomic Mapping and Ablation for Ventricular Arrhythmias. JACC Cardiovasc Imaging 2013;6(1):42-52.
14. Zeppenfeld K, Tops LF, Bax JJ, Schalij MJ. Images in cardiovascular medicine. Epicardial radiofrequency catheter ablation of ventricular tachycardia in the vicinity of coronary arteries is facilitated by fusion of 3-dimensional electroanatomical mapping with multislice computed tomography. Circulation 2006;114(3):e51-e52.
15. Dickfeld T, Kato R, Zviman M, Lai S, Meininger G, Lardo AC, Roguin A, Blumke D, Berger R, Calkins H, Halperin H. Characterization of radiofrequency ablation lesions with gadolinium-enhanced cardiovascular magnetic resonance imaging. J Am Coll Cardiol 2006;47(2):370-8.
16. Tian J, Ahmad G, Mesubi O, Jeudy J, Dickfeld T. Three-dimensional delayed-enhanced cardiac MRI reconstructions to guide ventricular tachycardia ablations and assess ablation lesions. Circ Arrhythm Electrophysiol 2012;5(2):e31-e35.
17. Desjardins B, Morady F, Bogun F. Effect of epicardial fat on electroanatomical mapping and epicardial catheter ablation. J Am Coll Cardiol 2010;56(16):1320-7.
18. Atienza F, Arenal A, Perez-David E, Elizaga J, Ortuno JE, Ledesma-Carbayo MJ, Sanchez-Quintana D, Fernandez-Aviles F. New diagnostic and therapeutic approaches to treat ventricular tachycardias originating at the summit of the left ventricle: role of merged hemodynamic-MRI and alternative ablation sources. Circ Arrhythm Electrophysiol 2013;6(6):e80-e84.
19. Oloriz T, Silberbauer J, Maccabelli G et al. Catheter ablation of ventricular arrhythmia in nonischemic cardiomyopathy: anteroseptal versus inferolateral scar sub-types. Circ Arrhythm Electrophysiol 2014;7(3):414-23.
20. Desjardins B, Crawford T, Good E, Oral H, Chugh A, Pelosi F, Morady F, Bogun F. Infarct architecture and characteristics on delayed enhanced magnetic resonance imaging and electroanatomic mapping in patients with postinfarction ventricular arrhythmia. Heart Rhythm 2009;6(5):644-51.
21. Sasaki T, Miller CF, Hansford R et al. Myocardial structural associations with local electrograms: a study of postinfarct ventricular tachycardia pathophysiology and magnetic resonance-based noninvasive mapping. Circ Arrhythm Electrophysiol 2012;5(6):1081-90.
22. Stevens SM, Tung R, Rashid S et al. Device artifact reduction for magnetic resonance imaging of patients with implantable cardioverter-defibrillators and ventricular tachycardia: late gadolinium enhancement correlation with electroanatomic mapping. Heart Rhythm 2014;11(2):289-98.
23. Rashid S, Rapacchi S, Vaseghi M, Tung R, Shivkumar K, Finn JP, Hu P. Improved late gadolinium enhancement MR imaging for patients with implanted cardiac devices. Radiology 2014;270(1):269-74.
24. Valles E, Bazan V, Marchlinski FE. ECG criteria to identify epicardial ventricular tachycardia in nonischemic cardiomyopathy. Circ Arrhythm Electrophysiol 2010;3(1):63-71.
25. Bazan V, Gerstenfeld EP, Garcia FC, Bala

R, Rivas N, Dixit S, Zado E, Callans DJ, Marchlinski FE. Site-specific twelve-lead ECG features to identify an epicardial origin for left ventricular tachycardia in the absence of myocardial infarction. Heart Rhythm 2007;4(11):1403-10.

26. Berruezo A, Mont L, Nava S, Chueca E, Bartholomay E, Brugada J. Electrocardiographic recognition of the epicardial origin of ventricular tachycardias. Circulation 2004; 109(15):1842-7.
27. Wijnmaalen AP, Schalij MJ, von der Thusen JH, Klautz RJ, Zeppenfeld K. Early reperfusion during acute myocardial infarction affects ventricular tachycardia characteristics and the chronic electroanatomic and histological substrate. Circulation 2010; 121(17):1887-95.
28. Higham PD, Adams PC, Murray A, Campbell RW. Plasma potassium, serum magnesium and ventricular fibrillation: a prospective study. Q J Med 1993;86(9):609-17.
29. Akar FG, Rosenbaum DS. Transmural electrophysiological heterogeneities underlying arrhythmogenesis in heart failure. Circ Res 2003;93(7):638-45.
30. Saumarez RC, Chojnowska L, Derksen R, Pytkowski M, Sterlinski M, Huang CL, Sadoul N, Hauer RN, Ruzyllo W, Grace AA. Sudden death in noncoronary heart disease is associated with delayed paced ventricular activation. Circulation 2003;107(20): 2595-600.
31. Kawara T, Derksen R, de Groot JR, Coronel R, Tasseron S, Linnenbank AC, Hauer RN, Kirkels H, Janse MJ, de Bakker JM. Activation delay after premature stimulation in chronically diseased human myocardium relates to the architecture of interstitial fibrosis. Circulation 2001;104(25):3069-75.

NEDERLANDSE SAMENVATTING

De onderzoeken die worden beschreven in dit proefschrift concentreren zich op structurele afwijkingen en mechanismen die ten grondslag liggen aan hartritmestoornissen. In de verschillende studies werd gebruik gemaakt van driedimensionale reconstructies van het hart op basis van CT-scans, MRI-scans en katheter-mapping en er werden ritmestoornissen en reacties op elektrische stimulatie geanalyseerd. Dit alles om het begrip van kamerritmestoornissen te verbeteren, zodat in de toekomst effectievere behandelingen kunnen worden ontwikkeld. Hieronder volgt een samenvatting van de achtergrond, de verschillende onderzoeken en de conclusies van dit proefschrift.

Inleiding

Patiënten met structurele hartziekte hebben een verhoogd risico op plotse hartdood door kamerritmestoornissen zoals ventrikeltachycardieën (VT's) en ventrikelfibrilleren (VF). In de afgelopen decennia zijn er belangrijke inzichten verkregen in het onderliggende substraat en de mechanismen achter deze ritmestoornissen, maar er zijn nog veel aspecten onopgehelderd. Intussen is voor een pragmatische benadering gekozen door een inwendige defibrillator (implantable cardioverter difibrillator, ICD) te implanteren bij patiënten die VT of VF hebben overleefd of een verhoogd risico hebben op plotse hartdood. De ICD's hebben op deze manier talloze levens gered en zijn niet meer weg te denken uit de huidige klinische praktijk. Het is echter belangrijk om te realiseren dat ICD's levensbedreigende ritmestoornissen zoals VT en VF kunnen stoppen, maar niet voorkomen. Elektrische ICD shocks zijn potentieel traumatisch voor de patiënt en worden geassocieerd met een verhoogde mortaliteit. Behandelingen om recidiverende kamerritmestoornissen te voorkomen, zoals anti-aritmische medicatie en katheterablatie van VT's, zijn daarom des te belangrijker geworden in het tijdperk van de ICD's. Momenteel wordt katheterablatie van VT's door veel cardiologen, mede vanwege de aanzienlijke recidiefkansen, pas toegepast als medicijnen niet meer werken. Eerdere onderzoeken hebben laten zien dat ongeveer de helft van de patiënten in het eerste jaar na de ablatie minstens één recidief heeft, maar ook dat bij ongeveer tweederde van de patiënten het aantal ritmestoornissen met tenminste 75% is reduceerd. Een redelijk resultaat gezien de complexiteit van het ziektebeeld, maar er is nog veel winst te behalen.

In dit proefschrift wordt, zoals in **hoofdstuk 1** gesteld, geprobeerd een bijdrage te leveren aan een beter begrip van het substraat en de mechanismen achter verschillende typen kamerritmestoornissen bij patiënten met structurele hartziekte, zodat in de toekomst meer effectieve, geindividualiseerde en substraatgerichte behandelingen ontwikkeld kunnen worden.

Deel I van dit proefschrift concentreert zich op integratie van beeldvormende technieken tijdens VT-ablatie, met het doel om meer inzicht te krijgen in het substraat voor VT en de ablatiebehandeling te optimaliseren.

Hoofdstuk 2 biedt een overzicht van de toepassingen, potentiele voordelen en de beperkingen van verschillende beeldvormende technieken. Eén van de belangrijkste hiervan is CT vanwege de hoge spatiële resolutie, waardoor onder andere de anatomie van het hart, het beloop van de kransslagaders en vet aan de buitenzijde van het hart uitstekend kunnen worden afgebeeld. Een andere belangrijke techniek is MRI vanwege de uitstekende weefselkarakterisatie, waardoor het substraat gedetailleerd in beeld kan worden gebracht.

In het geval van monomorfe VT's (d.w.z. kamerritmestoornissen met een stabiele ECG-morfologie) bestaat het substraat over het algemeen uit een re-entry circuit (kortsluitingscircuit) door een litteken, wat bijvoorbeeld is ontstaan na een hartinfarct. Met elektroanatomische substraatmapping worden traag geleidende gebieden binnen het litteken, meestal de oorzaak van re-entry circuits, geïdentificeerd zodat deze middels ablatie kunnen worden uitgeschakeld. Epicardiaal (aan de buitenzijde van het hart) wordt substraatmapping bemoeilijkt door vet, wat net als litteken de gemeten voltages verlaagt. In **hoofdstuk 3** worden zowel CT- als MRI-beelden met elektroanatomische maps geïntegreerd om een compleet inzicht te krijgen in laag gevolteerde en traag geleidende gebieden aan de buitenzijde van het hart (met elektroanatomische maps), het litteken (met MRI) en epicardiaal vet (met CT). Er wordt aangetoond dat een bipolair voltage ≤1.81 mV en een unipolair voltage ≤7.95 mV de beste afkapwaarden zijn om litteken van (relatief) gezond myocard te onderscheiden in gebieden zonder vet. In gebieden met vet kunnen elektrogrammen en de epicardiale vetdikte gebaseerd op CT worden gebruikt.

In **hoofstuk 4** worden met behulp van integratie van MRI twee typische substraatpatronen beschreven in een serie van 19 patiënten met non-ischemische cardiomyopathie (d.w.z. hartziekte niet veroorzaakt door kransslagaderproblemen). Bij 17 van de 19 patiënten werd ófwel een anteroseptaal, óf een inferolateraal substraat aangetoond en elk type was geassocieerd met specifieke typen ritmestoornissen en een beste benaderingswijze (van de binnenzijde of de buitenzijde van het hart). Na publicatie van deze studie zijn deze resultaten gerepliceerd door andere onderzoeksgroepen en is het belang voor de prognose aangetoond.

Zoals hierboven al genoemd bestaat het substraat in het geval van monomorfe VT's over het algemeen uit een re-entry circuit (kortsluitingscircuit) door een litteken. In **hoofdstuk 5** worden de eigenschappen van kritieke delen van deze re-entry circuits (en zodoende doelen voor ablatie) geanalyseerd met behulp van MRI-integratie tijdens VT-ablatie. De kritieke gebieden werden gekenmerkt door een hoge littekentransmuraliteit en een hoge signaalintensiteit op MRI. Het overgrote deel was gelokaliseerd op

hoogstens 5 mm van >75% transmuraal litteken en tevens op hoogstens 5 mm van de overgang tussen de kern en het randgebied van het litteken. Deze eigenschappen kunnen worden gebruikt om kritieke gebieden sneller te identificeren tijdens VT-ablaties.

Samenvattend heeft CT- en MRI-integratie tijdens VT-ablatie belangrijke inzichten opgeleverd. MRI-integratie kan helpen om het substraat te identificeren, de juiste benadering te kiezen en te leiden naar relevante gebieden. CT-integratie kan helpen om complicerende anatomische factoren zoals epicardiaal vet en kransslagaders te visualiseren. Nieuwe beeldvormende technieken kunnen de toegevoegde waarde mogelijk verder verhogen. Uiteindelijk zullen gerandomiseerde trials uitgevoerd moeten worden om de effecten van CT- en MRI-integratie op de duur van de ingreep, complicaties en resultaten te bepalen.

In **deel II** van dit proefschrift worden het substraat, de mechanismen en de behandeling van verschillende typen kamerritmestoornissen geanalyseerd bij patiënten met ischemische en non-ischemische hartziekte (d.w.z. hartziekte respectievelijk wel en niet veroorzaakt door kransslagaderproblemen).

Hoofdstuk 6 concentreert zich op de identificatie van VT's met een epicardiale oorsprong bij patiënten met non-ischemische cardiomyopathie. Voor deze ritmestoornissen kan een punctie onder het borstbeen nodig zijn om de ablatiekatheter in het hartzakje op te voeren zodat er aan de buitenzijde van het hart kan worden gebrand. In dit onderzoek werden eerder beschreven ECG criteria voor de identificatie van epicardiale VT's toegepast op standaard ECG's en op 100 mm/s ECG's op elektrofysiologiesystemen bij 36 patiënten die een gecombineerd endo- en epicardiale VT-ablatie ondergingen. Uit de analyses bleek dat géén van de ECG criteria goed kon differentiëren tussen endocardiale en epicardiale VT's wanneer deze werden toegepast op 100 mm/s ECG's op electrofysiologiesystemen, maar wel als deze werden toegepast op standaard ECG's. Er werd geconcludeerd dat de ECG criteria niet betrouwbaar zijn bij het bepalen van de beste benadering voor de ablatie indien deze worden toegepast op klinisch gedocumenteerde VT's. Waarschijnlijk is MRI voor dit doeleinde een betrouwbaarder hulpmiddel.

Als besloten wordt tot epicardiale mapping en ablatie, dan kan dit ná de ingreep gecompliceerd worden door pijn op de borst en ECG-veranderingen die ook bij een spontane pericarditis (d.w.z. een ontsteking van het hartzakje) worden gezien. In **hoofdstuk 7** wordt het effect van intrapericardiale (in het hartzakje) en systemische corticosteroïden op deze pijn en ECG-veranderingen geanalyseerd bij 85 patiënten die een epicardiale VT-ablatie ondergingen. Gedurende de afgelopen jaren evolueerde het beleid in het LUMC van géén steroïden, via systemische steroïden naar uiteindelijk intrapericardiale steroïden. In de laatste groep patiënten trad substantieel minder pericarditis-achtige pijn op de borst op dan in de twee eerdere groepen. Alhoewel het

hier niet om een gerandomiseerde studie gaat, werden de behandelingen niet-selectief toegepast in opeenvolgende patiënten en waren de effecten groot, wat suggereert dat er daadwerkelijk een gunstig effect is van intrapericardiale steroïden op pijn op de borst na de ingreep. Om dit definitief te bewijzen zou echter een gerandomiseerd onderzoek noodzakelijk zijn.

Er zijn slechts beperkte gegevens beschikbaar over de uitkomst na VT-ablatie bij patiënten met non-ischemische cardiomyopathie, met name wat betreft de waarde van het testen op induceerbaarheid van VT's na ablatie. In **hoofdstuk 8** beschrijven wij een groep van 45 patiënten met non-ischemische cardiomyopathie die VT-ablatie onderging. De sterkste voorspeller voor recidieven was de induceerbaarheid van VT's na ablatie. Ook de induceerbaarheid van niet-klinische (meestal snelle) VT's ná ablatie was geassocieerd met een hogerere recidiefkans. Dit betekent niet noodzakelijkerwijs dat deze meestal snelle, niet-klinische VT's ook altijd benaderd moeten worden tijdens de ablatie – de induceerbaarheid van dit soort VT's kan ook een marker zijn van een complexer of (deels) functioneel bepaald substraat, wat moeilijk met ablatie behandeld kan worden. In de toekomst moet daarom worden bepaald of het benaderen van dit soort VT's de prognose na ablatie verbetert.

In het algemeen blijft het moeilijk de oorzaak voor een recidief na ablatie te achterhalen. Zijn deze te wijten aan de timing van de ingreep, niet-geïdentificeerde of niet-bereikbare substraten, ontoereikende of herstellende ablatie-laesies, een evoluerend substraat, progressief hartfalen of andere factoren? Het is belangrijk dat er in de toekomst meer inzicht wordt verkregen op dit gebied.

Hoofdstuk 9 richt zich op de invloed van reperfusietherapie (bijv. dotter- en stentbehandeling) ten tijde van een acuut hartinfarct op de latere induceerbaarheid, snelheid en het optreden van VT's bij patiënten met ischemische hartziekte. Er werd een grote groep patiënten met een hartinfarct onderzocht die een elektrofysiologisch onderzoek hebben ondergaan vóór implantatie van een ICD. Het niet hebben gekregen van reperfusietherapie was een onafhankelijke voorspeller voor tragere geïnduceerde VT's en voor het optreden van terechte ICD-therapie (pacing of shocks) tijdens follow-up. Of deze relatie (deels) wordt verklaard door een grotere littekentransmuraliteit bij patiënten zonder reperfusietherapie, wat geassocieerd is met VT's zoals ook beschreven in hoofstuk 5, is nog onopgehelderd.

Het accuraat kunnen voorspellen van ritmestoornissen wordt niet alleen nagestreefd bij patiënten met een eerder hartinfarct, maar ook bij patiënten met een non-ischemische cardiomyopathie, zodat preventieve behandelingen kunnen worden toegepast bij patiënten met een hoog risico. Eerdere studies hebben gecombineerde eindpunten gebruikt, maar verschillende typen ritmestoornissen hebben waarschijnlijk verschillende onderliggende substraten en daarmee verschillende voorspellers. Monomorfe VT wordt normaliter veroorzaakt door een stabiel re-entry circuit, terwijl polymorfe VT en

VF (beide met een wisselende morfologie op het ECG) worden veroorzaakt door één of meer onstabiele circuits of rotors. In **hoofdstuk 10** wordt de invloed van de aanwezigheid van litteken in het hart en haar karakteristieken op het optreden van verschillende typen ritmestoornissen geanalyseerd bij 87 patiënten met non-ischemische cardiomyopathie die een MRI-scan en ICD-implantatie hebben ondergaan. De aanwezigheid van litteken voorspelde het optreden van monomorfe VT, maar niet van polymorfe VT en VF. Kenmerken van het litteken die voorspellend waren voor monomorfe VT waren uitgebreidheid van de kern, lokalisering in de basale segmenten en de grootte van het gebied met 51-75% transmuraliteit. Deze eigenschappen kunnen in de toekomst worden gebruikt om patiënten met een hoog risico op monomorfe VT te identificeren. Er werden geen voorspellers voor polymorfe VT of VF geïdentificeerd.

Hoofdstuk 11 richt zich op het substraat en de mechanismen van polymorfe VT en VF bij patiënten met non-ischemische cardiomyopathie. Om de inzichten in het substraat en de mechanismen achter kamerritmestoornissen bij non-ischemische cardiomyopathie te verbeteren, startten wij in 2011 met de Leidse Non-ischemische Cardiomyopathiestudie. In deze prospectieve cohortstudie worden patiënten uitgebreid geanalyseerd middels MRI, echocardiografie, 24-uurs Holters, inspanningstests, bloedonderzoek, een invasief elektrofysiologisch onderzoek, hartbiopsie, een MIBG-scan en genetische analyse van 55 relevante genen. De eerste resultaten van dit onderzoek worden gepresenteerd in hoofdstuk 11. In deze eerste studie werd bij 40 patiënten met non-ischemische cardiomyopathie en 20 controlepatiënten met een structureel normaal hart tijdens een elektrofysiologisch onderzoek de QRS-duur gemeten na elektrische stimulatie, als een eenvoudige marker voor vertraagde activatie en daarmee mogelijk een voorspeller voor polymorfe VT en VF. Verbreding van het QRS-complex na elektrische stimulatie bleek inderdaad duidelijk geassocieerd met de opwekbaarheid van polymorfe VT's. Een nieuw onderzoeksproject binnen de Leidse Non-ischemische Cardiomyopathiestudie zal de voorspellende waarde van progressieve activatievertraging na elektrische stimulatie voor spontane polymorfe VT en VF tijdens follow-up analyseren.

CONCLUSIE

Bij patiënten die VT-ablatie ondergaan biedt integratie van beeldvormende technieken toegevoegde waarde op het gebied van planning, substraatidentificatie en het leiden naar kritieke gebieden voor VT's. Bij patiënten met een oud hartinfarct of een non-ischemische cardiomyopathie bepalen de aanwezigheid, de uitbreiding en de kenmerken van litteken het toekomstige optreden en de karakteristieken van monomorfe VT's. Progressieve activatievertraging na elektrische stimulatie is geassocieerd met de opwekbaarheid van polymorfe VT bij patiënten met non-ischemische cardiomyopathie.

De studies beschreven in dit proefschrift dragen bij aan een beter begrip van het substraat en de mechanismen van kamerritmestoornissen bij patiënten met ischemische en non-ischemische hartziekte. Dit is de meest belangrijke voorwaarde voor de ontwikkeling van meer effectieve, geïndividualiseerde en substraatgerichte behandelingen voor kamerritmestoornissen in de toekomst.

DANKWOORD

Velen hebben op heel verschillende manieren een bijdrage geleverd aan dit proefschrift en wil ik graag bedanken. Patiënten door onbaatzuchtig in te stemmen met invasieve onderzoeken om een toekomstige generatie te helpen. Mijn promotores prof. dr. Katja Zeppenfeld en prof. dr. Martin Schalij ieder op geheel eigen wijze door hun sterke visie, humor en het altijd nastreven van het hoogste niveau. De promotiecommissie door de kritische beoordeling van het manuscript. Collega's door hun onmisbare hulp bij onderzoeksprojecten, stimulerende discussies en de nodige ontspanning tijdens lunches en congressen. Tenslotte mijn vrienden en familie, in het bijzonder mijn ouders, zus en paranimfen Fons en Rutger, door al het waardevolle buiten het werk.

LIST OF PUBLICATIONS

Critical QRS prolongation after premature stimulation is associated with polymorphic ventricular tachycardia in nonischemic cardiomyopathy: results from the Leiden Nonischemic Cardiomyopathy Study

Piers SR, Askar SFA, Venlet J, Kapel GFL, de Riva Silva M, Jongbloed JJDH, van Tintelen JP, Schalij MJ, Pijnappels DA, Zeppenfeld K
Accepted for publication in Heart Rhythm

Fatigue as presenting symptom and a high burden of premature ventricular contractions are independently associated with increased ventricular wall stress in patients with normal left ventricular function.

van Huls van Taxis CF, Piers SR, de Riva Silva M, Dekkers OM, Pijnappels DA, Schalij MJ, Wijnmaalen AP, Zeppenfeld K.
Circ Arrhythm Electrophysiol. 2015, Epub ahead of print.

Myocardial scar predicts monomorphic ventricular tachycardia but not polymorphic ventricular tachycardia or ventricular fibrillation in nonischemic dilated cardiomyopathy.

Piers SR, Everaerts K, van der Geest RJ, Hazebroek MR, Siebelink HM, Pison LA, Schalij MJ, Bekkers SC, Heymans S, Zeppenfeld K.
Heart Rhythm. 2015;12(10):2106-14.

Reassessing noninducibility as ablation endpoint of post-infarction ventricular tachycardia: the impact of left ventricular function.

De Riva Silva M, Piers SR, Kapel GF, Watanabe M, Venlet J, Trines SA, Schalij MJ, Zeppenfeld K.
Circ Arrhythm Electrophysiol. 2015;8(4)853-62.

The relationship between time from myocardial infarction, left ventricular dyssynchrony, and the risk for ventricular arrhythmia: speckle-tracking echocardiographic analysis.

Leong DP, Hoogslag GE, Piers SR, Höke U, Thijssen J, Marsan NA, Schalij MJ, Zeppenfeld K, Bax JJ, Delgado V.
J Am Soc Echocardiogr. 2015;28(4):470-7.

Re-entry using anatomically determined isthmuses: a curable ventricular tachycardia in repaired congenital heart disease.

Kapel GF, Reichlin T, Wijnmaalen AP, Piers SR, Holman ER, Tedrow UB, Schalij MJ, Stevenson WG, Zeppenfeld K.
Circ Arrhythm Electrophysiol. 2015;8(1):109-9.

Automated left ventricle segmentation in late gadolinium-enhanced MRI for objective myocardial scar assessment.

Tao Q, Piers SR, Lamb HJ, van der Geest RJ.
J Magn Reson Imaging. 2015;42(2):390-9.

Preprocedural magnetic resonance imaging for image-guided catheter ablation of scar-related ventricular tachycardia.

Tao Q, Piers SR, Lamb HJ, Zeppenfeld K, van der Geest RJ.
Int J Cardiovasc Imaging. 2015;31(2):369-77.

Left-sided ablation of ventricular tachycardia in adults with repaired tetralogy of Fallot: a case series.

Kapel GF, Reichlin T, Wijnmaalen AP, Tedrow UB, Piers SR, Schalij MJ, Hazekamp MG, Jongbloed MR, Stevenson WG, Zeppenfeld K.
Circ Arrhythm Electrophysiol. 2014;7(5):889-97.

CMR-based identification of critical isthmus sites of ischemic and nonischemic ventricular tachycardia.

Piers SR, Tao Q, de Riva Silva M, Siebelink HM, Schalij MJ, van der Geest RJ, Zeppenfeld K.
JACC Cardiovasc Imaging. 2014;7(8):774-84.

Influence of steroid therapy on the incidence of pericarditis and atrial fibrillation following percutaneous epicardial mapping and ablation for ventricular tachycardia.

Piers SR, Dyrda K, van Huls van Taxis CF, Schalij MJ, Zeppenfeld K.
Circ Arrhythm Electrophysiol. 2014;7(4):671-6.

Endocardial or epicardial ventricular tachycardia in nonischemic cardiomyopathy? The role of 12-lead ECG criteria in clinical practice.

Piers SR, de Riva Silva M, Kapel GF, Trines SA, Schalij MJ, Zeppenfeld K.
Heart Rhythm. 2014;11(6):1031-9.

Managing ventricular tachycardia: total atrioventricular block after ablation in a patient with nonischemic dilated cardiomyopathy.

Piers SR, Zeppenfeld K.
In: Yu CM, Hayes DL, Auricchio A, eds. Cases in cardiac resynchronization therapy. Philadephia, W.B. Saunders; 2014:163-69.

Prevention of effective cardiac resynchronization therapy by frequent premature ventricular contractions in a patient with nonischemic cardiomyopathy.

Piers SR, Zeppenfeld K.
In: Yu CM, Hayes DL, Auricchio A, eds. Cases in cardiac resynchronization therapy. Philadephia, W.B. Saunders; 2014:171-77.

Contrast-enhanced MRI-derived scar patterns and associated ventricular tachycardias in nonischemic cardiomyopathy: implications for the ablation strategy.

Piers SR, Tao Q, van Huls van Taxis CF, Schalij MJ, van der Geest RJ, Zeppenfeld K.
Circ Arrhythm Electrophysiol. 2013;6(5):875-83.

Imaging-guided Ventricular Tachycardia Ablation.

Piers SR, Zeppenfeld K.
Arrhythmia & Electrophysiology Review 2013;2(2):128–34

Outcome of ventricular tachycardia ablation in patients with nonischemic cardiomyopathy: the impact of noninducibility.

Piers SR, Leong DP, van Taxis CF, Tayyebi M, Trines SA, Pijnappels DA, Delgado V, Schalij MJ, Zeppenfeld K.
Circ Arrhythm Electrophysiol. 2013;6(3):513-21.

Real-Time Integration of MDCT-Derived Coronary Anatomy and Epicardial Fat: Impact on Epicardial Electroanatomic Mapping and Ablation for Ventricular Arrhythmias.

van Huls van Taxis CF, Wijnmaalen AP, Piers SR, van der Geest RJ, Schalij MJ, Zeppenfeld K.
JACC Cardiovasc Imaging. 2013;6(1):42-52.

Epicardial substrate mapping for ventricular tachycardia ablation in patients with non-ischaemic cardiomyopathy: a new algorithm to differentiate between scar and viable myocardium developed by simultaneous integration of computed tomography and contrast-enhanced magnetic resonance imaging.

Piers SR, van Huls van Taxis CF, Tao Q, van der Geest RJ, Askar SF, Siebelink HM, Schalij MJ, Zeppenfeld K.
Eur Heart J. 2013;34(8):586-96.

Electrophysiological characteristics of ventricular tachyarrhythmias in cardiac sarcoidosis versus arrhythmogenic right ventricular cardiomyopathy.

Dechering DG, Kochhäuser S, Wasmer K, Zellerhoff S, Pott C, Köbe J, Spieker T, Piers SR, Bittner A, Mönnig G, Breithardt G, Wichter T, Zeppenfeld K, Eckardt L.
Heart Rhythm. 2013;10(2):158-64.

Bipolar ablation of ventricular tachycardia in a patient after atrial switch operation for dextro-transposition of the great arteries.

Piers SR, Dyrda K, Tao Q, Zeppenfeld K.
Circ Arrhythm Electrophysiol 2012;5(2):e38-40

Early Reperfusion Therapy Affects Inducibility, Cycle Length and Occurrence of Ventricular Tachycardia Late After Myocardial Infarction.

Piers SR, Wijnmaalen AP, Borleffs CJ, van Huls van Taxis CF, Thijssen J, van Rees JB, Cannegieter SC, Bax JJ, Schalij MJ, Zeppenfeld K.
Circ Arrhythm Electrophysiol. 2011;4(2):195-201.

Predictors of Death and Occurrence of Appropriate Implantable Defibrillator Therapies in Patients with Chronic Ischemic Cardiomyopathy.

Ng AC, Bertini M, Borleffs CJ, Delgado V, Biersma E, Piers SR, Thijssen J, Nucifora G, Shanks M, Ewe SH, Biffi M, van de Veire NR, Leung DY, Schalij MJ, Bax JJ.
Am J Cardiol. 2010;106(11):1566-73.

Prediction of Atrial Fibrillation in Patients with Implantable Cardioverter Defibrillator and Heart Failure.

Bertini M, Borleffs CJ, Delgado V, Ng AC, Piers SR, Shanks M, Antoni ML, Biffi M, Boriani G, Schalij MJ, Bax JJ, Van de Veire NR.
Eur J Heart Fail. 2010;12(10):1101-10.

Atherosclerotic Plaque Histology and Clinical Outcome after Carotid Endarterectomy.

Hellings WE, Peeters W, Moll FL, Piers SR, van Setten J, Van der Spek PJ, de Vries JP, Seldenrijk KA, De Bruin PC, Vink A, Velema E, de Kleijn DP, Pasterkamp G.
Circulation 2010; 121(17):1941-50.

CURRICULUM VITAE

Sebastiaan Piers werd in 1986 geboren in Utrecht en groeide op in de omgeving van 's Hertogenbosch. Hij behaalde in 2004 cum laude zijn examen aan gymnasium Beekvliet te St. Michielsgestel, waarna hij startte met de studie geneeskunde aan de Universiteit Utrecht. Tijdens een bijbaan op de afdeling cardiologie in het UMC Utrecht raakte hij door ritmemonitors geïnteresseerd in de cardiologie, waarop hij een tweetal co-schappen cardiologie volgde in het St. Antonius ziekenhuis te Nieuwegein. In zijn laatste studiejaar was Sebastiaan actief betrokken bij een electrofysiologisch onderzoeksproject in het Leids Universitair Medisch Centrum en startte aldaar na het afronden van zijn studie in 2011 met een promotietraject onder begeleiding van prof. dr. K. Zeppenfeld en prof. dr. M.J. Schalij. Het onderzoek concentreerde zich op het substraat en de mechanismen van kamerritmestoornissen bij patiënten met structurele hartziektes – het resultaat werd op diverse (inter)nationale congressen gepresenteerd en staat in dit proefschrift beschreven. Sebastiaan startte op 1 apri 2014 met zijn vooropleiding interne geneeskunde in het Onze Lieve Vrouwe Gasthuis te Amsterdam (opleider dr. Y.F.C. Smets) en zal per 1 april 2016 beginnen op de afdeling cardiologie in het Alrijne ziekenhuis te Leiderdorp (opleider dr. C.J.H.J. Kirchhof), waarna hij zijn opleiding tot cardioloog zal vervolgen in het Leids Universitair Medisch Centrum (opleider prof. dr. M.J. Schalij).